



# dielectric properties of nanofluids : dielectric strength, static electrization, partial discharges and surface discharges

Hocine Khelifa

## ► To cite this version:

Hocine Khelifa. dielectric properties of nanofluids: dielectric strength, static electrization, partial discharges and surface discharges. Autre. Ecole Centrale de Lyon, 2024. Français. NNT: 2024ECDL0048 . tel-04921428

HAL Id: tel-04921428

<https://theses.hal.science/tel-04921428v1>

Submitted on 30 Jan 2025

**HAL** is a multi-disciplinary open access archive for the deposit and dissemination of scientific research documents, whether they are published or not. The documents may come from teaching and research institutions in France or abroad, or from public or private research centers.

L'archive ouverte pluridisciplinaire **HAL**, est destinée au dépôt et à la diffusion de documents scientifiques de niveau recherche, publiés ou non, émanant des établissements d'enseignement et de recherche français ou étrangers, des laboratoires publics ou privés.

**THESE**

Présentée devant

**L'ECOLE CENTRALE DE LYON**

Pour obtenir le grade de

**DOCTEUR**

(Arrêté du 30/03/1992)

**Spécialité : Génie Electrique**

Préparée au sein de

**L'ECOLE DOCTORALE**

**ELECTRONIQUE, ELECTROTECHNIQUE, AUTOMATIQUE**

**DE LYON**

par

**Hocine KHELIFA**

---

**DIELECTRIC PROPERTIES OF NANOFUIDS: DIELECTRIC STRENGTH,  
ELECTROSTATIC CHARGING TENDENCY, PARTIAL DISCHARGES AND  
SURFACE DISCHARGES**

---

*Soutenue le 18 décembre 2024 devant la commission d'examen :*

**JURY :**

<b>S. AGNEL</b>	<i>Professeur – Unisversité de Montpellier</i>	<b>Rapporteur</b>
<b>A. BEROUAL</b>	<i>Professeur – Ecole Centrale de Lyon</i>	<b>Directeur de thèse</b>
<b>A. HADDAD</b>	<i>Professeur – Université de Cardiff – Grande Bretagne</i>	<b>Rapporteur</b>
<b>J. MARTINEZ</b>	<i>Professeur – Université Paul Sabatier (UPS) - LAPLACE</i>	<b>Examinateur</b>
<b>M-A. RAULET</b>	<i>Maître de Conférence, HDR – Université Lyon 1, AMPERE</i>	<b>Examinateur</b>
<b>E. VAGNON</b>	<i>Maître de Conférence – Ecole Centrale de Lyon</i>	<b>Co-directeur de thèse</b>

## **DEDICATION**

*In memory of my mother and my brother Mahdi,*

*To my wife (F. Manar), my children (Tamime and Athyr), my father, and all my  
family,*

*And to all my friends.*

## **ACKNOWLEDGMENTS**

I sincerely thank my research supervisors, Professor Abderrahmane BEROUAL and Doctor Eric VAGNON, for their unwavering patience and generosity, particularly during the challenging moments I encountered. I am incredibly thankful for their confidence in my abilities and continual encouragement over the past four years, which has significantly impacted my journey. Their support in providing excellent working conditions was invaluable. Moreover, their clear and insightful advice throughout the writing process significantly eased my task and enabled me to produce this thesis.

I want to thank Professors Philippe DELACHARTRE and Dominique PLANSON, Director of EEA doctoral school and Professor at INSA Lyon, respectively, who kindly accepted to be on my thesis monitoring committee throughout these years.

I would also like to thank Professor Serge AGNEL from the *University of Montpellier* and Professor A. HADDAD from the *University of Cardiff – UK*, for agreeing to report on this thesis.

I also thank Professor J. MARTINEZ from University *Paul Sabatier (UPS) – LAPLACE* and M-A. RAULET, *Maître de Conférence, HDR – University of Lyon 1*, for agreeing to serve on this jury.

## TABLE OF CONTENTS

Dedication .....	ii
Acknowledgments .....	iii
Table of Contents.....	iv
Figures List.....	vii
Tables List .....	x
Abbreviations List .....	xii
General Introduction.....	1
Chapter 1 .....	5
State of the Art.....	5
1.1.    Introduction .....	6
1.2.1 History of nanofluids.....	6
1.2.2 Preparation of nanofluids .....	7
1.2.3 Stability of NFs .....	8
1.2.    On the impact of NPs on dielectrics performances of base liquids.....	11
1.3.1 Breakdown phenomena in nanofluids .....	11
1.3.2 PDs in nanofluids .....	15
1.3.3 Effect of nanoparticles on electrostatic charging tendency .....	17
1.3.    Statistical Analysis .....	19
1.4.1 Normal distribution .....	19
1.4.2 Weibull distribution (Appendix material).....	20
1.4.3 Goodness-of-fit tests (Anderson–Darling Fitting Test) .....	20
1.4.4 Two-Sample t-Test.....	21
1.4.    Electrical double layers .....	22
1.5.1 Helmholtz Double-Layer Theory [71]:.....	23
1.5.2 Gouy-Chapman Model (1910) and Chapman-Stern Model (1920s):.....	23
1.5.3 Stern-Gouy-Chapman Model (1957):.....	23
1.5.    Fractal analysis.....	23
1.6.    Health issue of nanoparticles .....	25
1.7.    Conclusion.....	26
Chapter 2 .....	27

Experimental Set-Up .....	27
2.1    Introduction .....	28
2.2    Materials.....	29
2.2.1    Nanoparticles .....	29
2.2.2    Dielectric liquids .....	30
2.2.3    Surfactant (Oleic Acid).....	32
2.3    Nanofluids preparation.....	33
2.4    Stability and stability assessment of nanofluids.....	34
•        Limited Charging:.....	35
•        Low Conductivity:.....	35
•        Lack of polarization:.....	35
2.5    Test bench.....	35
2.5.1    AC breakdown voltage measurements .....	35
2.5.2    Partial Discharge Characterization .....	36
2.5.3    Electrostatic charging tendency .....	38
2.5.4    Surface Discharge Characterization .....	39
2.6    Conclusion.....	41
Chapter 3. ....	43
AC Breakdown Voltage of Nanofluids-Based Synthetic and Naturel Esters and Mineral Oil.....	43
3.1    Introduction .....	44
3.2    Conducting nanoparticles .....	44
3.2.1    AC breakdown voltage .....	44
3.2.2    Anderson-Darling (AD) goodness-of-fit test.....	47
3.2.3    Weibull probability analysis .....	48
3.3    Semi-Conducting nanoparticles .....	55
3.3.1    AC breakdown voltage .....	55
3.3.2    Anderson-Darling (AD) goodness-of-fit test.....	56
3.3.3    Weibull probability analysis .....	56
3.4    Insulating nanoparticles .....	59
3.4.1    AC breakdown voltage .....	59
3.4.2    Anderson-Darling (AD) goodness-of-fit test.....	65
3.4.3    Weibull probability analysis .....	67
3.5    Discussion .....	76

3.6 Conclusion.....	81
CHAPTER 4.....	82
Effect of Nanoparticles on the Partial Discharge Activity, Electrostatic Charging Tendency, and Surface Discharge .....	82
4.1 Introduction .....	83
4.2 Partial Discharge Activity .....	84
4.2.1 Conducting NPs.....	84
4.2.2 Insulating NPs .....	93
4.2.2 Discussion of NPs effect on PDs activity .....	96
4.3 Electrostatic charging tendency .....	97
4.3.1 Synthetic ester with Fe <sub>3</sub> O <sub>4</sub> , CuO, and C <sub>60</sub> .....	97
4.3.2 Natural ester (Midel 1204) with MgO.....	101
4.3.3 Natural ester (FR3) with C <sub>60</sub> .....	104
4.4 Creeping discharges .....	107
4.4.1 Synthetic ester with Fe <sub>3</sub> O <sub>4</sub> , Al <sub>2</sub> O <sub>3</sub> (20-30 nm), and C <sub>60</sub> .....	107
4.4.2 Natural ester with Fe <sub>3</sub> O <sub>4</sub> , Al <sub>2</sub> O <sub>3</sub> (20-30 nm), and C <sub>60</sub> .....	110
4.4.3 Discussion.....	113
4.5 Conclusion.....	114
General Conclusion .....	115
References .....	118
Appendix A - Two-Sample t-Test .....	127
Appendix B - Anderson–Darling fitting test .....	128
Related Works.....	129
Journal Articles.....	129
International Conferences.....	130
Résumé de thèse en Français .....	- 1 -
Abstract .....	I
Résumé .....	II

## FIGURES LIST

<b>Figure 2.1</b> Chemical structure of Oleic Acid [96].....	32
<b>Figure 2.2</b> Preparation procedure of Nanofluids.....	34
<b>Figure 2.3</b> Electrodes configuration.....	36
<b>Figure 2.4</b> The experimental test bench.....	37
<b>Figure 2.5</b> Voltage profile (RMS value) was applied to samples during the PD test.....	38
<b>Figure 2.6</b> Diagram of spinning disk system for ECT quantification.....	38
<b>Figure 2.7</b> Creeping discharges investigation test bench.....	40
<b>Figure 2.8</b> Creeping discharge image at the surface of solid insulator immersed in pure NE at 58 kV with the circumscribed circle.....	41
<b>Figure 3.1</b> Mean breakdown voltages of nanofluid containing $\text{Fe}_3\text{O}_4$ at different concentrations for (a) synthetic ester, (b) natural ester, and (c) mineral oil .....	45
<b>Figure 3.2</b> Mean breakdown voltages of nanofluid containing fullerene (4-8 nm) at different concentrations for (a) synthetic ester, (b) natural ester, and (c) mineral oil. ....	46
<b>Figure 3.3</b> Mean breakdown voltages of nanofluid containing Gr at different concentrations for (a) synthetic ester, (b) natural ester, and (c) mineral oil.....	47
<b>Figure 3.4</b> Weibull probability plots of breakdown voltages of nanofluid containing $\text{Fe}_3\text{O}_4$ at different concentrations for (a) synthetic ester, (b) natural ester, and (c) mineral oil.....	50
<b>Figure 3.5</b> Weibull probability plots of breakdown voltages of nanofluid containing $\text{C}_{60}$ at different concentrations for (a) synthetic ester, (b) natural ester, and (c) mineral oil.....	51
<b>Figure 3.6</b> Weibull probability plots of breakdown voltages of nanofluid containing Gr at different concentrations for (a) synthetic ester, (b) natural ester, and (c) mineral oil.....	52
<b>Figure 3.7</b> Mean breakdown voltages of nanofluid containing $\text{ZnO}$ at different concentrations for (a) synthetic ester, (b) natural ester, and (c) mineral oil. ....	56
<b>Figure 3.8</b> Weibull probability plots of breakdown voltages of nanofluid containing $\text{ZnO}$ at different concentrations for (a) synthetic ester, (b) natural ester, and (c) mineral oil.....	58

<b>Figure 3.9</b> Mean breakdown voltages of nanofluid containing Al <sub>2</sub> O <sub>3</sub> (20-30 nm) at different concentrations for (a) synthetic ester, (b) natural ester, and (c) mineral oil .....	61
<b>Figure 3.10</b> Mean breakdown voltages of nanofluid containing Al <sub>2</sub> O <sub>3</sub> (50 nm) at different concentrations for (a) synthetic ester, (b) natural ester, and (c) mineral oil .....	62
<b>Figure 3.11</b> Mean breakdown voltages of nanofluid containing ZrO <sub>2</sub> at different concentrations for (a) synthetic ester, (b) natural ester, and (c) mineral oil .....	63
<b>Figure 3.12</b> Mean breakdown voltages of nanofluid containing SiO <sub>2</sub> at different concentrations for (a) synthetic ester, (b) natural ester, and (c) mineral oil .....	65
<b>Figure 3.13</b> Weibull probability plots of breakdown voltages of nanofluid containing Al <sub>2</sub> O <sub>3</sub> (20-30 nm) at different concentrations for (a) synthetic ester, (b) natural ester, and (c) mineral oil .....	68
<b>Figure 3.14</b> Weibull probability plots of breakdown voltages of nanofluid containing Al <sub>2</sub> O <sub>3</sub> (50 nm) at different concentrations for (a) synthetic ester, (b) natural ester, and (c) mineral oil .....	69
<b>Figure 3.15</b> Weibull probability plots of breakdown voltages of nanofluid containing ZrO <sub>2</sub> at different concentrations for (a) synthetic ester, (b) natural ester, and (c) mineral oil.....	70
<b>Figure 3.16</b> Weibull probability plots of breakdown voltages of nanofluid containing SiO <sub>2</sub> at different concentrations for: (a) synthetic ester, (b) natural ester, and (c) mineral oil....	71
<b>Figure 3.17</b> Diagram illustrating the polarization of dielectric particles with (a) higher or (b) lower, and (c) equal polarization capacity compared to the base liquid. ....	77
<b>Figure 3.18</b> Inter-nanoparticle distance vs. concentration of different nanofluids. ....	80
<b>Figure 4.1</b> Voltage rise protocol for inception voltage search. ....	84
<b>Figure 4.2</b> Voltage Profile. ....	85
<b>Figure 4.3</b> PD pattern of SE and SE-based nanofluids with Fe <sub>3</sub> O <sub>4</sub> .....	86
<b>Figure 4.4</b> PD pattern of NE and NE-based nanofluids with Fe <sub>3</sub> O <sub>4</sub> .....	87
<b>Figure 4.5</b> Voltage profile (RMS value) applied to SE-based nanofluids with C <sub>60</sub> and Gr.	88
<b>Figure 4.6</b> PD pattern of SE and SE-based nanofluids with C <sub>60</sub> at 12 kV voltage level. ....	89
<b>Figure 4.7</b> PD pattern of NE and NE-based nanofluids with C <sub>60</sub> . ....	91

<b>Figure 4.8</b> PD pattern of SE and SE-based nanofluids with Gr at 12 kV voltage level .....	93
<b>Figure 4.9</b> PD pattern of SE and SE-based nanofluids with Al <sub>2</sub> O <sub>3</sub> (20-30 nm).....	95
<b>Figure 4.10</b> PD pattern of NE and NE-based nanofluids with Al <sub>2</sub> O <sub>3</sub> (20-30 nm).....	95
<b>Figure 4.11</b> Electrostatic charging tendency of (a) SE, (b) SE with 0.1 g/L Fe <sub>3</sub> O <sub>4</sub> , (c) SE with 0.1 CuO, and (d) SE with 0.1 g/L C <sub>60</sub> . ....	100
<b>Figure 4.12</b> Cumulative ECT after one hour of different liquids for different speeds.....	100
<b>Figure 4.13</b> Dependence of the ECT on the disk's rotational speed for different liquids. 100	
<b>Figure 4.14</b> Mean value of AC breakdown voltages of different concentrations of MgO for a gap distance d=2 mm. ....	101
<b>Figure 4.15</b> PD pattern of natural ester and NFs-based natural ester with MgO nanoparticles at 0.2 g/L, stressed with 120%*PDIV. ....	102
<b>Figure 4.16</b> Electrostatic charging tendency of (a) natural ester and (b) natural ester with MgO nanoparticles at 0.2 g/L. ....	104
<b>Figure 4.17</b> Electrostatic charging tendency of (a) FR3, (b) FR3 with 0.3 g/L C <sub>60</sub> , and (c) FR3 with 0.4 g/L C <sub>60</sub> .....	105
<b>Figure 4.18</b> Electrostatic charging tendency of pure FR3 and different nanofluids .....	106
<b>Figure 4.19</b> Creeping discharge image at the surface of solid insulator immersed in different liquids.....	108
<b>Figure 4.20</b> Final length $L_f$ of creeping discharge vs the applied voltage of (a) SE/Fe <sub>3</sub> O <sub>4</sub> , (b) SE/Al <sub>2</sub> O <sub>3</sub> , and (c) SE/C <sub>60</sub> .....	109
<b>Figure 4.21</b> Creeping discharge image at the surface of solid insulator immersed in different liquids.....	111
<b>Figure 4.22</b> Final length $L_f$ of creeping discharge vs the applied voltage of (a) FR3/Fe <sub>3</sub> O <sub>4</sub> , (b) FR3/Al <sub>2</sub> O <sub>3</sub> , and (c) FR3/C <sub>60</sub> .....	112

## TABLES LIST

<b>Table 1.1</b> Summary of different stability measuring techniques .....	10
<b>Table 2.1</b> Physicochemical Properties of Metal-Oxides and Carbonic-based NPs.....	29
<b>Table 2.2</b> Physicochemical Properties of Synthetic Ester, Midel 7131.....	30
<b>Table 2.3</b> Physicochemical Properties of Natural Ester, FR3. ....	31
<b>Table 2.4</b> Physicochemical Properties of Mineral Oil, Nydro 4000X. ....	32
<b>Table 3.1</b> AD goodness-of-fit test results of conducting NPs based NFs. ....	48
<b>Table 3.2</b> Scale and shape parameters of conducting NP-based NFs.....	49
<b>Table 3.3</b> AC BDV of Fe <sub>3</sub> O <sub>4</sub> nanofluids for different probability levels. ....	53
<b>Table 3.4</b> AC BDV of C <sub>60</sub> nanofluids for different probability levels.....	54
<b>Table 3.5</b> AC BDV of Gr nanofluids for different probability levels.....	55
<b>Table 3.6</b> Table AD goodness-of-fit test results of semi-conducting NPs-based NFs.....	57
<b>Table 3.7</b> Scale and shape parameters of semi-conducting NP-based NFs.....	57
<b>Table 3.8</b> The AC BDV of ZnO nanofluids for different probability levels. ....	59
<b>Table 3.9</b> Table AD goodness-of-fit test results of insulating NPs based NFs.....	66
<b>Table 3.10</b> Scale and shape parameters of insulating NPs-based NFs. ....	67
<b>Table 3.11</b> The AC BDV of Al <sub>2</sub> O <sub>3</sub> (20-30 nm) nanofluids for different probability levels.	72
<b>Table 3.12</b> The AC BDV of Al <sub>2</sub> O <sub>3</sub> (50 nm) nanofluids for different probability levels.....	73
<b>Table 3.13</b> The AC BDV of ZrO <sub>2</sub> nanofluids for different probability levels.....	74
<b>Table 3.14</b> The AC BDV of SiO <sub>2</sub> nanofluids for different probability levels. ....	75
<b>Table 3.15</b> Electrical properties of base liquids and conducting, semi-conducting, and dielectric NP. ....	78
<b>Table 3.16</b> Relaxation time of different nanofluids.....	78

<b>Table 4.1</b> Inception voltage, standard deviation, and enhancement percentage of synthetic and natural esters nanofluids Fe <sub>3</sub> O <sub>4</sub> .....	85
<b>Table 4.2</b> Q <sub>peak</sub> , Q <sub>avg</sub> , and NPDs/s, Standard deviation, and increment percentage of synthetic and natural esters nanofluids with Fe <sub>3</sub> O <sub>4</sub> .....	86
<b>Table 4.3</b> PD Activity of synthetic ester and synthetic ester-based nanofluids with 0.4 g/L C <sub>60</sub> .....	88
<b>Table 4.4</b> Inception voltage, standard deviation, and enhancement percentage of natural ester and C <sub>60</sub> nanofluids. ....	90
<b>Table 4.5</b> Q <sub>avg</sub> , Q <sub>peak</sub> , NPDs/s, standard deviation, and increment percentage of natural ester and C <sub>60</sub> nanofluids. ....	90
<b>Table 4.6</b> PD Activity of synthetic ester and synthetic ester-based nanofluids with 0.3 g/L Gr. ....	92
<b>Table 4.7</b> Inception voltage, standard deviation, and enhancement percentage of synthetic and natural esters nanofluids Al <sub>2</sub> O <sub>3</sub> (20-30 nm). ....	94
<b>Table 4.8</b> Q <sub>peak</sub> , Q <sub>avg</sub> , and NPDs/s, standard deviation, and increment percentage of synthetic and natural esters nanofluids with Al <sub>2</sub> O <sub>3</sub> . ....	94
<b>Table 4.9</b> Q <sub>avg</sub> , Q <sub>peak</sub> , and NPDs/s, standard deviation, and increment percentage of NE and NE-based NFs with MgO at 0.2 g/L .....	102

## ABBREVIATIONS LIST

<b>AC</b>	Alternating Current
<b>AD</b>	Anderson-Darling
<b>Al<sub>2</sub>O<sub>3</sub></b>	Aluminum (II) Oxide
<b>BDV</b>	Breakdown Voltage
<b>BTA</b>	Benzotriazoles
<b>CDF</b>	Cumulative Distribution Function
<b>CQD</b>	Carbon Quantum Dots
<b>C<sub>60</sub></b>	Fullerene
<b>DLS</b>	Dynamic Light Scattering
<b>ECT</b>	Electrostatic Charging Tendency
<b>EDL</b>	Electrical Double Layer
<b>EM</b>	Electron Microscopy
<b>FE</b>	Finite Element
<b>Fe<sub>3</sub>O<sub>4</sub></b>	Iron (III) Oxide
<b>FR3</b>	Natural Ester (Cargill)
<b>GTLTO</b>	Gas-to-Liquid Transformer Oil
<b>Gr</b>	Graphene
<b>IEC</b>	International Electrotechnical Commission
<b>MO</b>	Mineral Oil
<b>MgO</b>	Magnesium Oxide
<b>NE</b>	Natural Ester
<b>NF</b>	Nanofluid
<b>NP</b>	Nanoparticle
<b>PD</b>	Partial Discharge
<b>PDIV</b>	Partial Discharge Inception Voltage
<b>PDF</b>	Probability Density Function
<b>PMT</b>	Photomultiplier Tube
<b>RMS</b>	Root Mean Square
<b>SE</b>	Synthetic Ester
<b>SEM</b>	Scanning Electron Microscopy
<b>SiC</b>	Silicon Carbide

<b>SiO<sub>2</sub></b>	Silicon Dioxide
<b>TEM</b>	Transmission Electron Microscopy
<b>TiO<sub>2</sub></b>	Titanium Dioxide
<b>UV</b>	Ultraviolet
<b>ZrO<sub>2</sub></b>	Zirconium Dioxide
<b>ZnO</b>	Zinc Oxide

## **GENERAL INTRODUCTION**

The search for advanced and efficient dielectric materials has gained considerable momentum due to the growing need for reliable electrical insulation in modern power systems and high-voltage applications. Nanofluids (NFs), which consist of nanoparticles (NPs) dispersed in traditional dielectric liquids, have emerged as a promising solution to enhance the performance of insulating materials. By incorporating NPs such as metal oxides (e.g.,  $\text{Al}_2\text{O}_3$ ,  $\text{Fe}_3\text{O}_4$ ) and carbon-based nanomaterials (e.g., fullerene, graphene), NFs have shown the potential to improve various dielectric properties, including breakdown voltage, partial discharge resistance, electrostatic charging tendency, and surface discharge.

This work explores developing, preparing, and characterizing NFs based on different base liquids-synthetic esters, natural esters, and mineral oils, commonly used in transformer insulation. The research delves into the history and evolution of NFs, preparation methods (such as one-step and two-step techniques), stabilization mechanisms, and factors influencing their performance, such as NP type, size, concentration, and surface modification. The study reviews the theoretical foundations and experimental findings related to the impact of NPs on electrical properties, emphasizing understanding the mechanisms that lead to enhanced dielectric strength, suppression of partial discharges, and reduction in electrostatic charging phenomena.

This research aims to identify optimal combinations of NPs and base fluids that yield significant improvements in insulation properties, opening up opportunities for their use in industrial settings. The subsequent chapters focus on experimental setups and methodologies, the effects of NPs on dielectric properties, and detailed statistical analyses to validate the findings.

The manuscript consists of four chapters. The first chapter summarizes the state of the art and knowledge of nanofluids (NFs) and their applications in electrical insulation. The different methods for fabricating stable NFs, the effect of nanoparticles on the breakdown voltage (BDV) of base liquids, the mechanisms involved in their improvement or deterioration of BDV, and the statistical methods for analyzing the experimental results are discussed. It also addresses the effects of NPs on the electrostatic charging tendency (ECT) of fluids and partial discharge (PDs) activity. The electrical double-layer models, fractal analysis-based models of discharges in electrical media, and the health effects of nanoparticles are also presented.

The second chapter presents the different types of nanoparticles and the basic liquids/oils used to prepare the nanofluids (NFs) to be investigated, the methods for preparing these NFs as well as the different experimental setups used to explore more particularly the dielectric strength of these NFs, their electrostatic charging tendency (ECT), the partial discharges initiation threshold voltage as well as the development of discharges propagating at NFs/solid interfaces.

The insulating liquids used as base fluids are synthetic ester (SE), natural ester (NE), and mineral oil (MO). The incorporated nanoparticles (NPs) are conducting ( $\text{Fe}_3\text{O}_4$ ,  $\text{C}_{60}$ , Gr), semi-conducting (ZnO and CuO), and insulating ( $\text{Al}_2\text{O}_3$ ,  $\text{ZrO}_2$ ,  $\text{SiO}_2$ , and MgO) NPs.

The physicochemical and the shape of the investigated nanoparticles (NPs) are described. The role of surfactants in ensuring the stability of NFs is also discussed; the surfactants play a crucial role in preventing the aggregation of NPs and maintaining their dispersion in dielectric liquids. The preparation methods of NFs, including the one-step and two-step techniques, are developed. The emphasis is placed on the practical considerations that influence the choice of NFs preparation method. This is of great interest to researchers and engineers, especially in evaluating the stability and dispersion maintenance of NPs in nonpolar liquids, which is essential for their practical application in power systems.

The experimental setups and methodologies used to evaluate the performance of NFs for insulation in electrical components and systems are described in detail; these investigations being crucial for understanding the behavior of NFs under electrical stress for optimizing their properties for industrial use.

In Chapter 3, we present the experimental results of measuring the AC breakdown voltage (AC BDV) of the nanofluids (NF) we prepared. The experimental data are then analyzed using statistical tools such as the Anderson-Darling goodness-of-fit test and Weibull probability analysis, and the voltages corresponding to 1%, 10%, and 50% risk levels were determined.

Chapter 4 explores the effects of the different types of NPs on partial discharges (PDs) activity, electrostatic charging tendency (ECT), and surface discharges behavior in various insulating fluids under high-voltage conditions. The objective is to highlight the potential advantages and limitations of using NFs in electrical insulation systems. Specifically, we investigate how nanoparticles can affect the inception and magnitude of

partial discharges, potentially by improving or deteriorating the insulation performance depending on their type and concentration. By improving the breakdown voltage or reducing the severity of discharges, nanoparticles can enhance the longevity and reliability of electrical equipment.

The effect of NPs on ECT must be investigated before introducing NFs in high-voltage equipment. Indeed, the accumulation of charge due to the motion of insulating fluids can lead to equipment failure if not properly managed. NPs may influence this tendency by altering charge mobility and dispersion within the liquid, thus reducing or increasing the buildup of static charges.

NPs also influence surface discharges, which occur along the interface of solid and liquid insulation. These discharges can degrade insulation materials over time, and NPs may help suppress or exacerbate this process by modifying the fluids' surface properties and dielectric behavior.

## **CHAPTER 1**

### **STATE OF THE ART**

## 1.1. Introduction

The quest for more efficient and advanced dielectric materials has grown over the years, driven by the ever-expanding applications of electrical devices in modern society. Recently, nanofluids (NFs) have emerged as a promising dielectric material class, combining traditional liquid dielectrics' advantages with remarkable improvements that offer the NPs.

This chapter presents a synthetic review of NFs for dielectric insulation applications. It discusses the different methods for fabricating stable NFs, the impact of nanoparticles on the breakdown voltage (BDV) of NFs, the mechanisms involved in their improvement or deterioration, and the statistical methods for analyzing the experimental results. It also addresses the effects of NPs on the electrostatic charging tendency (ECT) of fluids and partial discharge activity.

The electrical double-layer models, fractal analysis-based models of discharges in electrical media, and the health effects of nanoparticle use are also presented.

### 1.2.1 History of nanofluids

NFs are a relatively recent development in molecular liquids science and engineering [1]. The history of NFs dates back to the early 1990s when researchers began exploring the concept of dispersing NPs in a base liquid to improve its thermal properties. Here is a brief overview of the history of NFs.

1. The concept of NFs was first proposed by Choi and Eastman in 1995 [1]. They defined NFs as colloidal suspensions of NPs in a base liquid, where the particle size generally ranges in size from 1 to 100 nm. Their initial focus was on using NFs to improve the heat transfer characteristics of conventional heat transfer fluids. Their work underlines the tremendous ability of NPs to significantly increase the thermal conductivity of base liquids. Since then, a great deal of research has been carried out in various fields, including materials science, engineering, chemistry, and physics, to study NFs' properties and potential applications.
2. A huge milestone was reached at the end of the 1990s when researchers began to conduct experimental studies on improving the thermal conductivity offered by adding NPs. Stephen U.S. Choi led the first significant laboratory to work on NFs [2], [3], [4].

3. In the early 2000s, researchers started developing theoretical and numerical models to understand better the mechanisms responsible for the enhanced thermal conductivity of NFs. Theoretical models, such as the practical medium theory [5] and the Hamilton-Crosser model [6], were proposed to predict the thermal conductivity of NFs based on the properties of NPs and base liquids. The Hamilton-Crosser model has been extended and applied to all types of NPs, not just spherical ones [7], [8].
4. Challenges and Optimization (2000s - Present): Despite the potential benefits of NFs, challenges have been faced, such as NPs sedimentation, aggregation, and instability. Researchers have been working on optimizing the stability and dispersion of NFs and investigating the effects of NPs concentration, size, and shape on their properties.

### **1.2.2 Preparation of nanofluids**

The process of creating NFs involves integrating NPs into a base liquid through either a one-step direct synthesis approach or a two-step method of NPs dispersion.

#### **❖ One-step method**

The one-step method is a process for preparing NPs directly in their base liquid without the need for multiple intermediate steps such as particle drying, storage, and NPs dispersion [9], [10]. This synthesis procedure enables NPs to be synthesized and dispersed simultaneously in the base liquid, resulting in more stable NPs than the two-step method. This methodology minimizes the risk of particle agglomeration during the drying process.

Some of the key advantages of this method include:

- 1) Simultaneous synthesis of NPs and dispersion in a base liquid eliminates the need for separate storage, drying, and transportation steps that could lead to particle aggregation
- 2) The ability to prepare stable NFs without requiring additional stabilizers.
- 3) Greater control over NPs size and shape during the synthesis process.
- 4) A more stable NFs compared to the two-step method.

However, the one-step method cannot produce large quantities of NFs, and it is challenging to evenly expand their applicability with small volumes. The two-step method is still useful for applications that require large volumes.

❖ *Two-step method*

The second method proposes a two-step technique to prepare NFs. In the first processing step, NPs, nanofibers, or nanotubes are produced as a dry powder by suitable techniques [9], [11]. Then, the nanosized powder is dispersed in the fluid. This stepwise method isolates the synthesis of NPs from the preparation of NFs [9]. As a result, aggregation could occur in both steps, especially during NP drying, storing, and transporting. This method is problematic as aggregation leads to the fall of clusters under gravity, decreases thermal conductivity, and affects the dielectric properties. To address this issue, techniques such as ultrasonic agitation (treatment) and adding surfactants to the base liquid are often used to minimize particle aggregation and improve dispersion behavior.

Some of the key advantages of this method include:

- 1) The two-step method provides greater control of the NPs concentration in the NFs, as the NPs are pre-weighed before being dispersed in the base liquid.
- 2) This method can be used with a wide range of NPs and base liquids, making it a polyvalent technique for preparing NFs.
- 3) This method is easily scalable, making it suitable for large-scale production of NFs.

However, the two-step method is less stable, and producing NFs with the same stability as the one-step method is quite challenging.

#### **1.2.3 Stability of NFs**

The stability of an NF refers to its ability to maintain a uniform and homogeneous distribution of solid particles (or colloids) within a liquid medium over an extended period without undergoing significant settling or agglomeration [12], [13], [14], [15], [16], [17]. In other words, a stable suspension ensures that the dispersed NPs remain evenly distributed throughout the base liquid without phase separation, sedimentation, or flocculation. Stability is a critical factor facing the widespread NFs in various industries and applications, directly influencing their performances and characteristics. The stability of NFs is essential to maintain their enhanced properties, such as improved thermal and dielectric performances.

#### *1.2.3.1 Stabilization mechanisms of nanofluids*

Stabilizing NFs is fundamental/vital to prevent particle agglomeration and ensure NFs stability and uniform dispersion in the base fluid. In general, two types of stabilization mechanisms, namely electrostatic stabilization and steric stabilization, have been reported to increase the repulsive interaction among NPs. Electrostatic stabilization relies on the surface charge of NPs to create repulsive forces among NPs [13], [18]. Electrostatic repulsion can be achieved by modifying the surface charge through a suitable functionalization technique or pH adjustment [13], [18], [19], [20]. This process prevents particles from getting too close to each other and forming clumps. Common methods include surface modification with charged polymers or surfactants, pH adjustment, or using electrolytes to manipulate the ionic strength of the NFs. This stabilization technique is particularly effective for charged or polar NPs suspended in a polar medium. Meanwhile, steric stabilization is based on the steric hindrance effect caused by polymers or molecules adsorbed on the NP's surface. These adsorbed molecules create a protective layer that prevents close contact between NPs [13], [17], [19], [20]. The steric repulsion arising from the polymer chains or large molecules helps maintain the NFs dispersion stability [18], [19].

However, combining these two stabilization mechanisms to achieve the dispersion of NPs is possible. This combination is termed electro-steric stabilization [13]. In this scenario, polymer chains are affixed to the surfaces of charged particles, or polyelectrolyte chains are attached to the surfaces of uncharged particles. When two particles with modified surfaces approach each other, electrostatic and steric stabilization mechanisms work together to prevent agglomeration.

#### *1.2.3.2 How to Enhance the Stability of Nanofluids*

There are various methods to improve the stability of NFs against aggregation and settling of NPs. Using surfactants or dispersants can impart repulsive forces between particles through electrostatic or steric effects[14], [21]. Modifying the NPs surface directly via functionalization changes surface chemistry to make the particles more compatible with the base fluid and easily dispersible [15]. Adjusting properties like pH and ionic strength alters the zeta potential and stabilizes particles through electrostatic repulsion [1]. Other techniques include ultra-sonication to break up aggregates, adding agents that affect the viscosity and may slow settling, and optimizing NPs characteristics and concentration for stability [22]. Considering NPs/base liquid interactions and

controlling the forces is key for producing stable NFs, which can be achieved by combining steric and electrostatic stabilization, which is the most effective way to create stable NFs with well-dispersed NPs.

#### 1.2.3.3 Technics to Evaluate the Stability of Nanofluids

Therefore, the stability evaluation techniques of NFs have become an essential aspect of their application. Several methods have been developed to evaluate the stability of NFs, including sedimentation, zeta potential measurement, dynamic light scattering, and rheological studies. These techniques assess particle behavior in the base fluid and can provide important information for optimizing NF applications. Table 1.1 shows the various methods for evaluating the stability of NFs and their limitations.

**Table 1.1** Summary of different stability measuring techniques

Tech.	Description	Limitations
Zeta potential ( $\xi$ -potential)	$\xi$ -potential is the electric charge that develops at the interface between an NPs or surface and a liquid, affecting (reflecting) particle stability and interactions among them [15], [18], [19], [23], [24], [25], [26]. The absolute value of $\xi$ -potential varying between 30 and 60 mV indicates good stability, and above 60 mV shows excellent stability.	This technique requires dilute samples for performing the tests [27], and it does not provide any information about attractive forces, which indicates that there may be a possibility of instability of NFs with an instability limit of $\xi$ -potential [28].
Dynamic Light Scattering (DLS)	DLS is a technique used to determine the size distribution of particles in a solution based on the way they scatter light. It measures the Brownian motion of particles in a solution and calculates their size and size distribution based on the motion of the particles [15], [18], [19], [26]. It is commonly used in the characterization of nanomaterials and biomolecules in solution.	As for $\xi$ -potential, a dilute sample is required [27]. Another limitation is that DLS assumes that particles are spherical [26], [27] and may not accurately measure particles with complex shapes or particles that are not perfectly spherical. In addition, DLS measures the hydrodynamic diameter of particles, which is different from their physical diameter.

UV	In the UV (ultraviolet) visual spectroscopy method, the amount of light absorbed by the NFs indicates the concentration of NPs [29].	This does not apply to highly concentrated and dark-colored NFs. Additionally, it is also time-consuming.
Centrifugation	Centrifugation measures particle sedimentation rate to evaluate NF stability. Faster sedimentation indicates poor stability, while slower sedimentation suggests better stability [30].	It does not provide information on the aggregation state of particles or the stability of the dispersion under specific environmental conditions.
Electron Microscopy (EM) Methods	EM methods include Transmission Electron Microscopy (TEM), which visualizes thin samples in high resolution using electrons, and Scanning Electron Microscopy (SEM), which provides detailed 3D surface imaging [31], [32], [33], [34]. These techniques are essential for studying nanoscale structures in various fields, such as materials science, biology, and nanotechnology.	Despite these advantages, sample preparation can be complex, often requiring ultra-thin sections. Using electron microscopy methods in research may not be feasible due to their high cost and limited budgets.

## 1.2. On the impact of NPs on dielectrics performances of base liquids

NFs have attracted great attention in various fields due to their exceptional thermal and electrical properties. In electrical insulation, NFs have emerged as a promising frontier. This review examines the main studies on the influence of NPs (conducting, semi-conducting, and insulating) on the breakdown strength, partial discharges, and electrostatic charging tendency of transformer oils (mineral oil and synthetic and natural esters). These studies highlight the expected dielectric performances related to the use of NPs, offering insight into potential applications in electrical systems where improved insulation is paramount.

### 1.3.1 Breakdown phenomena in nanofluids

The breakdown voltage (BDV) of transformer oils must be measured to ensure electrical insulation capabilities. BDV measurement of oil under AC, DC, and impulse

voltage to analyze their behavior. The AC breakdown voltage measurements of the NFs need to be accomplished according to international standards, like IEC or ASTM standards. In the following, we present the state of knowledge on the BDVs of NFs depending on their nature, size, concentration, and type of base fluid/liquid.

#### *1.3.1.1 AC and impulse breakdown voltages*

Segal et al. [35] were the first to discover the promising applications of NPs as insulating liquids. They experimentally investigated the AC and impulse BDVs of NFs-based transformer oil and magnetite NPs. They found that the AC BDV was close to that of the base liquid, but the positive impulse BDV increased by up to 50% compared to the base liquid. The impulse BDV for both needle polarities is nearly equal in the case of NFs, unlike base liquid, where the BDV in negative polarity is much higher. The results show a slower propagation of positive streamer in NFs, which explains the improved impulse breakdown performance. Accelerated aging experiments indicate good long-term stability of the colloidal insulating fluid.

Hwang et al. [36] studied the effect of conductive NPs on positive streamer propagation in transformer oil-based NFs through analytical charging dynamics expressions and an electrodynamic model (Chapter 3 provides more details of their model). The results indicate that conductive NPs such as magnetite rapidly charge, trap electrons, and convert them into slow negative particles. This suppresses the electric field wave-driving streamers, reducing the streamer velocity by ~36% compared to base liquid. The NP charging dynamics explain the experimentally observed improvement of BDV of NFs, since slower streamers require more time to cause breakdown at a given voltage. Even insulating NPs alter the electrodynamics and slow streamers by reducing the conductivity in the streamer tail.

Sima et al. [37] investigated the effect of conducting, semi-conducting, and dielectric NPs on the insulation performance of transformer oil through experiments and modeling. Tests showed NPs increased the positive impulse BDV of base liquid; conducting Fe<sub>3</sub>O<sub>4</sub> NPs having the largest effect. The NPs were found to trap electrons through potential wells formed by induced (conducting NPs) or polarized (insulating NPs) surface charges, slowing streamer propagation. Modeling of positive streamers in NFs showed that they reduce streamer velocity and radius compared to base liquid. The higher the NPs conductivity or permittivity relative to the base liquid, the greater the electron trapping effect. Overall, adding NPs to transformer oil, especially the conductive

ones like  $\text{Fe}_3\text{O}_4$ , can significantly improve the dielectric strength by suppressing streamer development through electron trapping mechanism.

Peppas et al. [38] statistically investigated and compared the AC BDVs of mineral oil, natural ester FR3, and their corresponding NFs with  $\text{Fe}_3\text{O}_4$  NPs, using different electrode configurations. Various statistical distributions, including Normal, Weibull, Gumbel, and Generalized Extreme Value, are subjected to goodness-of-fit tests. These tests evaluate how well these distributions fit the data being analyzed. In most cases, the experimental data followed the generalized extreme value distribution better than others. Results showed that NFs exhibited increased BDVs compared to the mineral and natural esters oils.

Ibrahim et al. [39] presented theoretical and experimental studies to understand the role of NPs in improving the dielectric strength of transformer oil. They discussed already published breakdown mechanisms and proposed a new mechanism based on particle charging. Experiments validate that NPs can hold positive or negative charges when exposed to an electric field, depending on their material and characteristics. Adding positively and negatively charged particles further increased the BDV compared to only one charge type. Overall, the results prove the efficacy of the proposed theoretical charging and breakdown mechanisms for NFs.

Khaled et Beroual [40] studied the influence of conductive  $\text{Fe}_3\text{O}_4$  and insulating  $\text{Al}_2\text{O}_3$  and  $\text{SiO}_2$  NPs on the AC dielectric strength of synthetic ester Midel 7131. Normal and Weibull distributions are used to statistically analyze the AC BDVs at 1, 10, and 50% risk level probabilities. Results show that the AC BDVs data for most NFs obey to both distributions. Adding NPs improves the dielectric strength, but the enhancement depends on the concentration, size, and nature of the NPs. An optimal concentration exists for maximum dielectric strength improvement. Adding magnetic  $\text{Fe}_3\text{O}_4$  NPs provides the best enhancement of 48% compared to base liquid, against 32% for  $\text{SiO}_2$  NPs and 25-35% for  $\text{Al}_2\text{O}_3$  NPs.

Here is a summary of the three proposed mechanisms explaining how NPs can improve the dielectric strength of liquids:

❖ *Electron Scavenging Hypothesis [36]:*

- ⊕ NPs quickly polarize and "scavenge" free electrons in the liquid when an electric field is applied. This leaves behind positive ions and negatively charged NPs.

- ⊕ The negatively charged NPs reduce the electric field buildup from the positive ions, hindering further liquid ionization.
- ⊕ If the NPs relaxation time is much faster than the streamer development time, this electron scavenging effect can suppress streamer initiation.
- ❖ *Hydrophilicity Hypothesis [41]:*
  - ⊕ Hydrophilic NPs adsorb water molecules in the insulating liquid onto their surface.
  - ⊕ This reduces the harmful effect of moisture content on the dielectric strength of the liquid.
  - ⊕ Experimental evidence indicates that hydrophilic SiO<sub>2</sub> NPs increase the dielectric strength of oil, while hydrophobic-coated SiO<sub>2</sub> NPs decrease it.

In the study conducted by Jin et al. [41], the NFs-based mineral oil with SiO<sub>2</sub> NPs with and without coating were compared (hydrophobic/hydrophilic). As a result, any differences observed in the measured dielectric strengths could be solely attributed to the hydrophilicity of the SiO<sub>2</sub> NPs. The findings revealed that SiO<sub>2</sub> NPs without coating effectively increased the dielectric strength of the host liquid. On the other hand, coated SiO<sub>2</sub> NPs decreased the dielectric strength of NFs compared to base liquid. This led to the postulation that the improvement in dielectric strength resulted from water adsorption occurring at the surface of the NPs.

- ❖ *Shallow Trap Hypothesis [37]:*
  - ⊕ NPs introduce additional shallow traps for electrons in the liquid.
  - ⊕ This reduces electron mobility and velocity in the liquid.
  - ⊕ Slower electron motion inhibits the development of streamers, which require fast electron motion ahead of the streamer head.
  - ⊕ Liquids with higher shallow trap density were found to have improved dielectric strength.

#### *1.3.1.2 DC breakdown voltage*

Although many studies have addressed the effect of NPs on the AC BDV of transformer oil, the DC BDV is even less investigated; two principal studies are reviewed here. The first one was conducted by Kopčanský et al. [32] in which they investigated the DC BDV of transformer oil-based NFs with magnetite NPs with different concentrations of magnetite nanoparticles. The results show that magnetic NPs can either improve or

degrade the DC BDV compared to the base liquid, depending on the NPs concentration. At low concentrations below 0.01 volume fraction, aggregation of the NPs is minimal, and the fluids have higher dielectric strength than the base liquid. However, at higher concentrations, above 0.01 volume fraction, extensive aggregation occurs and decreases the performances of NFs under DC breakdown. The aggregation effects are most significant when the external magnetic field is parallel to the electric field. The second one was done by Khaled et Beroual [42], in which they addressed the effect of adding different NPs ( $\text{Fe}_3\text{O}_4$ ,  $\text{Al}_2\text{O}_3$ , and  $\text{SiO}_2$ ) for different concentrations on the DC BDV of natural ester MIDEDEL 1204. The results show that small amounts of conducting  $\text{Fe}_3\text{O}_4$  and insulating  $\text{Al}_2\text{O}_3$  NPs can improve the DC BDV, with the best enhancement of around 10% obtained with 0.2 g/L of  $\text{Fe}_3\text{O}_4$  NPs. However,  $\text{SiO}_2$  NPs decreased the DC-BDV at all concentrations tested. They state that the DC BDV improvements with those NPs were slightly higher than previously reported results using AC voltage with the same base liquid [43]. These authors conclude that adding  $\text{Fe}_3\text{O}_4$  or  $\text{Al}_2\text{O}_3$  NPs at optimal concentrations between 0.1 g/L and 0.5 g/L can enhance the DC insulating performance of natural ester. However,  $\text{SiO}_2$  NPs decrease the DC BDV.

### **1.3.2 PDs in nanofluids**

Besides the investigations and possible mechanisms widely considered AC breakdown voltage, partial discharge (PDs) still needs to be studied. PDs occur in electrical systems when localized discharges/breakdowns happen within the insulation material. These discharges can lead to insulation degradation and complete system failure in the worst cases. When NFs are utilized as insulating materials in electrical systems, the study of PDs becomes essential due to their potential impact on the performance and reliability of the system. In this context, Herchl et al. [44] focused on the PDs behavior of NFs composed of magnetite NPs dispersed in transformer oil. They observed that the PDs current impulses were lowest at an NPs volume concentration of 0.0024 across different electrode gaps. This suggests there is an optimal concentration that minimizes PDs in the magnetic fluid. The results demonstrate that NPs concentration has a significant effect on the PDs. At higher concentrations of 0.019-0.032, the permittivity and loss factor increased substantially with the electric field, indicating that NPs aggregation effects occur. However, the PD activity was minimized at the optimal concentration of 0.0024, likely due to sufficient NP separation to prevent extensive clustering. The work reveals the complex relationship between NPs concentration, electric field, and the resulting PDs behavior in transformer oil-based magnetic NFs.

Jin et al. [45] investigated the PDs behavior of mineral oil-based NFs with silica and fullerene NPs using a time-resolved detection setup to measure parameters like inception voltage, discharge magnitude, and pulse characteristics. Under positive DC voltage, the NFs showed increased inception voltages and reduced total discharge magnitudes compared to mineral oil, along with fewer PD pulses per sequence. The voltage amplitude was lower with silica versus fullerene. However, there was no significant difference in PD behavior over mineral oil under negative DC voltage. The improved positive DC PD behavior is hypothesized to be from the NPs surfaces adsorbing impurities like moisture and acid in the oil, reducing their negative effects. Fourier transform infrared spectroscopy provided evidence that acid may react with the NPs. The results of this analysis are likely due to the NPs interacting with contaminants in the mineral oil.

Chandrasekar et al. [46] investigated the PDs characteristics of corn oil NFs with  $\text{SiO}_2$  and  $\text{TiO}_2$  NPs untreated and treated with carbon quantum dots (CQD). PD inception voltage was measured using needle-plane and rod-plane electrodes to simulate different discharge types. The CQD-treated NFs, especially  $\text{SiO}_2$  at lower concentrations, showed higher PDIV and lower PD magnitude and repetition rate versus untreated NPs or base corn oil. CQD- $\text{SiO}_2$  performed the best in reducing PD activity through improved NPs dispersion and moisture absorption by the  $\text{SiO}_2$ . PD time transition revealed that pure corn oil had the fastest increase in PD with voltage due to faster charge dissipation, while CQD NFs suppressed PD propagation. In summary, small additions of CQD-treated  $\text{SiO}_2$  NPs significantly increased the PDIV. They reduced the PD magnitude and repetition rate in corn oil, with the combination of the CQD treatment and  $\text{SiO}_2$  properties to enhance the PD resistance.

Atiya et al. [47] addressed the PDs behavior and mechanisms in mineral oil-based NFs with  $\text{TiO}_2$  and  $\text{Al}_2\text{O}_3$  NPs. The NFs showed increased PD inception voltages compared to mineral oil.  $\text{Al}_2\text{O}_3$  NFs with a thicker electrical double layer performed better. The PD repetition rate and magnitude were lower in the NFs at the same applied voltage. The time transition of PD events showed an increasing trend for mineral oil but a decreasing trend for the NFs. The electrical double layer (EDL) of NPs is hypothesized to trap charges and limit the impact of residual charges between PD events, reducing the repetition rate over time. Overall, the NP EDL plays a key role in suppressing PD activity by capturing charge carriers and delaying the PD charge buildup in the oil.  $\text{Al}_2\text{O}_3$  NFs with a thicker EDL performed the best in mitigating PD. They are the first to propose an

explanation of the effect of EDL around the NPs on PD activity. Imani et al. [48] showed that PD tend to be initiated predominantly at the positive half-cycle by increasing the concentration of conductive NPs ( $\text{Fe}_3\text{O}_4$ ), unlike pure liquid, which mainly appears at the negative half-cycle. According to them, this alternation could be due to the electro-hydrodynamic behavior of  $\text{Fe}_3\text{O}_4$  NF and to the orientation of the magnetizable magnetic NPs under sinusoidal voltage.

Koutras et al. [49] investigated the effect of SiC NPs on the PDs inception voltage (PDIV) of natural ester oil FR3. Three NFs were prepared with SiC NPs concentrations of 0.002%, 0.004%, and 0.008% by weight. The PD inception voltage was measured for insulating paper impregnated with each NFs sample. The 0.004% NFs showed the highest PDIV enhancement of 55.5% compared to paper impregnated with the base oil. This improvement in PDs resistivity events was attributed to the SiC NPs acting as electron traps. However, increasing the concentration to 0.008% decreased the PDIV compared to base liquid, likely due to NPs aggregation, which reduces the trapping process. The 0.004% NFs sample also showed lower PDs magnitude and a more regular pulse shape versus the 0.008% sample. In summary, small additions of SiC NPs can increase the PDIV of natural ester oil, but there is an optimal concentration beyond which NPs aggregation negatively impacts the PDs resistance.

Kurimský et al. [50] studied PDs in two transformer oils - a naphthenic oil (NTO) and a gas-to-liquid oil (GTLTO) - and NFs made from them using iron oxide NPs. PDs were detected electrically and acoustically. Discharges started at a lower voltage in NTO but had higher acoustic emission in GTLTO, attributed to its lower viscosity and permittivity. Adding NPs suppressed discharges more in NTO, increasing the inception voltage from 35 kV to 55 kV. NPs were less effective in GTLTO, possibly because its lower viscosity enabled more nanoparticle migration and aggregation near the electrode, increasing local field strength. Overall, the base oil properties significantly affected PDs behavior and NPs suppression effects, with acoustic emission providing additional insights into electrical detection.

### ***1.3.3 Effect of nanoparticles on electrostatic charging tendency***

In this section, previous studies on how NPs impact the electrostatic charging tendency (ECT) of transformer oil are reviewed, uncovering key findings and insights in this area of research. The ECT phenomenon is the result of forced oil flow, generating heat that must be dissipated from the active part, leading to the appearance of electrostatic

charges at the solid-liquid interface [51]. Furthermore, studies have shown that ECT is responsible for generating partial discharges (PD) at the locations where the electrostatic charges are accumulated, especially on pressboards in transformers [52], [53]. Amplifying these PD generates large amounts of gas, the most important being hydrogen, acetylene, ethylene, and methane, leading to the transformer ignition or even an explosion; this major problem needs to be resolved. In recent years, adding NPs to transformer oils has shown potential in reducing the ECT [54], [55], [56], [57].

Aksamit and Zmarzly [54] investigated the use of fullerene NPs as an inhibitor to reduce the streaming electrification in insulating mineral oil. The authors prepared 20 NFs with C<sub>60</sub>, for concentrations ranging from 0 to 0.512 g/L. Using a wireless rotary electrometer, they quantified the electrification current at different rotation speeds. The results showed that adding 0.1 to 0.2 g/L of fullerene NPs resulted in a more than 90% reduction in electrification current compared with base liquid under various hydrodynamic conditions. In addition, the C<sub>60</sub> additive altered the electrification mechanism. The authors conclude that C<sub>60</sub> fullerene, at optimal concentrations, effectively suppresses flux electrification in mineral oil.

In another work, Aksamit et al. [55] conducted a comparative ECT analysis of mineral oil and NFs-based mineral oil with fullerene NPs. Accordingly, NFs with six concentrations were prepared (0.01 g/L, 0.02 g/L, 0.05 g/L, 0.1 g/L, 0.2 g/L, and 0.3 g/L). In addition, the aging effect was also considered by preparing three (with fullerene) different NFs-based on fresh and aged mineral oil; samples were oxidized at the temperature of 110 °C with a presence of copper inhibitor, the first one for 24 h, and the second one for 96 h, which give in total three different liquids set [55]. The measuring system of ECT used in their work was the spinning disk (similar to this used in [54]), whose diameter measures 120 mm; the disk's speed reached 150 rpm. Minimal flow electrification was achieved at an optimal concentration of 0.1 g/L. Depending on the aging period, the fullerene concentration, and the disk rotation speed, a 30% to 90% reduction rate of ECT was reported.

Amalanathan et al. [56] investigated the flow electrification of natural ester and natural ester doped with TiO<sub>2</sub> NPs of 5 nm. The tests were carried out in a rotating system of a 6 mm thick disk with diameters of 30 mm, 40 mm, and 50 mm, whose rotational speed ranged from 0 to 600 rpm. The disk was covered on both sides with a 0.5 mm or 1.5 mm thick pressboard; the liquid temperature ranged from 30 °C to 100 °C. A comparison of flow electrification of natural ester and NFs-based natural ester

with/without surfactant (cetyl trimethyl ammonium bromide, CTAB) and anti-static additive 1,2,3-benzotriazoles (BTA) was performed. The obtained results showed that the electrification current increases with the increase in the thickness of the pressboard, the disk diameter, and its rotational speed. The temperature of the liquid increases the electrification current as well. The NF-based natural ester with TiO<sub>2</sub> NPs (0.05 g/L) and CTAB surfactant (1 mg/L) showed a higher susceptibility to streaming electrification than the host liquid.

In a recent investigation, Zdanowski [57] studied the effect of fullerene NPs on the ECT of mineral oil and synthetic and natural esters. Five concentrations of fullerene NPs were addressed, ranging from 0.025 g/L to 0.35 g/L. He reported that the disk rotation speed significantly impacts the ECT of all liquids. Moreover, adding fullerene NPs to fresh mineral oil shows an increased electrification flow, while a reduction was observed in the case of aged mineral oil [26]. The ECT of NFs-based synthetic and natural esters also depends on the doping concentration of fullerene NPs; it was observed that the optimum concentration of fullerene NPs that manifests the lowest ECT is in the range from 0.1 g/L to 0.2 g/L.

### **1.3. Statistical Analysis**

The most commonly used methods used for statistical analysis of the breakdown voltage (BDVs) of dielectrics liquids are the normal and Weibull distribution laws [38], [43], [49], [58], [59], [60], [61], [62]; a detailed explanation of how the curve lines are plotted is presented in Chapter 2. The Anderson–Darling (AD) [63], [64], Shapiro–Wilk [65], and Kolmogorov–Smirnov [66], [67] goodness-of-fit tests can be used to check if experimental data follows a probabilistic distribution; the AD test is utilized as it applies to both probability laws. To compare two data sets and verify if they are statistically different, a *t*-test is used [68], which is called the Welch *t*-test [69].

#### **1.4.1 Normal distribution**

The normal probability distribution, or Gaussian distribution, is a fundamental statistical probability distribution. It is a statistical term describing a symmetrical curve resembling a bell. This graph illustrates that most data points are clustered around the mean, with some points located further away from the mean (on either side of the mean value). Two primary parameters determine the distribution: the mean ( $\mu$ ), the symmetry axis of the distribution, and the standard deviation ( $\sigma$ ), which measures how much the

data is spread out. The probability density function (*PDF*) of the normal distribution is given by:

$$PDF(x, \mu, \sigma) = \frac{1}{\sigma\sqrt{2\pi}} \times e^{-\left(\frac{x-\mu}{\sqrt{2\sigma^2}}\right)^2} \quad (1.1)$$

#### 1.4.2 Weibull distribution (Appendix material)

The Weibull distribution is named after Waloddi Weibull, who first described it in the 1950s. The Weibull distribution is a commonly used statistical model in survival analysis. It estimates the time until a system fails or the lifetime of individuals in a population. It is also helpful in engineering, economics, and environmental sciences, where accurate modeling of time-to-event data is essential for informed decision-making. In most cases, the statistical analysis of random parameters outcomes (AC BDV or partial discharges, ...etc.) is done using the Weibull distribution, which allows the evaluation of those parameters at different risk levels.

The probability density function (*PDF*) of the Weibull distribution is given by:

$$PDF(x, \alpha, \beta) = \frac{\beta}{\alpha} \times \left(\frac{x}{\alpha}\right)^{\beta-1} \times e^{-\left(\frac{x}{\alpha}\right)^\beta} \quad (1.2)$$

Where:

- $x$ : The random variable.
- $\alpha$ : The scale parameter determines the distribution's location. It's a positive actual number.
- $\beta$ : The shape parameter which determines the shape of the distribution. Also known as the Weibull slope.

The cumulative distribution function (*CDF*) of the Weibull distribution is the integral of its *PDF* (equation (1)):

$$CDF(x) = 1 - e^{-\left(\frac{x}{\alpha}\right)^\beta} \quad (1.3)$$

#### 1.4.3 Goodness-of-fit tests (Anderson–Darling Fitting Test)

Before conducting a detailed statistical analysis, one or more tests must often be performed to determine whether the sample appears to be drawn from a specific

probability distribution, such as the Normal or Weibull distribution. This step is mandatory for tests that require fitting verification, such as the *t*-test, which involves the normality of the data samples [68]. The Anderson-Darling (AD) fitting test [63], [64] will be conducted as a preferred choice among the many available tests. The AD goodness-of-fit test does not require any assumptions that need the estimation of parameters. Therefore, there is no need for prior verification to perform this test. The formula giving the AD statistic is shown below [63], [64], [70]

$$AD^2(x) = -n - \sum_{i=1}^n \frac{2i-1}{n} \times [\ln(CDF(x_i)) + \ln(1-CDF(x_{n+1-i}))] \quad (1.4)$$

where,  $\{x_1 < \dots < x_n\}$  are the ordered  $x$  random variable points;  $i$  and  $n$  are the number of data points in the sample and  $i^{\text{th}}$  sample, respectively.

The next step consists of calculating the corresponding *p*-value using the *AD* statistic [64]

$$p\text{-value} = \begin{cases} e^{(1.294-5.709\times AD+0.019\times AD^2)} & AD \geq 0.60 \\ e^{(0.918-4.279\times AD-1.380\times AD^2)} & 0.34 < AD < 0.60 \\ 1 - e^{(-8.318+42.796\times AD-59.938\times AD^2)} & 0.20 < AD \leq 0.34 \\ 1 - e^{(-13.436+101.140\times AD-223.730\times AD^2)} & AD \leq 0.20 \end{cases} \quad (1.5)$$

Then, the *p*-value is calculated for the data set and compared to the 0.05 significance level. If the *p*-value is less than or equal to the chosen significance level, reject the null hypothesis that the data follows the distribution being tested; it needs to be rejected; otherwise, the null hypothesis that the data follows the distribution can be accepted.

#### 1.4.4 Two-Sample *t*-Test

The *t*-test is a statistical method frequently used to compare the means of two independent samples. The hypothesis tested usually determines whether the difference between the two means equals a certain value, known as  $d$ . Often, the hypothesis is that the two means are equal, which means  $d = 0$ . Given two sets of data (BDVs, for example, of base liquid and NF sample), the Welch *t*-test is conducted according to the following steps:

- The calculation of the *t*-value (two-sample *t*-test, called the Welch *t*-test) is given by the formula below [68]:

$$t = \frac{\bar{x}_1 - \bar{x}_2 - \Delta}{\sqrt{\frac{s_1^2}{n_1} + \frac{s_2^2}{n_2}}} \quad (1.6)$$

where  $\bar{x}_1$  and  $\bar{x}_2$  are the mean values of sets 1 and 2, respectively,  $\Delta$  is the hypothesized difference (0 for equal and 1 for unequal means),  $s_1$  and  $s_2$  are the standard deviations of sets 1 and 2, respectively, and  $n_1$  and  $n_2$  are the sizes of set 1 and 2, respectively.

- The degree of freedom ( $df$ ) for the Welch  $t$ -test is given by the formula below [68]

$$df = \frac{\left( \frac{s_1^2}{n_1} + \frac{s_2^2}{n_2} \right)^2}{\frac{\left( \frac{s_1^2}{n_1} \right)^2}{n_1 - 1} + \frac{\left( \frac{s_2^2}{n_2} \right)^2}{n_2 - 1}} \quad (1.7)$$

- The  $df$  value is then used to determine the critical values from the  $t$ -value table. Because this is a one-tailed test, the alpha level is 0.05.

The following step consists of looking up  $t_{1-\alpha, df} (\alpha = 0.05, 1 - \alpha = 0.95, df)$  value in the  $t$ -table [68], and looking for the critical value corresponding to the limit  $t$ -value for a known degree of freedom.

- If  $t$ -value  $\geq t_{1-\alpha, df}$ , the null hypothesis cannot be rejected, and the two data sets appear different.
- If  $t$ -value  $< t_{1-\alpha, df}$ , the null hypothesis is rejected in this case, and the two data sets do not appear different.

## 1.4. Electrical double layers

When two phases interact, they develop a potential difference at the interface, particularly when solid and liquid surfaces are involved. As a result of electro-neutrality, the solid surface acquires an electric charge of one sign, while the fluid surface acquires a charge of the opposite sign. This creates what is known as an electrical double layer (EDL). Multiple models have been proposed to explain the charge distribution in the double layer, among them the Helmholtz model (1853), the Gouy-Chapman model (1910

and 1913), and the Stern model. EDL models offer a basic tool for understanding the complex interplay of electrical forces occurring in the solid/electrolyte solution.

The history of electrical double layer (EDL) models is closely tied to electrochemistry development and understanding of the behavior of charged interfaces in electrolyte solutions. EDL studies have evolved, with various models proposed to explain and describe the observed phenomena. Below is a quick summary of the significant events throughout the history of EDL models:

#### **1.5.1 Helmholtz Double-Layer Theory [71]:**

Helmholtz introduced one of the earliest models to describe the formation of an EDL at the charged surface/electrolyte solution interface. According to his model, a layer of adsorbed ions is formed at the surface, creating a charged layer with excess charges. Beyond the contact surface, ions form a diffuse region with a gradually decreasing concentration, similar to the distribution observed in the plan's capacity.

#### **1.5.2 Gouy-Chapman Model (1910) and Chapman-Stern Model (1920s):**

The Gouy-Chapman model further developed the understanding of the EDL by incorporating the concept of ions being distributed according to the Boltzmann distribution [72], [73], [74]. Thus, the electric potential decreases exponentially as we move away from the surface of the liquid bulk [72], [73], [74]. The model describes the distribution of ions in a diffuse layer around a charged surface in a one-dimensional manner [75]. The Chapman-Stern model later extended the Gouy-Chapman model by introducing the concept of the "inner Helmholtz plane" or the "Stern layer," where ions are specifically adsorbed on the charged surface [75], [76], [77].

#### **1.5.3 Stern-Gouy-Chapman Model (1957):**

Stern's model is a more comprehensive and accurate description of the electrical double layer than the Gouy-Chapman models. It integrates the concepts from both models, considering the diffuse layer and the adsorbed layer of ions. This model provides a realistic explanation, especially for highly charged EDLs, when the Gouy-Chapman model fails to do so.

### **1.5. Fractal analysis**

The fractal nature of dielectric breakdown patterns has been explored through experimental studies of discharge structures like Lichtenberg figures and electrical trees,

as well as theoretical modeling and computer simulations [78], [79], [80], [81]. Fractal analysis provides a way to characterize the complex branching morphology of these breakdown patterns [81], [82], [83]. Key findings show that the patterns exhibit self-similarity and can be described by non-integer fractal dimension typically between 1 and 2 [80]. The fractal dimension depends on factors like the nonlinearity between growth probability, electric field, and stochastic elements in the growth process [84]. Comparisons between simulations and experiments show consistent fractal characteristics. Fractal analysis has proven helpful in understanding the underlying dynamics and morphology of dielectric breakdown patterns. Since the introduction of fractal geometries in 1978 by Mandelbrot and Aizenman [85], many models describing the fractal analysis of discharges have been proposed. Sawada et al. [81] used computer simulations to study the fractal properties of randomized branching patterns parameterized by a tip growth priority factor  $R$ . The patterns showed approximate self-similarity with two associated fractal dimensions - an "inner" dimension measuring fine structure with a phase transition-like jump from  $\sim 1.6$  to  $\sim 1.2$  at  $R \approx 35$  and an "outer" dimension measuring the overall framework that remained close to 2. The authors propose a mechanism of alternating "stretching" and "filling" branch growth periods to explain the behaviors. The work provides an early demonstration of phase transition phenomena in the fractal dimensions of randomized branching patterns.

Niemeyer et al. [80] were some of the first to propose using fractal analysis to characterize dielectric breakdown patterns like Lichtenberg figures. They introduced a simple stochastic model and showed that it produces fractal branching structures similar to those in the experiments. This demonstrated the applicability of fractal concepts. For simulated patterns with growth probability proportional to the field, the fractal dimension is  $D \approx 1.75$ , consistent with experiments on planar discharges.

Vincent et al. [79] utilize a lattice-based model to simulate the growth of electrical trees in a dielectric material between electrodes. They compared different lattice growth models, including those that considered nearest neighbor and diagonal bonding. The dielectric was represented as a rectangular grid of discrete points. Tree growth occurs stochastically by adding bonds between lattice points one at a time. The probability of adding a bond is proportional to the local electric field, which is calculated by solving Laplace's equation on the grid with three points fixed at zero potential. The field exponent  $q$  controls the field dependence. Two versions are compared: one only allows nearest neighbor bonds on the square grid  $(i,j)$  and  $(i,j \pm 1)$  or  $(i,j)$  and  $(i \pm 1,j)$ , and one also includes

diagonal bonds  $(i,j)$  and  $(i\pm1,j\pm1)$ . After a tree spans the gap, its morphology and propagation time are analyzed. By varying  $q$ , different degrees of branching are obtained, enabling the exploration of fractal characteristics like dimension. This simple lattice growth model can relate the morphology and growth dynamics of simulated electrical trees in dielectrics.

Wiesmann and Zeller [78] propose a fractal model to describe dielectric breakdown and pre-breakup phenomena in solid dielectrics. It introduced key modeling concepts like local growth probabilities based on field strength. Two key parameters are introduced: the breakdown field  $F_c$ , which sets a threshold for growth, and the sustaining field  $F_s$ , which supports breakdown. Their model generated pre-breakdown tree structures. It improves the understanding of dielectric aging, pre-breakdown, and fracture mechanisms in solids [78].

## **1.6. Health issue of nanoparticles**

Despite the potential benefits of using nanomaterials in thermal and dielectric applications, it is important to acknowledge the potential health concerns associated with their use. The impact of NPs on human health is still being studied and not fully established [86], [87], [88]. Therefore, it is crucial to consider these potential health risks when using NPs and take necessary precautions to ensure their safe use [86], [87], [88]. NPs can enter the body through different routes, such as inhalation, ingestion, or injection [86], [87], [88], [89], [90]. Once inside the body, they tend to accumulate in organs and tissues and interact with biological molecules [89], [90], [91]. Several studies suggest that NPs can lead to inflammation, oxidative damage, and genetic mutations [86], [87], [90], [91], [92]. Moreover, some NPs may cause a pro-inflammatory effect, leading to respiratory diseases such as asthma and lung cancer [86], [88]. Other factors that can influence the impact of NPs on health include the size and shape of the NPs, the route of exposure, and the duration and frequency of exposure. For example, NPs smaller than 50 nm in dimension are more likely to enter the bloodstream and accumulate in organs. While NPs hold great promise for industrial applications, their impact on human health is a complex issue that requires further research. Proper safety precautions must be taken when handling NPs, extreme risks must be taken into account, and guidelines must be implemented to ensure their safe use.

## **1.7. Conclusion**

This chapter presents a general description of NFs, including history, preparation, and stability concerns. A literature review on the effect of different NPs types on the dielectric properties was carried out, showing the tremendous ability of different NPs' natures (conducting, semi-conducting, or insulating) on the enhancements of dielectric performance. Thus, the analysis of previous works showed that the improvements in breakdown voltages, partial discharges, and/or electrostatic charging tendency strongly depend on many parameters such as NPs type (depending on conductivity), size, concentration, surface modification, and/or base liquid, highlighting the factors that influence the dielectric performances of base liquid. Consequently, it is necessary to evaluate the effect of each factor to study and better understand their impact on the final performances and try to optimize the NFs characteristics (NPs selection, size, concentration, and base liquid choice) in view of eventual use in the dielectric application. This goal requires testing various combination base liquids/NPs at different concentrations. The coming chapters aim to determine how this can be achieved. In addition, the various experimental set-ups and methods used to characterize dielectrically NFs (breakdown voltage and partial discharges measurements, electrostatic charging tendency quantification, and creeping discharges characterization) are presented in Chapter 2.

## **CHAPTER 2**

### **EXPERIMENTAL SET-UP**

## **2.1 Introduction**

This chapter presents the different nanoparticles and the basic liquids/oils used to prepare the nanofluids (NFs) to be investigated, the methods for preparing these NFs as well as the different experimental setups used to explore more particularly the dielectric strength of these NFs, their electrostatic charging tendency (ECT), the partial discharges initiation threshold voltage as well as the development of discharges propagating at NFs/solid interfaces.

The physicochemical and geometrical characteristics of the investigated nanoparticles (NPs) are described. The role of surfactants in ensuring the stability of NFs is also discussed; the surfactants playing a crucial role in preventing the aggregation of NPs and maintaining their dispersion in dielectric liquids. The preparation methods of NFs, including the one-step and two-step techniques are developed. The emphasis is placed on the practical considerations that influence the choice of NFs preparation method. This is of great interest for researchers and engineers, especially in evaluating the stability and dispersion maintenance of NPs in nonpolar liquids, which is essential for their practical application in power systems.

The experimental setups and methodologies used for evaluating the performance of NFs for insulation in electrical components and systems are described in details. These investigations are crucial for understanding the behavior of NFs under electrical stress. This is urgent for optimizing their properties for industrial use.

## 2.2 Materials

### 2.2.1 Nanoparticles

The nanoparticles (NPs) we investigate are either spherical or nanosheets (lamellar/non-spherical). The spherical NPs are metal oxides namely Aluminum oxide ( $\text{Al}_2\text{O}_3$ ), Iron III oxide ( $\text{Fe}_3\text{O}_4$ ), Silicone oxide ( $\text{SiO}_2$ ), Titanium dioxide ( $\text{TiO}_2$ ), Copper oxide ( $\text{CuO}$ ), Zinc oxide ( $\text{ZnO}$ ), Zirconium oxide or Zirconia ( $\text{ZrO}_2$ ); and two carbonic NPs, namely, fullerene ( $\text{C}_{60}$ ) which are spherical NPs and graphene (Gr) which are nanosheet NPs. These NPs are conductive ( $\text{Fe}_3\text{O}_4$ ,  $\text{C}_{60}$ , and Gr), semiconducting ( $\text{ZnO}$  and  $\text{CuO}$ ), and insulating ( $\text{Al}_2\text{O}_3$ ,  $\text{SiO}_2$ ,  $\text{ZrO}_2$ , and  $\text{MgO}$ ). Their main characteristics are given (Table 2.1).

**Table 2.1** Physicochemical Properties of Metal-Oxides and Carbonic-based NP.

	Diameter (nm)	Specific surface area ( $\text{m}^2/\text{g}$ )	Density ( $\text{g}/\text{cm}^3$ )	Purity (%)	$\epsilon_r$	Remarks
<b>Spherical NPs</b>						
Metal-oxides NPs						
$\text{Fe}_3\text{O}_4$	20	40	5.1	99.5	80	Conducting
$\text{CuO}$	30-50	20-50	6.4	>99	10-30	Semi-
$\text{ZnO}$	25	19±5	5.6	99.5	8.5	conducting
$\text{ZrO}_2$	20 – 30	15 – 35	4.8 – 6.0	99	10 – 23	
$\text{SiO}_2$	10 – 20	60 – 100	0.6 – 1.8	99	3.9	
$\text{Al}_2\text{O}_3$	20 – 30/50	120 – 140 / 80	3 – 3.98	99.9	9 – 10.1	Insulating
$\text{MgO}$	20	50	3.58	>99	9.8	
Carbon-based NPs						
$\text{C}_{60}$	4 – 8	–	3.4	99.5	2.2	Conducting
<b>Nanosheet NPs</b>						
$<15\mu\text{m}$ and						
Gr	thickness (nm): 11- 15	40	0.8-1.8	99.5	6.9	Conducting

### 2.2.2 Dielectric liquids

Three types of liquids are used as base fluids: synthetic ester, natural ester, and mineral oil. These liquids are commonly used in oil-filled apparatus especially in transformers. Each offers distinct physicochemical properties that influence their performance under various conditions. The liquids under study are all fresh oils that have undergone filtration treatment.

#### 2.2.2.1 Synthetic ester

The synthetic ester used as the base liquid is MIDEI 7131 transformer oil supplied by M&I Materials, UK; its physicochemical properties are shown in Table 2.2 [93].

**Table 2.2** Physicochemical Properties of Synthetic Ester, Midel 7131.

Property	Midel 7131
Density at 20 (°C)	0.97
Kinematic Viscosity (mm <sup>2</sup> /sec)	
at 40 °C	29
at -20 °C	1440
Pour point (°C)	-56
Flash point (°C)	260
Fire point (°C)	316
Water content (ppm)	50
AC BDV “60Hz” (kV)	>75
Dissipation factor at 90°C	< 0.008

### 2.2.2.2 *Natural ester*

The natural ester used as the base liquid is FR3 transformer oil provided by Cargill, USA. FR3 is readily biodegradable and has high fire and low pour points. The main characteristics of this liquid are summarized in Table 2.3 [94].

**Table 2.3** Physicochemical Properties of Natural Ester, FR3.

Property	FR3
Density at 20 °C	0.92
Kinematic Viscosity (mm <sup>2</sup> /sec)	
at 40 °C	32 – 34
at 0 °C	190
Pour point (°C)	(-18) – (-23)
Flash point (°C)	320 – 350
Fire point (°C)	350 – 360
Water content (ppm)	< 50
AC BDV “60Hz” (kV)	> 70
Dissipation factor at 90°C	< 0.02

### 2.2.2.3 *Mineral oil*

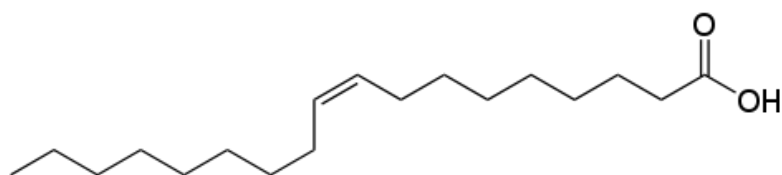
The mineral oil used as the base liquid is NYTRO 4000X transformer oil, supplied by Nynas. This particular type of transformer oil is inhibited and offers enhanced oxidation stability. The inclusion of NYTRO 4000X in the system is aimed at extending the transformer's lifespan by reducing the need for maintenance. The key characteristics of NYTRO 4000X, including detailed information, can be found in Table 2.4 [95].

**Table 2.4** Physicochemical Properties of Mineral Oil, Nytro 4000X.

Property	Nyro 4000X
Density at 20 °C	0.87
Kinematic Viscosity (mm <sup>2</sup> /sec)	
at 40 °C	9.2
at -30 °C	851
Pour point (°C)	-54
Flash point (°C)	140
Fire point (°C)	> 200
Water content (ppm)	< 20
AC BDV "60 Hz" (kV)	
Before treatment	40 – 60
After treatment	> 70
Dissipation factor at 90°C	< 0.001

### 2.2.3 Surfactant (Oleic Acid)

Incorporating a surfactant in NFs is essential to promote uniform dispersion and stability of the NPs, ensuring optimal performance and preventing particle agglomeration. One of the mainly used surfactants in dielectric applications is Oleic acid [96]. Oleic acid (OA) is a monounsaturated omega-9 fatty acid, classified as unsaturated fat [96]. It is commonly found in various oils and fats, particularly olive oil. Chemically, oleic acid is a long-chain carboxylic acid with an 18-carbon chain and a cis double bond at the ninth carbon from the omega end. The chemical formula is C<sub>18</sub>H<sub>34</sub>O<sub>2</sub> [96]. Figure 2.1 shows the chemical structure of Oleic acid [96].

**Figure 2.1** Chemical structure of Oleic Acid [96].

The solubility of OA in transformer oil is an essential property of NF formulation. It directly affects the efficiency and effectiveness of the surfactant in dissolving or dispersing in the desired solvent or medium. The solubility of OA in transformer oil can vary depending on factors such as temperature, pressure, and the exact composition of the transformer oil. Oleic acid is considered a nonpolar molecule since it lacks any

charged groups [21], [97]. This nonpolar nature makes it more soluble in nonpolar organic solvents.

### **2.3 Nanofluids preparation**

There are two main methods for preparing nanofluids. The first one consists of combining NPs synthesis and NFs preparation in a single step (one-step method), where NPs are directly prepared by physical vapor deposition or a liquid chemical method. In this method, the drying, storage, transport, and dispersion processes of NPs are avoided [18]. Hence, NPs agglomeration is minimized, and fluid stability is increased. The downside of this method is the limited volume of the prepared NFs, which constrains its range of applications. That has been the method of choice used so far, before the recent shift to the two-step method. The second method proposes a two-step technique to prepare NFs. In the first processing step, nanoparticles, nanofibers, or nanotubes are produced as a dry powder by suitable techniques [11], [18]. Then, the nanosized powder is dispersed in the fluid. This stepwise method isolates the synthesis of NPs from the preparation of NFs [18]. As a result, aggregation could occur in both steps, especially during NPs drying, storing, and transporting. This method is problematic as aggregation leads to the fall of clusters under gravity, decreases thermal conductivity, and affects the dielectric properties. To address this issue, some techniques, such as ultrasonic agitation (treatment) and adding surfactants to the fluids, are often used to minimize particle aggregation and improve the dispersion.

In this work, the two-step method has been employed to prepare the NF samples. As well as being simple, the technique is practical and thus suitable for our needs in laboratory scale (volume and stability). The preparation steps for NFs are shown in Figure 2.2. The base liquid is first purified (removal of impurities) using a micro membrane filter and a vacuum pump. Oleic acid (supplied by Sigma-Aldrich) is then added, and the mixture is stirred for five minutes using the high-speed rotor-stator disperser at room temperature to mix the solution. The mass ratio of oleic acid (OA) to ester is 0.75 wt.%; this fraction essentially depends on the size and the concentration of the NPs. Therefore, the NFs are prepared by dispersing the nanoparticles at concentrations ranging from 0.1 to 0.5 g / L (0.01 to 0.05 wt.%). The NFs then undergo a stirring process for 20 minutes with the disperser to better disperse the NPs in the ester. Subsequently, the samples of NFs are subjected to an ultrasound process for two hours to avoid agglomeration and sedimentation caused by attractive/repulsive forces. The ultrasound device (500 W, 20

kHz, 25 mm low-intensity solid probe) operates in pulsed mode ([10s 5s], i.e., 10 s of operation and 5 s of rest).

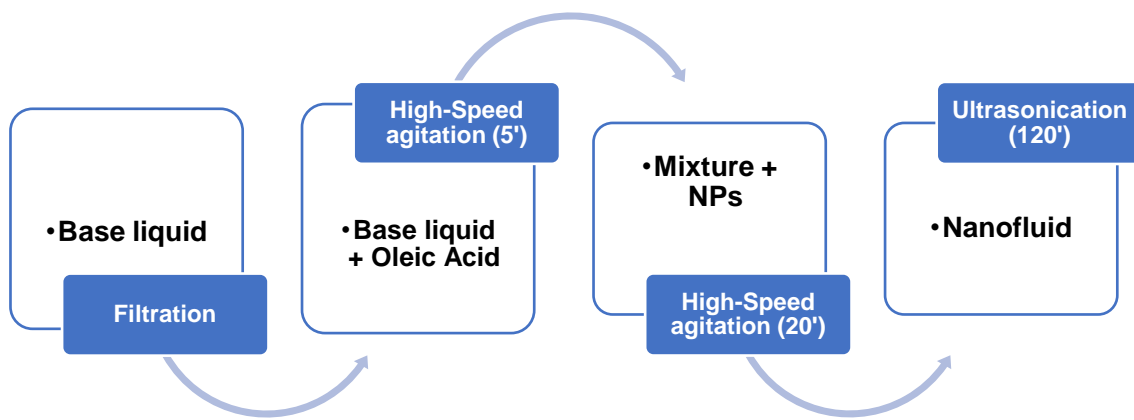


**Figure 2.2** Preparation procedure of Nanofluids.

## 2.4 Stability and stability assessment of nanofluids

The stability of NFs is crucial in a variety of technological applications. The ability to control and maintain the dispersion of NPs in the liquid matrix is paramount to achieving the desired properties and functionalities. However, problems arise regarding non-polar liquids, such as transformer oils or hydrophobic solvents, that can compromise NF stability. The significant challenges in achieving and maintaining stability in these non-polar liquids require innovative solutions.

Non-polar liquids often lack the mechanisms inherent in NPs stabilization, such as electrostatic repulsion or hydrogen bonding [21], [97], which are more common in polar liquids. Consequently, achieving and maintaining NPs dispersion in non-polar liquids becomes daunting. The absence of solid interfacial interaction can lead to agglomeration or sedimentation of NPs over time, diminishing the effectiveness of NFs in applications where stability is fundamental. Overcoming these difficulties requires innovative approaches, such as NPs surface modification or the introduction of stabilizing agents, to improve the colloidal stability of NFs in non-polar liquids, thereby ensuring their applicability and performance.

Several techniques for the stability evaluation have been used and proven to be effective [18], including (i) sedimentation and centrifugation techniques, (ii) Zeta potential ( $\zeta$ ) analysis, and (iii) Spectral absorbance analysis.

Zeta potential is a key parameter in colloidal science and characterizes the electrokinetic potential of particles suspended in a liquid. Measuring zeta potential in non-polar liquids is particularly challenging compared to polar liquids for the reasons highlighted below:

- **Limited Charging:** Zeta potential relies on charges on the particle surface. In non-polar liquids, it is often challenging for particles to acquire a significant charge because these liquids typically do not support the dissociation of ions. As a result, the limited availability of charged species makes it difficult to establish a stable electrical double layer around the particles.
- **Low Conductivity:** Zeta potential measurements involve monitoring particle movement under an electric field, and the conductivity of the liquid is crucial for this. Non-polar liquids usually have low conductivity, resulting in weak electric fields and, consequently, weak electrokinetic effects. This can make it challenging to observe and measure the subtle changes in particle behavior needed for accurate zeta potential determination.
- **Lack of polarization:** In polar liquids, the electric field can induce polarization, separating charges and creating a stable double layer around the particles. Non-polar liquids lack this inherent ability to polarize, making establishing and maintaining the necessary charged environment for zeta potential measurements harder.

## 2.5 Test bench

### 2.5.1 AC breakdown voltage measurements

AC Breakdown voltage measurements are conducted using oil tester BAUR DTA 100 C. The voltage application method and measurement are the same for all our tests. After the sample positioning and distance setting, a wait time of ten minutes is respected before running the test. According to the IEC 60156 [98], the electrodes consist of two spheres of 12.5 mm diameter, separated by a distance of 2.5 mm. The voltage increment is two kV/s until the breakdown occurs. Two minutes between successive measurements

are respected for all series (six measurements per series). Then, an average of six values is saved. We should have sufficient data for specific concentrations for statistical analysis. Hence, three series are measured for each liquid/NF concentration. The AC-BDV data were then analyzed using Weibull distribution. This method is the most used for analyzing the AC-BDV so far. Finally, the *p*-value is calculated to check the goodness-of-fit, and the voltages corresponding to the cumulative probability of 1%, 10%, and 50% are determined and compared.

### 2.5.2 Partial Discharge Characterization

#### a) Test set up

The Baur cell has been customized to the specified electrode arrangement, as shown in Figure 2.3. The PDs test is performed in a needle-plane electrode configuration with a gap spacing of 5 mm at the same voltage level in the case of comparison of a base liquid and their corresponding NFs. The tip radius curvature is ten  $\mu\text{m}$ , while the plane circular electrode has a 35 mm diameter, made from brass. The PDs inception voltages (PDIVs), average charge ( $Q_{\text{avg}}$ ), peak charge ( $Q_{\text{peak}}$ ), and number of PDs (NPDs/s) are measured for each sample that underwent five PD tests. The PD comparison is performed in compliance with IEC 60270. The phase-resolved PD pattern is also compared between the base liquid and the NF sample.

Figure 2.4 shows the experimental test bench; it consists of a high-voltage generator and a PD measurement circuit. The high voltage is generated using a cascade of 24/230 V and 0.23/25 kV transformers inside a Faraday cage. The 24/230 V transformer is controlled from the outside with an Arduino-based card via the Techron 7224 amplifier. The PDs investigation in the three liquids has complied with the IEC 60270 standard



**Figure 2.3** Electrodes configuration

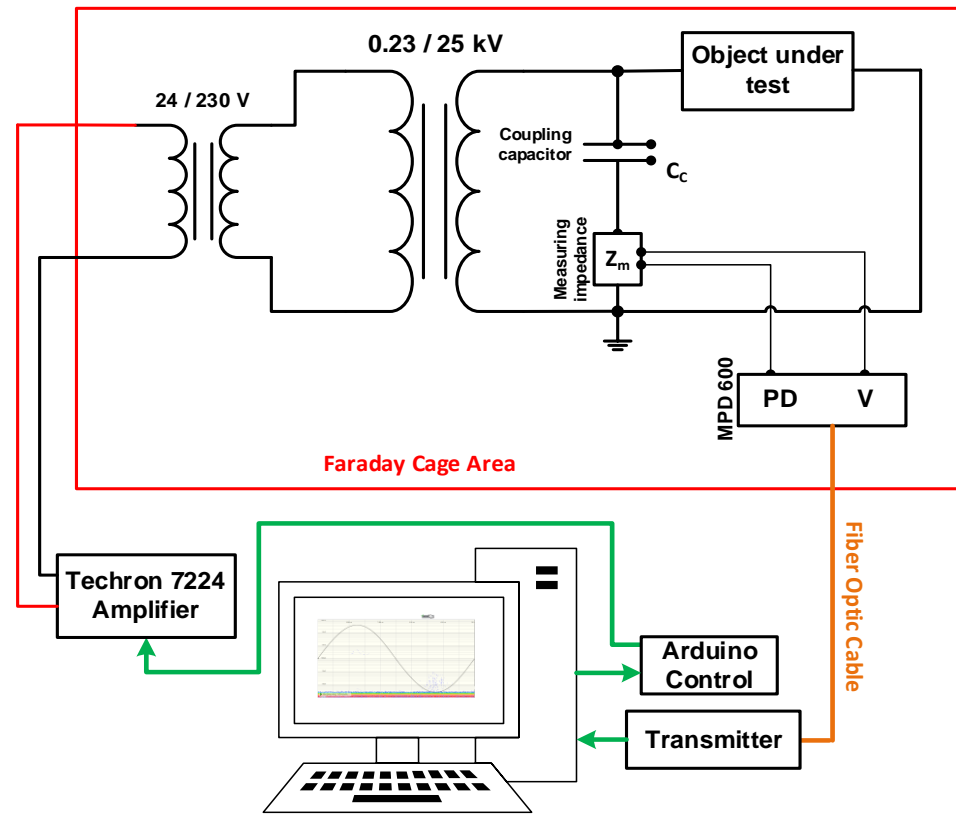


**Figure 2.4** The experimental test bench.

method using a commercially available Omicron system. The PD measurement circuit consists of a coupling capacitor ( $C_c$ ) and measuring impedance ( $Z_m$ ). The PD signal, thus measured by the  $Z_m$ , is treated by the MPD 600 module, and the information is transmitted using fiber optic cable to avoid interferences. Before PDs tests, the electrical measurement circuit was calibrated by IEC 60270 using CAL 542 provided by Omicron.

#### b) Testing strategy

During PDs tests, the applied voltage (RMS value) follows the profile in Figure 2.5. The voltage was increased/decreased during rising/falling with a rate of 0.5 kV/s, and the voltage was kept at its maximum value for 32 s. The PDIV for the base liquids and corresponding NFs samples were observed and recorded during voltage rising time. Other parameters are computed during the plateau, such as the average charge ( $Q_{avg}$ ) and number of PDs ( $NPDs/s$ ). Their values represent the average PD charge magnitude and the number of PDs per second during the 30 s of the maximum applied voltage. A waiting time of 5 s at zero voltage (separating two measurements) was respected. To ensure the reproducibility of PDs results, the described profile was repeated five times with each liquid.

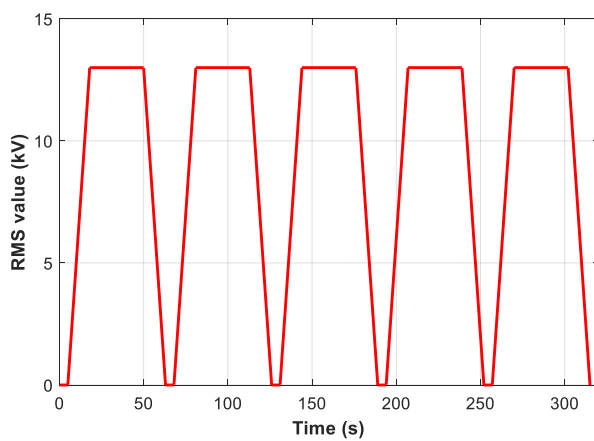


**Figure 2.5** Voltage profile (RMS value) was applied to samples during the PD test.

### 2.5.3 Electrostatic charging tendency

Figure 2.6 depicts the diagram of the spinning disk system for ECT quantification. ECT studies were performed using a rotating disc system identical to that reported in previous work [99]. CIGRE has adopted this system for ECT quantification resulting from solid-liquid interaction in which the pressboard covers both sides of the disk [51]. The disk measures 150 mm in diameter and 7.5 mm in thickness and is positioned in the center of the tank. The tank measures 170 mm in inner diameter and 120 mm in height. A DC motor drove the rotating disk. Using a stabilized DC source, the disk's rotating speed was

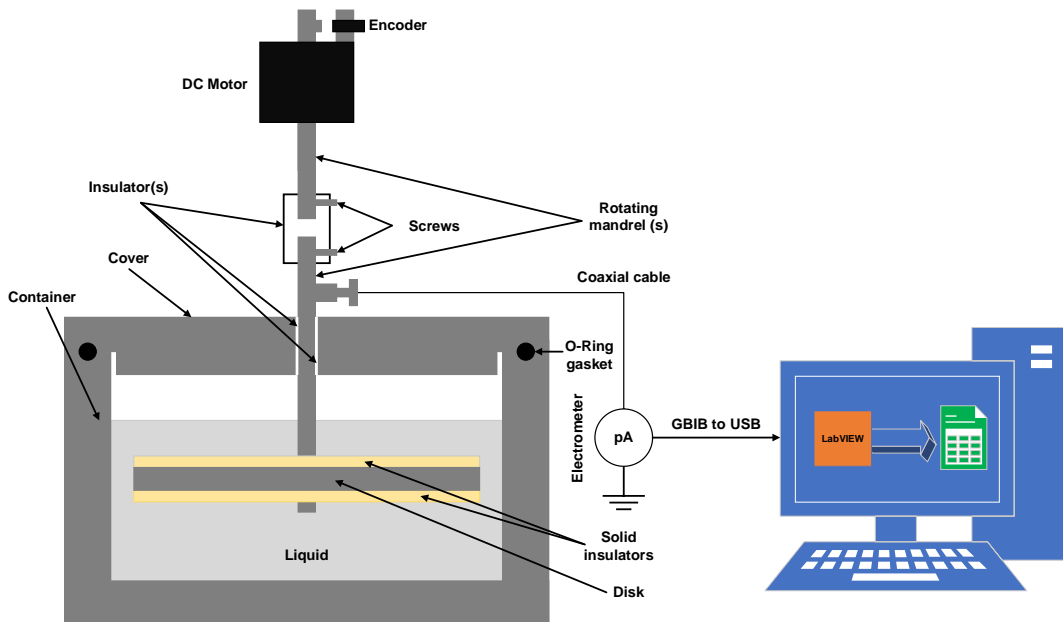


**Figure 2.6** Diagram of spinning disk system for ECT quantification.

varied between 200 ( $\pm 20$ ) to 700 ( $\pm 20$ ) rpm. An encoder provided the speed monitoring. The electrification parameters (charge) were simultaneously recorded via a data acquisition solution developed using LabVIEW™. The charge measurement was ensured using a pico-electrometer from KEITHLEY (6517A), inserted between the tank and the earth. The obtained data are saved into an Excel file, allowing for efficient further analysis.

#### 2.5.4 Surface Discharge Characterization

Figure 2.7 gives the schematic diagram of the experimental setup for the creeping discharge characterization. In the present work, only the optical characterization of radial discharges is addressed based on the measurement of their stopping length. The images were filmed using a CCD camera (SONY XC-HR58, 1 image per 20 ms at the maximal resolution: 767x580 px) connected to a computer via a video acquisition card (Matrox Meteor II/Multi-Channel). A manual trigger was used to start image recording and to trigger the pulse generator a few microseconds later.

The test cell consists of a cylindrical core of 90 mm height and 110 mm inner diameter; it contains a liquid-solid insulating system and a point-to-plane electrode arrangement. The top cover of the test cell is transparent to permit capturing the discharge images; it also serves as a mechanical support for the tip electrode and ensures it is always in the center of solid material. The lower cover (flat electrode) is connected to the ground (low-voltage electrode). The flat electrode, a key component in the NF sample testing process, consists of a thin brass plate 12 mm thick and 85 mm in diameter. It is covered with a solid Teflon insulator (blocked electrode), 2 mm thick, with sufficient dielectric strength to prevent breakdown. This design allows us to perform several tests and measurements on the same oil sample, ensuring accurate and consistent results. The sharp electrode (high-voltage electrode) has a tip with a radius of curvature of  $10.0 \pm 0.5 \mu\text{m}$ . It is made of tungsten. The tip is replaced when its profile deviates from the original. The radius of curvature is measured using a Nikon Eclipse LV150 microscope. In addition, the liquid is changed if a bypass occurs to avoid uncertainties in the results, which would affect the comparison.

The test uses a two-stage Marx generator (200 kV-2 kJ) to produce a standard positive lightning impulse wave of 1.2/50  $\mu\text{s}$ .

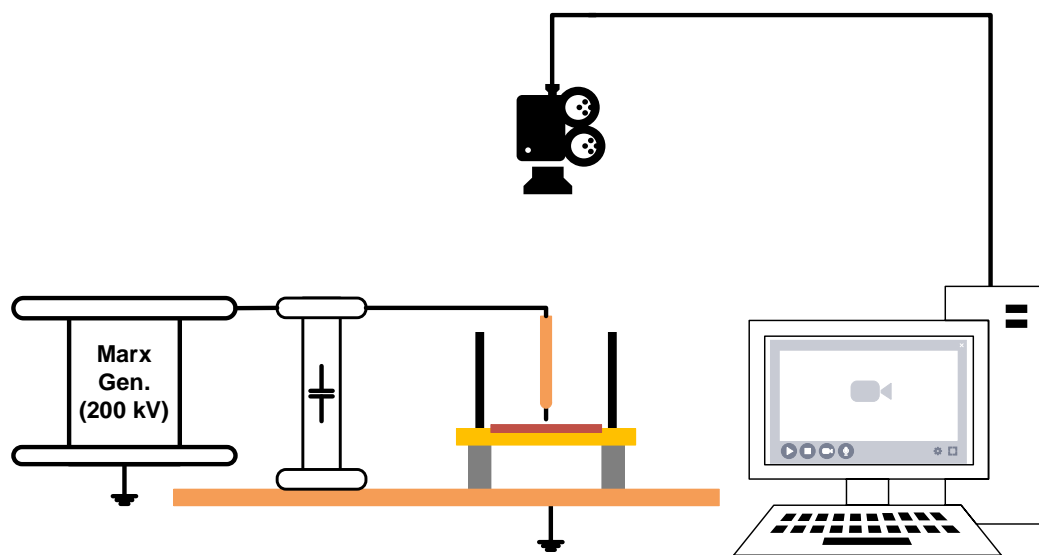


**Figure 2.7** Creeping discharges investigation test bench.

A program that allows the calculation of the stopping length from the recorded images was developed based on MATLAB software. The calculation method is divided into three main steps, as described below:

a) Picture-taking

- Frame Limitation: The frame is limited to the solid insulator border contained in the image to ensure consistency and relevance of the data.
- A sequence of images is captured and saved for analysis. This is done to have multiple frames from which the necessary one can be chosen.
- The image that contains the discharge is selected from the sequence. This image will then be used for further calculations.

b) Stopping length calculation (Figure 2.8):

- Using custom software developed on MATLAB, a circle with an adjustable diameter is drawn. This circle is critical as it will help measure the discharge's extent later.
- The circle's diameter is adjusted manually with the fixed center until the discharge is fully enclosed within the circle (Figure 2.8). This step might require precise adjustments to ensure the discharge's outer edge matches the circle's periphery accurately.

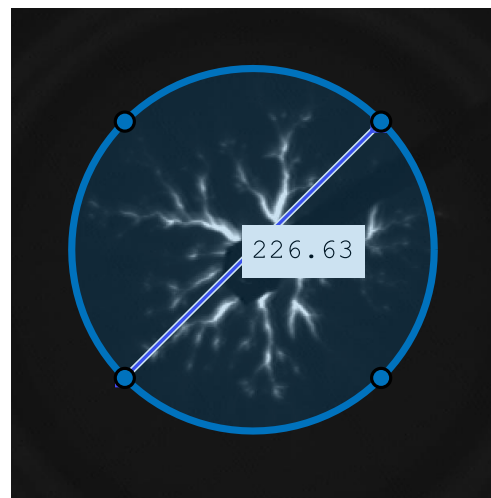


**Figure 2.8** Creeping discharge image at the surface of solid insulator immersed in pure NE at 58 kV with the circumscribed circle.

- The iterative distance tool within the MATLAB software measures the circle's diameter in pixels. This tool allows for high accuracy in finding the diameter's pixel length.
- c) The stopping length is calculated using the formula given below:

$$L_f (\text{mm}) = \frac{\text{Diam. of the discharge (px)}}{\text{Diam. of the frame (px)}} \times \frac{\text{Solide Diam. (mm)}}{2} \quad (2.1)$$

## 2.6 Conclusion

In conclusion, Chapter 2 described the experimental setup for studying the dielectric properties of nanofluids (NFs), focusing on preparation and testing methods. Through careful selection of NPs and base liquids, the chapter highlights the role of surfactants such as Oleic acid in maintaining NPs dispersion, which is crucial for stability in non-polar liquids such as transformer oils. Both one-step and two-step preparation methods are discussed, with the latter chosen for its practicality in laboratory-scale applications. In addition, this chapter details methodologies for measuring various electrical properties, such as AC breakdown voltage, partial discharge, electrostatic charge tendency, and surface discharge, using specific test configurations that align with industry standards (e.g. IEC 60156 and 60270). Chapter 3 presents the AC breakdown

voltage measuring results of the various nanofluids we prepared. In contrast, Chapter 4 will treat the partial discharge characterization, electrostatic charge tendency, and surface discharge development.

## **CHAPTER 3.**

### **AC BREAKDOWN VOLTAGE OF NANOFUIDS-BASED SYNTHETIC AND NATUREL ESTERS AND MINERAL OIL**

### 3.1 Introduction

In recent years, much work has been carried out in the search for new insulating fluids or improving the properties of existing fluids with a view to their applications in oil-filled electrical components and systems. Among the properties that have been the subject of intense research is the dielectric strength.

This chapter presents the experimental results of measuring the AC breakdown voltage (AC BDV) of the nanofluids (NF) we prepared before and their statistical analyses. These analyses are performed using statistical tools such as the Anderson-Darling goodness-of-fit test and Weibull probability analysis.

As a reminder, the considered nanofluids used as base fluids synthetic ester (SE), natural ester (NE), and mineral oil (MO) with the incorporated nanoparticles (NPs) are conducting ( $\text{Fe}_3\text{O}_4$ ,  $\text{C}_{60}$ , Gr), semi-conducting (ZnO, and CuO), and insulating ( $\text{Al}_2\text{O}_3$ ,  $\text{ZrO}_2$ ,  $\text{SiO}_2$ , and MgO) NPs.

Note that some NFs have a breakdown voltage higher than that which our voltage source can provide (100 kV) for the electrode gap dictated by the standard (2.5 mm), mainly those based on synthetic ester (SE). In that case, the measurements were carried out with a reduced spacing of the electrodes, i.e., 2 mm, the comparison being made on the basis of the dielectric strength.

So, unless otherwise stated, BDV tests are carried out following IEC 60156 (with a 2.5 mm electrode gap distance). Three series of six measurements were performed, giving 18 points, which were considered sufficient for the statistical analysis. Next, the conformity of AC BDV data for 2 mm and 2.5 mm electrode gap to Weibull distribution was analyzed using Anderson-Darling statistics. Finally, the Weibull curve lines were plotted, and the voltages corresponding to 1%, 10%, and 50% risk levels were determined.

### 3.2 Conducting nanoparticles

#### 3.2.1 AC breakdown voltage

Figures 3.1 – 3.3 illustrate the mean AC BDV and max/min values of base liquids and different NFs with  $\text{Fe}_3\text{O}_4$ ,  $\text{C}_{60}$ , and Gr for various concentrations, respectively. As mentioned in the previous section, the breakdown does not occur for a 2.5 mm electrode gap with  $\text{Fe}_3\text{O}_4$ ,  $\text{C}_{60}$ , and Gr with the SE; the AC BDV with a 2 mm electrode gap distance is considered to compare the NFs with SE under the same experimental conditions.

As depicted in Figure 3.1,  $\text{Fe}_3\text{O}_4$  NPs generally enhance the performance of various NFs, except for those containing NE at concentrations of 0.1 g/L and 0.5 g/L. Specifically:

- SE-based NFs see improvements ranging from 22% to 37%, with the highest enhancement at 0.4 g/L.
- NE-based NF experiences a maximum improvement of about 13.5% at 0.4 g/L.
- MO-based NFs show gains between 7.8% and 21%, peaking at 0.3 g/L.

As depicted in Figure 3.2,  $\text{C}_{60}$  NPs positively influence all NFs except those with NE at a concentration of 0.1 g/L. The specific improvements are as follows:

- SE-based NFs show enhancements ranging from 5.5% to 13%, with the maximum enhancement occurring at 0.4 g/L.
- NE-based NFs achieve a maximal improvement of about 13% at 0.4 g/L.

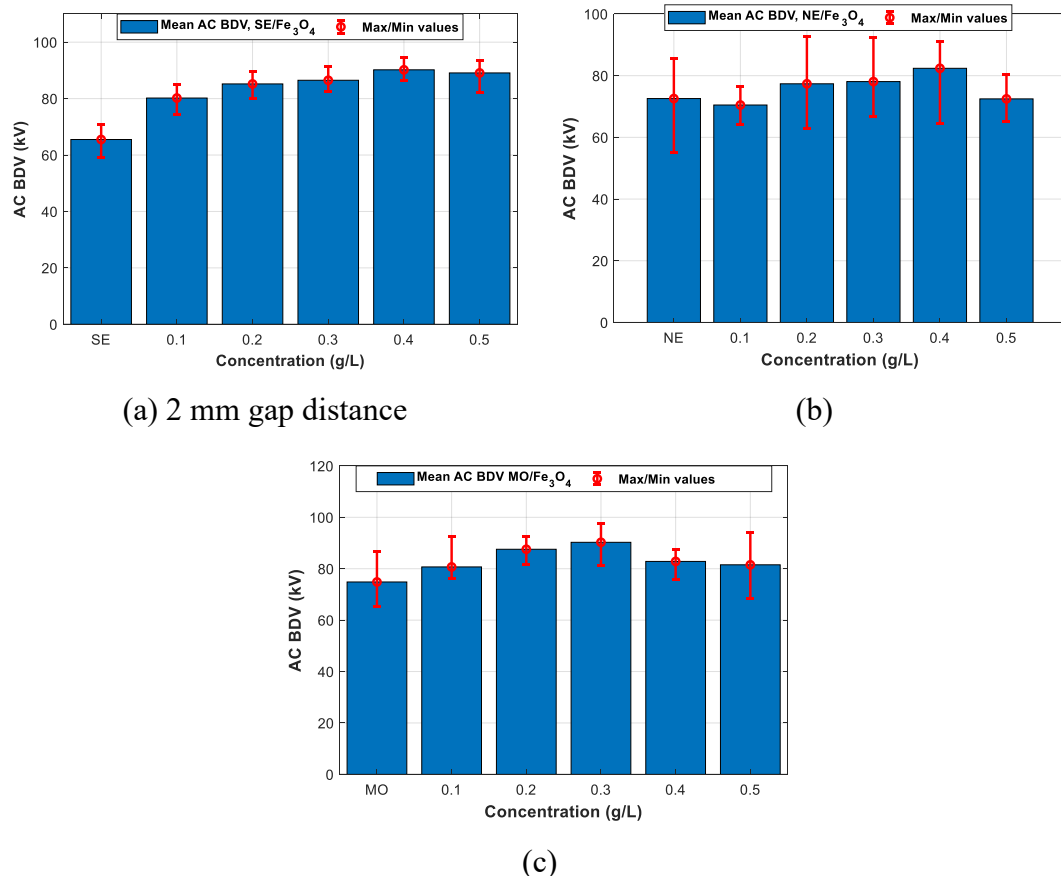


**Figure 3.1** Mean breakdown voltages of nanofluid containing  $\text{Fe}_3\text{O}_4$  at different concentrations for (a) synthetic ester, (b) natural ester, and (c) mineral oil.

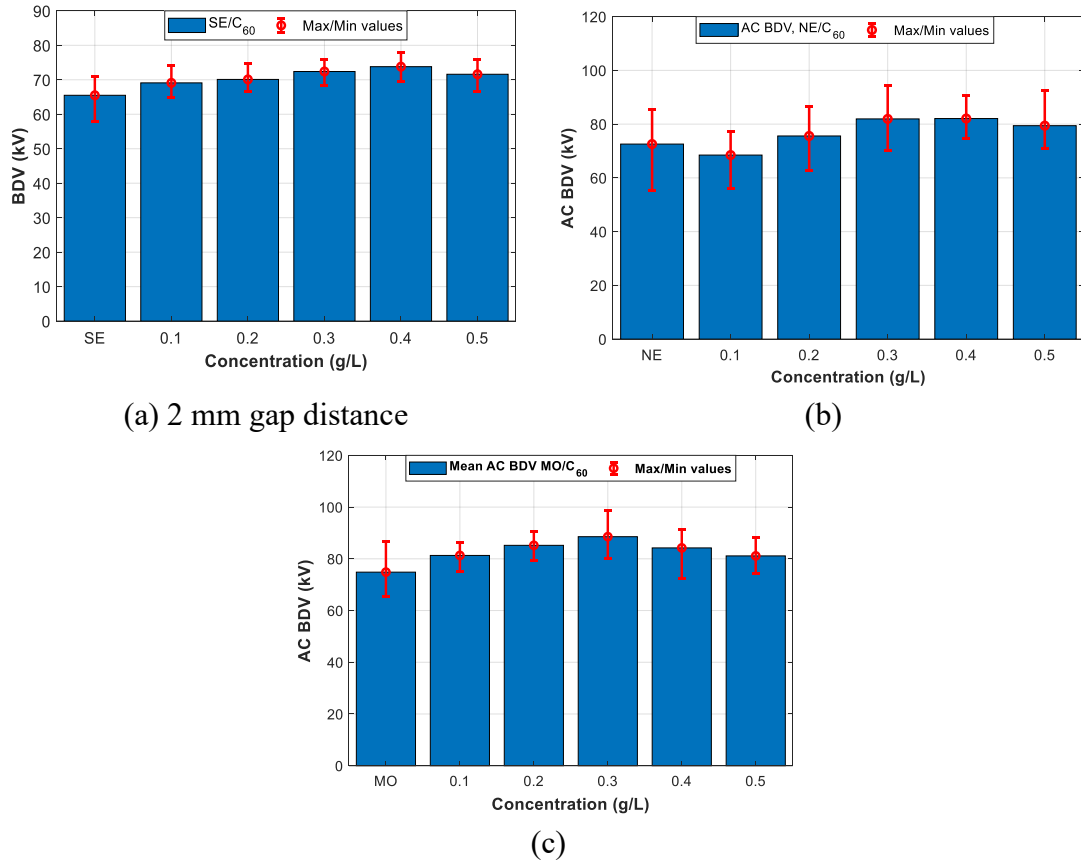


**Figure 3.2** Mean breakdown voltages of nanofluid containing fullerene (4-8 nm) at different concentrations for (a) synthetic ester, (b) natural ester, and (c) mineral oil.

- MO-based NFs experience gains between 8.4% and 18.3%, with the highest increment at 0.3 g/L.

As depicted in Figure 3.3, similar to the effects of the other conducting NPs, Gr NPs positively influence the AC BDV of the three liquids, except for those with NE at a concentration of 0.5 g/L. The improvements are as follows:

- SE-based NFs show enhancements ranging from 8.2 % to 16.6 %, with the maximum enhancement occurring at 0.3 g/L.
- Another type of NF with NE achieves a maximal improvement of about 12.8 % at 0.3 g/L.
- MO-based NFs experience gains between 7.4% and 18.5%, with the highest increment at 0.3 g/L.

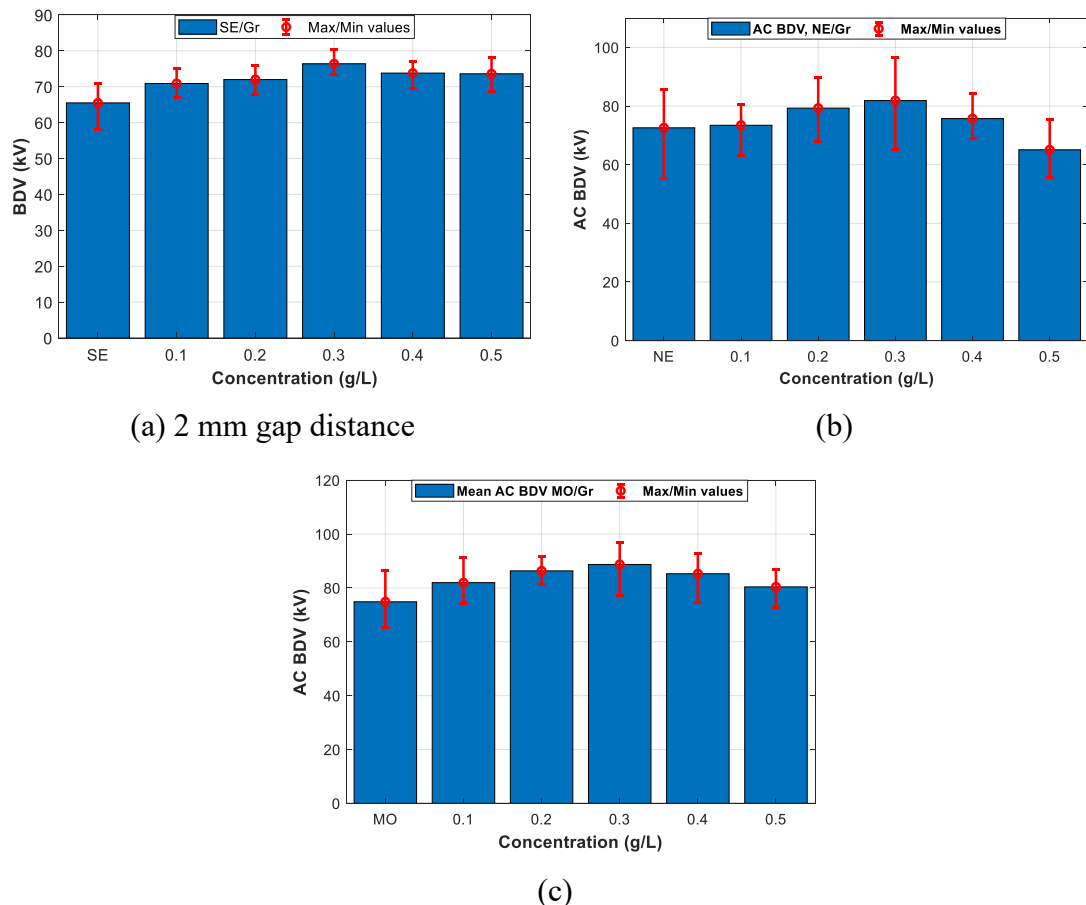


**Figure 3.3** Mean breakdown voltages of nanofluid containing Gr at different concentrations for (a) synthetic ester, (b) natural ester, and (c) mineral oil.

### 3.2.2 Anderson-Darling (AD) goodness-of-fit test

A goodness-of-fit test is required to use the Weibull fit curves safely. The Anderson-Darling fitting test checks if this distribution law obeys the experimental data. Table 3.1 summarizes the results of the AD fitting test for conducting NPs. Most cases, the AC BDV data of all liquids with conducting NPs obey the Weibull distribution. For SE, when tested with  $\text{Fe}_3\text{O}_4$ , most concentrations (0.1 to 0.5 g/L) were accepted, except for 0.4 g/L, which was rejected with a  $p$ -value less than 0.04. With  $\text{C}_{60}$  and Gr, all concentrations were accepted. All concentrations were accepted for NE with  $\text{Fe}_3\text{O}_4$  and Gr, but one concentration (0.5 g/L) was rejected with  $\text{C}_{60}$  NPs ( $p$ -value = 0.01). MO exhibited more variability: with  $\text{Fe}_3\text{O}_4$ , most concentrations were accepted except for 0.1 and 0.4 g/L, which were rejected with  $p$ -values less than 0.03. All concentrations were accepted with  $\text{C}_{60}$ ; with Gr, most concentrations were accepted except for 0.2 g/L ( $p$ -value < 0.02).

**Table 3.1** AD goodness-of-fit test results of conducting NPs based NFs.

m/V (g/L)	<i>p</i> -value	Decision	m/V (g/L)	<i>p</i> -value	Decision	m/V (g/L)	<i>p</i> -value	Decision
SE	0.20	Accepted	NE	0.63	Accepted	MO	0.10	Accepted
SE NF with $\text{Fe}_3\text{O}_4$								
0.1	0.42	Accepted	0.1	0.57	Accepted	0.1	0.03<	Rejected
0.2	0.24	Accepted	0.2	0.18	Accepted	0.2	0.83	Accepted
0.3	0.44	Accepted	0.3	0.54	Accepted	0.3	0.12	Accepted
0.4	0.0387<	Rejected	0.4	0.21	Accepted	0.4	0.03<	Rejected
0.5	0.15	Accepted	0.5	0.72	Accepted	0.5	0.50	Accepted
SE NF with $\text{C}_{60}$								
0.1	0.38	Accepted	0.1	0.66	Accepted	0.1	0.49	Accepted
0.2	0.31	Accepted	0.2	0.81	Accepted	0.2	0.47	Accepted
0.3	0.30	Accepted	0.3	0.60	Accepted	0.3	0.08	Accepted
0.4	0.57	Accepted	0.4	0.21	Accepted	0.4	0.67	Accepted
0.5	0.50	Accepted	0.5	0.01<	Rejected	0.5	0.44	Accepted
SE NF with Gr								
0.1	0.14	Accepted	0.1	0.15	Accepted	0.1	0.22	Accepted
0.2	0.57	Accepted	0.2	0.61	Accepted	0.2	0.02<	Rejected
0.3	0.46	Accepted	0.3	0.20	Accepted	0.3	0.68	Accepted
0.4	0.29	Accepted	0.4	0.45	Accepted	0.4	0.13	Accepted
0.5	0.25	Accepted	0.5	0.75	Accepted	0.5	0.86	Accepted

### 3.2.3 Weibull probability analysis

In the following, the experimental results are statistically analyzed using the Weibull distribution law [70]. This statistical law is among the most probabilistic distributions used to analyze the BDV data of dielectric liquids. Therefore, it constitutes a valuable tool in predicting breakdown voltages at low-risk levels. Hence, it provides hopeful information about the health state of the fluid under test. Furthermore, apart from being beneficial for the probability estimation of an AC BDV at different risk levels, the Weibull distribution constitutes a means lifetime estimator of insulation liquid; hence, the equipment. Table 3.2 provides the scale ( $\alpha$ ) and shape ( $\beta$ ) parameters of the Weibull distribution for different NFs with conducting NPs ( $\text{Fe}_3\text{O}_4$ ,  $\text{C}_{60}$ , and Gr) at various concentrations, analyzed using three different liquids: SE, NE, and MO. For  $\text{Fe}_3\text{O}_4$ , SE

**Table 3.2** Scale and shape parameters of conducting NP-based NFs.

Fe <sub>3</sub> O <sub>4</sub>						
	SE		NE		MO	
Concentration (g/L)	$\alpha$ (scale)	$\beta$ (shape)	$\alpha$ (scale)	$\beta$ (shape)	$\alpha$ (scale)	$\beta$ (shape)
0.0	65.15	10.52	75.73	11.65	76.76	18.96
0.1	84.18	17.48	72.09	23.11	83.85	12.16
0.2	83.66	19.09	80.88	10.56	88.90	35.67
0.3	87.95	21.62	81.30	11.83	92.35	23.18
0.4	92.20	28.40	85.38	15.61	84.69	27.69
0.5	91.42	21.70	74.56	17.90	84.22	14.88
C <sub>60</sub>						
	SE		NE		MO	
Concentration (g/L)	$\alpha$ (scale)	$\beta$ (shape)	$\alpha$ (scale)	$\beta$ (shape)	$\alpha$ (scale)	$\beta$ (shape)
0.1	71.19	13.98	71.19	13.98	82.74	29.48
0.2	75.62	12.73	78.75	12.73	86.76	29.75
0.3	85.07	13.30	85.07	13.30	90.86	18.46
0.4	84.15	19.80	84.14	19.80	86.04	24.75
0.5	82.05	13.81	82.05	13.81	83.01	22.27
Gr						
	SE		NE		MO	
Concentration (g/L)	$\alpha$ (scale)	$\beta$ (shape)	$\alpha$ (scale)	$\beta$ (shape)	$\alpha$ (scale)	$\beta$ (shape)
0.1	73.81	17.43	75.81	17.43	84.33	17.15
0.2	82.01	14.97	82.01	14.97	87.89	28.50
0.3	85.74	10.29	85.74	10.29	90.81	22.12
0.4	77.72	18.88	77.72	18.88	87.82	19.28
0.5	67.68	12.71	67.68	12.71	82.22	23.89

shows an increase in the scale parameter from 72.09 at 0.1 g/L to 92.20 at 0.4 g/L, then a slight decrease to 91.42 at 0.5 g/L, with the shape parameter rising significantly from 11.65 to 28.40 and then dropping to 21.70. NE fluctuates, peaking in the scale parameter at 85.38 and having the shape parameter highest at 23.11 for 0.1 g/L. MO shows a general increase in the scale parameter, peaking at 92.35, and high variability in the shape parameter, peaking at 35.67 for 0.2 g/L. For C<sub>60</sub>, both SE and NE exhibit similar trends, with the scale parameter peaking at 85.07 and the shape parameter slightly fluctuating but reaching 19.80. MO for C<sub>60</sub> also shows a peak in the scale parameter at 90.86 g/L and significant fluctuations in the shape parameter, peaking at 29.75. For Gr, SE sees the scale parameter increasing to 85.74 at 0.3 g/L and the shape parameter peaking at 17.43 for 0.1 g/L. NE follows a similar pattern, while the MO method shows a peak in the scale parameter at 90.81 and the highest shape parameter at 28.50 for 0.2 g/L.

Generally, for all NFs, the scale parameter increases with concentration up to a point before stabilizing or decreasing slightly, while the shape parameter shows more variability. Comparing the liquids, SE and NE display similar trends, while MO shows higher scale parameters and more significant fluctuations in shape parameters.

The shape and scale parameters plot the Weibull diagram for NF with SE, NE, and MO with  $\text{Fe}_3\text{O}_4$ ,  $\text{C}_{60}$ , and Gr NPs at different concentrations are given in Figures 3.4 – 3.6). These plots help predict the likelihood of failure at various voltage levels. The Weibull distribution, characterized by its shape and scale parameter, models the statistical behavior of BDV. The shape parameter indicates how the failure rate changes under stress, while the scale parameter represents the characteristic life or the point at which 63.2% of samples have failed.

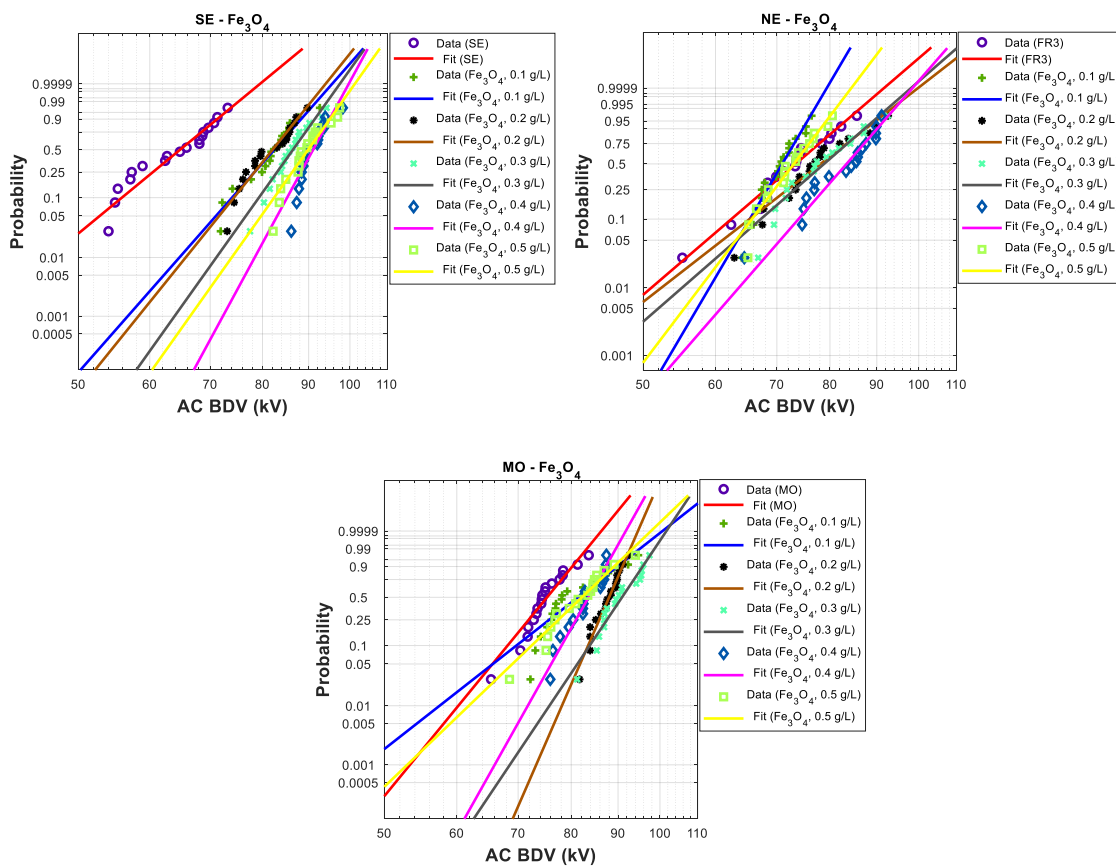


**Figure 3.4** Weibull probability plots of breakdown voltages of nanofluid containing  $\text{Fe}_3\text{O}_4$  at different concentrations for (a) synthetic ester, (b) natural ester, and (c) mineral oil.

### 3. AC Breakdown Voltage of Nanofluids-Based SE, NE, and MO

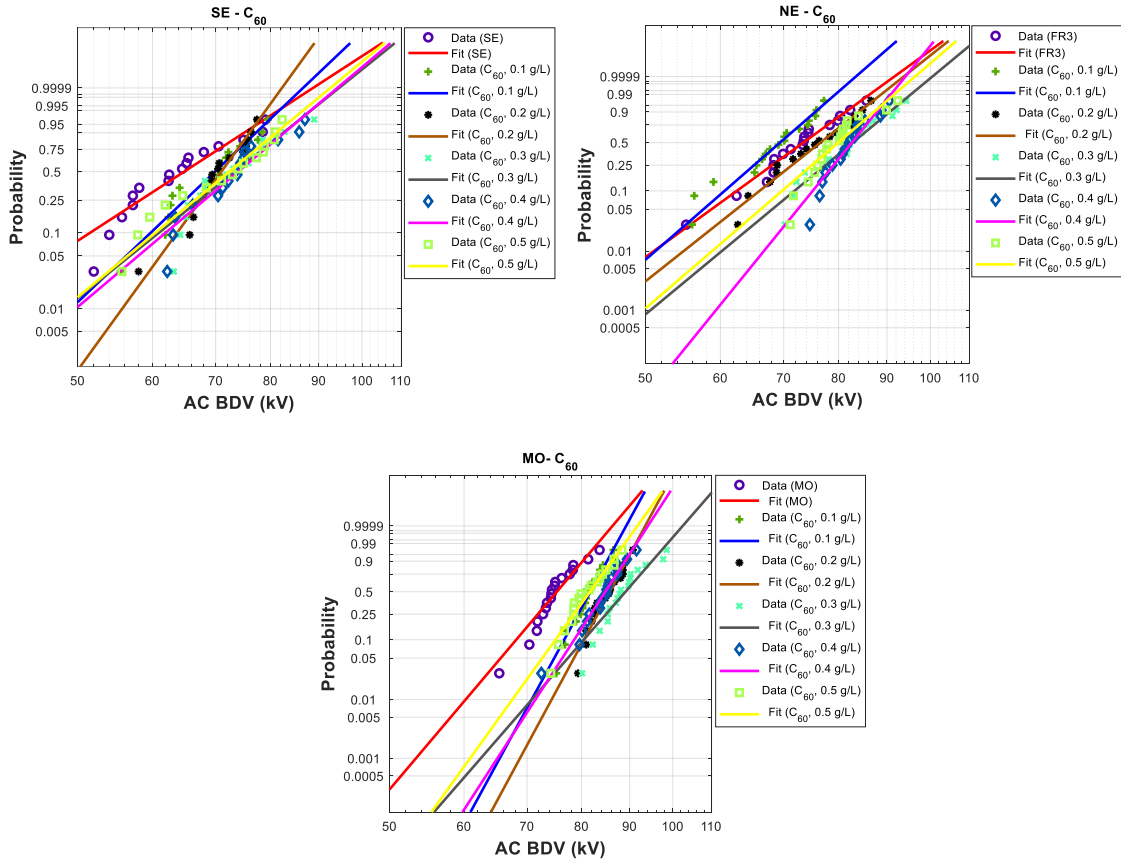


**Figure 3.5** Weibull probability plots of breakdown voltages of nanofluid containing C<sub>60</sub> at different concentrations for (a) synthetic ester, (b) natural ester, and (c) mineral

- 1

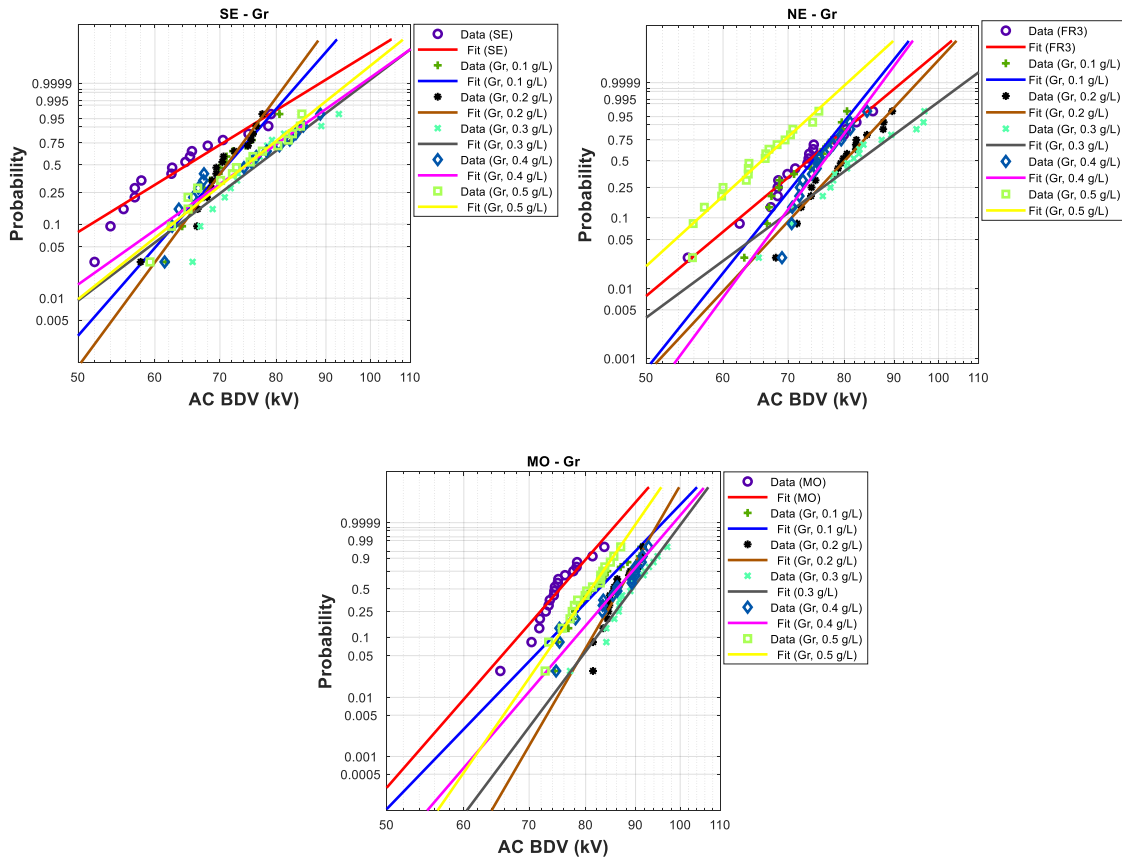


**Figure 3.6** Weibull probability plots of breakdown voltages of nanofluid containing Gr at different concentrations for (a) synthetic ester, (b) natural ester, and (c) mineral oil.

Weibull curves are utilized to calculate the breakdown voltage (BDV) at low probability levels, such as 1%, 10%, and 50%. These levels provide the AC BDV at specific probability levels. The process involves assessing the probability levels from the lowest to the highest AC BDV by increasing the BDV by 0.1 kV at each step. Subsequently, the AC BDV at the desired probability level is selected, and the results are presented in Tables 3.3 to 3.5. Table 3.3 provides the AC BDV and percentage increment for  $\text{Fe}_3\text{O}_4$  NFs in different base oils (SE, NE, and MO) at varying concentrations (0.1 to 0.5 g/L) and probability levels (1%, 10%, 50%). In SE base oil, the BDV shows a significant increase with  $\text{Fe}_3\text{O}_4$  NPs addition, particularly at 0.3 g/L and 0.4 g/L concentrations, where increments exceed 50%. NE base oil shows mixed results, with BDV increasing modestly up to 0.4 g/L concentration but showing some decrements at higher concentrations and probability levels, and the increments are less pronounced than with SE oil. For MO base oil, the addition of  $\text{Fe}_3\text{O}_4$  NPs results in substantial BDV increments, especially at 0.2 g/L and 0.3 g/L concentrations, where the BDV increases up

**Table 3.3** AC BDV of Fe<sub>3</sub>O<sub>4</sub> nanofluids for different probability levels.

Fe <sub>3</sub> O <sub>4</sub>						
	1 %		10 %		50 %	
	BDV (kV)	Increment (%)	BDV (kV)	Increment (%)	BDV (kV)	Increment (%)
SE	0.0	46.50	—	55.90	—	64.90
	0.1	64.70	39.14	74.10	32.56	82.50
	0.2	65.80	41.51	74.40	33.09	82.10
	0.3	71.10	52.90	79.30	41.86	86.50
	0.4	78.50	68.82	85.20	52.42	91.10
	0.5	74.00	59.14	82.50	47.58	89.90
NE	0.0	51.10	—	62.50	—	73.40
	0.1	59.10	15.66	65.40	04.64	71.00
	0.2	52.40	02.54	65.40	04.64	78.30
	0.3	55.20	08.02	67.30	07.68	78.90
	0.4	63.60	24.46	74.00	18.40	83.50
	0.5	57.70	12.92	65.80	05.28	73.10
MO	0.0	60.30	—	68.20	—	75.30
	0.1	57.50	-4.64	69.70	02.20	81.40
	0.2	78.20	29.68	83.50	22.43	88.00
	0.3	75.80	25.70	83.90	23.02	91.00
	0.4	71.80	19.07	78.10	14.52	83.60
	0.5	61.90	02.65	72.50	06.30	82.20

to 29.68% and 25.70%, respectively, at the 1% probability level, and up to 23.02% and 20.85% at the 50% probability level.

The provided data in Table 3.4 includes AC BDV values at different probability levels (1%, 10%, and 50%) for NFs containing C<sub>60</sub> dispersed in SE, NE, and MO. The data also highlights the percentage increment in BDV compared to the base fluid. The AC BDV data for NFs containing C<sub>60</sub> demonstrates that the BDV generally increases with the concentration of C<sub>60</sub>, with the most significant improvements observed at lower concentrations (0.2 g/L to 0.4 g/L) across all matrices (SE, NE, MO). These increments are more pronounced at the 1% probability level, indicating enhanced reliability and performance of the NFs in high-stress conditions. Consistent trends in SE and NE suggest similar interactions of C<sub>60</sub> with these fluids, while MO shows higher base BDV values and significant improvements with the addition of C<sub>60</sub>.

**Table 3.4** AC BDV of C<sub>60</sub> nanofluids for different probability levels.

C <sub>60</sub>						
	1 %		10 %		50 %	
	BDV (kV)	Increment (%)	BDV (kV)	Increment (%)	BDV (kV)	Increment (%)
SE	0.0	46.50	—	55.90	—	64.90
	0.1	49.20	05.80	59.80	06.90	69.90
	0.2	55.80	20.00	63.80	14.13	71.00
	0.3	48.40	04.08	61.00	09.12	73.40
	0.4	49.80	07.00	62.00	10.90	74.00
	0.5	48.30	03.80	60.50	08.22	72.40
NE	0.0	51.10	—	62.50	—	73.40
	0.1	51.40	00.60	60.70	-02.88	69.40
	0.2	54.90	07.40	66.00	05.60	76.60
	0.3	60.20	17.80	71.90	15.04	82.80
	0.4	66.70	30.50	75.20	20.32	82.70
	0.5	58.80	15.10	69.80	11.68	80.00
MO	0.0	60.30	—	68.20	—	75.30
	0.1	70.80	17.40	76.70	12.46	81.80
	0.2	74.40	23.40	80.50	18.03	85.80
	0.3	70.90	17.60	80.50	18.03	89.10
	0.4	71.50	18.60	78.60	15.24	84.80
	0.5	67.60	12.10	75.10	10.11	81.70

Table 3.5 details the AC BDV at different probability levels (1%, 10%, and 50%) and the percentage increment of Gr NFs. For SE base oil, as the concentration increases to 0.1 g/L, 0.2 g/L, and 0.3 g/L, the BDV increases consistently, reaching its peak at 0.4 g/L concentration before declining at 0.5 g/L. The increments range from 2.80% to 21.29%, depending on the concentration and probability level. NE base oil shows similar trends with consistent increases in BDV up to 0.4 g/L concentration and a slight decrease at 0.5 g/L. For MO base oil, the initial BDV values are higher, starting at 60.30 kV, 68.20 kV, and 75.30 kV. The BDV increases significantly with the addition of Gr NPs, showing the highest increments at 0.2 g/L and 0.3 g/L concentrations, with up to 31.36% improvement at the 10% probability level.

**Table 3.5** AC BDV of Gr nanofluids for different probability levels.

Gr						
	1 %		10 %		50 %	
	BDV (kV)	Increment (%)	BDV (kV)	Increment (%)	BDV (kV)	Increment (%)
SE	0.0	46.50	—	55.90	—	64.90
	0.1	54.10	16.34	63.10	12.88	71.30 09.86
	0.2	56.40	21.29	64.20	14.84	71.20 09.70
	0.3	50.40	08.30	63.60	13.77	76.60 18.03
	0.4	47.80	02.80	61.30	09.66	74.70 15.10
	0.5	50.20	07.95	62.50	11.80	74.60 14.90
NE	0.0	51.10	—	62.50	—	73.40 —
	0.1	58.30	14.09	66.70	06.72	74.30 01.23
	0.2	60.30	18.00	70.60	12.96	80.10 09.13
	0.3	54.90	07.44	69.00	10.40	82.80 12.81
	0.4	61.00	19.37	69.00	10.40	76.30 03.95
	0.5	47.20	-7.63	56.80	-9.12	65.80 -10.35
MO	0.0	60.30	—	68.20	09.12	75.30 —
	0.1	64.50	06.97	74.00	18.40	82.60 09.69
	0.2	74.80	24.05	81.30	30.08	86.80 15.27
	0.3	73.80	22.39	82.10	31.36	89.40 18.73
	0.4	69.20	14.76	78.20	25.12	86.20 14.48
	0.5	67.90	12.60	74.90	19.84	81.00 07.57

### 3.3 Semi-Conducting nanoparticles

#### 3.3.1 AC breakdown voltage

Figure 3.7 gives the mean AC BDV and max/min values for the base liquids and the various NFs with ZnO for different concentrations, respectively. As previously mentioned, the breakdown does not occur for a 2.5 mm electrode gap with ZnO for SE. As depicted in Figure 3.7, ZnO NPs generally enhance the performance of various NFs, except for those containing NE at concentrations of 0.1 g/L and 0.5 g/L. Specifically:

- SE-based NFs see improvements ranging from 5.8% to 19.38%, with the highest enhancement at 0.4 g/L.

- NE-based NF experiences a maximum improvement of about 5.7% at 0.3 g/L.

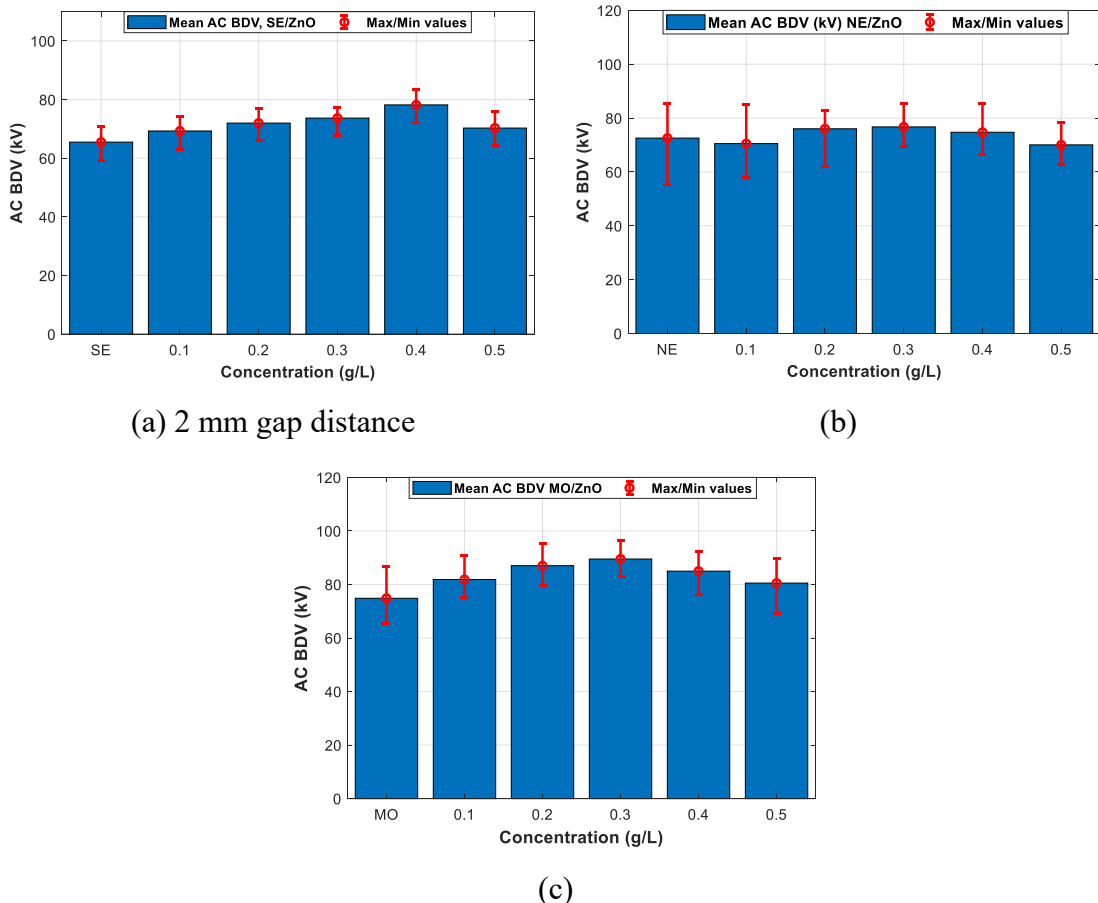


**Figure 3.7** Mean breakdown voltages of nanofluid containing ZnO at different concentrations for (a) synthetic ester, (b) natural ester, and (c) mineral oil.

- MO-based NFs show gains between 7.6% and 19.59%, peaking at 0.3 g/L.

### 3.3.2 Anderson-Darling (AD) goodness-of-fit test

Table 3.6 presents the results of an AD goodness-of-fit test on semi-conducting NP-based NFs. The NFs analyzed include SE, NE, and MO, each integrated with ZnO NPs at various concentrations (0.1 g/L to 0.5 g/L). For SE NFs, the *p*-values generally indicated acceptance of the null hypothesis across most concentrations, except at 0.5 g/L. Similar trends were observed for NE and MO NFs, with most concentrations showing acceptance, highlighting the suitability of these NFs under test conditions.

### 3.3.3 Weibull probability analysis

Table 3.7 lists the scale and shape parameters for ZnO for each NF type, showing variations in values corresponding to different concentrations. Similar to conducting NPs,

**Table 3.6** Table AD goodness-of-fit test results of semi-conducting NPs-based NFs.

m/V (g/L)	<i>p</i> -value	Decision	m/V (g/L)	<i>p</i> -value	Decision	m/V (g/L)	<i>p</i> -value	Decision
SE	0.20	Accepted	NE	0.63	Accepted	MO	0.10	Accepted
SE NF with ZnO								
0.1	0.0564	Accepted	0.1	0.07	Accepted	0.1	0.34	Accepted
0.2	0.37	Accepted	0.2	0.22	Accepted	0.2	0.07	Accepted
0.3	0.70	Accepted	0.3	0.28	Accepted	0.3	0.11	Accepted
0.4	0.60	Accepted	0.4	0.49	Accepted	0.4	0.32	Accepted
0.5	0.0247<	Rejected	0.5d	0.72	Accepted	0.5	0.41	Accepted

**Table 3.7** Scale and shape parameters of semi-conducting NP-based NFs.

Concentration (g/L)	ZnO					
	SE		NE		MO	
	$\alpha$ (scale)	$\beta$ (shape)	$\alpha$ (scale)	$\beta$ (shape)	$\alpha$ (scale)	$\beta$ (shape)
0.0	65.15	10.52	75.73	11.65	76.76	18.96
0.1	80.42	14.98	73.54	10.92	84.08	18.46
0.2	73.24	22.07	78.42	18.23	89.34	18.81
0.3	76.82	14.33	78.92	17.75	91.54	24.04
0.4	80.36	21.95	77.15	15.35	87.37	19.38
0.5	71.24	20.78	72.18	16.92	83.13	16.57

those values were utilized to plot the Weibull curves, as illustrated in Figure 3.8. Those plots are then used to evaluate the BDV. Table 3.8 records BDV percentages at different ZnO concentrations, showing increments across 1%, 10%, and 50% probabilities levels.

For SE, the BDV starts at 46.50 kV for 1%, 55.90 kV for 10%, and 64.90 kV for 50% without ZnO. With increasing ZnO concentration, there is significantly improvement in BDV, especially at 0.4 g/L ZnO, where the BDV increases by 40.22% for the 1% probability level. However, there are some fluctuations at 0.3 g/L and 0.5 g/L concentrations.

In the case of NE, for 0.1 g/L ZnO, BDV decreases across all probability levels, with the most significant negative increment at 1% (-5.48%). Positive increments begin at 0.2 g/L ZnO, peaking at 19.37% for the 1% probability level. The increment values show a general trend of improvement, with some decline at the 0.5 g/L concentration.

For MO, positive increments are observed at all ZnO concentrations, with the highest at 0.3 g/L ZnO (25.37% for the 1% probability level). The pattern of increments

is generally consistent and positive, indicating an overall increase in BDV with higher ZnO concentrations, up to 0.4 g/L.

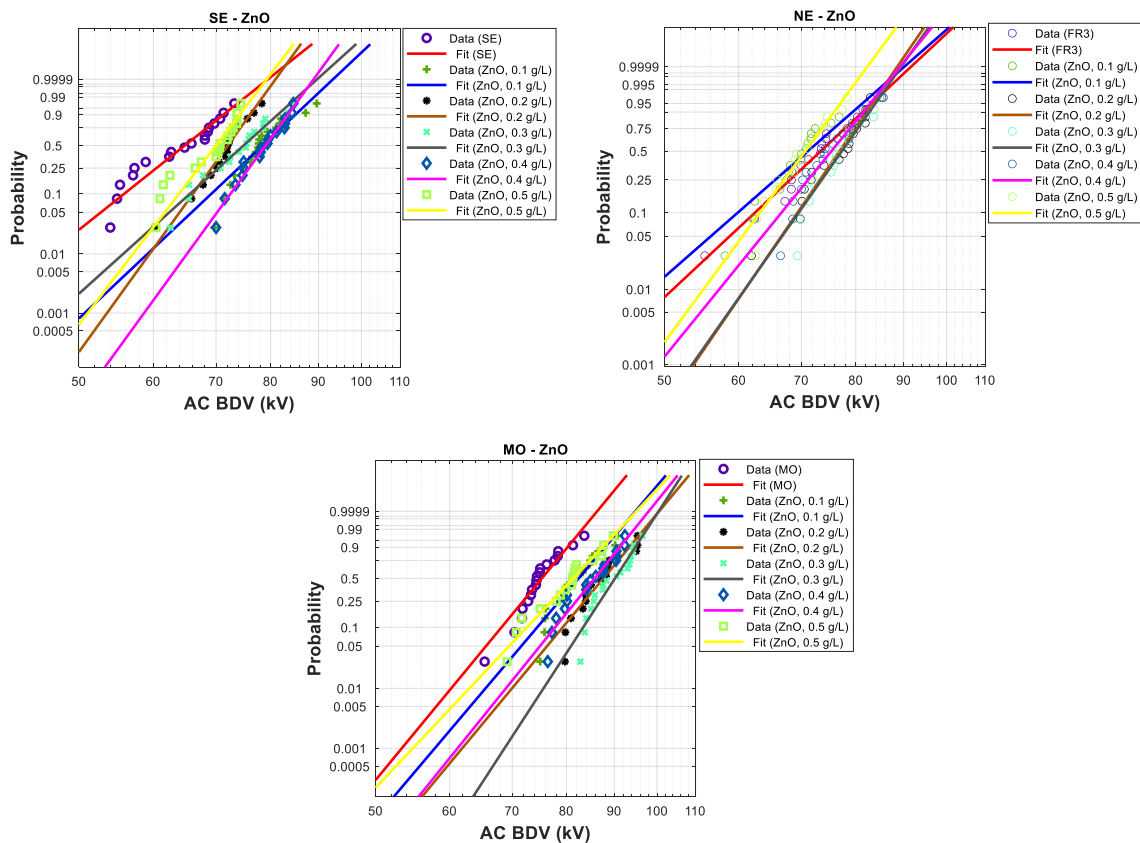


**Figure 3.8** Weibull probability plots of breakdown voltages of nanofluid containing ZnO at different concentrations for (a) synthetic ester, (b) natural ester, and (c) mineral oil.

Adding ZnO NPs generally enhances the BDV of base oils, with variations depending on the type of oil and the concentration of ZnO. SE shows significant improvements with some fluctuations, and NE exhibits mixed results with initial

decreases. Following improvements, MO demonstrates steady and significant increases in BDV with increasing ZnO concentration.

**Table 3.8** The AC BDV of ZnO nanofluids for different probability levels.

ZnO						
	1 %		10 %		50 %	
	BDV (kV)	Increment (%)	BDV (kV)	Increment (%)	BDV (kV)	Increment (%)
SE	0.0	46.50	–	55.90	–	64.90
	0.1	59.20	27.31	69.30	23.97	78.50
	0.2	59.50	27.96	66.20	18.43	72.10
	0.3	55.80	20.00	65.70	17.53	74.90
	0.4	65.20	40.22	72.60	29.87	79.10
	0.5	57.10	22.80	64.00	14.49	70.00
NE	0.0	51.10	–	62.50	–	73.40
	0.1	48.30	-5.48	59.90	-4.16	71.20
	0.2	61.00	19.37	69.40	11.04	76.90
	0.3	60.90	19.18	69.40	11.04	77.40
	0.4	57.20	11.94	66.70	06.72	75.40
	0.5	55.00	07.63	63.20	01.12	70.70
MO	0.0	60.30	–	68.20	–	75.30
	0.1	65.60	08.79	74.50	09.24	82.50
	0.2	70.00	16.09	79.30	16.28	87.70
	0.3	75.60	25.37	83.40	22.29	90.20
	0.4	69.00	14.43	77.80	14.08	85.80
	0.5	63.00	04.48	72.60	06.45	81.40

## 3.4 Insulating nanoparticles

### 3.4.1 AC breakdown voltage

Figure 3.9 illustrates the mean BDV of NFs containing Al<sub>2</sub>O<sub>3</sub> NPs (20-30 nm) at different concentrations across SE, NE, and MO. For SE, the mean BDV shows an increasing trend with adding Al<sub>2</sub>O<sub>3</sub> NPs.

- At lower concentrations, there is a noticeable increase in BDV, indicating that small amounts of NPs significantly enhance the dielectric strength of the SE.

---

### *3. AC Breakdown Voltage of Nanofluids-Based SE, NE, and MO*

---

- The trend suggests that the dielectric improvement stabilizes or slightly increases with higher concentrations of Al<sub>2</sub>O<sub>3</sub> NPs.
- The highest improvement is about 44% at 0.3 g/L.

Similar to SE, the NE increases BDV by adding Al<sub>2</sub>O<sub>3</sub> NPs.

- The increment is more pronounced at lower concentrations, stabilizing at higher concentrations.
- The NE appears to benefit from the presence of Al<sub>2</sub>O<sub>3</sub> NPs, showing an overall enhancement in dielectric strength.
- The best concentration is 0.2 g/L, which improves it by 10.44%.

MO also shows an increase in BDV with the addition of Al<sub>2</sub>O<sub>3</sub> NPs.

The pattern is consistent with synthetic and natural esters, with the most significant improvements observed at lower concentrations.

- Higher concentrations of NPs continue to show improvement, but at a reduced rate compared to lower concentrations. The optimal concentration is about 0.3 g/L, manifesting as an increment of 25.33%.

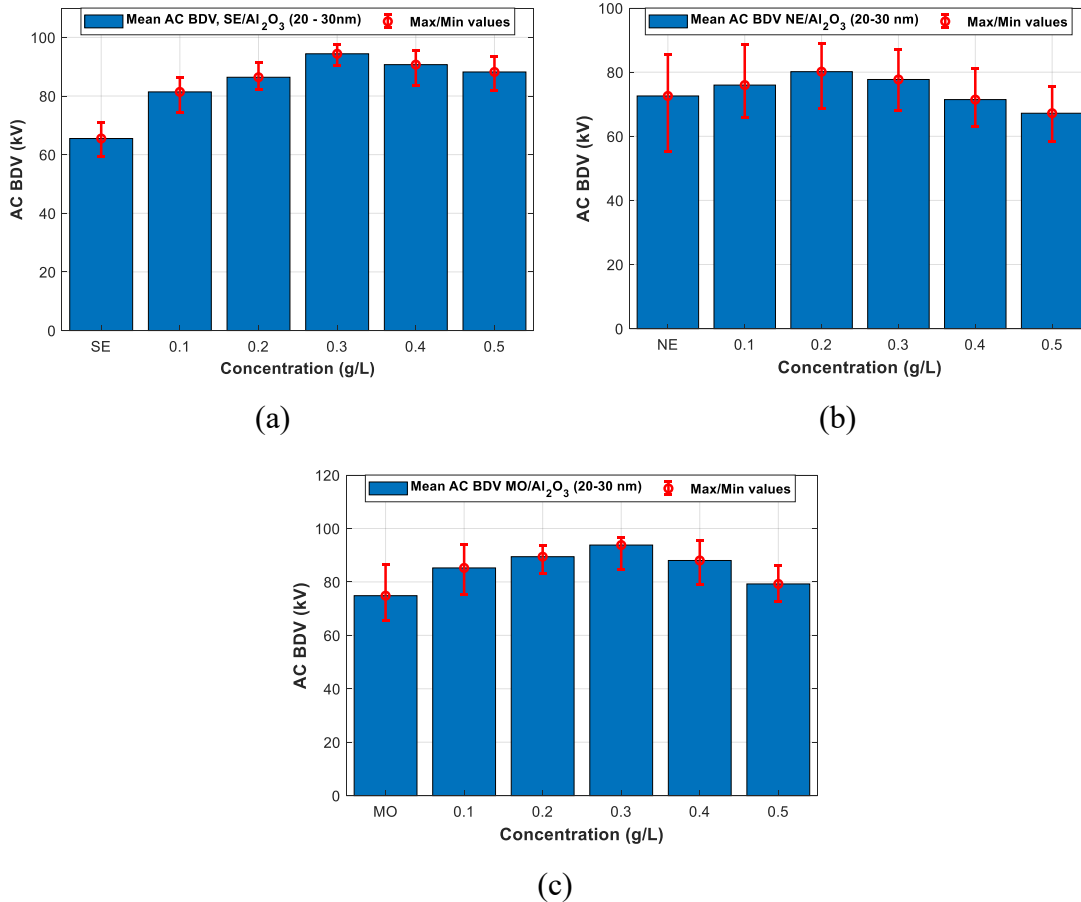


**Figure 3.9** Mean breakdown voltages of nanofluid containing  $\text{Al}_2\text{O}_3$  (20-30 nm) at different concentrations for (a) synthetic ester, (b) natural ester, and (c) mineral oil.

Figure 3.10 illustrates the mean breakdown voltages of NFs containing  $\text{Al}_2\text{O}_3$  NPs (50 nm) at different concentrations for SE, NE, and MO.

For SE, the mean BDV increases with the addition of  $\text{Al}_2\text{O}_3$  NPs.

- The increase is significant at lower concentrations and continues to rise with higher concentrations, though at a reduced rate.
- The dielectric enhancement is apparent, showing that larger  $\text{Al}_2\text{O}_3$  NPs effectively improve the BDV of SE.
- The best concentration is 0.4 g/L, which improves 42.13% at 0.4 g/L.

The BDV of NE increases with the addition of  $\text{Al}_2\text{O}_3$  (50 nm) NPs.

- The most significant improvements are seen at a concentration of 0.2 g/L, with a steady increase observed at higher concentrations.
- The trend suggests that NE benefits from the larger NPs, improving its dielectric properties.
- The highest improvement is about 11.54% at 0.2 g/L.

MO shows an increase in BDV with adding 50 nm  $\text{Al}_2\text{O}_3$  NPs.

- The pattern is similar to SE and NE, with the highest improvements at lower concentrations.
- Higher concentrations still have positive effects, but the rate of increase is slowing down.
- 0.3 g/L manifests the best improvements with 19.60% of improvement.

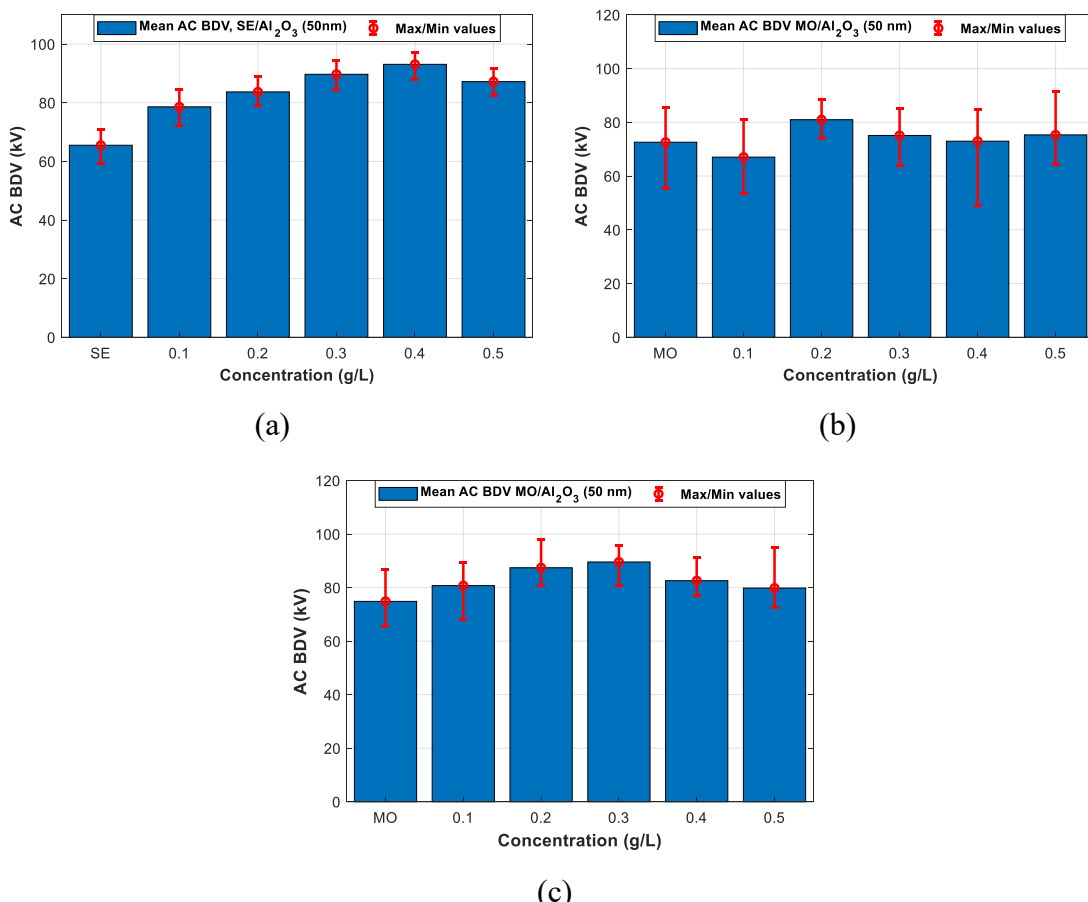


**Figure 3.10** Mean breakdown voltages of nanofluid containing  $\text{Al}_2\text{O}_3$  (50 nm) at different concentrations for (a) synthetic ester, (b) natural ester, and (c) mineral oil.

Both Figures 3.9 and 3.10 demonstrate that adding  $\text{Al}_2\text{O}_3$  NPs, regardless of their size, improves the dielectric strength of SE, NE, and MO. The most substantial improvements in BDV are observed at lower NPs concentrations, with the enhancement effect stabilizing or slightly increasing at higher concentrations. Comparison of the two figures indicates that the size of the NPs (20-30 nm vs. 50 nm) affects the degree of improvement; in other words, for small NPs (which means higher surface contact), the best improvements are reached at lower concentrations, with both sizes contributing positively to the dielectric properties of the base oils.

Figure 3.11 includes an analysis of the mean BDV of nanofluids containing  $\text{ZrO}_2$  NPs at different concentrations for SE, NE, and MO.

For SE, the mean BDV increases with the addition of  $\text{ZrO}_2$  NPs.

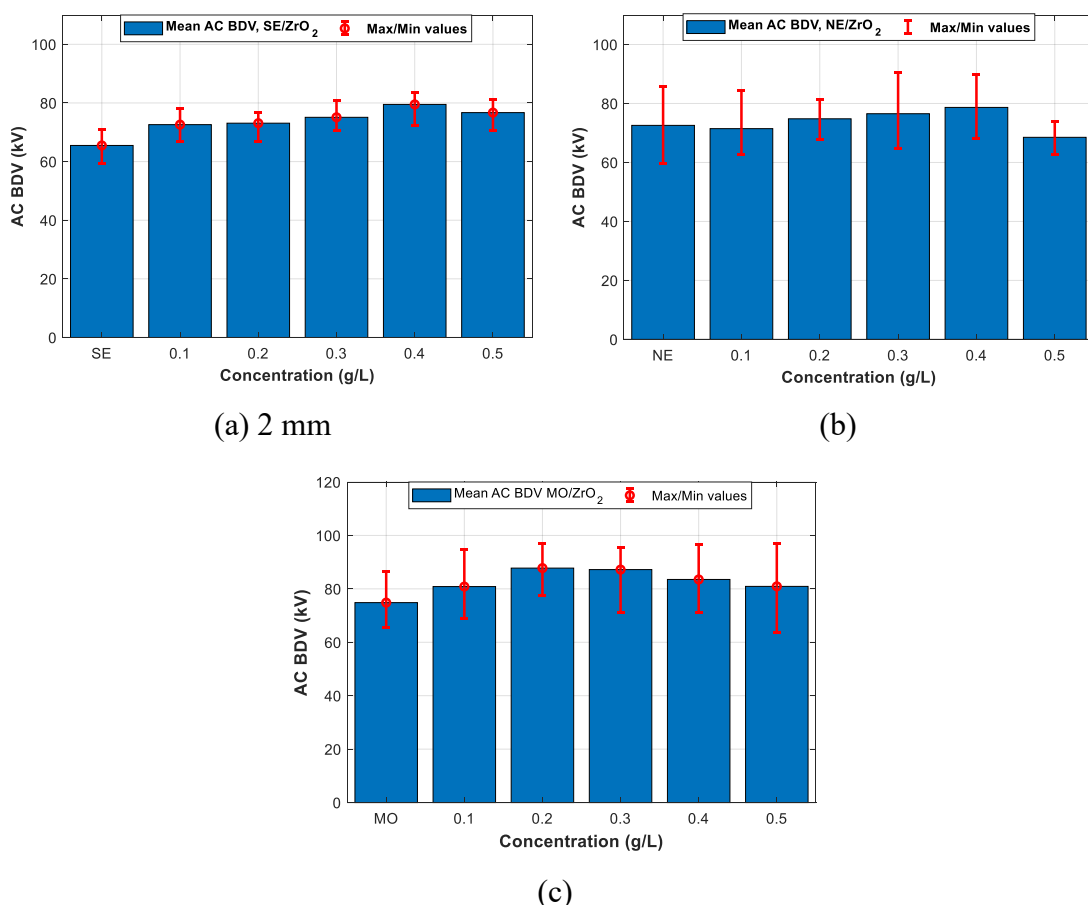


**Figure 3.11** Mean breakdown voltages of nanofluid containing  $\text{ZrO}_2$  at different concentrations for (a) synthetic ester, (b) natural ester, and (c) mineral oil.

- At lower concentrations, there is a noticeable enhancement in BDV, indicating that even small amounts of ZrO<sub>2</sub> NPs can significantly improve the dielectric strength.
- As the concentration of ZrO<sub>2</sub> increases, the BDV continues to rise to 0.4 g/L, showing a trend of consistent improvement.

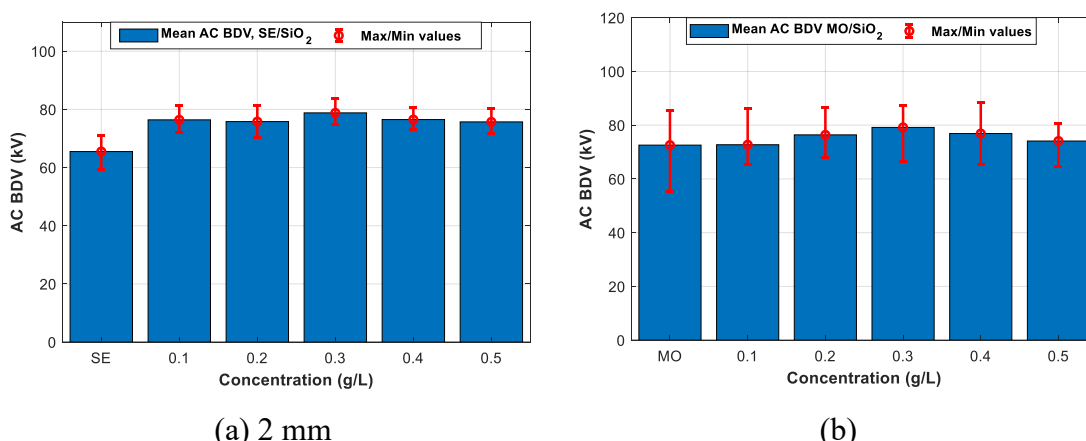
Similar to SE, the NE shows increased BDV by adding ZrO<sub>2</sub> nanoparticles.

- The improvement is more pronounced at lower concentrations, with a steady increase as the concentration increases.
- The NE benefits from the presence of ZrO<sub>2</sub> NPs up to the optimal concentration of 0.4 g/L, enhancing its dielectric properties.

MO exhibits an increase in BDV with the addition of ZrO<sub>2</sub> NPs.

- The pattern of improvement is consistent with that of SE and NE, with significant improvements at lower concentrations and a steady increase at higher concentrations.
- The addition of ZrO<sub>2</sub> NPs effectively enhances the dielectric strength of MO with an optimal concentration of 0.2 g/L.

The analysis of these three graphs in Figure 3.12 reveals the impact of SiO<sub>2</sub> NPs concentration on the AC BDV of different liquids: SE, NE, and MO. All three liquids show improvement in AC BDV with adding NPs, but to varying degrees. MO exhibits the highest base BDV and the most significant absolute improvement, peaking at about 90 kV at a concentration of 0.3 g/L. SE shows consistent improvement across



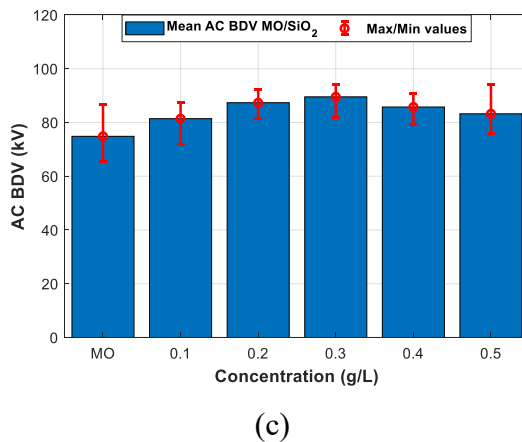


**Figure 3.12** Mean breakdown voltages of nanofluid containing  $\text{SiO}_2$  at different concentrations for (a) synthetic ester, (b) natural ester, and (c) mineral oil.

concentrations, peaking at 0.3 g/L. NE demonstrates a moderate increase, reaching its maximum at 0.3 g/L (9% compared to SE), but with more variability in measurements. Interestingly, all fluids show an optimal NPs concentration range of 0.2-0.3 g/L, suggesting a common improvement mechanism. Beyond this range, there's a slight decline in performance for all fluids. This consistency in optimal concentration across different base fluids indicates that while the magnitude of improvement varies, the underlying physics of how NPs enhance dielectric strength may be similar.

### 3.4.2 Anderson-Darling (AD) goodness-of-fit test

Table 3.9 presents the AD goodness-of-fit test results for NFs with different insulating NPs across three base oils: SE, NE, and MO. The table includes *p*-values and decisions (Accepted or Rejected) for each combination of NPs, liquid type, and concentration.

For  $\text{Al}_2\text{O}_3$  NPs (20-30 nm), SE shows acceptance of the null hypothesis at concentrations ranging from 0.1 g/L to 0.2 g/L and 0.4 g/L to 0.5 g/L, but rejection at 0.3 g/L with a *p*-value of 0.0066. NE and MO accept  $\text{Al}_2\text{O}_3$  (20-30 nm) at all tested concentrations. For  $\text{Al}_2\text{O}_3$  NPs (50 nm), SE accepts concentrations of 0.1 g/L, 0.3 g/L to 0.5 g/L while rejecting at 0.2 g/L with a *p*-value of 0.0012. Both NE and MO accept all concentrations of  $\text{Al}_2\text{O}_3$  (50 nm).

For  $\text{ZrO}_2$  NPs, SE accepts concentrations from 0.1 g/L to 0.4 g/L but rejects at 0.5 g/L with a *p*-value of 0.0408. NE accepts all concentrations except for 0.2 g/L, which is rejected with a *p*-value of 0.049. MO accepts all concentrations of  $\text{ZrO}_2$ . For  $\text{SiO}_2$  NPs,

### 3. AC Breakdown Voltage of Nanofluids-Based SE, NE, and MO

SE accepts concentrations of 0.1 g/L, 0.2 g/L, 0.3 g/L, and 0.5 g/L, but rejects 0.4 g/L with a *p*-value of 0.0381. NE rejects lower concentrations of 0.1 g/L and 0.2 g/L with *p*-values of 0.0494 and 0.034, respectively, but accepts higher concentrations. MO accepts all concentrations of SiO<sub>2</sub>.

**Table 3.9** AD goodness-of-fit test results of insulating NPs based NFs.

m/V (g/L)	<i>p</i> -value	Decision	m/V (g/L)	<i>p</i> -value	Decision	m/V (g/L)	<i>p</i> -value	Decision
SE	0.20	Accepted	NE	0.63	Accepted	MO	0.10	Accepted
SE NF with Al <sub>2</sub> O <sub>3</sub> (20-30 nm)			NE NF with Al <sub>2</sub> O <sub>3</sub> (20-30 nm)			MO NF with Al <sub>2</sub> O <sub>3</sub> (20-30 nm)		
0.1	0.88	Accepted	0.1	0.37	Accepted	0.1	0.57	Accepted
0.2	0.22	Accepted	0.2	0.69	Accepted	0.2	0.40	Accepted
0.3	0.0066<	Rejected	0.3	0.056	Accepted	0.3	0.09	Accepted
0.4	0.30	Accepted	0.4	0.30	Accepted	0.4	0.95	Accepted
0.5	0.84	Accepted	0.5	0.82	Accepted	0.5	0.27	Accepted
SE NF with Al <sub>2</sub> O <sub>3</sub> (50 nm)			NE NF with Al <sub>2</sub> O <sub>3</sub> (50 nm)			MO NF with Al <sub>2</sub> O <sub>3</sub> (50 nm)		
0.1	0.06	Accepted	0.1	0.20	Accepted	0.1	0.66	Accepted
0.2	0.0012<	Rejected	0.2	0.18	Accepted	0.2	0.21	Accepted
0.3	0.68	Accepted	0.3	0.61	Accepted	0.3	0.90	Accepted
0.4	0.51	Accepted	0.4	0.69	Accepted	0.4	0.29	Accepted
0.5	0.38	Accepted	0.5	0.08	Accepted	0.5	0.16	Accepted
SE NF with ZrO <sub>2</sub>			NE NF with ZrO <sub>2</sub>			MO NF with ZrO <sub>2</sub>		
0.1	0.08	Accepted	0.1	0.07	Accepted	0.1	0.29	Accepted
0.2	0.88	Accepted	0.2	0.049<	Rejected	0.2	0.57	Accepted
0.3	0.21	Accepted	0.3	0.34	Accepted	0.3	0.56	Accepted
0.4	0.24	Accepted	0.4	0.45	Accepted	0.4	0.25	Accepted
0.5	0.0408<	Rejected	0.5	0.77	Accepted	0.5	0.51	Accepted
SE NF with SiO <sub>2</sub>			NE NF with SiO <sub>2</sub>			MO NF with SiO <sub>2</sub>		
0.1	0.93	Accepted	0.1	0.0494	Rejected	0.1	0.69	Accepted
0.2	0.54	Accepted	0.2	0.034	Rejected	0.2	0.84	Accepted
0.3	0.34	Accepted	0.3	0.17	Accepted	0.3	0.79	Accepted
0.4	0.0381<	Rejected	0.4	0.269	Accepted	0.4	0.47	Accepted
0.5	0.2678	Accepted	0.5	0.280	Accepted	0.5	0.06	Accepted

### 3.4.3 Weibull probability analysis

Table 3.10 provides the scale and shape parameters for NFs containing different insulating NPs across SE, NE, and MO. These parameters are essential for plotting the Weibull statistical distribution of the BDV data, as illustrated in Figures 3.13 to 3.16. As for the other liquids presented above, those plots are then used to calculate the voltage at different probabilities.

**Table 3.10** Scale and shape parameters of insulating NPs-based NFs.

Al <sub>2</sub> O <sub>3</sub> (20-30 nm)						
Concentration (g/L)	SE		NE		MO	
	$\alpha$ (scale)	$\beta$ (shape)	$\alpha$ (scale)	$\beta$ (shape)	$\alpha$ (scale)	$\beta$ (shape)
0.0			75.30	11.65		
0.1	78.50	13.85	78.80	13.26	87.36	20.41
0.2	88.31	25.34	82.76	16.50	90.76	38.87
0.3	95.09	27.76	79.98	16.91	95.09	47.29
0.4	92.88	40.11	73.50	16.87	90.05	23.63
0.5	89.81	16.28	69.29	16.53	81.12	22.30
Al <sub>2</sub> O <sub>3</sub> (50 nm)						
Concentration (g/L)	SE		NE		MO	
	$\alpha$ (scale)	$\beta$ (shape)	$\alpha$ (scale)	$\beta$ (shape)	$\alpha$ (scale)	$\beta$ (shape)
0.1	80.52	20.85	70.17	10.18	82.93	19.34
0.2	85.49	26.65	76.85	10.23	89.60	18.65
0.3	93.54	19.61	77.77	14.39	91.24	27.64
0.4	94.54	27.68	82.93	21.18	84.34	20.84
0.5	94.44	29.38	78.22	11.63	82.65	16.22
ZrO <sub>2</sub>						
Concentration (g/L)	SE		NE		MO	
	$\alpha$ (scale)	$\beta$ (shape)	$\alpha$ (scale)	$\beta$ (shape)	$\alpha$ (scale)	$\beta$ (shape)
0.1	87.44	19.42	73.83	13.66	83.83	13.06
0.2	89.94	23.48	76.45	22.50	90.30	18.40
0.3	91.90	26.97	79.40	12.71	90.11	17.17
0.4	93.57	27.26	81.07	16.13	86.74	12.65
0.5	90.95	22.42	69.95	25.20	84.46	10.64
SiO <sub>2</sub>						
Concentration (g/L)	SE		NE		MO	
	$\alpha$ (scale)	$\beta$ (shape)	$\alpha$ (scale)	$\beta$ (shape)	$\alpha$ (scale)	$\beta$ (shape)
0.1	77.49	24.06	75.31	12.80	83.05	26.52
0.2	76.94	15.46	78.92	14.60	88.73	34.32
0.3	81.74	18.63	81.17	20.66	90.99	36.37
0.4	77.83	18.36	79.61	13.93	87.38	29.82
0.5	77.45	16.21	76.18	19.98	85.86	15.25

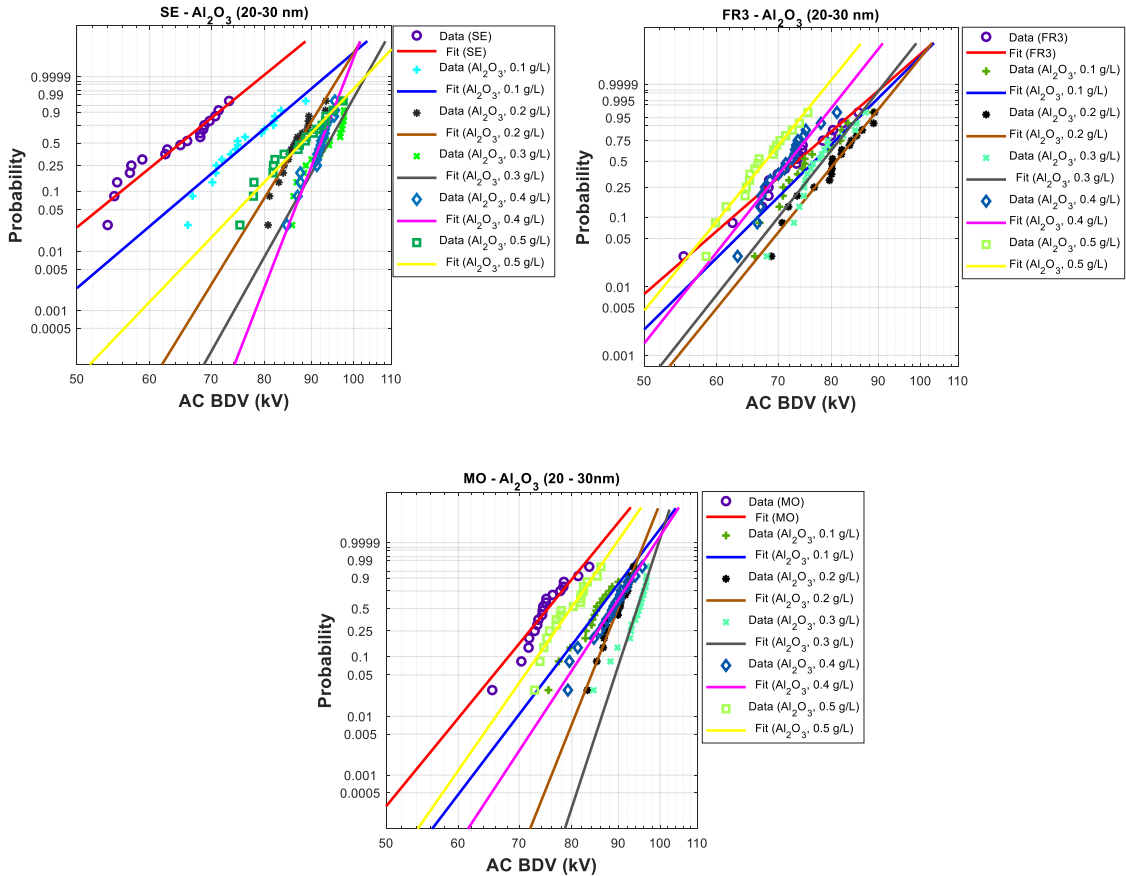


**Figure 3.13** Weibull probability plots of breakdown voltages of nanofluid containing  $\text{Al}_2\text{O}_3$  (20-30 nm) at different concentrations for (a) synthetic ester, (b) natural ester, and (c) mineral oil.

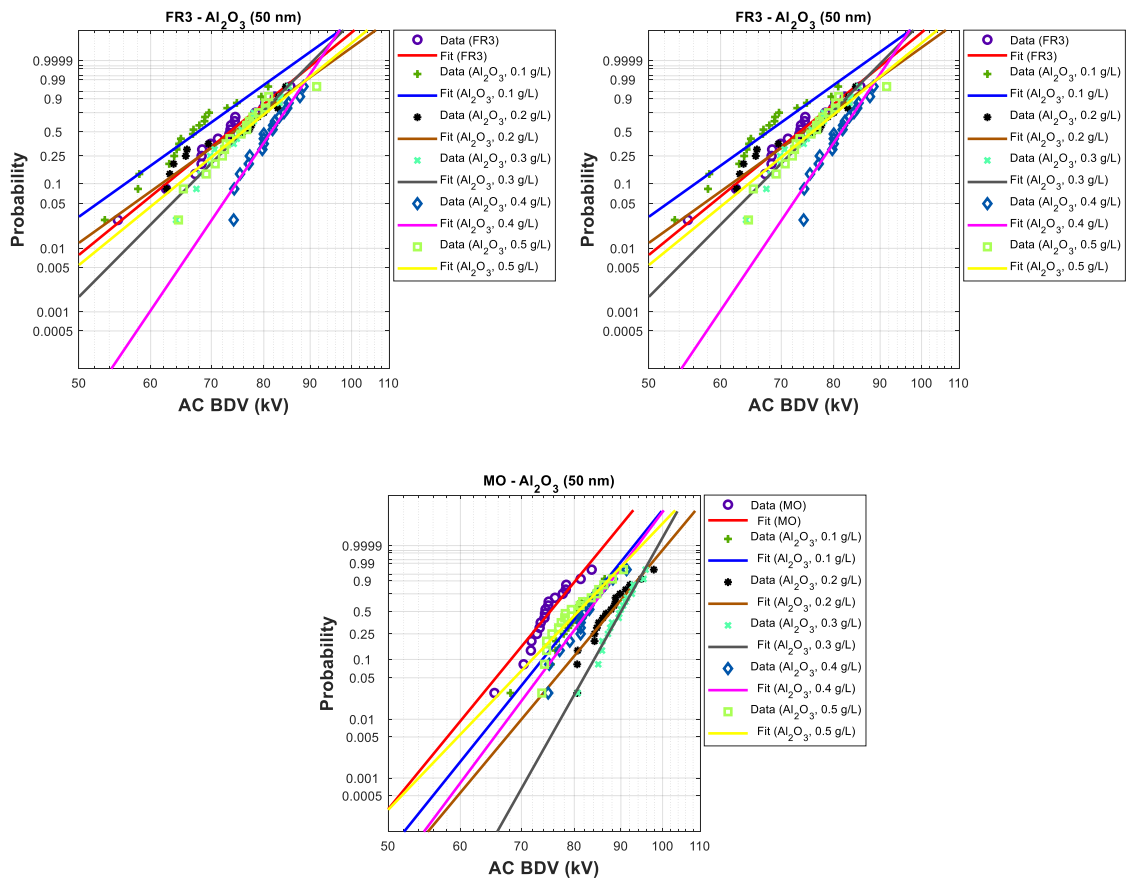


**Figure 3.14** Weibull probability plots of breakdown voltages of nanofluid containing  $\text{Al}_2\text{O}_3$  (50 nm) at different concentrations for (a) synthetic ester, (b) natural ester, and (c) mineral oil.

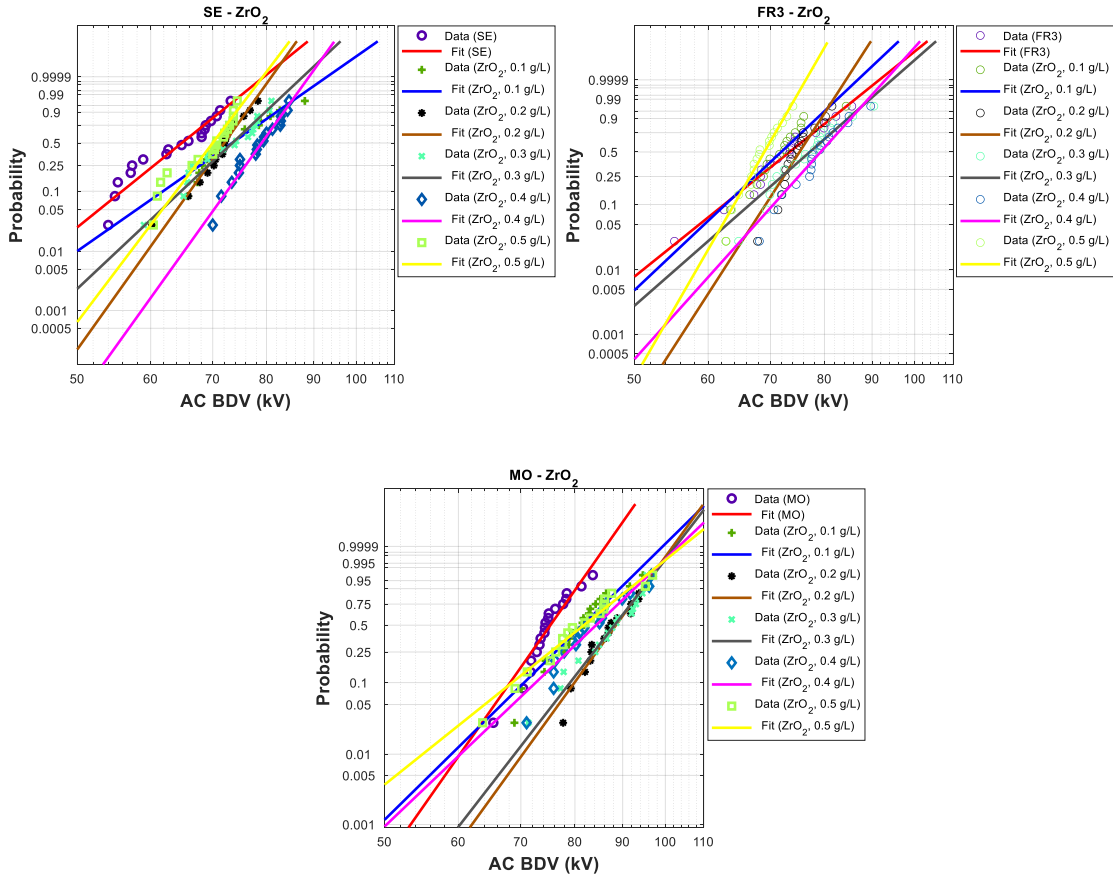


**Figure 3.15** Weibull probability plots of breakdown voltages of nanofluid containing  $\text{ZrO}_2$  at different concentrations for (a) synthetic ester, (b) natural ester, and (c) mineral oil.

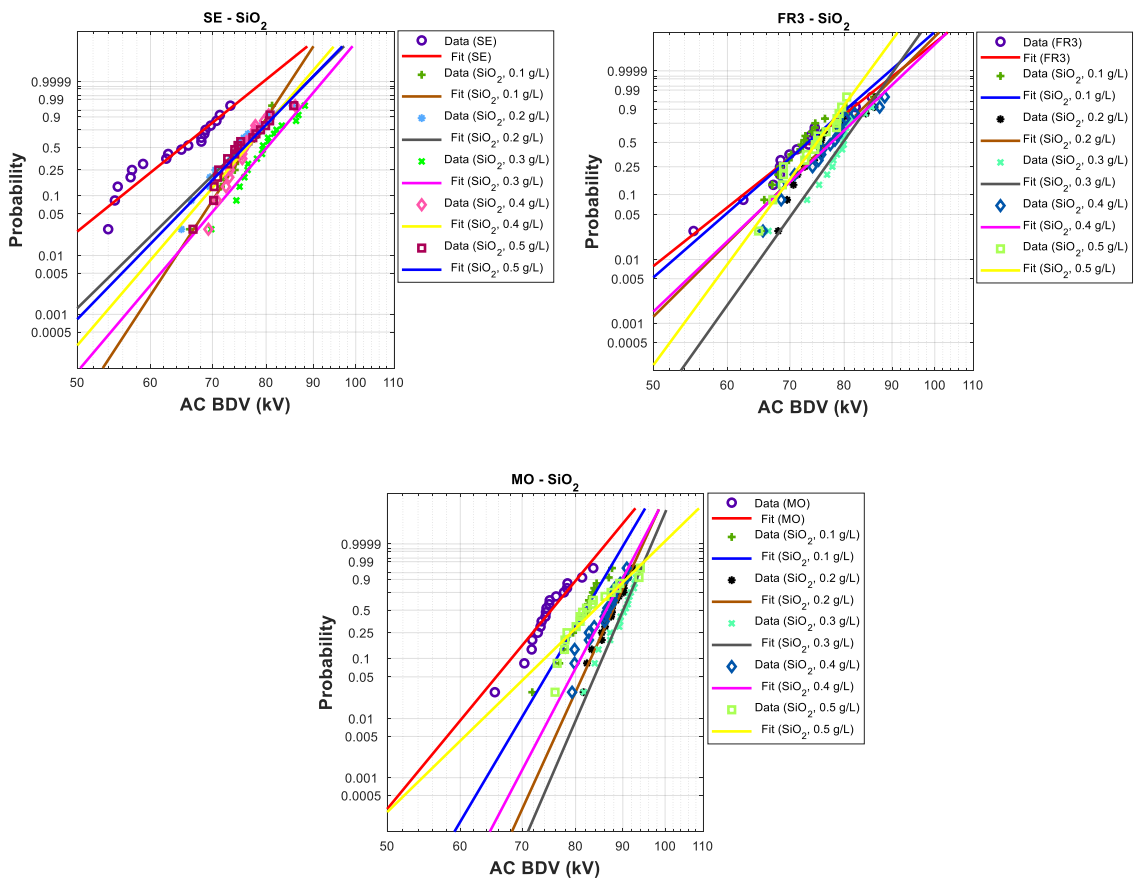


**Figure 3.16** Weibull probability plots of breakdown voltages of nanofluid containing  $\text{SiO}_2$  at different concentrations for: (a) synthetic ester, (b) natural ester, and (c) mineral oil.

### 3. AC Breakdown Voltage of Nanofluids-Based SE, NE, and MO

Table 3.11 shows BDV values and percentage increases for SE, NE, and MO with different concentrations of Al<sub>2</sub>O<sub>3</sub> NPs (20-30 nm). For SE, BDV increases significantly with higher concentrations of Al<sub>2</sub>O<sub>3</sub>, peaking at 0.4 g/L with an increase of 78.28% for 1% probability.

- At 0.5 g/L, the BDV decreases but substantially increases over the base value.
- Optimal concentration appears to be around 0.3-0.4 g/L.

For NE, the BDV shows initial improvement at 0.1 g/L, peaking at 0.2 g/L with a 22.70% increase for 1% probability.

- BDV decreases at higher concentrations, particularly at 0.5 g/L, where negative increments are observed.
- The optimal concentration is around 0.2 g/L.

**Table 3.11** The AC BDV of Al<sub>2</sub>O<sub>3</sub> (20-30 nm) nanofluids for different probability levels.

Al <sub>2</sub> O <sub>3</sub> (20-30 nm)						
	1 %		10 %		50 %	
	BDV (kV)	Increment (%)	BDV (kV)	Increment (%)	BDV (kV)	Increment (%)
SE	0.0	46.50	–	55.90	–	64.90
	0.1	55.20	18.71	66.70	19.32	76.90
	0.2	73.70	58.49	80.90	44.72	87.10
	0.3	80.60	73.33	87.70	56.89	93.90
	0.4	82.90	78.28	87.90	57.25	92.10
	0.5	67.70	45.59	78.30	40.07	87.90
NE	0.0	51.10	–	62.50	–	73.40
	0.1	55.70	09.00	66.60	6.56	76.70
	0.2	62.70	22.70	72.30	15.68	81.00
	0.3	61.00	19.37	70.10	12.16	78.30
	0.4	56.00	09.59	64.40	03.04	72.00
	0.5	52.50	02.74	60.50	-3.20	67.80
MO	0.0	60.30	–	68.20	–	75.30
	0.1	69.80	15.75	78.30	14.81	85.90
	0.2	80.70	33.83	85.70	25.66	89.90
	0.3	86.30	43.12	90.70	32.99	94.40
	0.4	74.20	23.05	81.90	20.09	88.70
	0.5	66.00	09.45	73.40	07.62	79.90

### 3. AC Breakdown Voltage of Nanofluids-Based SE, NE, and MO

In the case of MO, the BDV steadily increases with concentration, peaking at 0.3 g/L with a 43.12% increase for 1% probability.

- The increment decreases slightly at 0.4 g/L but remains positive.
- Optimal concentration is around 0.3 g/L.

Table 3.12 shows BDV values for Al<sub>2</sub>O<sub>3</sub> NPs (50 nm) across the same base oils.

- The BDV significantly increases with NPs concentration, peaking at 0.5 g/L with a 73.76% increase for 1% probability.
- Optimal concentration is around 0.4-0.5 g/L.

For NE, the lower concentrations result in negative increments, but BDV improves significantly at 0.4 g/L with a 30.72% increase for 1% probability. The optimal concentration is around 0.4 g/L. The BDV increases steadily in the case of MO, peaking at 0.3 g/L with a 28.19% increase for a 1% probability.

**Table 3.12** The AC BDV of Al<sub>2</sub>O<sub>3</sub> (50 nm) nanofluids for different probability levels.

Al <sub>2</sub> O <sub>3</sub> (50 nm)							
	1 %		10 %		50 %		
	BDV (kV)	Increment (%)	BDV (kV)	Increment (%)	BDV (kV)	Increment (%)	
SE	0.0	46.50	–	55.90	–	64.90	–
	0.1	64.60	38.92	72.30	29.34	79.20	22.03
	0.2	72.00	54.84	78.60	40.61	84.40	30.05
	0.3	74.00	59.14	83.50	49.37	91.90	41.60
	0.4	80.10	72.26	87.20	55.99	93.40	43.91
	0.5	80.80	73.76	87.50	56.53	93.30	43.76
NE	0.0	51.10	–	62.50	–	73.40	–
	0.1	44.70	-12.52	56.30	-9.92	67.70	-7.77
	0.2	49.10	-3.91	61.70	-1.28	74.20	01.09
	0.3	56.50	10.57	66.60	6.56	75.90	03.41
	0.4	66.80	30.72	74.60	19.36	81.60	11.17
	0.5	52.70	03.13	64.50	03.20	75.80	03.27
MO	0.0	60.30	–	68.20	–	75.30	–
	0.1	65.40	08.46	73.90	08.36	81.40	08.10
	0.2	70.10	16.25	79.50	16.57	87.90	16.73
	0.3	77.30	28.19	84.20	23.46	90.10	19.65
	0.4	67.70	12.27	75.80	11.14	82.90	10.09
	0.5	62.30	03.32	72.00	05.57	80.90	07.44

### 3. AC Breakdown Voltage of Nanofluids-Based SE, NE, and MO

- The increment decreases at 0.4 g/L but remains positive.
- Optimal concentration is around 0.3 g/L.

Table 3.13 presents BDV values for ZrO<sub>2</sub> NPs. For SE, the BDV increases with concentration, peaking at 0.4 g/L with a 20.20% increase for 1% probability, with an optimal concentration around 0.4 g/L. For NE, the BDV shows significant improvement at 0.2 g/L with a 22.40% increase for 1% probability.

- BDV decreases at higher concentrations, particularly at 0.5 g/L, where a negative increment is observed.
- Optimal concentration is around 0.2-0.3 g/L.

Contrary to the two liquids, MO shows a steadily increased BDV, peaking at 0.2 g/L with a 23.30% increase for 1% probability with an optimal concentration of around 0.2-0.3 g/L.

**Table 3.13** The AC BDV of ZrO<sub>2</sub> nanofluids for different probability levels.

<b>ZrO<sub>2</sub></b>						
	1 %		10 %		50 %	
	BDV (kV)	Increment (%)	BDV (kV)	Increment (%)	BDV (kV)	Increment (%)
SE	0.0	46.50	–	55.90	–	64.90
	0.1	69.00	04.86	77.90	03.87	85.90
	0.2	74.00	12.50	81.80	09.07	88.60
	0.3	77.50	17.80	84.60	12.80	90.70
	0.4	79.10	20.20	86.20	14.90	92.40
	0.5	74.10	12.60	82.30	09.73	89.50
NE	0.0	51.10	–	62.50	–	73.40
	0.1	52.80	03.52	62.70	00.32	71.90
	0.2	62.40	22.40	69.20	10.70	75.30
	0.3	55.30	08.43	66.60	06.56	77.20
	0.4	61.00	19.60	70.60	13.00	79.30
	0.5	58.30	14.30	64.00	02.40	69.00
MO	0.0	60.30	–	68.20	–	75.30
	0.1	59.00	03.30	70.60	06.00	81.60
	0.2	70.40	23.30	80.00	20.10	88.60
	0.3	69.00	20.80	79.10	18.80	88.30
	0.4	60.30	05.60	72.70	09.15	84.30
	0.5	55.00	-3.70	68.60	03.00	81.80

### 3. AC Breakdown Voltage of Nanofluids-Based SE, NE, and MO

Finally, Table 3.14 shows BDV values for SiO<sub>2</sub> NPs with the same matrix. For SE, The BDV increases, peaking at 0.4 g/L with a 37.63% increase for 1% probability with an optimal concentration around 0.3-0.4 g/L.

The initial concentrations with NE show minor improvements, peaking at 0.3 g/L with a 27.20% increase for a 1% probability.

- BDV improves significantly at higher concentrations.
- Optimal concentration is around 0.3-0.4 g/L.

In the case of MO, BDV increases steadily, peaking at 0.3 g/L with a 33.00% increase for a 1% probability.

- The increment decreases at 0.4 g/L but remains positive.
- The optimal concentration is around 0.3 g/L.

**Table 3.14** The AC BDV of SiO<sub>2</sub> nanofluids for different probability levels.

SiO <sub>2</sub>						
	1 %		10 %		50 %	
	BDV (kV)	Increment (%)	BDV (kV)	Increment (%)	BDV (kV)	Increment (%)
SE	0.0	46.50	—	55.90	—	64.90
	0.1	64.00	37.63	70.60	26.30	76.40
	0.2	57.20	23.01	66.60	19.14	75.20
	0.3	63.90	37.42	72.50	29.70	80.20
	0.4	60.60	30.32	68.90	23.26	76.30
	0.5	58.40	25.59	67.50	20.75	75.80
NE	0.0	51.10	—	62.50	—	73.40
	0.1	52.60	2.94	63.20	23.68	73.20
	0.2	57.60	12.72	67.70	32.49	77.00
	0.3	65.00	27.20	72.80	42.47	79.80
	0.4	57.30	12.13	67.80	32.68	77.60
	0.5	60.60	18.59	68.10	33.27	74.90
MO	0.0	60.30	—	68.20	—	75.30
	0.1	69.90	15.92	76.40	12.02	82.00
	0.2	77.60	28.69	83.20	21.99	87.80
	0.3	80.20	33.00	85.60	25.51	90.10
	0.4	74.90	24.21	81.10	18.91	86.40
	0.5	63.50	05.31	74.10	8.65	83.90

### **3.5 Discussion**

Although most studies suggest that NPs' trapping behavior is responsible for improved AC BDV of NFs, this mechanism remains debatable. The key to understanding this mechanism, the effect of NPs (conducting, semi-conducting, or insulating) on the AC dielectric strength of the base liquid, lies in the appearance of surface charge distribution at the interface between NPs and the base fluid with different conductivities and/or relative permittivities, subjected to a uniform applied electric field ( $E_0$ ). According to Sima et al. [37] and Morgan and Green [100], the surface of NPs contains induced and polarized charges, induced charges in the case of conducting NPs, and polarized charges in the case of insulating NPs (dielectric polarization) [37], [100]. Contrary to the idea that a material has only one of the two properties (induced or polarized charges), some materials have both (such as conducting  $\text{Fe}_3\text{O}_4$  with high relative permittivity, i.e.,  $\epsilon_r = 80$ ). In addition, there is a difference in charge density on both sides of the particle, which results in an effective or induced dipole across the particle (two hemispheres with opposite signs) aligned with the applied field [100]. This concept is known as polarizability, as shown in Figure 3.17. Three cases can be distinguished based on the above:

- The first case is when the polarizability of the NP is more significant than the base liquid. That means there are more charges inside the interface (NP side) than outside (liquid side), resulting in a surface charge density difference on both sides. So, an induced dipole is aligned with the field applied through the particle [100]. A suitable example of this case would be a conducting NP (or NP 'insulating or conducting' with a high dielectric constant) in an insulating liquid with a low dielectric constant.
- The second case is when the polarizability of the NP is less significant than the base liquid, meaning there are fewer charges inside the interface (NP side) than outside (liquid side). The resulting dipole points in the opposite direction. This could be an insulating NP suspended in a liquid with a high dielectric constant or conductivity.
- The third case is when the NP and base liquid polarizability are the same, with no net dipole.

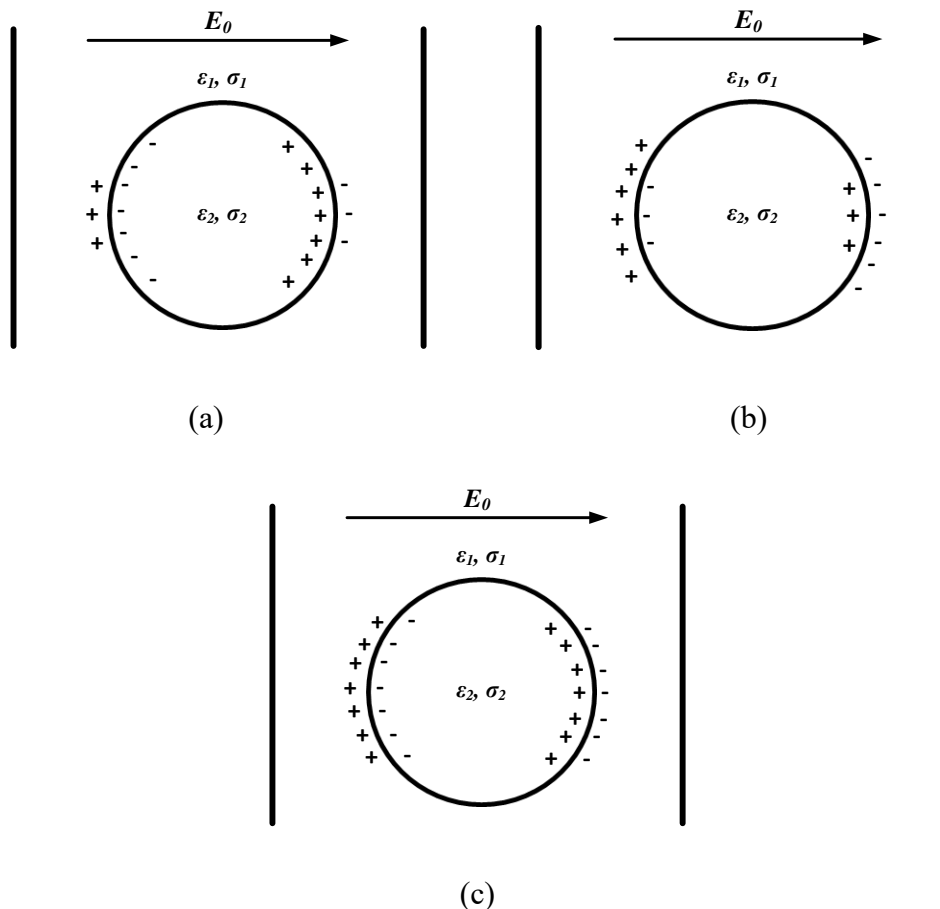


**Figure 3.17** Diagram illustrating the polarization of dielectric particles with (a) higher or (b) lower, and (c) equal polarization capacity compared to the base liquid.

Obviously, the second and the third cases do not correspond to our study since, in most cases, the NPs conductivity and/or permittivity is higher than that of base liquid.

In the present work, conducting, semi-conducting, and insulating NPs are investigated, so the process of charge appearance varies from charge induction to charge polarization [37]; the improvement in the AC BDV in a sphere-to-sphere electrode configuration (quasi-uniform electric field) when adding conducting, semi-conducting, and insulating nanomaterials to SE, NE, and MO, stressed with an AC high-voltage source is possibly due to the electron trapping caused by the formation of the surface charge density. The electrons originating from either ionization or injection move quickly and are trapped by the positively charged pole until saturation. Upon saturation, the negatively charged NPs are considered motionless compared to the mobility of electrons, slowing the streamer's propagation by reducing its velocity and enhancing the BDV of NFs

### 3. AC Breakdown Voltage of Nanofluids-Based SE, NE, and MO

compared to base liquids. Conducting NPs (e.g., Fe<sub>3</sub>O<sub>4</sub>, C<sub>60</sub>, and Gr) induces charges and charges up rapidly due to their fast charge relaxation time constant. Dielectric NPs (e.g., Al<sub>2</sub>O<sub>3</sub>, SiO<sub>2</sub>, ZrO<sub>2</sub>) develop polarized surface charges more slowly. Both types of NPs are capable of capturing electrons despite their differences. The relaxation time constant can be calculated as follows [37].

$$\tau = \left( \frac{2\epsilon_1 + \epsilon_2}{2\sigma_1 + \sigma_2} \right) \quad (3.1)$$

Where  $\epsilon_{1,2}$ ,  $\sigma_{1,2}$  are the permittivities and conductivities of base liquid and NP, respectively. Tables 3.15 and 3.16 show the electrical properties and the relaxation time of different NFs, respectively. If the material is perfectly conductive, such as Fe<sub>3</sub>O<sub>4</sub> NPs, the relaxation time is of the order of 1 to  $10 \times 10^{-14}$  s, which is very quick compared to

**Table 3.15** Electrical properties of base liquids and conducting, semi-conducting, and dielectric NP.

	MO	SE	NE	Fe <sub>3</sub> O <sub>4</sub>	C <sub>60</sub>	Gr	ZnO	Al <sub>2</sub> O <sub>3</sub>	ZrO <sub>2</sub>	SiO <sub>2</sub>
$\epsilon_r$	2.2	3.8	3.2	80	2.2	6.6	9	9.8	25	4
$\sigma$ ( $S \cdot m^{-1}$ )		$10^{-12} - 10^{-10}$		$10^4$	$10^{-6}$	$10^4$	$10^{-6} - 10^{-3}$	$10^{-12}$	$10^{-12}$	$10^{-14}$

**Table 3.16** Relaxation time of different nanofluids.

NFs	Relaxation time (s)	NFs	Relaxation time (s)	NFs	Relaxation time (s)
Conducting nanoparticles					
SE	$7.75 \cdot 10^{-14}$	SE	$8.67 \cdot 10^{-5}$	SE	$1.25 \cdot 10^{-14}$
Fe <sub>3</sub> O <sub>4</sub>	$7.64 \cdot 10^{-14}$	C <sub>60</sub>	$7.60 \cdot 10^{-5}$	Gr	$1.15 \cdot 10^{-14}$
NE		NE		NE	
MO	$7.47 \cdot 10^{-14}$	MO	$5.84 \cdot 10^{-6}$	MO	$0.97 \cdot 10^{-14}$
Semi-conducting nanoparticles					
		SE	$1.47 \cdot 10^{-7}$		
		ZnO	$1.36 \cdot 10^{-7}$		
		NE			
		MO	$1.18 \cdot 10^{-7}$		
Insulating nanoparticles					
SE	51.33	SE	4.12	SE	51.07
Al <sub>2</sub> O <sub>3</sub>	NE	ZrO <sub>2</sub>	NE	SiO <sub>2</sub>	NE
	47.79		3.97		45.79
MO	41.89	MO	3.71	MO	36.98

nanoseconds involved in streamer growth. In the case of insulating NPs, the relaxation time is very slow compared to the time growth of the streamer. These results may be wordy in explaining the beneficial effect of insulating NPs in suppressing streamer growth. In fact, in insulating NPs with high permittivity compared to base liquid, the permittivity mismatch creates the surface charge and, hence, a potential wall at the NP/base liquid interface. The potential distribution generated by the induced and polarized surface charge on a conducting and insulating NP is expressed as [37]

$$\varphi_i = -E_0 r \cos(\theta) - \frac{1}{8} \times \left( \frac{\sigma_1 - \sigma_2}{2\sigma_1 + \sigma_2} \right) \times \frac{R^3 E_0}{r^2} \cos(\theta) \quad r \geq R \quad (3.2)$$

$$\varphi_p = -\frac{1}{8} \times \left( \frac{\varepsilon_1 - \varepsilon_2}{2\varepsilon_1 + \varepsilon_2} \right) \times \frac{D^3 E_0}{r^2} \cos(\theta) \quad r \geq R \quad (3.3)$$

Where  $D$  is the diameter of the NP,  $r$  corresponds to the distance from the NP's surface, and  $E_0$  is the electric field. Thus, the trapping process is not non-limited, and the saturation charges, which are defined as the amount of charges that each NP can trap, are given by the formula 3.4 (for conducting NPs) and 3.5 (for insulating NPs), below [37]

$$(\varphi_{sat})_{\text{conducting}} = -12\pi\varepsilon_1 E_0 R^2 \quad (3.4)$$

$$(\varphi_{sat})_{\text{insulating}} = -12\pi\varepsilon_1 E_0 R^2 \left( \frac{\varepsilon_2}{2\varepsilon_1 + \varepsilon_2} \right) \quad (3.5)$$

While the positive impact of adding NPs to an optimal concentration is explained, the decline observed beyond the optimal concentration also needs discussion. In the effort to explain the negative impact of adding certain NPs to base liquids, the mechanisms vary depending on whether the concentration is below or above the optimal one. For instance, when the concentration of conducting NPs exceeds the optimal concentration, the negative effect on AC BdV can be attributed to forming a conductive pathway between the electrodes in the case of conducting NPs. This occurs because an increase in concentration reduces the distance between the NPs. Another possible reason is the reduction of trapping capability due to cluster formation (due to Van der Waals attraction forces), which reduces the effective surface needed for successful trapping events. The Van der Waals attraction forces are outlined below.

$$vdW_F = \frac{H}{12\pi D_s^2} \quad (3.6)$$

Where  $H$  is the Hamaker constant, and  $D_s$  is the separation distance between the NPs. The  $vdW_F$  is inversely proportional to the square of the inter-NPs distance.  $D_s$  can be expressed as follows.

$$D_s = \sqrt[3]{\frac{\left(\frac{4}{3} \times \pi r^3\right) \times \rho}{C}} \quad (3.7)$$

Where  $r$ ,  $\rho$  (g/L), and  $C$  (g/L) are the radius and density of NP and the concentration of NPs. The analysis assumes uniform NPs dispersion, a unique NPs size distribution (no Gaussian distribution), and no initial agglomeration.

Figure 3.18 shows the evolution of distance among  $\text{Fe}_3\text{O}_4$ ,  $\text{ZnO}$ , and  $\text{Al}_2\text{O}_3$  (20-30 nm and 50 nm) NPs as a function of concentration. It can be noted that upon concentration elevation, distance inter-NPs decreases, increasing  $vdW_F$  attraction forces. This increases the forces between NPs, and thence, the NPs tend to agglomerate. Additionally, in the case of  $\text{Fe}_3\text{O}_4$  NPs, the distance between the two NPs decreases (less than 50 nm), approaching their diameter (20 nm). In contrast,  $\text{Al}_2\text{O}_3$  (50 nm) NF shows reduced risks of distance reduction across all concentration ranges.  $\text{Al}_2\text{O}_3$  (20-30 nm) and  $\text{ZnO}$  have the same inter-NP distance range. Thus, the two NPs behave roughly the same when the concentration increases.

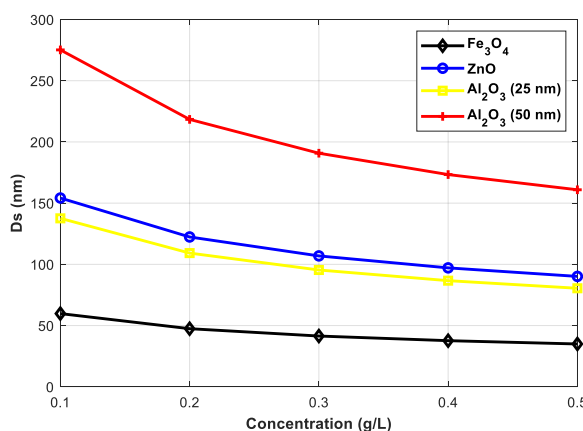


**Figure 3.18** Inter-nanoparticle distance vs. concentration of different nanofluids.

The reduction in distance and the formation of clusters may justify the existence of an optimal concentration, ensuring a good compromise between trapping and space among NPs. The trapping and de-trapping process refers to releasing the captured electrons from the NPs. Trapping and de-trapping of electrons reduce their mobility, leading to increased recombination of space charges in the NF and restricting the space charge density. This inhibits and delays the development of streamers, enhancing breakdown strength. The depth of potential walls characterizes the trapping and de-trapping.

### **3.6 Conclusion**

The comprehensive study presented in this chapter highlights the significant impact of NPs additives on the dielectric properties of synthetic ester, natural ester, and mineral oil. The experimental results demonstrate that incorporating nanoparticles such as  $\text{Fe}_3\text{O}_4$ ,  $\text{C}_{60}$ , Gr,  $\text{ZnO}$ ,  $\text{Al}_2\text{O}_3$ ,  $\text{ZrO}_2$ , and  $\text{SiO}_2$  can markedly enhance the AC breakdown voltage of these base liquids. Each type of NPs exhibited unique interactions with the fluids, with optimal concentrations identified for maximum dielectric improvement. The Anderson-Darling goodness-of-fit test and Weibull probability analysis confirmed the reliability and statistical significance of the observed enhancements. These findings suggest promising advancements in developing high-performance dielectric fluids for electrical insulation applications, paving the way for further research and potential industrial implementation.

## **CHAPTER 4**

### **EFFECT OF NANOPARTICLES ON THE PARTIAL DISCHARGE ACTIVITY, ELECTROSTATIC CHARGING TENDENCY, AND SURFACE DISCHARGE**

## 4.1 Introduction

The experimental study of NPs in insulating fluids is crucial for understanding their impact on partial discharges (PD), electrostatic charging tendencies (ECT), and surface discharges at solid/liquid interface. When dispersed in dielectric fluids, NPs influence these liquids' electrical properties and behavior under high-voltage conditions. Specifically, nanoparticles can affect the inception and magnitude of partial discharges, potentially improving or deteriorating the insulation performance depending on their type and concentration. The addition of nanoparticles like  $\text{Fe}_3\text{O}_4$ ,  $\text{Al}_2\text{O}_3$ , or  $\text{C}_{60}$  can alter the electric field distribution and dielectric properties, affecting the onset voltage, frequency, and intensity of these discharges. By improving the breakdown voltage or reducing the severity of discharges, nanoparticles can enhance the longevity and reliability of electrical equipment. However, the effect of nanoparticles is complex and varies depending on the base fluid and nanoparticle material, with some combinations showing improved performance and others leading to increased discharge activity.

ECT, another crucial parameter, is affected by the presence of NPs. The accumulation of charge due to the motion of insulating fluids can lead to equipment failure if not properly managed. NPs may influence this tendency by altering charge mobility and dispersion within the liquid, thus reducing or increasing the buildup of static charges.

NPs also influence surface discharges, which occur along the interface of solid and liquid insulation. These discharges can degrade insulation materials over time, and NPs may help suppress or exacerbate this process by modifying the fluids' surface properties and dielectric behavior.

This chapter explores these effects, presenting how different types of NPs impact the PDs, ECT, and surface discharge behavior in various insulating fluids. It highlights the potential advantages and limitations of using NPs in electrical insulation systems.

## 4.2 Partial Discharge Activity

### 4.2.1 Conducting NPs

#### 4.2.1.1 Synthetic and natural esters with $Fe_3O_4$

The first step for the PD test methodology is determining the inception voltage (PDIV) for each liquid, as shown in Figure 4.1. The voltage is increased every 10 seconds by 0.5 kV until the inception voltage is reached for a charge threshold of 1 pC. This operation is repeated five times. Then, an average inception voltage is calculated. In the second step, every liquid is subjected to a  $120\%*(PDIV)_{avg}$  to ensure the PD regime is reached. The voltage profile comprises five identical periods (Figure 4.2); each consists of increasing/decreasing phases with a speed of 1 kV/s, a voltage plateau of 32 s ( $120\%*(PDIV)_{avg}$ ), and a rest time of 5 s. The PD study is carried out following IEC 60270 standard. The average charge ( $Q_{avg}$ ), peak charge ( $Q_{peak}$ ), and number of PDs per second (NPDs/s) are measured during the plateau for each liquid, let be five times in total, and the mean and standard deviation are calculated. The data collected represent the average of the five measurements carried out. In addition, the phase-resolved PD is also compared for the three liquids.

The PDIV of the SE and NE is compared to the corresponding nanofluids with  $Fe_3O_4$  for optimal concentrations, those giving the highest AC BDV, and the results are given in Table 4.1. The PDIV increases from 9.04 kV to 9.22 kV when 0.4 g/L  $Fe_3O_4$  NPs

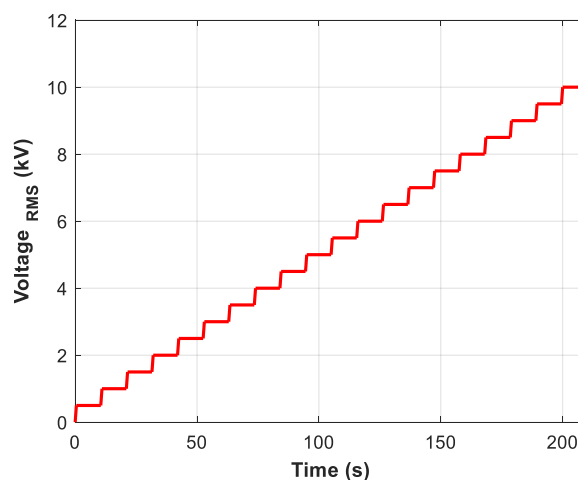


**Figure 4.1** Voltage rise protocol for inception voltage search.

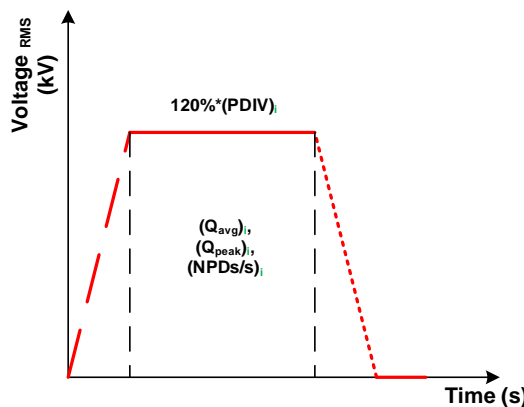


**Figure 4.2** Voltage Profile.

**Table 4.1** Inception voltage, standard deviation, and enhancement percentage of synthetic and natural esters nanofluids  $\text{Fe}_3\text{O}_4$ .

	Mean (kV)	St.Dev	Increment (%)
<b>SE</b>	9.04	0.38	—
<b>0.4 g/L <math>\text{Fe}_3\text{O}_4</math> NF</b>	9.22	0.64	1.99
<b>NE</b>	9.01	0.40	—
<b>0.4 g/L <math>\text{Fe}_3\text{O}_4</math> NF</b>	9.26	0.04	2.77

are added to SE. The same tendency can be observed with NE as a base liquid; adding 0.4 g/L of  $\text{Fe}_3\text{O}_4$  increases it from 9.04 kV to 9.26 kV.

As explained above, to ensure that the PDs regime is reached, every liquid is stressed during the plateau, imposing  $120\% \times (\text{PDIV})_{avg}$ . The results of this analysis are presented in Table 4.2. Compared to SE, fewer PDs per second have been observed for the SE-based  $\text{Fe}_3\text{O}_4$  NF. The  $\text{Fe}_3\text{O}_4$  NPs negatively impact  $Q_{avg}$  and  $Q_{peak}$  of SE. In the case of NE as base liquid, adding  $\text{Fe}_3\text{O}_4$  NPs decreases the  $Q_{avg}$  and the NPDs/s of SE while it increases the  $Q_{peak}$ . Adding  $\text{Fe}_3\text{O}_4$  NPs is more favorable to reducing PD activity with NE than SE.

Figures 4.3 and 4.4 show the PD patterns of SE and NE and their corresponding NFs  $\text{Fe}_3\text{O}_4$ , respectively. The PD activity starts at the negative polarity peak ( $270^\circ$  electrical degrees) and a few seconds after, at the positive ( $90^\circ$ ) electrical degrees) with less activity and a high charge level).

**Table 4.2** Q<sub>peak</sub>, Q<sub>avg</sub>, and NPDs/s, Standard deviation, and increment percentage of synthetic and natural esters nanofluids with Fe<sub>3</sub>O<sub>4</sub>.

		Q <sub>peak</sub> (pC)	Q <sub>avg</sub> (pC)	NPDs/s (PDs/s)
<b>Synthetic ester-based NFs</b>				
SE	<b>Mean</b>	190.8	13.77	60.14
	<b>St.Dev</b>	67.60	0.47	8.35
	<b>Incr. (%)</b>	—	—	—
<b>0.4 g/L Fe<sub>3</sub>O<sub>4</sub> NF</b>	<b>Mean</b>	427.32	17.25	45.55
	<b>St.Dev</b>	83.25	1.44	6.47
	<b>Incr. (%)</b>	123.96	25.27	-24.26
<b>Natural ester-based NFs</b>				
NE	<b>Mean</b>	397,9	4.04	41.08
	<b>St.Dev</b>	101.3	0.46	3.53
	<b>Incr. (%)</b>	—	—	—
<b>0.4 g/L Fe<sub>3</sub>O<sub>4</sub> NF</b>	<b>Mean</b>	177.5	11.15	27.58
	<b>St.Dev</b>	56.50	0.613	3.845
	<b>Incr. (%)</b>	-55.39	175.4	-32.86

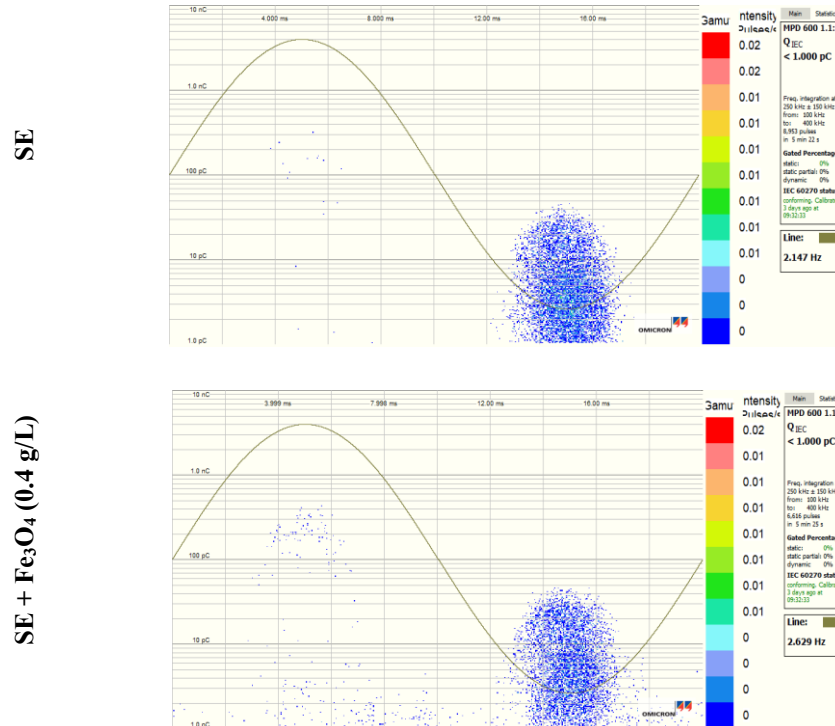


**Figure 4.3** PD pattern of SE and SE-based nanofluids with Fe<sub>3</sub>O<sub>4</sub>.

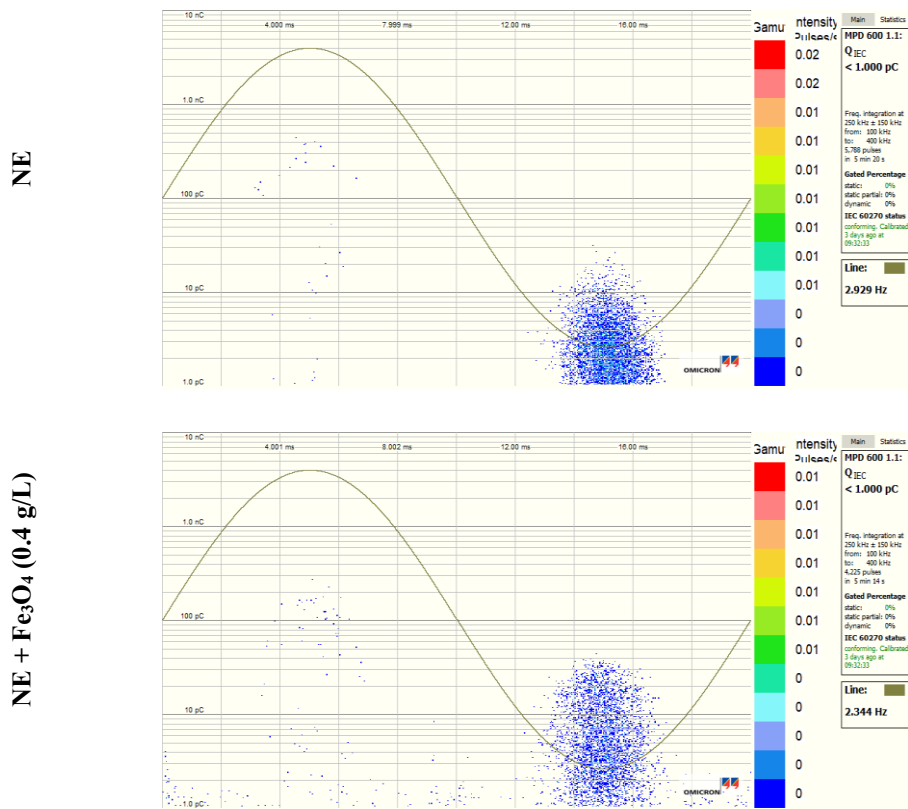


**Figure 4.4** PD pattern of NE and NE-based nanofluids with  $\text{Fe}_3\text{O}_4$ .

#### 4.2.1.2 Synthetic and natural esters with $C_{60}$

Figure 4.5 shows the profile of the voltage RMS value applied to SE-based NFs with  $C_{60}$  and Gr. This setup was implemented at the start of the thesis work and improved as the project progressed (against the final setup presented in Figures 4.1 and 4.2). The voltage rises and falls with 1kV/s speed, 12 kV as the maximum value, kept for 30 seconds, and 5 seconds of rest is respected between two successive tests. This voltage profile was applied five times for each sample, and five PD tests were performed for each liquid.

Table 4.3 presents the average and standard deviation of PDIV,  $Q_{\text{avg}}$ ,  $Q_{\text{peak}}$ , NPDs/s, and PDEV values obtained from electrical measurement for the SE and SE-based NFs with 0.4 g/L  $C_{60}$  for a PDs threshold level of 2 pC. The PDIV value of SE-based NF with  $C_{60}$  at 0.4 g/L is higher than that of SE, which was enhanced by about 5.1% compared to base liquid. Furthermore, the lower  $Q_{\text{avg}}$ ,  $Q_{\text{peak}}$ , and NPDs/s for SE-based NF with  $C_{60}$  demonstrates that  $C_{60}$  NP enhanced the performance of the SE liquid with a lower PD

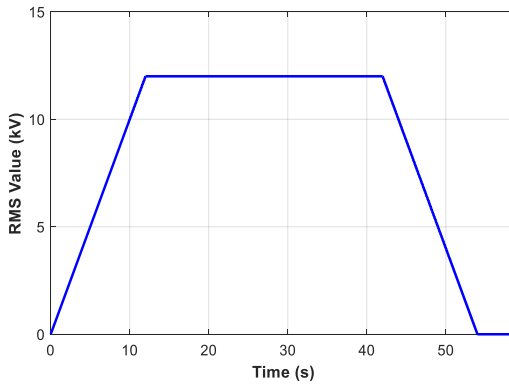


**Figure 4.5** Voltage profile (RMS value) applied to SE-based nanofluids with C<sub>60</sub> and Gr.

**Table 4.3** PD Activity of synthetic ester and synthetic ester-based nanofluids with 0.4 g/L C<sub>60</sub>.

		PDIV s (kV)	Q <sub>peak</sub> (pC)	Q <sub>avg</sub> (pC)	NPDs/s (PDs/s)	PDEVs (kV)
SE	Mean	10.47	205	14.3	42	8.07
	St.Dev	0.58	68	1	2	0.73
	Incr. (%)	—	—	—	—	—
0.4 g/L C <sub>60</sub> NF	Mean	11.01	134	11.7	24	6.86
	St.Dev	5	9	1	1	1.48
	Incr.(%)	0.362	-34.6	-18.1	-42	-14.98

activity. The PDEVs results show that the pure SE gives the best extinction voltage compared to the C<sub>60</sub> NFs. It was decreased by about 14.98% with SE-based NFs with C<sub>60</sub> compared to SE.

Figure 4.6 shows the PD patterns of SE and SE-based NF with 0.4 g/L C<sub>60</sub>, at 12kV (RMS) voltage level. For all cases, it was observed that the PD activity began with the appearance of PDs at the peak of negative polarity (270° electrical degrees) and just after at the peak of positive polarity (90° electrical degrees) with less important activity. Furthermore, it was noticed that C<sub>60</sub> NF shows the lowest activity in terms of PD activity compared to SE. Based on partial discharge measurements, with a higher PDIV and a lower PD activity, it can be said that adding C<sub>60</sub> NPs enhances the performance of the pure liquid against PD activity.

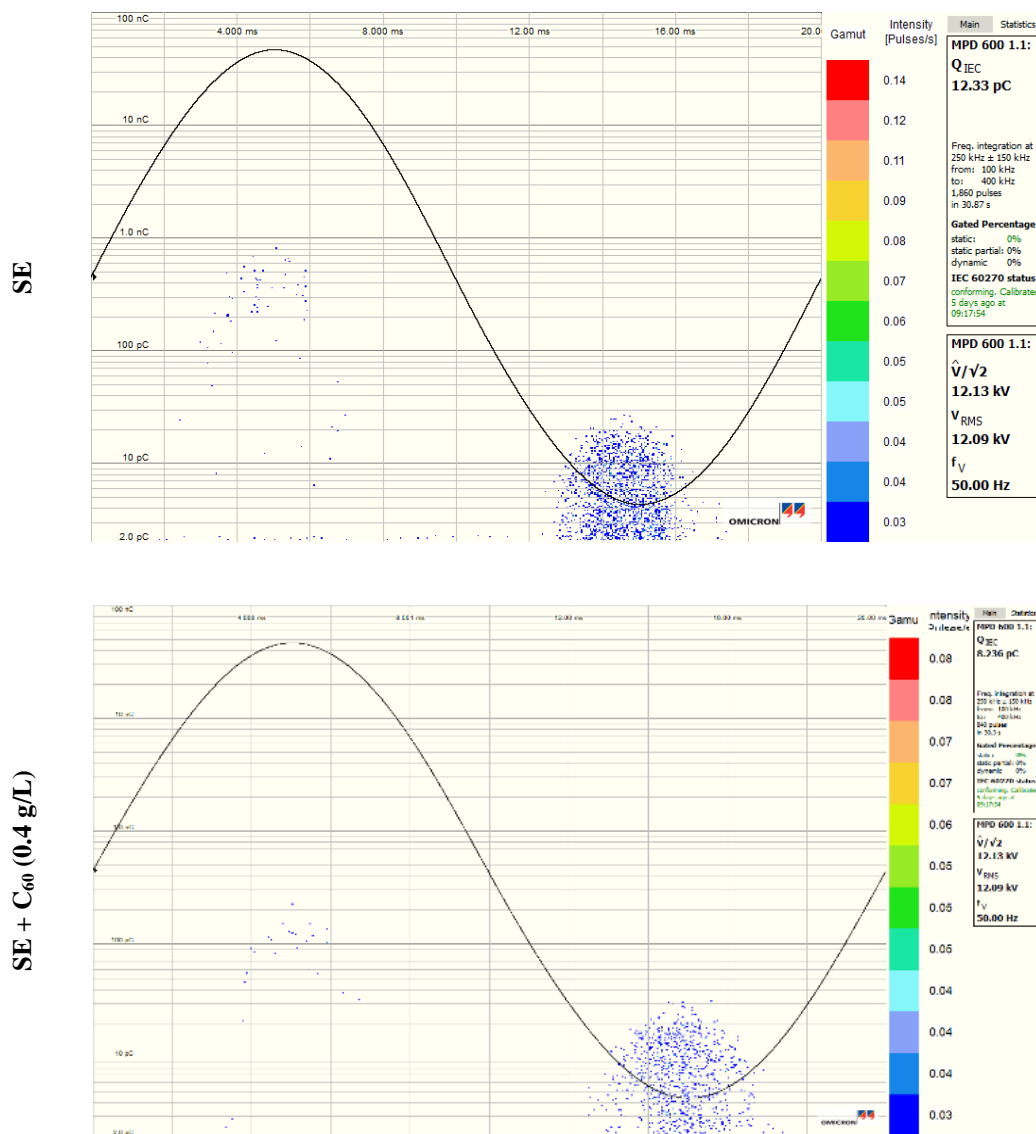


**Figure 4.6** PD pattern of SE and SE-based nanofluids with C<sub>60</sub> at 12 kV voltage level.

The PDIV of the NE and NE-based NFs with 0.3 g/L and 0.4 g/L of C<sub>60</sub> is determined according to the protocol described in Figure 4.1 and Figure 4.2; the results are presented in Table 4.4. It can be observed that the PDIV decreases from 9.14 kV to 8.04 kV when 0.3 g/L of C<sub>60</sub> NPs were added and decreases from 9.14 kV to 7.72 kV when 0.4 g/L C<sub>60</sub> NPs were added. The decreases are 12.11% and 15.60% in the case of C<sub>60</sub> NFs at a concentration of 0.3 g/L and 0.4 g/L, respectively. Now, the voltage profile described in Figure 4.2 is applied to the three liquids, imposing a plateau voltage equal to 120%\*PDIV. The results are depicted in Table 4.5. For the two NE-based NFs with C<sub>60</sub>, more PDs per second than the base liquid have been observed.

**Table 4.4** Inception voltage, standard deviation, and enhancement percentage of natural ester and C<sub>60</sub> nanofluids.

	Mean (kV)	St.Dev	Increment (%)
<b>NE</b>	9.14	0.65	—
<b>0.3 g/L C<sub>60</sub> NF</b>	8.04	0.5	-12.11
<b>0.4 g/L C<sub>60</sub> NF</b>	7.72	0.37	-15.60

**Table 4.5** Q<sub>avg</sub>, Q<sub>peak</sub>, NPDs/s, standard deviation, and increment percentage of natural ester and C<sub>60</sub> nanofluids.

	Q <sub>peak</sub> (pC)	Q <sub>avg</sub> (pC)	NPDs/s (PDs/s)
<b>Natural ester-based NFs</b>			
<b>NE</b>	<b>Mean</b>	812.86	43.25
	<b>St.Dev</b>	109.82	2.36
	<b>Incr. (%)</b>	—	—
<b>0.3 g/L C<sub>60</sub> NF</b>	<b>Mean</b>	105.31	9.10
	<b>St.Dev</b>	20.15	15.77
	<b>Incr. (%)</b>	-87.04	+178.68
<b>0.4 g/L C<sub>60</sub> NF</b>	<b>Mean</b>	127.28	15.19
	<b>St.Dev</b>	20.03	17.96
	<b>Incr. (%)</b>	-84.34	+303.92

Although a lower PDIV and higher NPs/s, a lower Q<sub>avg</sub> and Q<sub>peak</sub> for the NE-based NFs with C<sub>60</sub> compared to the base liquid, lower Q<sub>peak</sub> indicates that NPs eliminate or reduce the effect of PDs with high charge value. In addition, the reduction in Q<sub>avg</sub> is significant, which means that even if the PD regime is reached at a slightly lower voltage value than the base liquid, this reduction might indicate a less intense PD regime and, therefore, less harmful for the liquid.

Figure 4.7 shows the PDs patterns of NE and NE-based NFs with C<sub>60</sub> at 0.3 g/L and 0.4 g/L, respectively, at a 120%\*PDIV (RMS) voltage level. The PD activity begins at the negative polarity peak (270° electrical degrees), and just after, at the positive polarity peak (90° electrical degrees) with less important activity and a higher charge level. Furthermore, it is noticed that adding C<sub>60</sub> NPs has a positive impact on the charge peak of the NE.

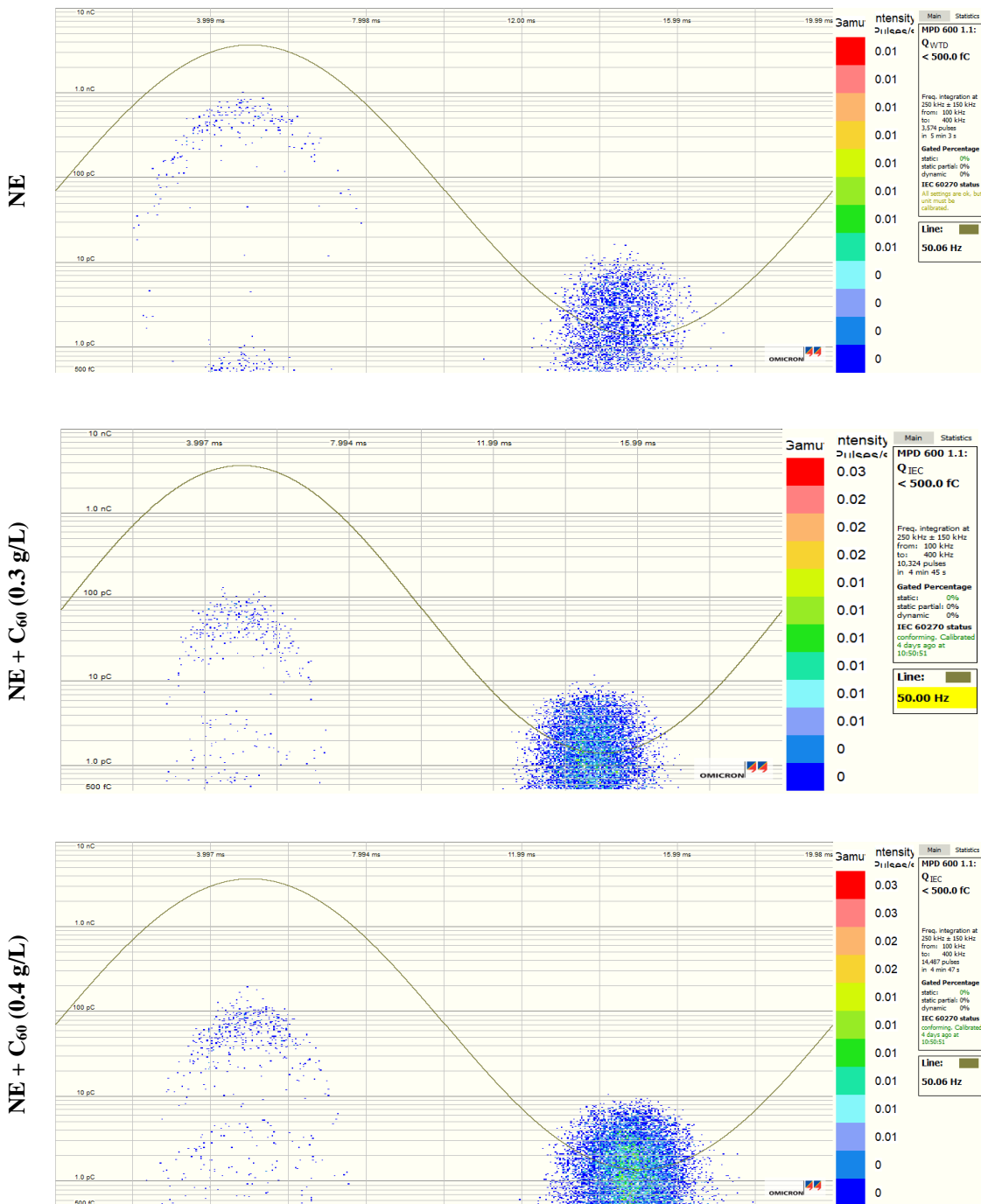


**Figure 4.7** PD pattern of NE and NE-based nanofluids with C<sub>60</sub>.

#### 4.2.1.3 Synthetic ester with Gr

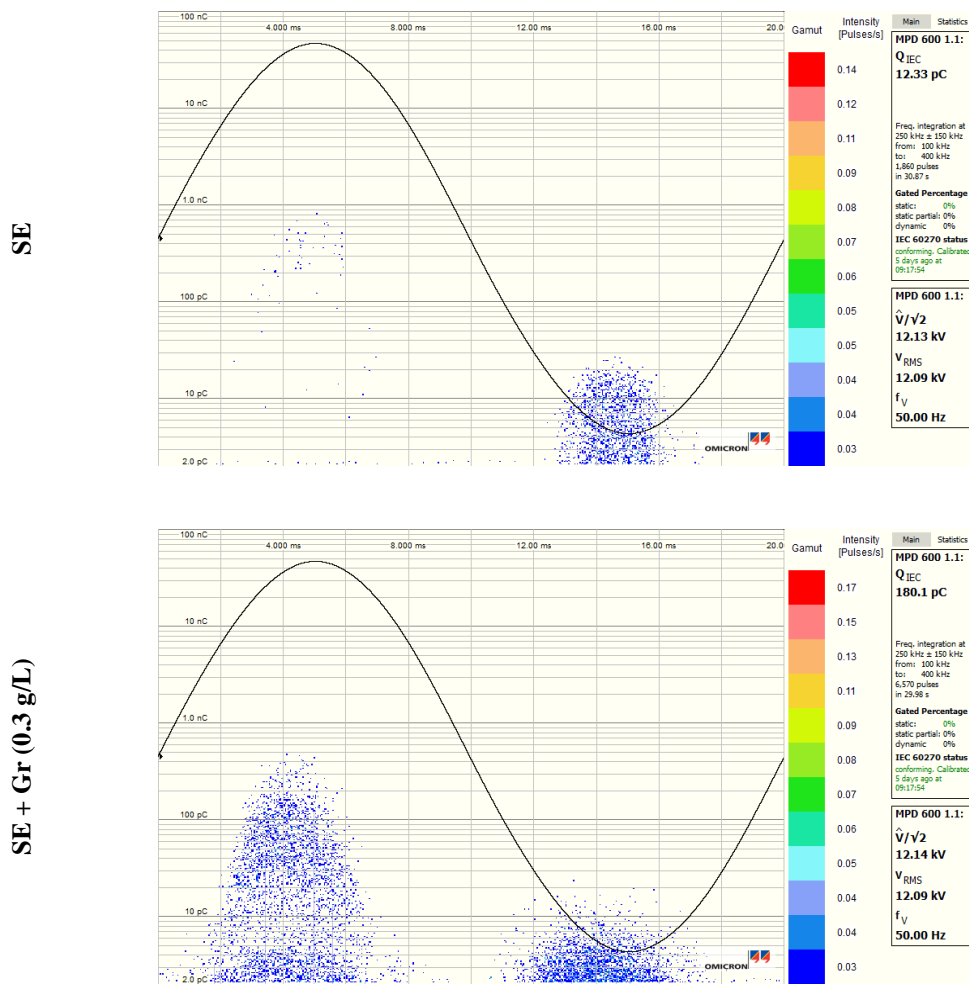
The same setup presented in Figure 4.5 has been used again to analyze the PDs of SE and SE-based NFs with Gr. As for the C<sub>60</sub> NFs, the voltage rises and falls with 1 kV/s speed, 12 kV as the maximum value, kept for 30 seconds, and 5 seconds of rest is respected between two successive tests. This voltage profile was applied five times for each sample, and five PD tests were performed for each liquid.

Table 4.6 provides the mean and standard deviation of the PDIV, Q<sub>avg</sub>, Q<sub>peak</sub>, NPDs/s, and PD Extinction Voltage values for SE and SE-based NFs with 0.3 g/L Gr at a PDs threshold level of 2 pC. The PDIV value of SE-based NFs with 0.3 g/L Gr is lower than that of SE, which decreased by about 33% compared with the base liquid. In addition, higher Q<sub>avg</sub>, Q<sub>peak</sub>, and NPDs/s for SE-based NF with Gr demonstrate that Gr NP degrades the performance of the SE liquid with a higher PD activity. The results of the PDEV show that the SE provides the best extinction voltage compared with the Gr NFs. It was decreased by about 40% with SE-based NFs with Gr compared to SE.

Figure 4.8 illustrates the PD profiles of SE and SE-based NF with 0.3 g/L Gr at a 12 kV (RMS) voltage level. As for all the NFs samples, it was noticed that the PD activity begins with the appearance of PD at the negative polarity peak (270° electrical degrees) and just after at the positive polarity peak (90° electrical degrees). Contrary to other NPs, adding Gr to SE is manifested by an intense PD activity on positive polarity compared to the negative one. Therefore, the addition of Gr NPs to the SE has a negative impact on its PD activity.

**Tabl 4.6** PD Activity of synthetic ester and synthetic ester-based nanofluids with 0.3 g/L Gr.

		PDIVs (kV)	Q <sub>peak</sub> (pC)	Q <sub>avg</sub> (pC)	NPDs/s (PDs/s)	PDEVs (kV)
<b>Synthetic ester-based NFs</b>						
SE	<b>Mean</b>	10.47	205	14.3	42	8.07
	<b>St.Dev</b>	0.58	68	1	2	0.73
	<b>Incr. (%)</b>	–	–	–	–	–
0.3 g/L Gr NF	<b>Mean</b>	6.983	573	124.4	250	4.890
	<b>St.Dev</b>	0.582	67	5	3	0.387
	<b>Incr. (%)</b>	-33.34	+180	+770	+495	-39.40



**Figure 4.8** PD pattern of SE and SE-based nanofluids with Gr at 12 kV voltage level.

#### 4.2.2 Insulating NPs

##### 4.2.1.4 Synthetic and natural ester with $Al_2O_3$ (20-30 nm)

The same protocol presented in Figure 4.1 and Figure 4.2 is used for the PD activity quantification for SE and NE with  $Al_2O_3$  NPs. The study case analyzes the impact of  $Al_2O_3$  (20-30 nm) NPs on PD activity in both SE and NE. The findings reveal that adding  $Al_2O_3$  NPs influences various aspects of PD behavior. Adding 0.3 g/L of  $Al_2O_3$  NPs to SE results in a slight decrease in PDIV from 9.04 kV to 8.22 kV. Similarly, the PDIV decreases in NE from 9.04 kV to 8.61 kV when 0.2 g/L of  $Al_2O_3$  is added, indicating that the NPs may facilitate earlier PD initiation. Regarding PD activity, the  $Q_{avg}$  decreases

**Table 4.7** Inception voltage, standard deviation, and enhancement percentage of synthetic and natural esters nanofluids Al<sub>2</sub>O<sub>3</sub> (20-30 nm).

	Mean (kV)	St.Dev	Increment (%)
<b>SE</b>	9.04	0.38	—
<b>0.3 g/L Al<sub>2</sub>O<sub>3</sub> NF</b>	8.22	0.02	-9.07
<b>NE</b>	9.01	0.40	—
<b>0.2 g/L Al<sub>2</sub>O<sub>3</sub> NF</b>	8.61	0.49	-4.44

**Table 4.8** Q<sub>peak</sub>, Q<sub>avg</sub>, and NPDs/s, standard deviation, and increment percentage of synthetic and natural esters nanofluids with Al<sub>2</sub>O<sub>3</sub>.

		Q <sub>peak</sub> (pC)	Q <sub>avg</sub> (pC)	NPDs/s (PDs/s)
<b>Synthetic ester-based NFs</b>				
<b>SE</b>	<b>Mean</b>	190.8	13.77	60.14
	<b>St.Dev</b>	67.60	0.47	8.35
	<b>Incr. (%)</b>	—	—	—
<b>0.3 g/L Al<sub>2</sub>O<sub>3</sub> NF</b>	<b>Mean</b>	126.96	6.60	49.86
	<b>St.Dev</b>	98.6	1.50	8.29
	<b>Incr. (%)</b>	-33.45	-52	-17.09
<b>Natural ester-based NFs</b>				
<b>NE</b>	<b>Mean</b>	397,9	4.04	41.08
	<b>St.Dev</b>	101.3	0.46	3.53
	<b>Incr. (%)</b>	—	—	—
<b>0.2 g/L Al<sub>2</sub>O<sub>3</sub> NF</b>	<b>Mean</b>	116.0	6.22	20.66
	<b>St.Dev</b>	35.20	0.50	4.89
	<b>Incr. (%)</b>	-70.83	+53.69	-49.70

significantly by 52% in SE, showing improved performance, while in NE, Q<sub>avg</sub> increases by 53.69%, suggesting that the NPs have a variable effect depending on the base liquid. The Q<sub>peak</sub> decreases by 33.45% in SE and by 70.83% in NE, revealing that Al<sub>2</sub>O<sub>3</sub> NPs effectively reduce the highest PD charge levels in both liquids. Furthermore, the frequency of PD events (NPDs/s) decreases by 17.09% in SE and by 49.70% in NE with the addition of Al<sub>2</sub>O<sub>3</sub> NPs. The study concludes that Al<sub>2</sub>O<sub>3</sub> NPs improve PD characteristics by reducing peak charge levels and NPDs/s. However, their impact on the inception voltage and average charge varies between SE and NE.

#### 4. The effect of NPs on the PDs, ECT, and Surface discharges

The PD patterns associated with  $\text{Al}_2\text{O}_3$  NPs presented in Figures 4.9 and 4.10 show a clear reduction in PD activity for both SE and NE compared to the base liquids. In these

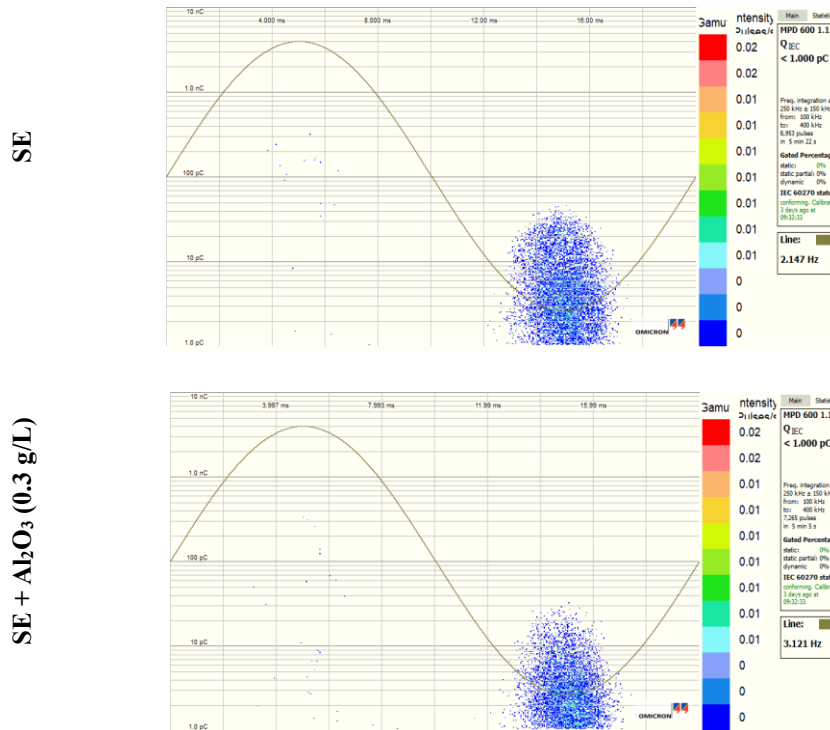


**Figure 4.9** PD pattern of SE and SE-based nanofluids with  $\text{Al}_2\text{O}_3$  (20-30 nm).

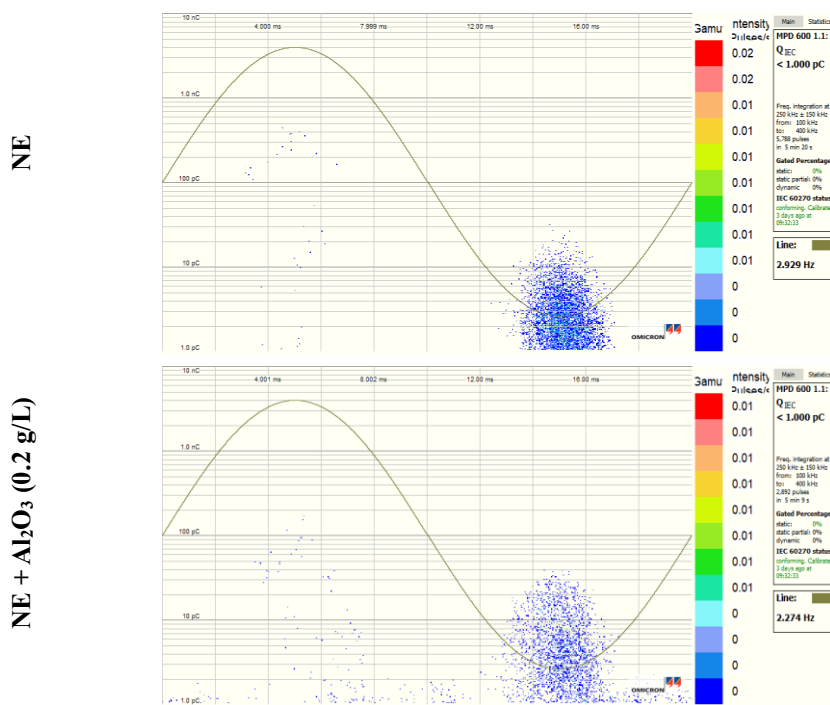


**Figure 4.10** PD pattern of NE and NE-based nanofluids with  $\text{Al}_2\text{O}_3$  (20-30 nm).

PD patterns, the activity typically starts during the negative polarity peak (around 270° electrical degrees) and continues, though less intensely, during the positive polarity peak (around 90° electrical degrees).

For both esters, introducing Al<sub>2</sub>O<sub>3</sub> NPs leads to fewer discharge events and reduced discharge magnitudes. This indicates that Al<sub>2</sub>O<sub>3</sub> NPs effectively suppress the initiation and propagation of PD. Specifically, the patterns show that the overall charge levels

#### **4.2.2 Discussion of NPs effect on PDs activity**

##### **4.2.2.1 Effect of Fe<sub>3</sub>O<sub>4</sub> and Al<sub>2</sub>O<sub>3</sub> on PDs of SE and NE**

The findings from this study reveal important insights into the role of NPs in enhancing the dielectric performance of ester-based insulating liquids. Introducing Fe<sub>3</sub>O<sub>4</sub> and Al<sub>2</sub>O<sub>3</sub> NPs leads to varying effects on PD activity, depending on the type of base liquid used.

For SE, Fe<sub>3</sub>O<sub>4</sub> NPs increase the severity of PD events, as evidenced by the higher Q<sub>avg</sub> and Q<sub>peak</sub> values. This suggests that Fe<sub>3</sub>O<sub>4</sub> may delay PD initiation but can also contribute to more intense discharge activity, potentially compromising the insulation performance. In contrast, Al<sub>2</sub>O<sub>3</sub> (20-30 nm) NPs significantly suppress PD activity in SE, reducing the frequency and severity of discharges. This highlights the potential of Al<sub>2</sub>O<sub>3</sub> as a more effective NPs for improving the PDs resistivity of synthetic esters.

For NE, Fe<sub>3</sub>O<sub>4</sub> NPs show a mixed impact, with reduced Q<sub>avg</sub> but increased Q<sub>peak</sub>, indicating a trade-off between the frequency and intensity of PD events. Al<sub>2</sub>O<sub>3</sub> NPs, on the other hand, display a more complex behavior, increasing Q<sub>avg</sub> but reducing Q<sub>peak</sub>. This suggests that while Al<sub>2</sub>O<sub>3</sub> can reduce the maximum discharge levels, it may also lead to more frequent PD occurrences in natural esters.

The PD patterns further support these observations, showing that both types of NPs can alter the phase-resolved PD characteristics of the liquids. Al<sub>2</sub>O<sub>3</sub> NPs, in particular, demonstrate a more vital ability to suppress discharge activity across both positive and negative polarity peaks, making them a more favorable option for enhancing insulation performance in high-voltage applications.

In conclusion, the study underscores the importance of selecting the appropriate nanoparticle type based on the specific insulating liquid and the desired dielectric performance. While Fe<sub>3</sub>O<sub>4</sub> nanoparticles may offer some benefits in delaying PD initiation, Al<sub>2</sub>O<sub>3</sub> nanoparticles appear to provide a more consistent improvement in

reducing PD severity and frequency, especially in synthetic ester liquids. Further research is recommended to optimize nanoparticle concentrations and explore their long-term stability in different insulating environments.

#### 4.2.2.2 Effect of $C_{60}$ and Gr NPs on PDs of SE and NE

The effects of  $C_{60}$  and Gr NPs on PD activity reveal contrasting behaviors.  $C_{60}$  generally improves insulation performance, while graphene appears to degrade it. For  $C_{60}$  NPs, the study shows promising results, particularly in SE. The increase in PDIV, coupled with the significant reduction in  $Q_{avg}$  and  $Q_{peak}$ , suggests that  $C_{60}$  can effectively suppress PD activity and improve the overall dielectric strength of SE. However, in NE, while  $C_{60}$  reduces the severity of individual discharges, it also increases PD frequency, highlighting a complex interaction between the NPs and the base liquid. This indicates that while  $C_{60}$  has potential as an additive for improving insulation performance, its effects may vary depending on the specific ester used.

On the other hand, Gr NPs exhibit a detrimental effect on the dielectric properties of SE. The significant decrease in PDIV and the significant increase in both  $Q_{avg}$  and  $Q_{peak}$  suggest that graphene worsens PD activity, leading to more frequent and severe discharges. The PD patterns further confirm this negative impact, showing intense activity, particularly during the positive polarity peak. This indicates that graphene may be unsuitable as an insulating material additive, especially for applications where minimizing PD activity is critical.

In summary, this study suggests that while  $C_{60}$  NPs can enhance the insulation performance of ester oils, particularly synthetic esters, Gr NPs may not be suitable for such applications. Further research is recommended to optimize the concentration and dispersion of  $C_{60}$  in different ester-based liquids and explore alternative NPs that may offer better performance than graphene.

### 4.3 Electrostatic charging tendency

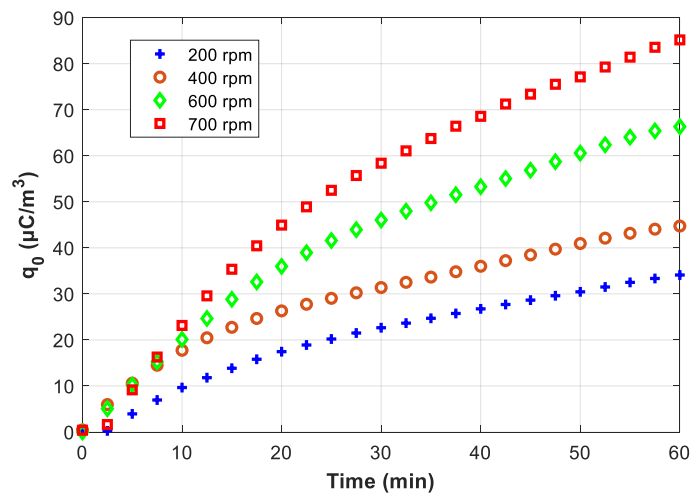
#### 4.3.1 Synthetic ester with $Fe_3O_4$ , $CuO$ , and $C_{60}$

Figures 4.11. (a), (b), (c), and (d) show the variation of liquid volume charge density (charge per liquid volume) with a spinning disk for SE, SE with  $Fe_3O_4$ , SE with  $CuO$ , and SE with  $C_{60}$ , at 0.1 g/L [101], for a rotating speed ranging from 200 to 700 rpm at room temperature. A 2 mm thick pressboard is used for this study. Those results indicate that an increase in the speed causes an increase in the ECT of pure SE and NFs-impregnated

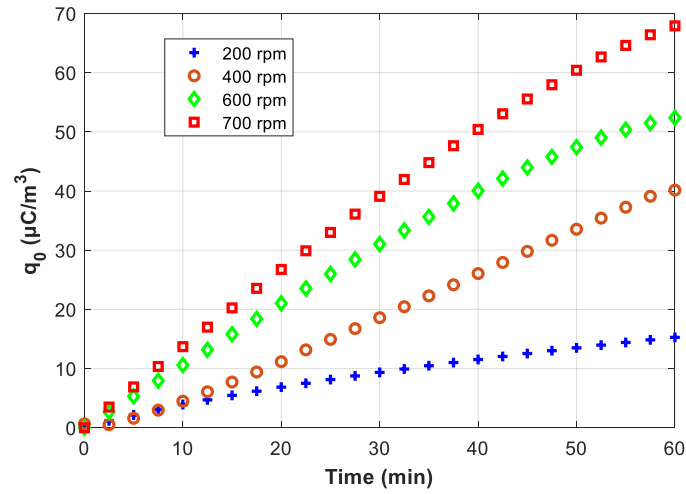
pressboards over time. The cumulative ECT for different rates after one hour is presented in Figure 4.12. A lower ECT is observed with the three NFs; the NFs somehow show a similar ECT at low speed (200 rpm); beyond that speed, the effect of CuO and C<sub>60</sub> NPs becomes more significant than Fe<sub>3</sub>O<sub>4</sub> NPs.

Nevertheless, the results mentioned above show that the three NPs considerably reduce the ECT of pure SE at low liquid flow velocity. On the other hand, in the case of a high liquid flow velocity, only NF-based SE with CuO and NF-based SE with C<sub>60</sub> could reduce it. In addition, Figure 4.13 shows the dependence of the cumulative ECT after one hour as a function of the disk's rotational speed for the four liquids; it can be observed that the ECT has a linear behavior with the increment of speed in the case of NFs-based SE with Fe<sub>3</sub>O<sub>4</sub> and C<sub>60</sub>, which move away in the case of pure SE and NF-based CuO. Therefore, it appears that CuO and C<sub>60</sub> NPs constitute potential inhibitor additives to reduce the flow electrification instead of 1,2,3-benzotriazole (BTA), whose effect on long-term aging and its negative impact on the breakdown voltage of insulation oil presents some uncertainties. The non-reproducibility of the experimental results with BTA meant that this additive was not retained as a solution against static electrification.

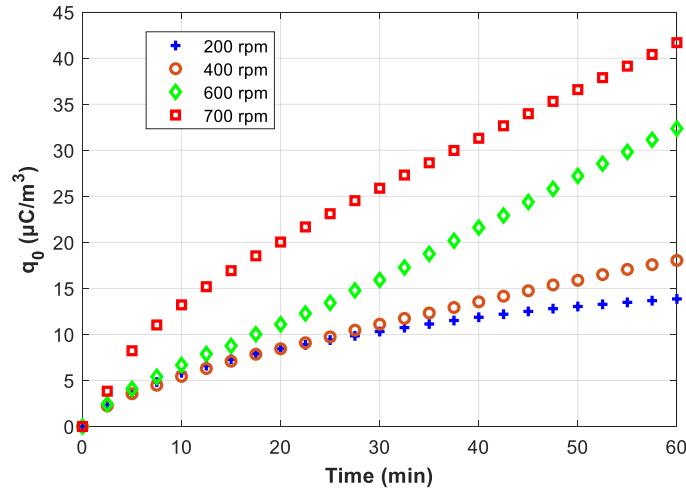
Paillat et al. [102] studied the ECT phenomena of ester oils compared to those of mineral oils; they suggested that the increase in the charge accumulation could be due to higher conductivity and/or viscosity or simply due to the different mechanisms. Many rheological studies show that the addition of NPs less impacts the viscosity of NFs than the temperature for low doping concentration [56], [103], [104]. Thus, the ECT may be more affected by the conductivity. Adding NPs may also affect the relaxation time since conductive and semi-conductive NPs reduce it [36], [37], favoring the charge displacement. Another impacting factor would be that the electronegative atoms/molecules contained in different NPs reduce ECT due to trapping mechanisms. Finally, it is quite hard to determine why the NFs-based CuO and C<sub>60</sub> NPs have less charge production than NF-based Fe<sub>3</sub>O<sub>4</sub> NPs, while these later improve AC BDV. This is certainly due to the interaction of NPs / pressboard, which differs depending on the NPs type. However, this initial tentative on ECT phenomena in different NFs-based fresh synthetic esters for one specific concentration permits identifying the potential inhibitor additives. However, the risks of ECT could be more/less important with the aging of synthetic ester, liquid nature (mineral oil and natural ester), and/or insulating NPs (Al<sub>2</sub>O<sub>3</sub>). Thus, further investigations should be planned to verify the effect of those parameters.



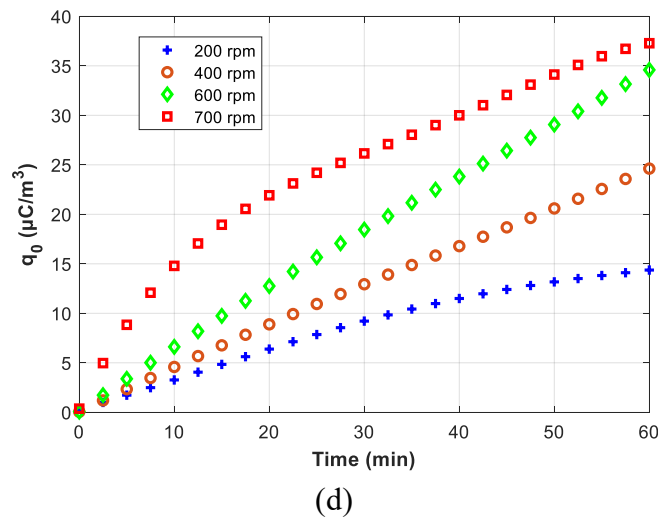
(a)



(b)



(c)



(d)

**Figure 4.11** Electrostatic charging tendency of (a) SE, (b) SE with 0.1 g/L  $\text{Fe}_3\text{O}_4$ , (c) SE with 0.1 CuO, and (d) SE with 0.1 g/L  $\text{C}_{60}$ .

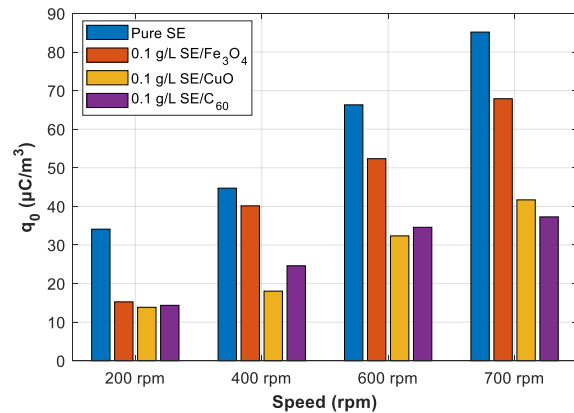


**Figure 4.12** Cumulative ECT after one hour of different liquids for different speeds.

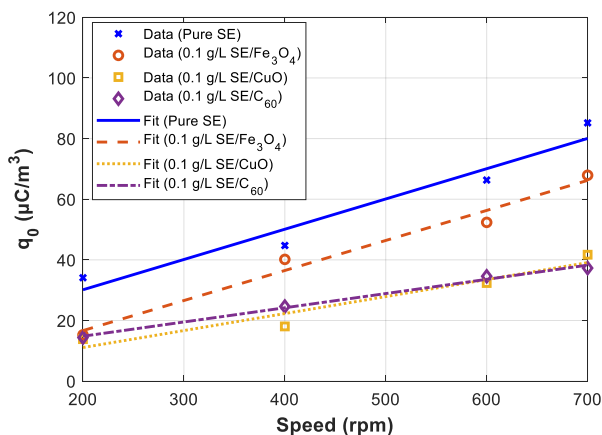


**Figure 4.13** Dependence of the ECT on the disk's rotational speed for different liquids.

#### 4.3.2 Natural ester (Midel 1204) with MgO

The ECT quantification involves testing the NE and NE with MgO at the optimal concentration of 0.2 g/L. This concentration was chosen for its superior AC BDV performance and notable PD resistance, as shown in Figures 4.14 and 4.15. As shown in Figure 4.14, the mean AC BDV increases with the increase of the doping concentrations up to optimal concentration (0.2 g/L). After, a decreasing tendency is observed with the increase in the doping concentration. It can be seen that the NFs-based NE with MgO NPs show the best improvement at 0.2 g/L with an increase of 21.85% compared to pure NE. The improvements are 12.85% at 0.1 g/L and around 15% at 0.3 g/L and 0.4 g/L. NFs-based NE with MgO at 0.5 g/L represents the only concentration where the AC BDV decreased compared to base liquid.

Then, the partial discharge activity was investigated on the base liquid and NFs-based NE with MgO at the optimal concentration (0.2 g/L). Figure 4.15 shows the PD patterns of NE and MgO NF at 0.2 g/L. Table 4.9 displays the mean, standard deviation, as well as the enhancement of average charge ( $Q_{avg}$ ), peak charge ( $Q_{peak}$ ), and number of PD per second (NPDs/s) values acquired through electrical measurements on NE and NF

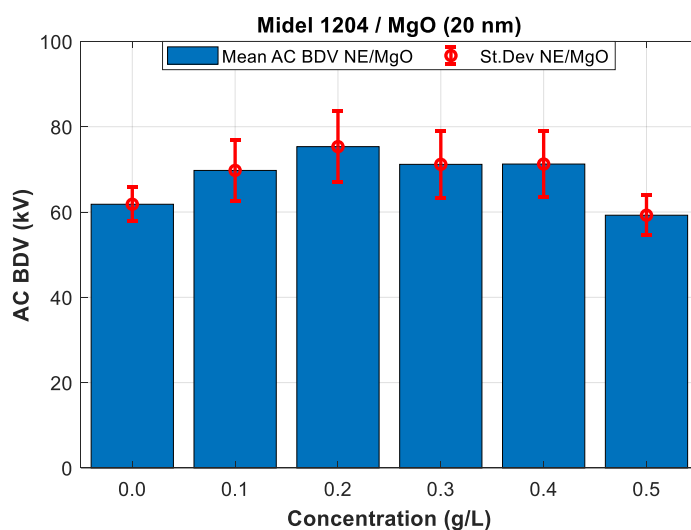
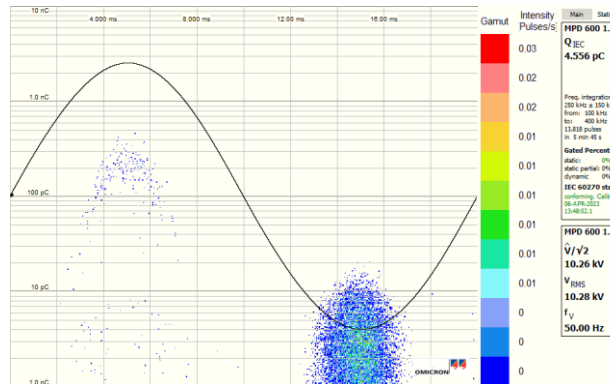


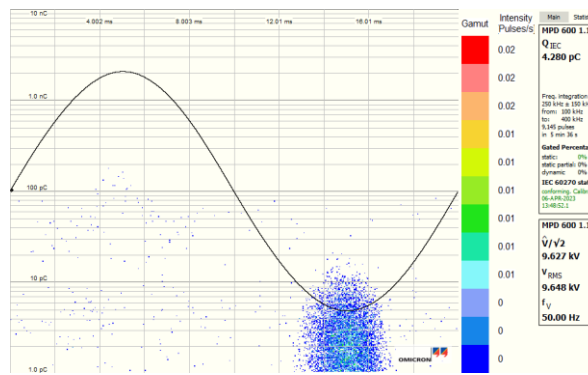
**Figure 4.14** Mean value of AC breakdown voltages of different concentrations of MgO for a gap distance d=2 mm.

#### 4. The effect of NPs on the PDs, ECT, and Surface discharges

samples tested at one pC threshold level. It is evident that adding MgO NPs at a doping



(a) Midel eN 1204



(b) Midel eN 1204 + MgO (0.2 g/L)

**Figure 4.15** PD pattern of natural ester and NFs-based natural ester with MgO nanoparticles at 0.2 g/L, stressed with 120%\*PDI.

**Table 4.9** Q<sub>avg</sub>, Q<sub>peak</sub>, and NPDs/s, standard deviation, and increment percentage of NE and NE-based NFs with MgO at 0.2 g/L

	Midel 1204	Midel 1204+MgO (0.2 g/L)
Q <sub>avg</sub> (pC)	16.54	4.53
Std. (pC)	4.40	0.47
Enhancement (%)	-	-72.55
Q <sub>peak</sub> (pC)	366.88	124.81
Std. (pC)	26.11	30.64
Enhancement (%)	-	-66.0
NPDs (PDs/s)	98.76	83.44
Std. (PDs/s)	4.73	7.16
Enhancement (%)	-	-15.51

#### *4. The effect of NPs on the PDs, ECT, and Surface discharges*

---

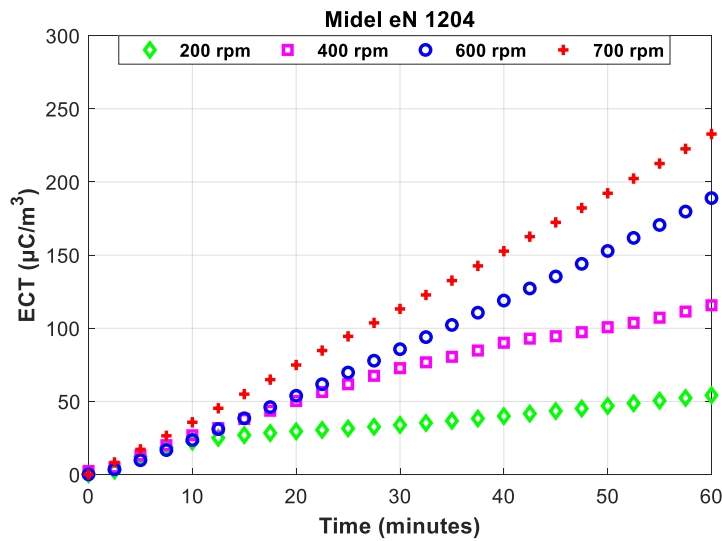
concentration of 0.2 g/L exhibits the improved performance of NE; the  $Q_{avg}$  and  $Q_{peak}$  are decreased by 66% and 72.55% compared to base liquid, respectively. In addition, there was a decrease in the number of PDs/s by approximately 15.5% compared to the base liquid. The reduction in PD characteristics (in  $Q_{avg}$ ,  $Q_{peak}$ , and NPDs/s) indicates an improvement in the performance of NE with the addition of MgO NPs at the optimal concentration.

Figure 4.16 shows the evolution of the volume charge density (charge per liquid volume) vs time for different spinning disk speeds for different liquids at room temperature. According to the results, the ECT of both NE (Figure 4.13. (a)) and NFs-based NE with MgO NPs (Figure 4.13. (b)) increases as the speed increases, except for the NF sample at 400 rpm and 600 rpm, which have an ECT that seems equal for a time higher than 40 minutes.

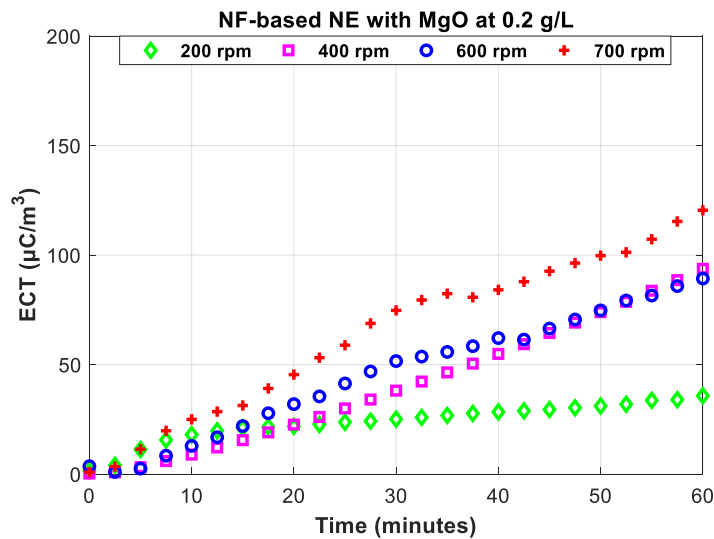
The results concerning the ECT level show the great potential of MgO NPs as a possible inhibitor of natural ester, Midel eN 1204. Several assumptions can be made about the mechanism behind such decrement:

- MgO NPs can act by increasing/decreasing the overall electronegativity of the liquid.
- NFs-based natural ester may have additional pathways for charge dispersal. When static charges are generated, NPs can facilitate the movement of charges, allowing them to dissipate more efficiently and preventing their build-up at the solid-liquid interface.
- NPs can act as electrostatic shields in transformer oil. They attract and neutralize static charges, reducing the overall charge imbalance and minimizing the electrostatic charging tendency of the oil.

However, it is difficult at this stage to conclude the mechanisms responsible for the decrease in the level of ECT of the natural ester observed in the presence of MgO NPs.



(a) Midel eN 1204



(a) Midel 1204 + MgO (0.2 g/L)

**Figure 4.16** Electrostatic charging tendency of (a) natural ester and (b) natural ester with MgO nanoparticles at 0.2 g/L.

#### 4.3.3 Natural ester (FR3) with $C_{60}$

Figures 4.17. (a) - 4.17. (c) show the variation in charge density (charge per fluid volume) for different fluids at rotational speeds from 200 to 700 rpm at room temperature. Those results indicate that an increase in the speed causes an increase in the ECT of pure FR3 and NFs-impregnated pressboards with  $C_{60}$  at 0.3 g/L and 0.4 g/L over time,

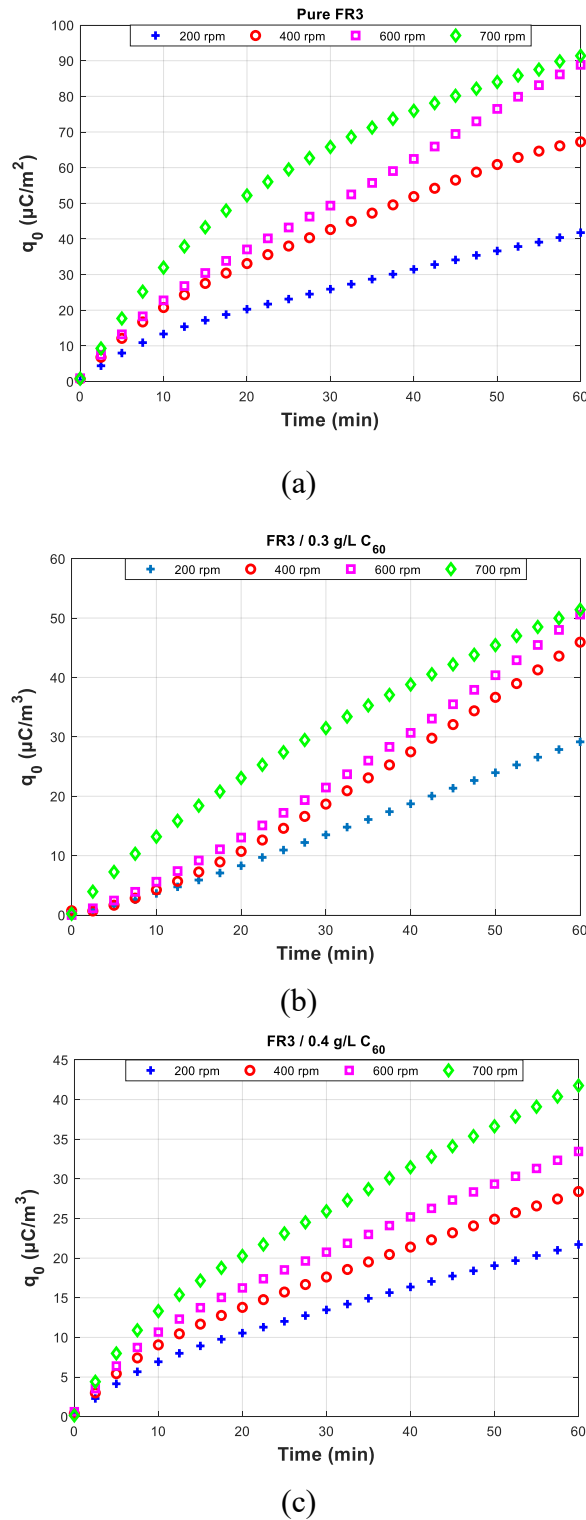


**Figure 4.17** Electrostatic charging tendency of (a) FR3, (b) FR3 with 0.3 g/L  $\text{C}_{60}$ , and (c) FR3 with 0.4 g/L  $\text{C}_{60}$ .

indicating the ECT's dependence on the speed rate. The cumulative electrostatic charge tendency (ECT) for different speed rates after one hour is presented in Figure 4.18.

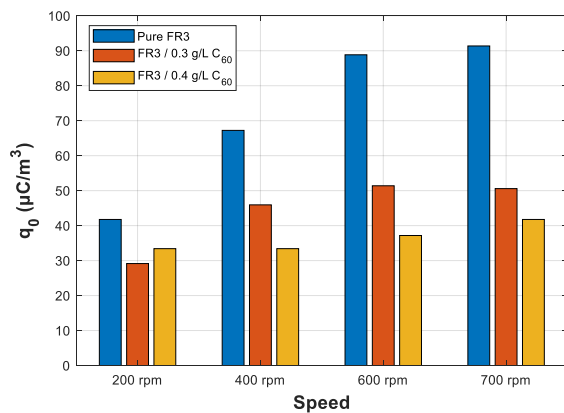


**Figure 4.18** Electrostatic charging tendency of pure FR3 and different nanofluids

On the other hand, it is observed that the two NFs show a reduced ECT level than the pure FR3, regardless of the flow velocity. These results generally show a high degree of agreement with the literature. In a similar work (nanofluid based on natural ester with  $\text{C}_{60}$ ), Zdanowski [57] studied the effect of fullerene NPs on the ECT of NE, Midel 1204. He observed that adding fullerene NPs to this latter for concentrations ranging from 0.025 g/L to 0.35 g/L considerably reduces its ECT level (60% of reduction of volume charge density  $q_w$  at a concentration of 0.35 g/L, which is the best concentration for comparison). He also reported that adding fullerene NPs to fresh mineral oil shows an increased electrification flow, while a reduction was observed in the case of aged mineral oil. The ECT of synthetic and natural esters-based NFs also depends on the doping concentration of fullerene NPs; it was reported that in most cases, a reduction was observed, and the optimum concentration of fullerene NPs that manifests the lowest ECT is in the range from 0.1 g/L to 0.2 g/L. Aksamit et al. [54] addressed the effect of fullerene NPs on the ECT of fresh mineral oil using a wireless rotating electrometer, 19 NFs were considered for concentrations ranging from 0.001 g/L to 0.512 g/L. The work underlined that fullerene NPs can significantly reduce the streaming electrification current in mineral transformer oil. The fullerene additive also causes a significant change in the flow electrification mechanism as indicated by current versus flow velocity relations. In similar work with quite an attention on the aging effect, Aksamit et al. [55] compared the ECT performances of mineral oil and mineral oil-based NFs doped with fullerene NPs; six NFs with different concentrations (0.01 g/L, 0.02 g/L, 0.05 g/L, 0.1 g/L, 0.2 g/L, and 0.3 g/L) were prepared. According to them, minimal flow electrification was achieved at an optimal concentration of 0.1 g/L. A 30% to 90% reduction rate of ECT was reported

depending on the aging period, the fullerene concentration, and the disk rotation speed [55].

#### **4.4 Creeping discharges**

Surface discharges, also known as creeping discharges, occur when an electric field causes discharges along the surface of insulating materials. If not properly prevented, these discharges can weaken the dielectric strength of the insulating systems and eventually lead to equipment failure. NPs have been shown to influence the behavior of AC BDV, PD activity, and ECT by different mechanisms.

This section will explore how different NPs, such as  $\text{Fe}_3\text{O}_4$ ,  $\text{Al}_2\text{O}_3$ , and  $\text{C}_{60}$ , affect surface discharge patterns of synthetic and natural esters, particularly the final length of the discharges under positive lightning impulse voltage (1.2/50  $\mu\text{s}$ ). A ceramic solid material of 6 mm is used for this analysis. By comparing the discharge activity in base liquid and different NFs, we can better understand the role of NPs in suppressing or modifying surface discharges, which is important for improving the durability and reliability of high-voltage equipment.

##### **4.4.1 Synthetic ester with $\text{Fe}_3\text{O}_4$ , $\text{Al}_2\text{O}_3$ (20-30 nm), and $\text{C}_{60}$**

###### **4.4.1.1 Creeping discharge patterns**

Figures 4.19. (a)-(d) show examples of creeping discharges propagating on the surface of solid insulator immersed in the SE and the corresponding NFs (with  $\text{Fe}_3\text{O}_4$ ,  $\text{Al}_2\text{O}_3$  (20-30 nm), and  $\text{C}_{60}$ ) under a 58 kV positive polarity voltage. It is important to note that the branches of the discharges follow circular paths (radial behavior) that appear to rotate around the tip electrode. Their shape, final length, and branch density depend on several parameters, such as the solid material's nature and thickness, the amplitude of applied voltage, and the NPs added to the base liquid. Others have also reported such observations [82], [105], [106], [107]. The creeping discharges in the SE and SE-based NFs have similar patterns (bush-like shape). Regardless of the liquid tested, increasing the applied voltage results in longer discharges and brighter discharge channels.

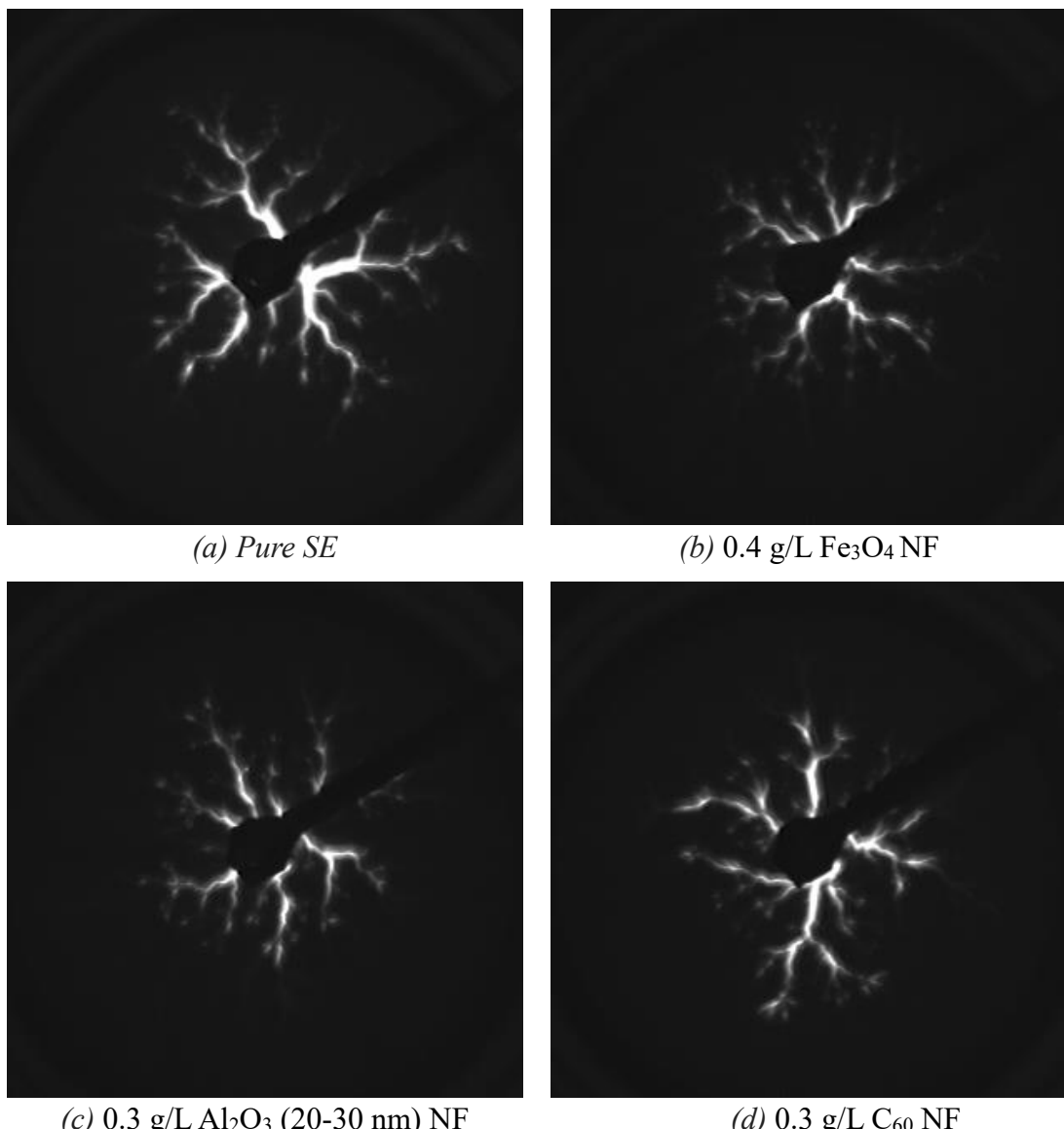


**Figure 4.19** Creeping discharge image at the surface of solid insulator immersed in different liquids.

#### 4.4.1.2 Stopping length of creeping discharges

Figure 4.20 shows the stopping length versus the applied voltage, ranging from 48 to 58 kV of SE and the corresponding NFs with  $\text{Fe}_3\text{O}_4$ ,  $\text{Al}_2\text{O}_3$ , and  $\text{C}_60$ . Note that the stopping length for voltage lower than 48 kV with SE and higher than 58 kV with  $\text{Fe}_3\text{O}_4$ ,  $\text{Al}_2\text{O}_3$ , and  $\text{C}_60$  NFs were measured. But, for comparison purposes, only the points with the same applied voltage were plotted.

The stopping length  $L_f$  increases quasi-linearly with the voltage  $U$ , whatever the type of liquid/NF. In the case of SE with  $\text{Fe}_3\text{O}_4$  and except with the 0.5 g/L at 54 kV,

concentrations of 0.3 g/L, 0.4 g/L, and 0.5 g/L positively impact the  $L_f$  whatever the voltage amplitude. In the majority of cases, 0.1 g/L and 0.2 g/L  $\text{Fe}_3\text{O}_4$  NFs show a negative impact regarding the  $L_f$ , regardless of the amplitude of the voltage. 0.3 g/L  $\text{Fe}_3\text{O}_4$  NF shows the best decrements in  $L_f$  compared to SE. In the case of  $\text{Al}_2\text{O}_3$  (20-30) nm NPs, concentrations of 0.1-0.3 g/L positively affect the  $L_f$  of SE regardless of the voltage amplitude, while higher concentrations increase the  $L_f$ . Those results show the capability

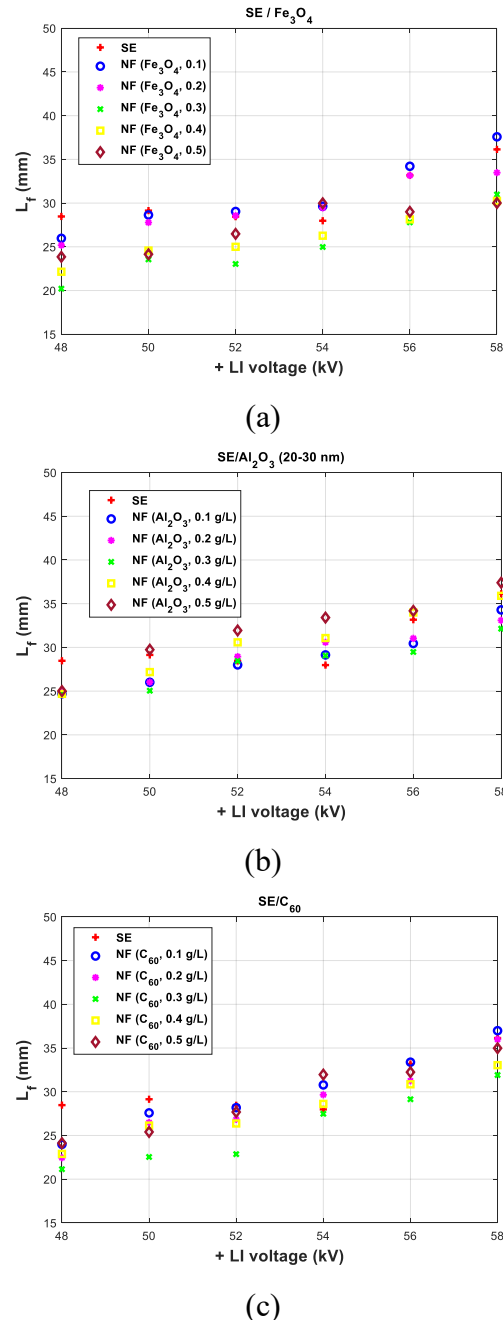


**Figure 4.20** Final length  $L_f$  of creeping discharge vs the applied voltage of (a) SE/ $\text{Fe}_3\text{O}_4$ , (b) SE/ $\text{Al}_2\text{O}_3$ , and (c) SE/ $\text{C}_{60}$ .

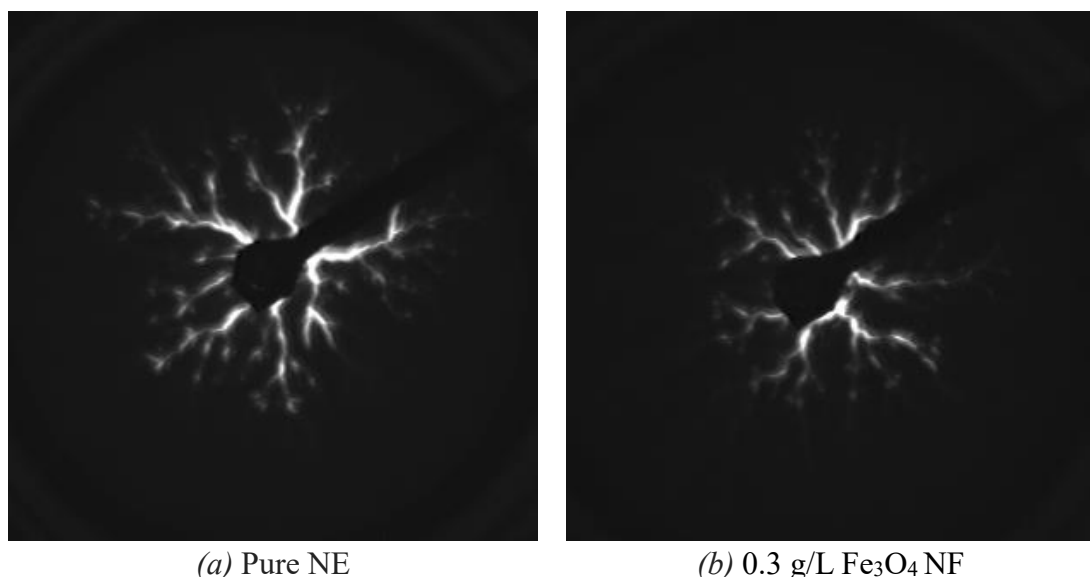
of alumina in reducing surface discharges of SE at lower concentrations, contrary to  $\text{Fe}_3\text{O}_4$ .

In the case of  $\text{C}_{60}$  NF, except for some points for each concentration, the  $L_f$  is more extended with base liquid than the corresponding NF for a given voltage. The decrease in the stopping length is between 1.49% (56 kV) and 13.23% (48 kV). It is quite clear that incorporating  $\text{Fe}_3\text{O}_4$ ,  $\text{Al}_2\text{O}_3$ , and  $\text{C}_{60}$  NPs may enhance the dielectric withstand of solid and liquid insulating systems.

#### **4.4.2 Natural ester with $\text{Fe}_3\text{O}_4$ , $\text{Al}_2\text{O}_3$ (20-30 nm), and $\text{C}_{60}$**

##### *4.4.2.1 Creeping discharge patterns*

Figures 4.21. (a)-(d) show examples of creeping discharges propagating on the surface of the solid insulator immersed in the FR3 and their corresponding NFs (with  $\text{Fe}_3\text{O}_4$ ,  $\text{Al}_2\text{O}_3$ , and  $\text{C}_{60}$ ) under a 58 kV positive polarity voltage. Similar to SE and SE-based NFs, the branches of the discharges appear to follow circular paths (radial behavior) around the tip electrode. The creeping discharges in the base liquid and NFs have similar patterns (bush-like shape). Furthermore, two significant differences could be underlined: (1) the main channels are much thicker in the case of  $\text{C}_{60}$  NF, with more lateral branches than the base liquid and  $\text{Fe}_3\text{O}_4$  and  $\text{Al}_2\text{O}_3$  NFs; and (2) the branches are even denser, and the emitted light is much weaker than that of the other liquids.



(a) Pure NE

(b) 0.3 g/L  $\text{Fe}_3\text{O}_4$  NF

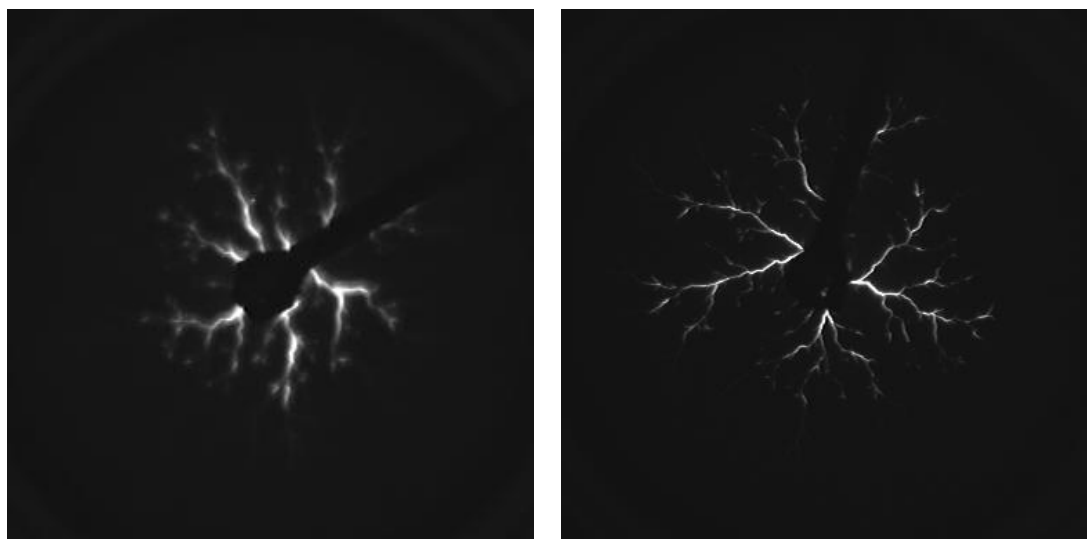


**Figure 4.21** Creeping discharge image at the surface of solid insulator immersed in different liquids.

#### 4.4.2.2 Stopping length of creeping discharges

Figure 4.22 illustrates the relationship between  $L_f$  and applied voltage, ranging from 48 to 58 kV for FR3 and the corresponding NF (containing  $\text{Fe}_3\text{O}_4$ ,  $\text{Al}_2\text{O}_3$ , and  $\text{C}_{60}$ ). Consistent with the observations for SE and their respective NFs, the  $L_f$  was measured for voltages lower than 48 kV with FR3 and higher than 58 kV with the  $\text{Fe}_3\text{O}_4$ ,  $\text{Al}_2\text{O}_3$ , and  $\text{C}_{60}$  NFs. However, only the data points corresponding to the same applied voltage were plotted. The  $L_f$  increases quasi-linearly with the voltage  $U$ , whatever the type of liquid/NF. In the case of SE with  $\text{Fe}_3\text{O}_4$ , only two concentrations (0.3 g/L and 0.4 g/L) positively impact the  $L_f$  regardless of the voltage amplitude. In most cases, 0.1 g/L, 0.2 g/L, and 0.5 g/L  $\text{Fe}_3\text{O}_4$  NFs negatively impact the  $L_f$ , regardless of the voltage amplitude. 0.3 g/L  $\text{Fe}_3\text{O}_4$  NF shows the best decrements in  $L_f$  compared to FR3. In contrast,  $\text{Al}_2\text{O}_3$  (20-30) nm NPs positively affect the  $L_f$  of FR3 regardless of the amplitude and NPs concentration. Those results show the capability of alumina in reducing surface discharges.

In the case of  $\text{C}_{60}$  NF, except for the first point, the stopping length is longer with base liquid than the corresponding NF for a given voltage. The decrease in the stopping length is between 1.49% (56 kV) and 13.23% (48 kV). It emerges from the above that adding  $\text{Fe}_3\text{O}_4$ ,  $\text{Al}_2\text{O}_3$ , and  $\text{C}_{60}$  NPs could be a solution to improve the dielectric withstand of solid/liquid insulating systems.

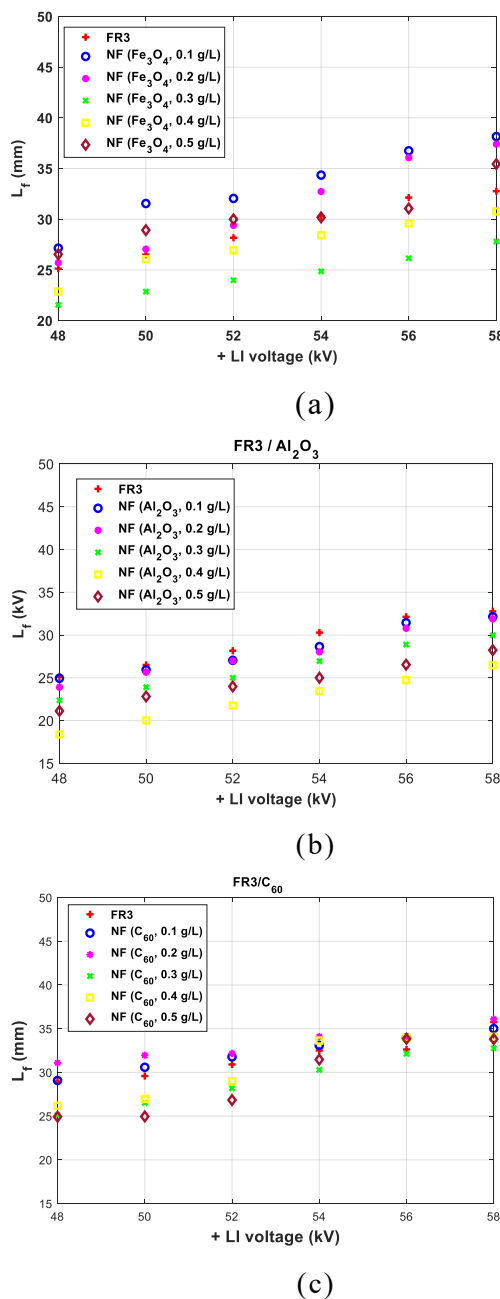


**Figure 4.22** Final length  $L_f$  of creeping discharge vs the applied voltage of (a) FR3/Fe<sub>3</sub>O<sub>4</sub>, (b) FR3/Al<sub>2</sub>O<sub>3</sub>, and (c) FR3/C<sub>60</sub>.

#### 4.4.3 Discussion

##### 4.4.3.1 Impact of Different Nanoparticles on Final Discharge Length

The analysis compares three NPs: Fe<sub>3</sub>O<sub>4</sub>, Al<sub>2</sub>O<sub>3</sub> (20-30 nm), and C<sub>60</sub>. The goal is to determine their effect on  $L_f$  of surface discharges when incorporated into SE and FR3 insulating liquids. For both esters, the creeping discharge length tends to increase quasi-linearly with the applied voltage. The influence of NPs can either enhance or suppress this increase depending on their type and concentration.

##### 4.4.3.2 Comparison between nanofluids and base liquids

###### a) Synthetic Ester:

Fe<sub>3</sub>O<sub>4</sub> NPs show varying impacts on  $L_f$  based on concentration. Higher concentrations (0.3 g/L and above) generally reduce the discharge length compared to lower concentrations (0.1 and 0.2 g/L), which can extend  $L_f$ . Al<sub>2</sub>O<sub>3</sub> NPs consistently reduce  $L_f$  at lower concentrations, making them more effective at improving dielectric strength at lower loadings. C<sub>60</sub> NPs generally show a shorter  $L_f$  than the base liquid across most conditions, indicating a more favorable impact on suppressing surface discharges.

###### b) Natural Ester:

The trends observed in SE tests are mirrored here, with some variations in the degree of  $L_f$  reduction. For instance, Al<sub>2</sub>O<sub>3</sub> again proves effective at reducing  $L_f$  across concentrations. The impact of Fe<sub>3</sub>O<sub>4</sub> NPs is inconsistent, with only specific concentrations leading to noticeable reductions in  $L_f$ , while, the effect of C<sub>60</sub> NPs remains less favorable for surface discharge suppression compared to the base liquid.

The results indicate that Al<sub>2</sub>O<sub>3</sub> is the most reliable NPs for reducing the  $L_f$  of creeping discharges, especially at lower concentrations. Fe<sub>3</sub>O<sub>4</sub> requires precise concentration control to achieve optimal performance, while C<sub>60</sub>'s role in discharge suppression remains less consistent.

## 4.5 Conclusion

The study has provided valuable insights into how NPs influence ester-based insulating liquids' electrical properties and insulation performance. The findings demonstrate that different types of NPs, including  $\text{Fe}_3\text{O}_4$ ,  $\text{Al}_2\text{O}_3$ ,  $\text{C}_{60}$ , and graphene, have varying effects on partial discharge (PD) activity, electrostatic charging tendencies (ECT), and surface discharges, depending on the type and concentration of NPs and the base liquid used.

Key conclusions from the chapter include:

**Partial Discharge Activity:** The introduction of NPs can either suppress or exacerbate PD activity based on the type of base liquid and NP concentration.  $\text{Al}_2\text{O}_3$  consistently reduces PD severity and number per second, particularly in SE, making it a favorable choice for improving insulation performance. In contrast,  $\text{Fe}_3\text{O}_4$ 's impact varies, with some improvements in delaying PD initiation and increasing discharge intensity under certain conditions.

**Electrostatic Charging Tendencies:** NPs such as  $\text{CuO}$ ,  $\text{MgO}$ , and  $\text{C}_{60}$  have shown potential in reducing ECT, particularly under higher liquid flow velocities, suggesting their role as effective additives for controlling static charge buildup in insulating systems. However, NP type, concentration, and fluid velocity affect the degree of ECT reduction observed.

**Surface Discharges:** The chapter findings suggest that adding NPs can enhance the dielectric strength of insulating systems by reducing the final length ( $L_f$ ) of surface discharges.  $\text{Al}_2\text{O}_3$  emerges as the most effective NP in this regard, while  $\text{Fe}_3\text{O}_4$  and  $\text{C}_{60}$  show mixed results depending on the applied voltage and concentration.

## **GENERAL CONCLUSION**

The research has provided significant evidence supporting the potential of nanofluids as advanced dielectric materials to enhance the insulation performance of transformer oils. The experimental investigations and statistical analyses reveal that incorporating NPs such as Fe<sub>3</sub>O<sub>4</sub>, Al<sub>2</sub>O<sub>3</sub>, C<sub>60</sub>, and Gr significantly influences the electrical properties of synthetic esters, natural esters, and mineral oils. Key findings indicate that including these nanoparticles can enhance the breakdown voltage, suppress partial discharge activity, reduce electrostatic charging tendencies and surface discharges although the extent of improvement depends on various factors, including the type of base liquid, nanoparticle material and size, concentration, etc.

In synthetic esters, Al<sub>2</sub>O<sub>3</sub> nanoparticles consistently show a significant reduction in partial discharge severity and frequency, making them a suitable choice for enhancing dielectric performance. Fe<sub>3</sub>O<sub>4</sub> nanoparticles, while improving some dielectric properties, exhibit mixed effects depending on the concentration used, with certain formulations showing increased partial discharge intensity. Carbon-based materials such as C<sub>60</sub> demonstrate promising results, particularly in reducing electrostatic charging, though their effectiveness may vary across different base liquids.

The research highlights the complexity of optimizing nanofluid formulations, as the interplay between NP characteristics and the dielectric properties of base fluids must be carefully managed to achieve the desired performance outcomes. Additionally, challenges related to NP stability, long-term dispersion, and the potential health risks associated with handling nanomaterials must be addressed to facilitate the safe and effective use of NFs in industrial applications.

Future work should focus on scaling up the preparation of stable and high-performance NFs, conducting long-term aging studies to assess their stability under operational conditions, and investigating the interactions between NPs and aging products in dielectric fluids. Furthermore, exploring novel NPs, such as hybrid nanomaterials and functionalized nanoparticles, could open new pathways for achieving even more

significant enhancements in electrical insulation. The findings of this research pave the way for the practical application of NFs in power transformers and other high-voltage equipment, contributing to improved reliability, safety, and efficiency in the energy sector.

## REFERENCES

- [1] S. U. Choi and J. A. Eastman, “Enhancing thermal conductivity of fluids with nanoparticles,” Argonne National Lab., IL (United States), 1995.
- [2] S. U. S. Choi, Z. G. Zhang, W. Yu, F. E. Lockwood, and E. A. Grulke, “Anomalous thermal conductivity enhancement in nanotube suspensions,” *Applied Physics Letters*, vol. 79, no. 14, pp. 2252–2254, Oct. 2001, doi: 10.1063/1.1408272.
- [3] P. Keblinski, S. R. Phillpot, S. U. S. Choi, and J. A. Eastman, “Mechanisms of heat flow in suspensions of nano-sized particles (nanofluids),” *International Journal of Heat and Mass Transfer*, vol. 45, no. 4, pp. 855–863, 2002, doi: [https://doi.org/10.1016/S0017-9310\(01\)00175-2](https://doi.org/10.1016/S0017-9310(01)00175-2).
- [4] S. U. S. Choi, X. Xu, P. Keblinski, and W. Yu, “NANOFLUIDS CAN TAKE THE HEAT”.
- [5] T. C. Choy, *Effective medium theory: principles and applications*, Second edition. in International series of monographs on physics, no. 165. Oxford: Oxford University Press, 2016.
- [6] R. L. Hamilton and O. K. Crosser, “Thermal Conductivity of Heterogeneous Two-Component Systems,” *Ind. Eng. Chem. Fund.*, vol. 1, no. 3, pp. 187–191, Aug. 1962, doi: 10.1021/i160003a005.
- [7] W. Yu and S. U. S. Choi, “The Role of Interfacial Layers in the Enhanced Thermal Conductivity of Nanofluids: A Renovated Maxwell Model,” *Journal of Nanoparticle Research*, vol. 5, no. 1/2, pp. 167–171, Apr. 2003, doi: 10.1023/A:1024438603801.
- [8] W. Yu and S. U. S. Choi, “The role of interfacial layers in the enhanced thermal conductivity of nanofluids: A renovated Hamilton?Crosser model,” *Journal of Nanoparticle Research*, vol. 6, no. 4, pp. 355–361, Aug. 2004, doi: 10.1007/s11051-004-2601-7.
- [9] W. Yu and H. Xie, “A review on nanofluids: preparation, stability mechanisms, and applications,” *Journal of nanomaterials*, vol. 2012, 2012.
- [10] N. A. C. Sidik, H. A. Mohammed, O. A. Alawi, and S. Samion, “A review on preparation methods and challenges of nanofluids,” *International Communications in Heat and Mass Transfer*, vol. 54, pp. 115–125, 2014.
- [11] M. Mehrali *et al.*, “Preparation, characterization, viscosity, and thermal conductivity of nitrogen-doped graphene aqueous nanofluids,” *J Mater Sci*, vol. 49, no. 20, pp. 7156–7171, Oct. 2014, doi: 10.1007/s10853-014-8424-8.
- [12] Y. Li, S. Tung, E. Schneider, and S. Xi, “A review on development of nanofluid preparation and characterization,” *Powder technology*, vol. 196, no. 2, pp. 89–101, 2009.
- [13] F. Yu *et al.*, “Dispersion stability of thermal nanofluids,” *Progress in Natural Science: Materials International*, vol. 27, no. 5, pp. 531–542, Oct. 2017, doi: 10.1016/j.pnsc.2017.08.010.

- [14] F. Ahmad, A. A. Khan, Q. Khan, and M. R. Hussain, “State-of-art in nano-based dielectric oil: A review,” *IEEE Access*, vol. 7, pp. 13396–13410, 2019.
- [15] S. Chakraborty and P. K. Panigrahi, “Stability of nanofluid: A review,” *Applied Thermal Engineering*, vol. 174, p. 115259, 2020, doi: <https://doi.org/10.1016/j.applthermaleng.2020.115259>.
- [16] A. G. N. Sofiah, M. Samykano, A. K. Pandey, K. Kadirkama, K. Sharma, and R. Saidur, “Immense impact from small particles: Review on stability and thermophysical properties of nanofluids,” *Sustainable Energy Technologies and Assessments*, vol. 48, p. 101635, 2021, doi: <https://doi.org/10.1016/j.seta.2021.101635>.
- [17] N. A. C. Sidik, H. A. Mohammed, O. A. Alawi, and S. Samion, “A review on preparation methods and challenges of nanofluids,” *International Communications in Heat and Mass Transfer*, vol. 54, pp. 115–125, May 2014, doi: 10.1016/j.icheatmasstransfer.2014.03.002.
- [18] W. Yu and H. Xie, “A Review on Nanofluids: Preparation, Stability Mechanisms, and Applications,” *Journal of Nanomaterials*, vol. 2012, pp. 1–17, 2012, doi: 10.1155/2012/435873.
- [19] F. Ahmad, “State-of-Art in Nano-Based Dielectric Oil: A Review,” vol. 7, p. 15, 2019.
- [20] N. Sezer, M. A. Atieh, and M. Koç, “A comprehensive review on synthesis, stability, thermophysical properties, and characterization of nanofluids,” *Powder Technology*, vol. 344, pp. 404–431, 2019, doi: <https://doi.org/10.1016/j.powtec.2018.12.016>.
- [21] Y. Nakama, “Surfactants,” in *Cosmetic Science and Technology*, Elsevier, 2017, pp. 231–244. doi: 10.1016/B978-0-12-802005-0.00015-X.
- [22] S. M. S. Murshed, K. C. Leong, and C. Yang, “Investigations of thermal conductivity and viscosity of nanofluids,” *International Journal of Thermal Sciences*, vol. 47, no. 5, pp. 560–568, May 2008, doi: 10.1016/j.ijthermalsci.2007.05.004.
- [23] P. Becher, “A Review of: ‘Fundamentals of Interface and Colloid Science: Vol.II - Solid/Liquid Interfaces’. J. Lyklema (with various contributors). Academic Press, London, 1995. \$65.00.,” *Journal of Dispersion Science and Technology*, vol. 18, no. 2, pp. 219–219, 1997, doi: 10.1080/01932699708943729.
- [24] T. F. Tadros, *Colloids in Paints: Colloids and Interface Science, Volume 6*. Wiley Online Library.
- [25] J. Lyklema, *Fundamentals of Interface and Colloid Science: Soft Colloids*. Elsevier, 2005.
- [26] A. S. Dukhin and P. J. Goetz, *Ultrasound for characterizing colloids: particle sizing, zeta potential, rheology*, 1st ed. in Studies in interface science, no. v. 15. Boston: Elsevier, 2002.
- [27] Malvern, “User Manual ZetaSizer ZS, Nano Series.” Apr. 2013.
- [28] P. Becher, “A Review of: ‘Fundamentals of Interface and Colloid Science: Vol.II - Solid/Liquid Interfaces’. J. Lyklema (with various contributors). Academic Press,

- London, 1995. \$65.00.,” *Journal of Dispersion Science and Technology*, vol. 18, no. 2, pp. 219–219, 1997, doi: 10.1080/01932699708943729.
- [29] Z. Huang *et al.*, “Electrical and thermal properties of insulating oil-based nanofluids: a comprehensive overview,” *IET Nanodielectrics*, vol. 2, no. 1, pp. 27–40, Mar. 2019, doi: 10.1049/iet-nde.2018.0019.
- [30] Y. Li, J. Zhou, S. Tung, E. Schneider, and S. Xi, “A review on development of nanofluid preparation and characterization,” *Powder Technology*, p. 13, 2009.
- [31] E. G. Atiya, D.-E. A. Mansour, R. M. Khattab, and A. M. Azmy, “Dispersion behavior and breakdown strength of transformer oil filled with TiO<sub>2</sub> nanoparticles,” *IEEE Trans. Dielect. Electr. Insul.*, vol. 22, no. 5, pp. 2463–2472, Oct. 2015, doi: 10.1109/TDEI.2015.004742.
- [32] P. Kopčanský, L. Tomčo, K. Marton, M. Koneracká, M. Timko, and I. Potočová, “The DC dielectric breakdown strength of magnetic fluids based on transformer oil,” *Journal of Magnetism and Magnetic Materials*, vol. 289, pp. 415–418, Mar. 2005, doi: 10.1016/j.jmmm.2004.11.117.
- [33] P. Kopčanský, L. Tomčo, K. Marton, M. Koneracká, I. Potočová, and M. Timko, “The experimental study of the DC dielectric breakdown strength in magnetic fluids,” *Journal of Magnetism and Magnetic Materials*, vol. 272–276, pp. 2377–2378, May 2004, doi: 10.1016/j.jmmm.2003.12.465.
- [34] J.-C. Lee, H.-S. Seo, and Y.-J. Kim, “The increased dielectric breakdown voltage of transformer oil-based nanofluids by an external magnetic field,” *International Journal of Thermal Sciences*, vol. 62, pp. 29–33, Dec. 2012, doi: 10.1016/j.ijthermalsci.2012.03.013.
- [35] V. Segal, A. Hjortsberg, A. Rabinovich, D. Nattrass, and K. Raj, “AC (60 Hz) and impulse breakdown strength of a colloidal fluid based on transformer oil and magnetite nanoparticles,” in *Conference Record of the 1998 IEEE International Symposium on Electrical Insulation (Cat. No.98CH36239)*, Arlington, VA, USA: IEEE, 1998, pp. 619–622. doi: 10.1109/ELINSL.1998.694869.
- [36] J. G. Hwang, M. Zahn, F. M. O’Sullivan, L. A. A. Pettersson, O. Hjortstam, and R. Liu, “Effects of nanoparticle charging on streamer development in transformer oil-based nanofluids,” *Journal of Applied Physics*, vol. 107, no. 1, p. 014310, Jan. 2010, doi: 10.1063/1.3267474.
- [37] W. Sima, J. Shi, Q. Yang, S. Huang, and X. Cao, “Effects of conductivity and permittivity of nanoparticle on transformer oil insulation performance: experiment and theory,” *IEEE Trans. Dielect. Electr. Insul.*, vol. 22, no. 1, pp. 380–390, Feb. 2015, doi: 10.1109/TDEI.2014.004277.
- [38] G. D. Peppas, V. P. Charalampakos, E. C. Pyrgioti, M. G. Danikas, A. Bakandritsos, and I. F. Gonos, “Statistical investigation of AC breakdown voltage of nanofluids compared with mineral and natural ester oil,” *IET Science, Measurement & Technology*, vol. 10, no. 6, pp. 644–652, Sep. 2016, doi: 10.1049/iet-smt.2016.0031.
- [39] M. E. Ibrahim, A. M. Abd-Elhady, and M. A. Izzularab, “Effect of nanoparticles on transformer oil breakdown strength: experiment and theory,” *IET Science,*

- Measurement & Technology*, vol. 10, no. 8, pp. 839–845, Nov. 2016, doi: 10.1049/iet-smt.2016.0104.
- [40] U. Khaled and A. Beroual, “AC dielectric strength of synthetic ester-based Fe<sub>3</sub>O<sub>4</sub>, Al<sub>2</sub>O<sub>3</sub> and SiO<sub>2</sub> nanofluids — conformity with normal and weibull distributions,” *IEEE Trans. Dielect. Electr. Insul.*, vol. 26, no. 2, pp. 625–633, Apr. 2019, doi: 10.1109/TDEI.2018.007759.
- [41] Huifei Jin, T. Andritsch, I. A. Tsekmes, R. Kochetov, P. H. F. Morshuis, and J. J. Smit, “Properties of Mineral Oil based Silica Nanofluids,” *IEEE Trans. Dielect. Electr. Insul.*, vol. 21, no. 3, pp. 1100–1108, Jun. 2014, doi: 10.1109/TDEI.2014.6832254.
- [42] U. Khaled and A. Beroual, “DC breakdown voltage of natural ester oil-based Fe<sub>3</sub>O<sub>4</sub>, Al<sub>2</sub>O<sub>3</sub>, and SiO<sub>2</sub> nanofluids,” *Alexandria Engineering Journal*, vol. 59, no. 6, pp. 4611–4620, Dec. 2020, doi: 10.1016/j.aej.2020.08.016.
- [43] U. Khaled and A. Beroual, “Statistical Investigation of AC Dielectric Strength of Natural Ester Oil-Based Fe<sub>3</sub>O<sub>4</sub>, Al<sub>2</sub>O<sub>3</sub>, and SiO<sub>2</sub> Nano-Fluids,” *IEEE Access*, vol. 7, pp. 60594–60601, 2019, doi: 10.1109/ACCESS.2019.2915517.
- [44] F. Herchl *et al.*, “Breakdown and partial discharges in magnetic liquids,” *J. Phys.: Condens. Matter*, vol. 20, no. 20, p. 204110, May 2008, doi: 10.1088/0953-8984/20/20/204110.
- [45] H. Jin, P. Morshuis, A. R. Mor, J. J. Smit, and T. Andritsch, “Partial discharge behavior of mineral oil based nanofluids,” *IEEE Trans. Dielect. Electr. Insul.*, vol. 22, no. 5, pp. 2747–2753, Oct. 2015, doi: 10.1109/TDEI.2015.005145.
- [46] S. Chandrasekar, J. Chandramohan, G. C. Montanari, and P. Uthirakumar, “Developing eco-friendly nanostructured oil: Partial discharge and breakdown voltage characterization of transformer corn oil,” *IEEE Trans. Dielect. Electr. Insul.*, vol. 27, no. 5, pp. 1611–1618, Oct. 2020, doi: 10.1109/TDEI.2020.008992.
- [47] E. G. Atiya, D.-E. A. Mansour, and M. A. Izzularab, “Partial Discharge Development in Oil-Based Nanofluids: Inception, Propagation and Time Transition,” *IEEE Access*, vol. 8, pp. 181028–181035, 2020, doi: 10.1109/ACCESS.2020.3027905.
- [48] M. T. Imani, P. Werle, J. F. Miethe, and N. C. Bigall, “Magnetite nanofluid as alternative for conventional insulating liquids,” in *2017 IEEE 19th International Conference on Dielectric Liquids (ICDL)*, Manchester: IEEE, Jun. 2017, pp. 1–4. doi: 10.1109/ICDL.2017.8124604.
- [49] K. N. Koutras, S. N. Tegopoulos, V. P. Charalampakos, A. Kyritsis, I. F. Gonos, and E. C. Pyrgioti, “Breakdown Performance and Partial Discharge Development in Transformer Oil-Based Metal Carbide Nanofluids,” *Nanomaterials*, vol. 12, no. 2, p. 269, Jan. 2022, doi: 10.3390/nano12020269.
- [50] J. Kurimský, M. Rajnák, M. Šárpataky, Z. Čonka, and K. Paulovičová, “Electrical and acoustic investigation of partial discharges in two types of nanofluids,” *Journal of Molecular Liquids*, vol. 341, p. 117444, Nov. 2021, doi: 10.1016/j.molliq.2021.117444.

- [51] J. Samat, “Summary of the TF activity since 1990 CIGRE Session,” CIGRE, Report CIGRE SC 15 WG 15-01, Task Force JWG 12/15-13-01, 1990.
- [52] L. Peyraque, C. Boisdon, A. Beroual, and F. Buret, “Static electrification and partial discharges induced by oil flow in power transformers,” *IEEE Trans. Dielect. Electr. Insul.*, vol. 2, no. 1, pp. 40–45, Feb. 1995, doi: 10.1109/94.368678.
- [53] M. Higaki, Y. Kako, M. Moriyama, M. Hirano, K. Hiraishi, and K. Kurita, “Static Electrification and Partial Discharges Caused by Oil Flow in Forced Oil Cooled Core Type Transformers,” *IEEE Trans. on Power Apparatus and Syst.*, vol. PAS-98, no. 4, pp. 1259–1267, Jul. 1979, doi: 10.1109/TPAS.1979.319438.
- [54] P. Aksamit and D. Zmarzly, “C60 as flow electrification inhibitor in mineral insulating oil,” *Journal of Electrostatics*, vol. 69, no. 3, pp. 195–199, Jun. 2011, doi: 10.1016/j.elstat.2011.03.009.
- [55] P. Aksamit, D. Zmarzly, and T. Boczar, “Electrostatic properties of aged fullerene-doped mineral oil,” *IEEE Trans. Dielect. Electr. Insul.*, vol. 18, no. 5, pp. 1459–1462, Oct. 2011, doi: 10.1109/TDEI.2011.6032816.
- [56] A. J. Amalanathan, R. Sarathi, N. Harid, and H. Griffiths, “Investigation on flow electrification of ester-based TiO<sub>2</sub> nanofluids,” *IEEE Trans. Dielect. Electr. Insul.*, vol. 27, no. 5, pp. 1492–1500, Oct. 2020, doi: 10.1109/TDEI.2020.008540.
- [57] M. Zdanowski, “Streaming Electrification of C60 Fullerene Doped Insulating Liquids for Power Transformers Applications,” *Energies*, vol. 15, no. 7, p. 2496, Mar. 2022, doi: 10.3390/en15072496.
- [58] A. Beroual and H. Duzkaya, “AC and Lightning Impulse Breakdown Voltages of Natural Ester Based Fullerene Nanofluids,” *IEEE Trans. Dielect. Electr. Insul.*, vol. 28, no. 6, pp. 1996–2003, Dec. 2021, doi: 10.1109/TDEI.2021.009772.
- [59] H. Khelifa, A. Beroual, and E. Vagnon, “Effect of Conducting, Semi-Conducting and Insulating Nanoparticles on AC Breakdown Voltage and Partial Discharge Activity of Synthetic Ester: A Statistical Analysis,” *Nanomaterials*, vol. 12, no. 12, p. 2105, Jun. 2022, doi: 10.3390/nano12122105.
- [60] H. Duzkaya and A. Beroual, “Statistical Analysis of AC Dielectric Strength of Natural Ester-Based ZnO Nanofluids,” *Energies*, vol. 14, no. 1, p. 99, Dec. 2020, doi: 10.3390/en14010099.
- [61] M. Fasehullah, F. Wang, and S. Jamil, “Significantly elevated AC dielectric strength of synthetic ester oil-based nanofluids by varying morphology of CdS nano-additives,” *Journal of Molecular Liquids*, vol. 353, p. 118817, May 2022, doi: 10.1016/j.molliq.2022.118817.
- [62] M. Fasehullah, F. Wang, S. Jamil, and M. S. Bhutta, “Influence of Emerging Semiconductive Nanoparticles on AC Dielectric Strength of Synthetic Ester Midel-7131 Insulating Oil,” *Materials*, vol. 15, no. 13, p. 4689, Jul. 2022, doi: 10.3390/ma15134689.
- [63] T. W. Anderson and D. A. Darling, “Asymptotic Theory of Certain ‘Goodness of Fit’ Criteria Based on Stochastic Processes,” *The Annals of Mathematical Statistics*, vol. 23, no. 2, pp. 193–212, 1952, doi: 10.1214/aoms/1177729437.

- [64] G. Marsaglia and J. Marsaglia, “Evaluating the Anderson-Darling Distribution,” *J. Stat. Soft.*, vol. 9, no. 2, 2004, doi: 10.18637/jss.v009.i02.
- [65] S. Shaphiro and M. Wilk, “An analysis of variance test for normality,” *Biometrika*, vol. 52, no. 3, pp. 591–611, 1965.
- [66] M. J. Crawley, *The R book*. John Wiley & Sons, 2012.
- [67] M. A. Stephens, “EDF statistics for goodness of fit and some comparisons,” *Journal of the American statistical Association*, vol. 69, no. 347, pp. 730–737, 1974.
- [68] S. Boslaugh and P. A. Watters, *Statistics in a nutshell: A desktop quick reference*. O'Reilly Media, Inc., 2012.
- [69] B. L. Welch, “The generalization of ‘STUDENT’S’problem when several different population variances are involved,” *Biometrika*, vol. 34, no. 1–2, pp. 28–35, 1947.
- [70] R. D'Agostino, *Goodness-of-fit-techniques*. Routledge, 2017.
- [71] J. Lyklema, *Fundamentals of interface and colloid science. Volume I: Fundamentals*. Academic Press, 1991.
- [72] M. Gouy, “Sur la constitution de la charge électrique à la surface d'un électrolyte,” *J. Phys. Theor. Appl.*, vol. 9, no. 1, pp. 457–468, 1910.
- [73] D. L. Chapman, “LI. A contribution to the theory of electrocapillarity,” *The London, Edinburgh, and Dublin Philosophical Magazine and Journal of Science*, vol. 25, no. 148, pp. 475–481, 1913, doi: 10.1080/14786440408634187.
- [74] J. Bikerman, “XXXIX. Structure and capacity of electrical double layer,” *The London, Edinburgh, and Dublin Philosophical Magazine and Journal of Science*, vol. 33, no. 220, pp. 384–397, 1942.
- [75] O. Stern, “Zur theorie der elektrolytischen doppelschicht,” *Zeitschrift für Elektrochemie und angewandte physikalische Chemie*, vol. 30, no. 21–22, pp. 508–516, 1924.
- [76] J. R. Macdonald, “Theory of the differential capacitance of the double layer in unadsorbed electrolytes,” *The Journal of Chemical Physics*, vol. 22, no. 11, pp. 1857–1866, 1954.
- [77] J. Bockris, M. Devanathan, and K. Müller, “On the structure of charged interfaces,” in *Electrochemistry*, Elsevier, 1965, pp. 832–863.
- [78] H. J. Wiesmann and H. R. Zeller, “A fractal model of dielectric breakdown and prebreakdown in solid dielectrics,” in *Conference on Electrical Insulation & Dielectric Phenomena — Annual Report 1986*, Claymont, DE: IEEE, Nov. 1986, pp. 385–390. doi: 10.1109/CEIDP.1986.7726472.
- [79] J. L. Vicente, A. C. Razzitte, and E. E. Mola, “Fractal characteristics of dielectric breakdown,” in *Proceedings of IEEE Conference on Electrical Insulation and Dielectric Phenomena - (CEIDP'94)*, Arlington, TX, USA: IEEE, 1994, pp. 524–531. doi: 10.1109/CEIDP.1994.592025.

- [80] L. Niemeyer, L. Pietronero, and H. J. Wiesmann, “Fractal Dimension of Dielectric Breakdown,” *Phys. Rev. Lett.*, vol. 52, no. 12, pp. 1033–1036, Mar. 1984, doi: 10.1103/PhysRevLett.52.1033.
- [81] Y. Sawada, S. Ohta, M. Yamazaki, and H. Honjo, “Self-similarity and a phase-transition-like behavior of a random growing structure governed by a nonequilibrium parameter,” *Phys. Rev. A*, vol. 26, no. 6, pp. 3557–3563, Dec. 1982, doi: 10.1103/PhysRevA.26.3557.
- [82] J. L. Jiosseu, G. M. Mengounou, and A. M. Imano, “Study of Creeping Discharges Propagating Along a Solid Insulating Surface Immersed in Mineral Oil and Palm Kernel Oil Methyl Ester Under Negative Lightning Impulse Voltage,” *IEEE Trans. Dielect. Electr. Insul.*, vol. 29, no. 5, pp. 1847–1856, Oct. 2022, doi: 10.1109/TDEI.2022.3199183.
- [83] A. Beroual, V.-H. Dang, M.-L. Coulibaly, and C. Perrier, “Investigation on creeping discharges propagating over pressboard immersed in mineral and vegetable oils under AC, DC and lightning impulse voltages,” *IEEE Trans. Dielect. Electr. Insul.*, vol. 20, no. 5, pp. 1635–1640, Oct. 2013, doi: 10.1109/TDEI.2013.6633693.
- [84] L. Kebbabi, “Caractérisation des décharges glissantes se propageant aux interfaces liquide/solide sous différentes formes de tension–Relation entre propriétés des matériaux et dimension fractale.,” PhD Thesis, École Centrale de Lyon, 2006.
- [85] B. B. Mandelbrot and M. Aizenman, “Fractals: Form, Chance and Dimension,” 1978. [Online]. Available: <https://api.semanticscholar.org/CorpusID:120246027>
- [86] M. Lungu, A. Neculae, M. Bunoiu, and C. Biris, Eds., *Nanoparticles' Promises and Risks: Characterization, Manipulation, and Potential Hazards to Humanity and the Environment*. Cham: Springer International Publishing, 2015. doi: 10.1007/978-3-319-11728-7.
- [87] R. J. Aitken, K. S. Creely, and C. L. Tran, *Nanoparticles: an occupational hygiene review*. Sudbury: HSE Books, 2004.
- [88] G. Ramachandran, Ed., *Assessing nanoparticle risks to human health*, Second edition. in Micro & nano technologies series. Amsterdam ; Boston: Elsevier/WA, William Andrew is an imprint of Elsevier, 2016.
- [89] K. Wang *et al.*, “Respiratory Exposure to Copper Oxide Particles Causes Multiple Organ Injuries via Oxidative Stress in a Rat Model,” *IJN*, vol. Volume 17, pp. 4481–4496, Sep. 2022, doi: 10.2147/IJN.S378727.
- [90] D. Gupta, P. Yadav, D. Garg, and T. K. Gupta, “Pathways of nanotoxicity: Modes of detection, impact, and challenges,” *Frontiers of Materials Science*, vol. 15, no. 4, pp. 512–542, Dec. 2021, doi: 10.1007/s11706-021-0570-8.
- [91] Z. Li *et al.*, “Cardiovascular Effects of Pulmonary Exposure to Single-Wall Carbon Nanotubes,” *Environ Health Perspect*, vol. 115, no. 3, pp. 377–382, Mar. 2007, doi: 10.1289/ehp.9688.
- [92] E. Mostovenko *et al.*, “Indirect mediators of systemic health outcomes following nanoparticle inhalation exposure,” *Pharmacology & Therapeutics*, vol. 235, p. 108120, Jul. 2022, doi: 10.1016/j.pharmthera.2022.108120.

- [93] M&I Materials, “MIDEL 7131, Synthetic Ester Transformer Fluid Fire safe and Biodegradable,” M&I Materials, UK, 2018.
- [94] Gargill, “Envirotemp FR3 fluid. Formulated for performance.” 2018.
- [95] Nynas, “NYTRO 4000 X,” Sweden, Nov. 2023. Accessed: Nov. 30, 2023. [Online]. Available: <https://www.nynas.com/en/products/transformer-oils/products/nytrop-4000x/>
- [96] “Oleic acid,” *Wikipedia*. Feb. 06, 2024. Accessed: Feb. 23, 2024. [Online]. Available: [https://en.wikipedia.org/w/index.php?title=Oleic\\_acid&oldid=1204007032](https://en.wikipedia.org/w/index.php?title=Oleic_acid&oldid=1204007032)
- [97] M. Ash and I. Ash, *Handbook of industrial surfactants*, 5th ed. Endicott, N.Y.: Synapse Information Resources, 2010.
- [98] International Electrotechnical Commission, “Insulating liquids – Determination of the Breakdown Voltage at Power Frequency – Test Method,” IEC 60156, Edition 3.0, 2018.
- [99] A. Beroual, H. Khelifa, and U. Khaled, “Comparison of electrostatic charging tendency of Jarylec and mineral oil,” *Electr Eng*, Sep. 2021, doi: 10.1007/s00202-021-01400-8.
- [100] H. Morgan and N. G. Green, *AC electrokinetics: colloids and nanoparticles*. in Microtechnologies and microsystems series, no. 2. Baldock: Research Studies Press, 2003.
- [101] H. Khelifa, A. Beroual, and E. Vagnon, “Effect of Conducting and Semiconducting Nanoparticles on the AC Breakdown Voltage and Electrostatic Charging Tendency of Synthetic Ester,” *IEEE Trans. Dielect. Electr. Insul.*, vol. 30, no. 4, pp. 1414–1421, Aug. 2023, doi: 10.1109/TDEI.2023.3261825.
- [102] T. Paillat, Y. Zelu, G. Morin, and C. Perrier, “Ester oils and flow electrification hazards in power transformers,” *IEEE Trans. Dielect. Electr. Insul.*, vol. 19, no. 5, pp. 1537–1543, Oct. 2012, doi: 10.1109/TDEI.2012.6311498.
- [103] P. C. Mishra, S. Mukherjee, S. K. Nayak, and A. Panda, “A brief review on viscosity of nanofluids,” *Int Nano Lett*, vol. 4, no. 4, pp. 109–120, Dec. 2014, doi: 10.1007/s40089-014-0126-3.
- [104] K. Bashirnezhad *et al.*, “Viscosity of nanofluids: A review of recent experimental studies,” *International Communications in Heat and Mass Transfer*, vol. 73, pp. 114–123, Apr. 2016, doi: 10.1016/j.icheatmasstransfer.2016.02.005.
- [105] A. Reffas, H. Moulai, and A. Beroual, “Creeping discharges propagating on natural ester oils/pressboard interface under AC and lightning impulse voltages,” *IEEE Trans. Dielect. Electr. Insul.*, vol. 25, no. 5, pp. 1814–1821, Oct. 2018, doi: 10.1109/TDEI.2018.007217.
- [106] J. L. Jiosseu, G. M. Mengounou, and A. M. Imano, “Experimental characterisation of positive creeping discharges propagating along an insulating surface immersed in vegetable and mineral oil,” *Journal of Electrostatics*, vol. 119, p. 103753, 2022.
- [107] L. Kebabi and A. Beroual, “Optical and electrical characterization of creeping discharges over solid/liquid interfaces under lightning impulse voltage,” *IEEE Trans.*

*Dielect. Electr. Insul.*, vol. 13, no. 3, pp. 565–571, Jun. 2006, doi: 10.1109/TDEI.2006.1657969.

## Appendix A - Two-Sample t-Test

Given two sets of data (AC BDV of base liquid and different NFs), the t-test is conducted in the following steps:

The calculation of the *t*-value (two-sample *t*-test, called Welch *t*-test) is given by the formula below [68]

$$t = \frac{\bar{x}_1 - \bar{x}_2 - \Delta}{\sqrt{\frac{s_1^2}{n_1} + \frac{s_2^2}{n_2}}} \quad 5$$

Where  $\bar{x}_1$  and  $\bar{x}_2$  are the mean values of set 1 and 2, respectively,  $\Delta$  is the hypothesized difference (0 for equal and 1 for unequal means),  $s_1$  and  $s_2$  are the standard deviations of set 1 and 2, respectively, and  $n_1$  and  $n_2$  are the sizes of set 1 and 2, respectively.

The degree of freedom (*df*) for the Welch *t*-test is given by the formula below [68]

$$df = \frac{\left( \frac{s_1^2}{n_1} + \frac{s_2^2}{n_2} \right)^2}{\frac{\left( \frac{s_1^2}{n_1} \right)^2}{n_1 - 1} + \frac{\left( \frac{s_2^2}{n_2} \right)^2}{n_2 - 1}} \quad 6$$

The *df* value is then used to determine the critical values from the *t*-value table. Because this is a one-tailed test, the alpha level is 0.05.

The following step consists in looking up  $t_{1-\alpha, df}(\alpha=0.05, 1-\alpha=0.95, df)$  value in the *t*-table [68], and looking for the critical value, which corresponds to the limit *t*-value for a known degree of freedom.

If  $t$ -value  $\geq t_{1-\alpha, df}$ , the null hypothesis cannot be rejected in this case, and the two data sets appear different.

If  $t$ -value  $< t_{1-\alpha, df}$ , the null hypothesis is rejected in this case, and the two data sets do not appear different.

## Appendix B - Anderson–Darling fitting test

The conformity check of the AC BdV outcomes to Weibull distribution was investigated using the Anderson–Darling fitting test (AD-Test) [63], [64], [70]; its formula is given below

$$AD^2(x) = -n - \sum_{i=1}^n \frac{2i-1}{n} \times [\ln(CDF(x_i)) + \ln(1 - CDF(x_{n+1-i}))] \quad 2$$

Where,  $\{x_1 < \dots < x_n\}$  are the ordered AC BdVs points; i and n are the number of data points in the sample and  $i^{\text{th}}$  sample, respectively. The cumulative distribution function (CDF) of Weibull distribution is given below:

$$CDF(x) = 1 - e^{-\left(\frac{x}{\beta}\right)^{\alpha}} \quad 1$$

The scale ( $\alpha$ ) and the shape ( $\beta$ ) parameters represent the AC BdV at a 63% risk level and the slope of the Weibull line curve, respectively.

The next step consists in calculating the corresponding p-value using AD statistic [64]

$$p\text{-value} = \begin{cases} e^{(1.294 - 5.709AD + 0.019AD^2)} & AD \geq 0.60 \\ e^{(0.918 - 4.279AD - 1.380AD^2)} & 0.34 < AD < 0.60 \\ 1 - e^{(-8.318 + 42.796AD - 59.938AD^2)} & 0.20 < AD \leq 0.34 \\ 1 - e^{(-13.436 + 101.140AD - 223.730AD^2)} & AD \leq 0.20 \end{cases} \quad 3$$

Finally, the p-value is compared to the significance level (0.05). Hence, if the p-value is less than or equal to 0.05, reject the null hypothesis that the Weibull distribution fits the data; else, accept the null hypothesis that the Weibull distribution fits the data.

## RELATED WORKS

### Journal Articles

- [1] **H. Khelifa**, E. Vagnon, and A. Beroual, “Effect of Zirconia Nanoparticles on the AC Breakdown Voltage of Mineral Oil, Synthetic, and Natural Esters,” *IEEE Transactions on Dielectrics and Electrical Insulation*, vol. 31, no. 2, pp. 731–737, 2024, doi: 10.1109/TDEI.2024.3364108.
- [2] **H. Khelifa**, P. Skotnicki, A. Beroual, E. Vagnon, and M. Jaroszewski, “Effect of MgO Nanoparticles on the AC Breakdown Voltage, Partial Discharge Activity, and Electrostatic Charging Tendency of Natural Ester,” *IEEE Transactions on Dielectrics and Electrical Insulation*, vol. 31, no. 3, pp. 1350–1358, 2024, doi: 10.1109/TDEI.2024.3374244.
- [3] **H. Khelifa**, A. Beroual, and E. Vagnon, “Effect of Conducting, Semi-Conducting and Insulating Nanoparticles on AC Breakdown Voltage and Partial Discharge Activity of Synthetic Ester: A Statistical Analysis,” *Nanomaterials*, vol. 12, no. 12, 2022, doi: 10.3390/nano12122105.
- [4] **H. Khelifa**, A. Beroual, and E. Vagnon, “Effect of Conducting and Semiconducting Nanoparticles on the AC Breakdown Voltage and Electrostatic Charging Tendency of Synthetic Ester,” *IEEE Transactions on Dielectrics and Electrical Insulation*, vol. 30, no. 4, pp. 1414–1421, 2023, doi: 10.1109/TDEI.2023.3261825.
- [5] **H. Khelifa**, E. Vagnon, and A. Beroual, “Effect of Fullerene and Graphene Nanoparticles on the AC Dielectric Strength of Natural Ester,” *Energies*, vol. 16, no. 4, 2023, doi: 10.3390/en16041995.
- [6] **H. Khelifa**, E. Vagnon, and A. Beroual, “AC Breakdown Voltage and Partial Discharge Activity in Synthetic Ester-Based Fullerene and Graphene Nanofluids,” *IEEE Access*, vol. 10, pp. 5620–5634, 2022, doi: 10.1109/ACCESS.2022.3140928.

## International Conferences

- [1] **H. Khelifa**, A. Beroual, and E. Vagnon, “Effect of Fullerene Nanoparticles on the Electrostatic Charging Tendency of Natural Ester FR3,” in *2023 IEEE 22nd International Conference on Dielectric Liquids (ICDL)*, 2023, pp. 1–4. doi: 10.1109/ICDL59152.2023.10209318.
- [2] **H. Khelifa**, A. Beroual, and E. Vagnon, “Effect of Fe<sub>3</sub>O<sub>4</sub> and Al<sub>2</sub>O<sub>3</sub> Nanoparticles on Creeping Discharges Propagating Over Solid-Natural Ester FR3 Interface Under Lightning Impulse Voltage,” in *2023 IEEE Conference on Electrical Insulation and Dielectric Phenomena (CEIDP)*, 2023, pp. 1–4. doi: 10.1109/CEIDP51414.2023.10410470.
- [3] **H. Khelifa**, E. Vagnon, and A. Beroual, “Effect of Fe<sub>3</sub>O<sub>4</sub> and Al<sub>2</sub>O<sub>3</sub> Nanoparticles on AC Breakdown Voltage and Partial Discharge Activity of Synthetic and Natural Esters,” in *2023 IEEE Conference on Electrical Insulation and Dielectric Phenomena (CEIDP)*, 2023, pp. 1–4. doi: 10.1109/CEIDP51414.2023.10410487.
- [4] **H. Khelifa**, S. Anand, A. Beroual, and E. Vagnon, “Comparison of Partial Discharge Activity in Synthetic Ester and Synthetic Ester-Based Fullerene Nanofluid Under AC 50 Hz,” in *2022 IEEE Electrical Insulation Conference (EIC)*, 2022, pp. 102–105. doi: 10.1109/EIC51169.2022.9833211.
- [5] **H. Khelifa**, E. Vagnon, and A. Beroual, “AC Dielectric Strength and Partial Discharge Activity in Naturel Ester and Naturel Ester-Based Fullerene Nanofluids,” in *2023 IEEE 22nd International Conference on Dielectric Liquids (ICDL)*, 2023, pp. 1–4. doi: 10.1109/ICDL59152.2023.10209333.
- [6] **H. Khelifa**, E. Vagnon, and A. Beroual, “AC Breakdown Voltage and Partial Discharge Activity in Synthetic Ester and Synthetic Ester-Based Zirconia Nanofluid,” in *2022 IEEE 21st International Conference on Dielectric Liquids (ICDL)*, 2022, pp. 1–4. doi: 10.1109/ICDL49583.2022.9830968.

## RESUME DE THESE EN FRANÇAIS

<u>Introduction Générale</u> .....	- 3 -
<u>Section 1</u> .....	- 4 -
<u>Techniques Experimentales</u> .....	- 4 -
<u>Matériaux et préparation des nanofluides</u> .....	- 5 -
<u>Dispositif expérimental et méthodes d'essai</u> .....	- 7 -
<u>Mesures de la tension de claquage en courant alternatif</u> .....	- 7 -
<u>Caractérisation de la décharge partielle (DP)</u> .....	- 7 -
<u>Tendance à la charge électrostatique (ECT)</u> .....	- 8 -
<u>Caractérisation des décharges de surface</u> .....	- 9 -
<u>Conclusion</u> .....	- 10 -
<u>Section 2</u> .....	- 11 -
<u>Tension de Claquage en Courant Alternatif des Nanofluides à base d'Esters Synthétiques et Naturels et d'Huile Minérale</u> .....	- 11 -
<u>Tension de claquage en AC des Nanoparticules conductrices</u> .....	- 12 -
<u>Tension de claquage en AC des Nanoparticules semi-conductrices</u> .....	- 15 -
<u>Tension de claquage en AC des Nanoparticules Isolantes</u> .....	- 16 -
<u>Discussion</u> .....	- 22 -
<u>Conclusion</u> .....	- 27 -
<u>Section 3</u> .....	- 29 -
<u>Effet des Nanoparticules sur l'Activité des Décharges Partielles, la Tendance à la Charge Electrostatique et la Décharge Surfacique</u> .....	- 29 -
<u>Activité de décharge partielle</u> .....	- 30 -
<u>NP conductrices</u> .....	- 30 -
<u>NPs isolantes</u> .....	- 35 -
<u>Discussion de l'effet des NP sur l'activité des DP</u> .....	- 37 -
<u>Tendances à la charge électrostatique</u> : .....	- 39 -
<u>Ester synthétique avec Fe<sub>3</sub>O<sub>4</sub>, CuO, et C<sub>60</sub></u> : .....	- 39 -

<u>Ester naturel (Midel 1204) avec MgO :</u>	- 39 -
<u>Ester naturel (FR3) avec C<sub>60</sub> :</u>	- 40 -
<u>Principales conclusions :</u>	- 40 -
<u>Décharge de surface</u> .....	- 40 -
<u>Ester synthétique avec Fe<sub>3</sub>O<sub>4</sub>, Al<sub>2</sub>O<sub>3</sub> (20-30 nm), et C<sub>60</sub></u> .....	- 41 -
<u>Ester naturel avec Fe<sub>3</sub>O<sub>4</sub>, Al<sub>2</sub>O<sub>3</sub> (20-30 nm), et C<sub>60</sub></u> .....	- 44 -
<u>Discussion</u> .....	- 47 -
<u>Conclusion</u> .....	- 48 -
<u>Conclusion Générale et Perspectives</u> .....	- 49 -

## **INTRODUCTION GENERALE**

La thèse examine le développement, la préparation et la caractérisation des nanofluides (NFs) afin d'améliorer les performances diélectriques des liquides d'isolation utilisés dans les transformateurs électriques. Les travaux incluent l'incorporation de divers types de nanoparticules (NPs) — conductrices ( $\text{Fe}_3\text{O}_4$ ,  $\text{C}_{60}$ , et Grphene), semi-conductrice ( $\text{CuO}$  et  $\text{MgO}$ ) et isolants ( $\text{Al}_2\text{O}_3$ ,  $\text{ZrO}_2$ , et  $\text{SiO}_2$ ), dans des liquides tels que les esters synthétiques et naturels, ainsi que les huiles minérales. L'objectif est d'optimiser des propriétés essentielles telles que la tension de claquage, la résistance aux décharges partielles, la tendance à la charge électrostatique et les caractéristiques de décharges de surface.

La méthodologie inclut une analyse historique des NFs, des techniques de préparation et de stabilisation, ainsi qu'une évaluation expérimentale des effets des caractéristiques des NPs (type, taille, concentration et traitement de surface) sur les propriétés diélectriques des liquides de base. Les données expérimentales sont analysées à l'aide d'outils statistiques tels que le test d'adéquation d'Anderson-Darling et l'analyse de probabilité de Weibull pour déterminer les niveaux de risque liés aux tensions de claquage.

Les résultats montrent que les NFs améliorent significativement les propriétés diélectriques en réduisant l'activité des décharges partielles, la tendance de charge électrostatique et la longueur des décharges de surface. L'ajout de NPs telles que  $\text{Fe}_3\text{O}_4$  et  $\text{Al}_2\text{O}_3$  contribue à renforcer la durabilité des équipements en isolant plus efficacement les composants électriques.

## **SECTION 1**

### **TECHNIQUES EXPERIMENTALES**

Cette section donne un aperçu complet de la configuration expérimentale et des méthodologies utilisées pour évaluer les propriétés diélectriques des nanofluides (NF) pour les applications d'isolation électrique. Elle commence par présenter les types de nanoparticules (NPs) et les liquides diélectriques de base utilisés pour préparer les NFs, ainsi que le rôle des surfactants pour assurer la stabilité des NPs. Plus précisément, l'acide oléique est présenté comme un surfactant essentiel pour empêcher l'agrégation des NP dans les liquides non polaires tels que les huiles de transformateur, garantissant ainsi une dispersion et une stabilité cohérentes, essentielles pour obtenir des performances diélectriques fiables.

## Matériaux et préparation des nanofluides

Dans cette thèse, diverses nanoparticules ont été utilisées, à savoir les oxydes métalliques conductrice ( $\text{Fe}_3\text{O}_4$ ), semi-conductrice ( $\text{CuO}$  et  $\text{MgO}$ ) et isolants ( $\text{Al}_2\text{O}_3$ ,  $\text{ZrO}_2$ , et  $\text{SiO}_2$ ) et des NP à base de carbone ( $\text{C}_{60}$  et Gr), dont les caractéristiques sont présentées dans le Tableau I.1. Les liquides de base, tels que l'ester synthétique (Midel 7131), l'ester naturel (FR3) et l'huile minérale (Nytro 4000X), sont couramment utilisés dans les transformateurs et ont été sélectionnés pour leurs propriétés physicochimiques spécifiques présentées dans le Tableau I.2.

**Tableau I.1** Propriétés physicochimiques des oxydes métalliques et des NP à base de carbone.

	Diamètre (nm)	Surface spécifique ( $\text{m}^2/\text{g}$ )	Densité ( $\text{g}/\text{cm}^3$ ) <sup>3</sup>	Pureté (%)	$\epsilon_r$	Remarques
<b>NPs sphériques</b>						
<b>NPs d'oxydes métalliques</b>						
$\text{Fe}_3\text{O}_4$	20	40	5.1	99.5	80	Conductrice
$\text{CuO}$	30-50	20-50	6.4	>99	10-30	Semi-
$\text{ZnO}$	25	19±5	5.6	99.5	8.5	Conductrice
$\text{ZrO}_2$	20 - 30	15 - 35	4.8 - 6.0	99	10 - 23	
$\text{SiO}_2$	10 - 20	60 - 100	0.6 - 1.8	99	3.9	
$\text{Al}_2\text{O}_3$	20 - 30/ 50	120 - 140 / 80	3 - 3.98	99.9	9 - 10.1	Isolante
$\text{MgO}$	20	50	3.58	>99	9.8	
<b>NPs à base de carbone</b>						
$\text{C}_{60}$	4 - 8	-	3.4	99.5	2.2	Conductrice
<b>Lamelles de nanoparticules</b>						
$<15\mu\text{m}$						
et						
Gr	l'épaisseur (nm) : 11-	40	0.8-1.8	99.5	6.9	Conductrice
15						

**Tableau I.3** Propriétés physicochimiques de SE, NE et MO.

Propriété	Midel 7131	FR3	Nytro 4000X
Densité à 20 °C)	0.97	0.92	0.87
Viscosité cinématique (mm <sup>2</sup> /sec)			
à 40 °C	29	32 - 34	9.2
Point d'écoulement (°C)	-56	-23 - (-18)	-54
Point d'éclair (°C)	260	320 - 350	140
Point d'ignition (°C)	316	350 - 360	> 200
Teneur en eau (ppm)	50	< 50	< 20
AC BDV "60Hz" (kV)	>75	> 70	> 70
Facteur de dissipation à 90°C	< 0.008	< 0.02	< 0.001

Chaque liquide a été filtré pour éliminer les impuretés avant l'intégration des NP. Les NF ont été préparés à l'aide d'une méthode en deux étapes (Figure I.1), où les NP ont d'abord été synthétisées sous forme de poudre sèche, puis dispersées dans le liquide de base. Cette approche, privilégiée pour l'extensibilité des applications en laboratoire, permet de relever des défis tels que l'agrégation des NP en utilisant des techniques telles que l'agitation ultrasonique et l'ajout de tensioactifs pour améliorer la stabilité.

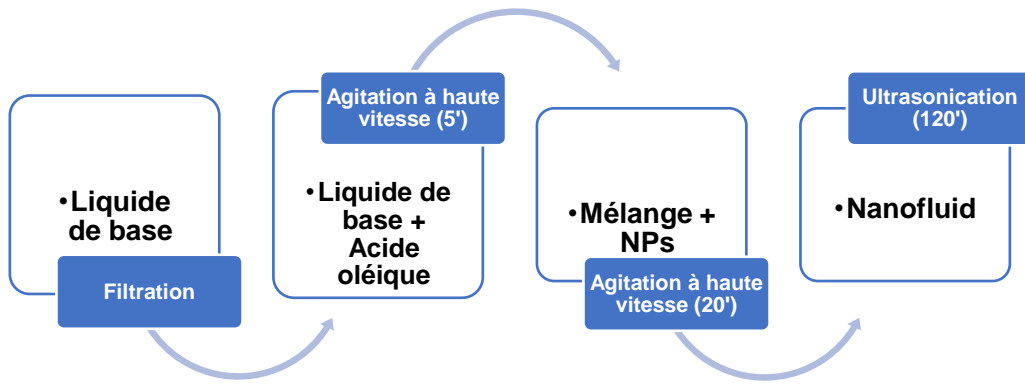


**Figure I.9** Procédure de préparation des nanofluides.

## Dispositif expérimental et méthodes d'essai

### *Mesures de la tension de claquage en courant alternatif*

Les essais de tension de claquage en courant alternatif (BDV) ont été réalisés à l'aide d'un testeur d'huile BAUR DTA 100 C avec des configurations d'électrodes spécifiques conformément aux normes IEC 60156. La tension de claquage des NF a été testée en augmentant progressivement la tension jusqu'au claquage, en enregistrant six mesures par série, chaque concentration de liquide/NP étant testée en trois séries. Les résultats ont été analysés à l'aide de la distribution de Weibull pour évaluer la fiabilité de la performance diélectrique, et des mesures statistiques telles que la valeur  $p$  ont été utilisées pour valider l'adéquation des données.

### *Caractérisation de la décharge partielle (DP)*

La Figure I.2 montre le dispositif expérimental pour la comparaison de DP de liquide de base et NF. Des tests de DP ont été réalisés avec une configuration d'électrode pointe-plan afin de déterminer la tension d'apparition de la DP (PDIV), la charge moyenne

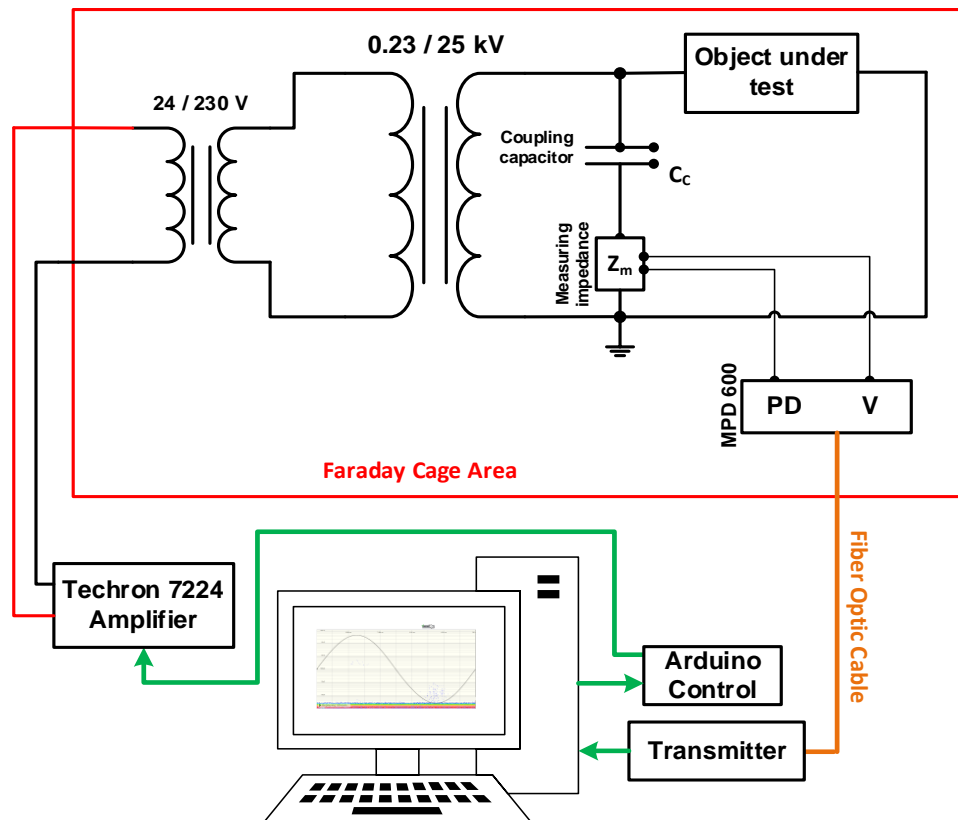


**Figure I.2** Le banc d'essai expérimental pour l'étude des DP.

( $Q_{avg}$ ), la charge de maximale ( $Q_{peak}$ ) et le taux d'occurrence de la DP (NPDs/s). Un générateur haute tension et un système Omicron ont été utilisés pour mesurer les DP conformément aux normes IEC 60270. L'étude des DP comprend la comparaison des modèles de DP entre les liquides de base et leurs NF, ce qui permet de comprendre comment la concentration et les propriétés des NP influencent le comportement de la décharge.

### *Tendance à la charge électrostatique (ECT)*

Les mesures ECT ont été effectuées à l'aide d'un système de disque rotatif adopté par les normes CIGRE, dont le schéma est donné dans la figure ci-dessous. Ce test a permis d'évaluer la charge générée à l'interface solide-liquide en raison de l'écoulement forcé de l'huile, un facteur critique dans la rupture de l'isolation. Le système de disque rotatif est entraîné à différentes vitesses de rotation, les données de charge étant enregistrées via un système d'acquisition basé sur LabVIEW. En observant comment les NP modifient l'ECT dans les huiles de transformateur, cette installation a permis d'identifier des formulations de NF qui réduisent la charge électrostatique et améliorent la durabilité de l'isolation.

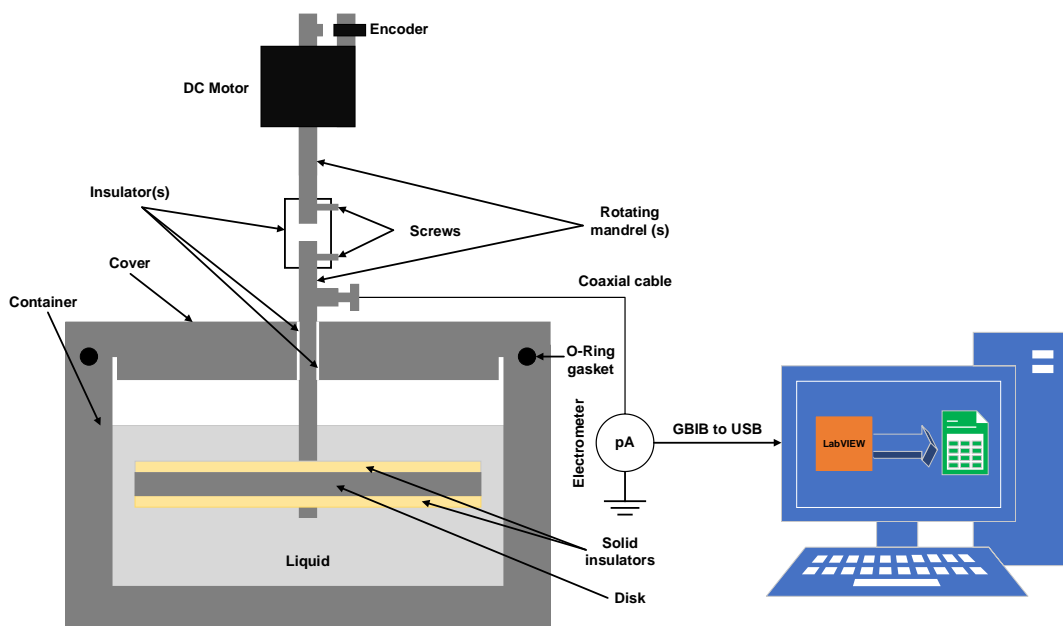


**Figure I.3** Diagramme du système de disque rotatif pour la quantification de l'ECT

### Caractérisation des décharges surfaciques

Des essais de décharge de surface, visant à observer la propagation de la décharge à travers les interfaces liquide-solide, ont été réalisés à l'aide d'une caméra à grande vitesse et d'un générateur de Marx à deux étages pour produire des ondes d'impulsion. La longueur d'arrêt de la décharge a été calculée à l'aide d'un logiciel MATLAB personnalisé. Cette analyse optique a fourni une vue détaillée des trajectoires de décharge, révélant comment les NP influencent la dynamique des décharges de surface dans les applications diélectriques.

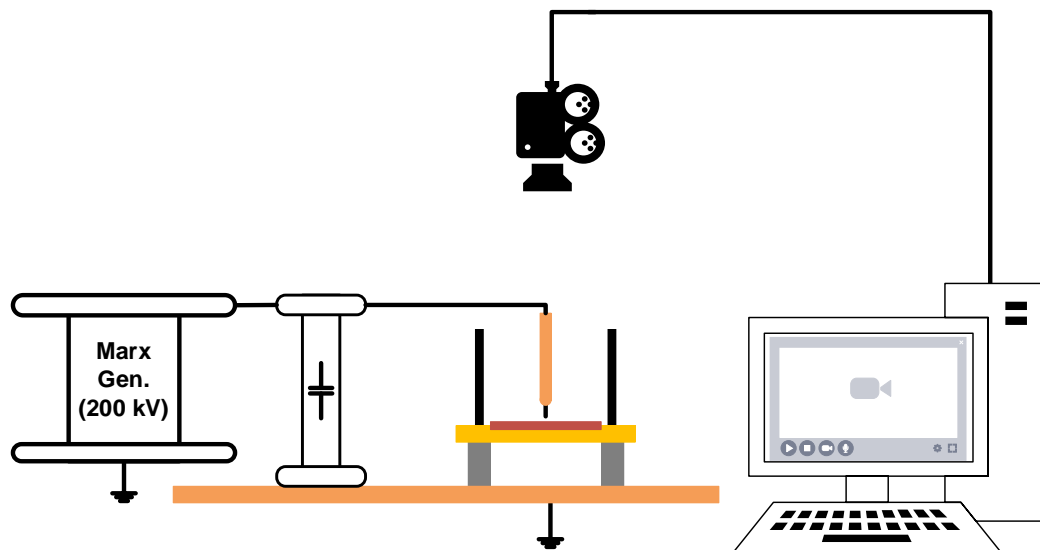


**Figure I.4** Banc d'essai d'investigation des décharges rampantes.

## **Conclusion**

La section 1 établit les bases expérimentales de l'analyse des NF en tant que diélectriques avancés, en détaillant les méthodes de préparation et d'essai des NF en fonction de multiples paramètres. L'approche systématique des évaluations de stabilité et de performance garantit que les NF sont évalués de manière approfondie pour les applications d'isolation, avec un accent particulier sur l'amélioration des propriétés de l'huile de transformateur. Les chapitres suivants examineront les résultats de la tension de claquage en courant alternatif, la caractérisation des décharges partielles et d'autres mesures de performance afin d'optimiser les formulations de NF pour les applications industrielles.

## **SECTION 2**

### **TENSION DE CLAQUAGE EN COURANT ALTERNATIF DES NANOFLUIDES A BASE D'ESTERS SYNTHETIQUES ET NATURELS ET D'HUILE MINERALE**

Ces dernières années, de nombreux travaux ont été menés pour trouver de nouveaux fluides isolants ou améliorer les propriétés des fluides existants en vue de leur application dans les composants et systèmes électriques remplis d'huile. Parmi les propriétés qui ont fait l'objet de recherches intensives figure la rigidité diélectrique.

Cette section présente les résultats expérimentaux de la mesure de la tension de claquage AC (AC BDV) des nanofluides (NF) que nous avons préparés auparavant, ainsi que leurs analyses statistiques. Ces analyses sont réalisées à l'aide d'outils statistiques tels que le test d'adéquation d'Anderson-Darling et l'analyse de probabilité de Weibull. Pour rappel, les nanofluides considérés utilisés comme fluides de base sont l'ester synthétique (SE, Midel 7131), l'ester naturel (NE, FR3), et l'huile minérale (MO, Nydro 4000X) avec les nanoparticules (NPs) incorporées conductrices ( $\text{Fe}_3\text{O}_4$ ,  $\text{C}_{60}$ , Gr), semi-conductrices ( $\text{ZnO}$ , et  $\text{CuO}$ ), et isolantes ( $\text{Al}_2\text{O}_3$ ,  $\text{ZrO}_2$ ,  $\text{SiO}_2$ , et  $\text{MgO}$ ).

A noter que certains NF ont une tension de claquage supérieure à celle que notre source de tension peut fournir (100 kV) pour l'écartement des électrodes dicté par la norme (2,5 mm), principalement ceux à base d'ester synthétique (SE). Dans ce cas, les mesures ont été effectuées avec un écartement réduit des électrodes, soit 2 mm, la comparaison se faisant sur base de la rigidité diélectrique.

Ainsi, sauf indication contraire, les tests BDV sont effectués conformément à la norme IEC 60156 (avec une distance de 2.5 mm entre les électrodes). Trois séries de six mesures ont été effectuées, ce qui a donné 18 points, considérés comme suffisants pour l'analyse statistique. Ensuite, la conformité des données AC BDV à la distribution de Weibull a été analysée à l'aide des statistiques d'Anderson-Darling. Enfin, les droites de la courbe de Weibull ont été tracées et les tensions correspondant aux niveaux de risque de 1 %, 10 % et 50 % ont été déterminées.

## Tension de claquage en AC des Nanoparticules conductrices

Les figures II.1 à II.3 illustrent les valeurs moyennes du AC BDV et du max/min des liquides de base et des différents NF avec  $\text{Fe}_3\text{O}_4$ , C<sub>60</sub>, et Gr pour diverses concentrations, respectivement. Comme mentionné dans la section précédente, le claquage ne se produit pas pour un écart d'électrode de 2.5 mm avec  $\text{Fe}_3\text{O}_4$ , C<sub>60</sub>, et Gr avec le SE ; l'AC BDV avec une distance d'écart d'électrode de 2 mm est considéré pour comparer les NF avec SE dans les mêmes conditions expérimentales. Comme le montre la figure II.1, les NP de  $\text{Fe}_3\text{O}_4$  améliorent généralement les performances de divers NF, à l'exception de ceux contenant de la NE à des concentrations de 0.1 g/l et 0.5 g/l. Plus précisément :

Les NP de  $\text{Fe}_3\text{O}_4$  améliorent généralement les performances de divers NF, à l'exception de ceux contenant de la NE à des concentrations de 0.1 g/l et 0.5 g/l. Plus précisément :

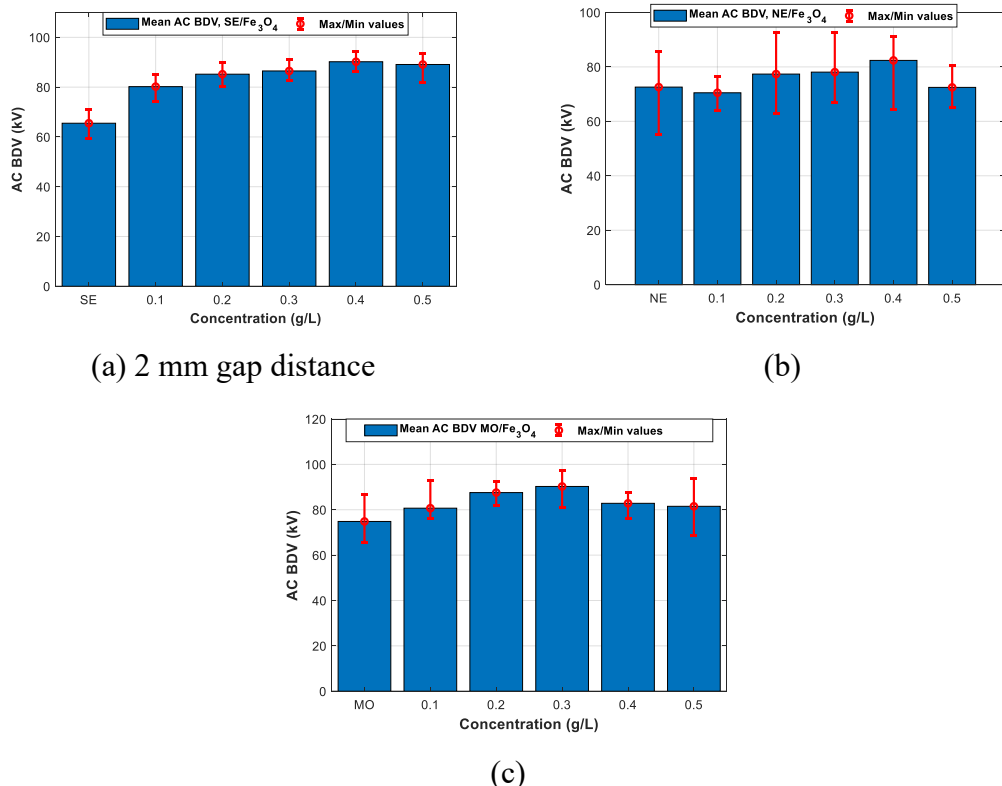


**Figure II.1** Tensions de claquage moyennes du nanofluide contenant  $\text{Fe}_3\text{O}_4$  à différentes concentrations pour (a) l'ester synthétique, (b) l'ester naturel et (c) l'huile minérale.

- Les NF à base de SE présentent des améliorations allant de 22 % à 37 %, l'amélioration la plus importante étant observée à 0.4 g/L.
- Le NF à base de NE présente une amélioration maximale d'environ 13.5 % à 0.4 g/L.
- Les NF à base de MO présentent des gains entre 7.8 % et 21 %, avec un pic à 0.3 g/L.

Comme le montre la figure II.2, les NP C<sub>60</sub> ont une influence positive sur toutes les NF, à l'exception de celles contenant de la NE à une concentration de 0.1 g/L. Les améliorations spécifiques sont les suivantes :

- Les NF à base de SE présentent des améliorations allant de 5.5 % à 13 %, l'amélioration maximale se produisant à 0.4 g/L.
- Les NF à base de NE atteignent une amélioration maximale d'environ 13 % à 0.4 g/L.
- Les NF à base de MO présentent des gains compris entre 8.4 % et 18.3 %, l'augmentation la plus forte étant observée à 0.3 g/L.

Comme les autres NPs conductrices, les NPs de Gr influencent positivement le BDV AC des trois liquides, à l'exception de ceux contenant de la NE à une concentration de 0.5 g/L. Les améliorations sont les suivantes :

- Les NF à base de SE présentent des améliorations allant de 8.2 % à 16.6 %, l'amélioration maximale se produisant à 0.3 g/L.
- Un autre type de NF avec NE permet d'obtenir une amélioration maximale d'environ 12.8 % à 0.3 g/L.
- Les NF à base de MO présentent des gains compris entre 7.4 % et 18.5 %, l'augmentation la plus forte étant observée à 0.3 g/L.

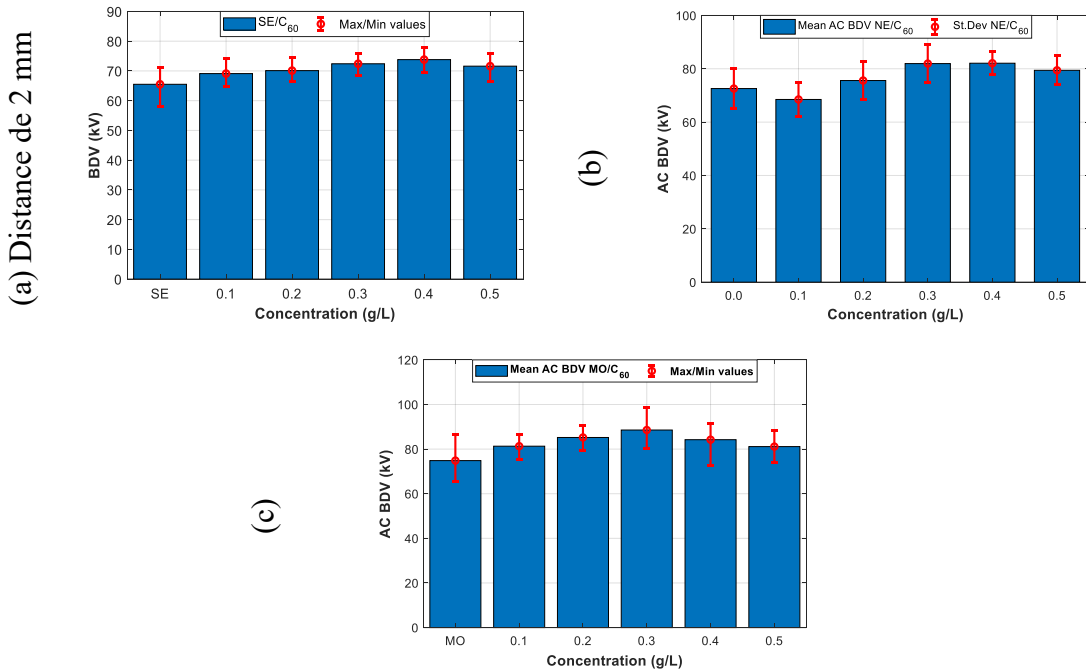


**Figure II.2** Tensions de claquage moyennes du nanofluide contenant du fullerène (4-8 nm) à différentes concentrations pour (a) l'ester synthétique, (b) l'ester naturel et (c) l'huile minérale.

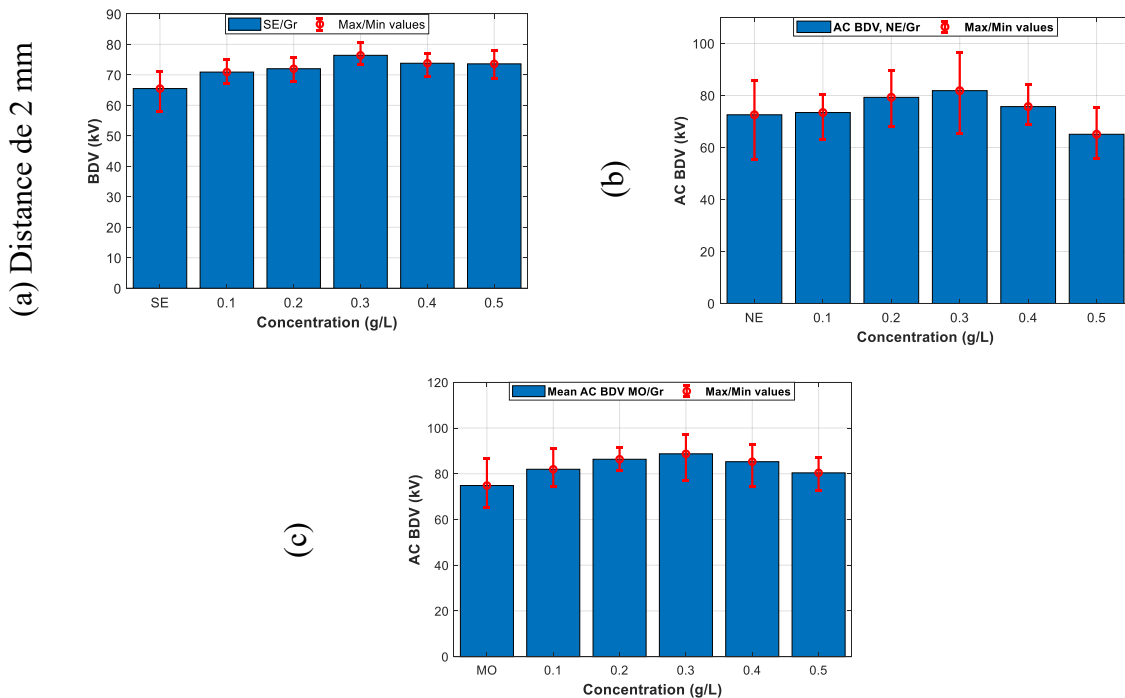


**Figure II.3** Tensions de claquage moyennes du nanofluide contenant du Graphène à différentes concentrations pour (a) l'ester synthétique, (b) l'ester naturel et (c) l'huile minérale.

## Tension de claquage en AC des Nanoparticules semi-conductrices

La figure II.4 donne les valeurs moyennes du AC BDV et du max/min pour les liquides de base et les différents NF avec ZnO pour différentes concentrations. Comme indiqué précédemment, le claquage ne se produit pas pour un écartement d'électrode de 2.5 mm avec ZnO pour SE. Comme le montre la figure II.4, les NP de ZnO améliorent généralement les performances des différents NF, à l'exception de ceux contenant de la NE à des concentrations de 0.1 g/L et 0.5 g/L. Plus précisément :

- NE-based NF experiences a maximum improvement of about 5.7% at 0.3 g/L.

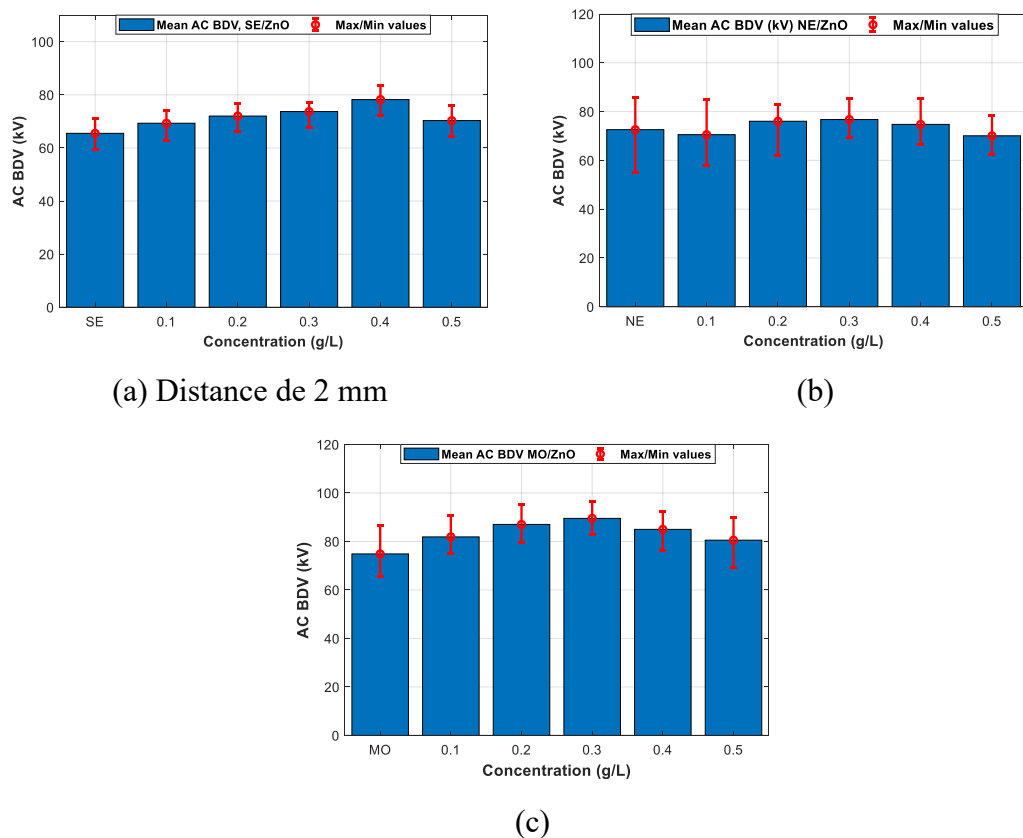


**Figure II.4** Tensions de claquage moyennes du nanofluide contenant du ZnO à différentes concentrations pour (a) l'ester synthétique, (b) l'ester naturel et (c) l'huile minérale.

- Les NF à base de SE présentent des améliorations allant de 5.8% à 19.38 %, l'amélioration la plus importante étant observée à 0.4 g/L.
- Le NF à base de NE présente une amélioration maximale d'environ 5.7% à 0.2 g/L.

- Les NF à base de MO présentent des gains entre 7.6 % et 19.59 %, avec un pic à 0.3 g/L.

### **Tension de claquage en AC des Nanoparticules Isolantes**

La figure II.5 illustre l'AC BDV moyen des NF contenant des NP d' $\text{Al}_2\text{O}_3$  (20-30 nm) à différentes concentrations dans les liquides de base SE, NE et MO.

Pour SE, le BDV moyen montre une tendance à l'augmentation avec l'ajout de NP d' $\text{Al}_2\text{O}_3$  (20-30 nm).

- À des concentrations plus faibles, on observe une augmentation notable du AC BDV, ce qui indique que de petites quantités de NP améliorent de manière significative la rigidité diélectrique du SE.
- La tendance suggère que l'amélioration diélectrique se stabilise ou augmente légèrement avec des concentrations plus élevées d' $\text{Al}_2\text{O}_3$  (20-30 nm).
- L'amélioration la plus importante est d'environ 44 % à 0.3 g/L.

Comme pour la SE, la NE augmente l'AC BDV en ajoutant des NP d' $\text{Al}_2\text{O}_3$  (20-30 nm).

- L'augmentation est plus prononcée à des concentrations plus faibles et se stabilise à des concentrations plus élevées.
- Le NE semble bénéficier de la présence des NPs  $\text{Al}_2\text{O}_3$  (20-30 nm), montrant une amélioration globale de la rigidité diélectrique.

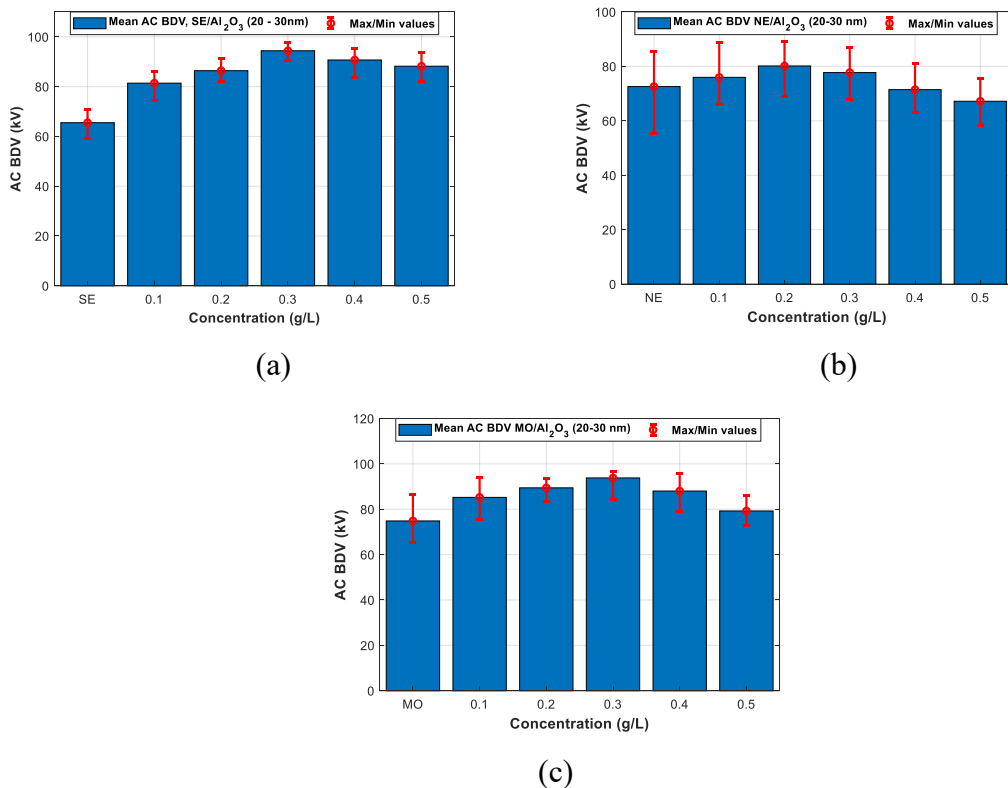


**Figure II.5** Tensions de claquage moyennes du nanofluide contenant du  $\text{Al}_2\text{O}_3$  (20-30 nm) à différentes concentrations pour (a) l'ester synthétique, (b) l'ester naturel et (c) l'huile minérale.

- La meilleure concentration est de 0.2 g/L, ce qui l'améliore de 10.44 %.

MO montre également une augmentation du BDV avec l'ajout d' $\text{Al}_2\text{O}_3$  NPs. Le schéma est similaire avec les esters synthétiques et naturels ; les améliorations les plus significatives étant observées à des concentrations plus faibles.

- Des concentrations plus élevées de NPs continuent à montrer une amélioration, mais à un taux réduit par rapport aux concentrations plus faibles. La concentration optimale est d'environ 0.3 g/L, ce qui se traduit par une augmentation de 25.33 %.

La figure II.6 illustre les tensions de claquage moyennes des NF contenant des NP d' $\text{Al}_2\text{O}_3$  (50 nm) à différentes concentrations pour SE, NE et MO.

Pour SE, l'AC BDV moyen augmente avec l'ajout de NPs  $\text{Al}_2\text{O}_3$  (50 nm)

- L'augmentation est significative à des concentrations plus faibles et continue à augmenter avec des concentrations plus élevées, bien qu'à un taux réduit.

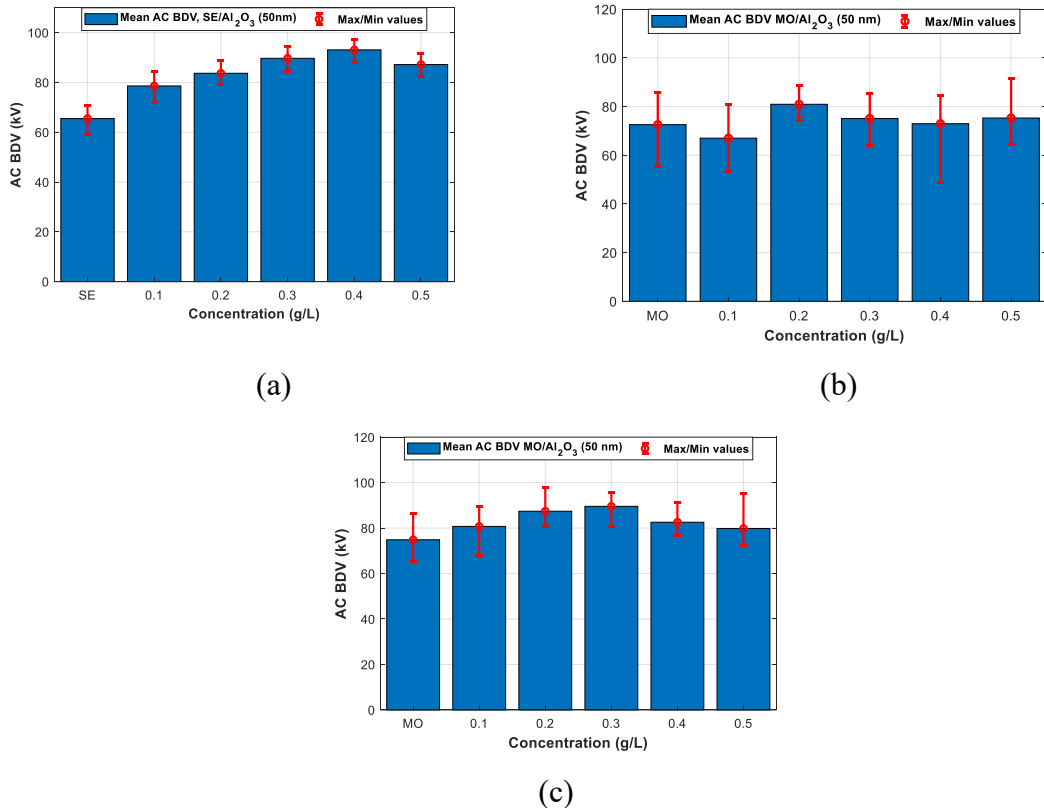


**Figure II.6** Tensions de claquage moyennes du nanofluide contenant Al<sub>2</sub>O<sub>3</sub> (50 nm) à différentes concentrations pour (a) l'ester synthétique, (b) l'ester naturel et (c) l'huile minérale.

- L'amélioration diélectrique est apparente, ce qui montre que des NP d'Al<sub>2</sub>O<sub>3</sub> (50 nm) plus grandes améliorent effectivement le BDV du SE.
- La meilleure concentration est 0.4 g/L, qui améliore L'AC BDV de 42.13 %.

Le BDV de NE augmente avec l'ajout de NPs Al<sub>2</sub>O<sub>3</sub> (50 nm)

- Les améliorations les plus significatives sont observées à des concentrations plus faibles, avec une augmentation régulière à des concentrations plus élevées.
- Cette tendance suggère que la NE bénéficie de la présence de NPs plus grandes, ce qui améliore ses propriétés diélectriques.
- L'amélioration la plus importante est d'environ 11.54 % à 0.2 g/L.

MO montre une augmentation du BDV avec l'ajout d' Al<sub>2</sub>O<sub>3</sub> (50 nm) NPs.

- Le schéma est similaire pour SE et NE, avec les améliorations les plus importantes à des concentrations plus faibles.

- Des concentrations plus élevées ont encore des effets positifs, mais le taux d'augmentation ralentit.
- C'est à 0.3 g/L que l'on observe les meilleures améliorations avec 19.60 % d'amélioration.

Les résultats ci-dessus montrent que l'ajout de NP d' $\text{Al}_2\text{O}_3$ , quelle que soit leur taille, améliore la rigidité diélectrique de SE, NE et MO. Les améliorations les plus importantes du BDV sont observées à des concentrations plus faibles de NP, l'effet d'amélioration se stabilisant ou augmentant légèrement à des concentrations plus élevées. La taille des NPs (20-30 nm vs. 50 nm) affecte le degré d'amélioration ; en d'autres termes, pour les petites NPs (ce qui signifie une surface de contact entre NP et liquide plus élevé), les meilleures améliorations sont obtenues à des concentrations plus faibles, les deux tailles contribuant positivement à l'amélioration d'AC BDV des huiles de base.

La figure II.7 comprend une analyse du AC BDV moyen des nanofluides contenant des NP de  $\text{ZrO}_2$  à différentes concentrations pour SE, NE et MO, comme illustré dans la figure II.6.

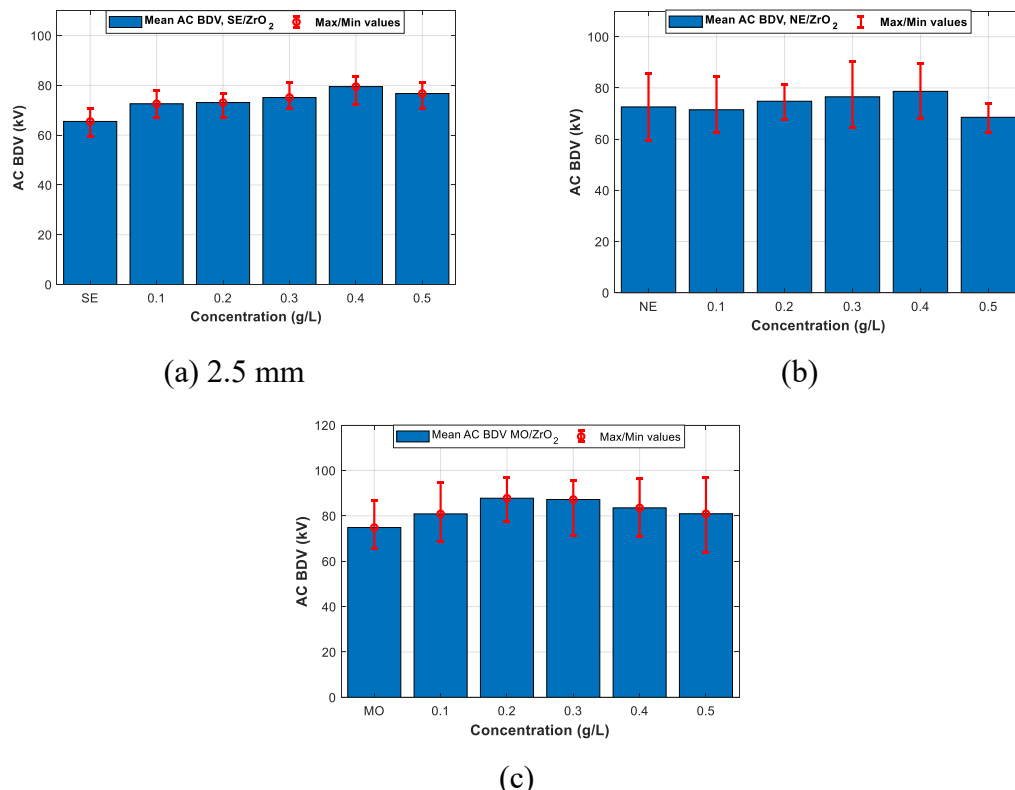


**Figure II.7** Tensions de claquage moyennes du nanofluide contenant  $\text{ZrO}_2$  à différentes concentrations pour (a) l'ester synthétique, (b) l'ester naturel et (c) l'huile minérale.

Pour le SE, le BDV moyen augmente avec l'ajout de NP de ZrO<sub>2</sub>.

- À des concentrations plus faibles, on observe une amélioration notable du AC BDV, ce qui indique que même de petites quantités de NP de ZrO<sub>2</sub> peuvent améliorer de manière significative la rigidité diélectrique.
- Au fur et à mesure que la concentration de ZrO<sub>2</sub> augmente, le BDV continue d'augmenter jusqu'à 0.4 g/L, montrant une tendance à l'amélioration constante.

NE bénéficie de la présence de NP de ZrO<sub>2</sub> de 0.2 g/L au 0.4 g/L jusqu'à la concentration optimale de 0.4 g/L, ce qui améliore ses propriétés diélectriques.

MO présente une augmentation du BDV avec l'ajout de NP de ZrO<sub>2</sub>.

- Le schéma d'amélioration est cohérent avec celui de SE et NE, avec des améliorations significatives à des concentrations plus faibles et une augmentation constante à des concentrations plus élevées.
- L'ajout de NP de ZrO<sub>2</sub> améliore efficacement la rigidité diélectrique de la MO avec une concentration optimale de 0.2 g/L.

L'analyse de ces trois graphiques dans la figure II.8 révèle l'impact de la concentration des NPs  $\text{SiO}_2$  sur l'AC BDV de différents liquides : SE, NE et MO. Les trois liquides montrent une amélioration du AC BDV avec l'ajout de  $\text{SiO}_2$ , mais à des degrés divers. MO présente le BDV de base le plus élevé et l'amélioration absolue la plus significative, avec un pic à environ 90 kV à une concentration de 0.3 g/L. SE montre une amélioration constante à travers les concentrations, avec un pic à 0.3 g/L. Le NE présente une augmentation modérée, atteignant son maximum à 0.3 g/L, mais avec une plus grande variabilité dans les mesures. Il est intéressant de noter que tous les fluides présentent des concentrations optimales de  $\text{SiO}_2$  comprise entre 0.2 et 0.3 g/L, ce qui suggère un mécanisme d'amélioration commun. Au-delà de cette plage, on observe une légère baisse des performances pour tous les fluides. Cette cohérence de la concentration optimale entre les différents fluides de base indique que si l'ampleur de l'amélioration varie, la physique sous-jacente de l'amélioration de la rigidité diélectrique par les NPs peut être similaire.

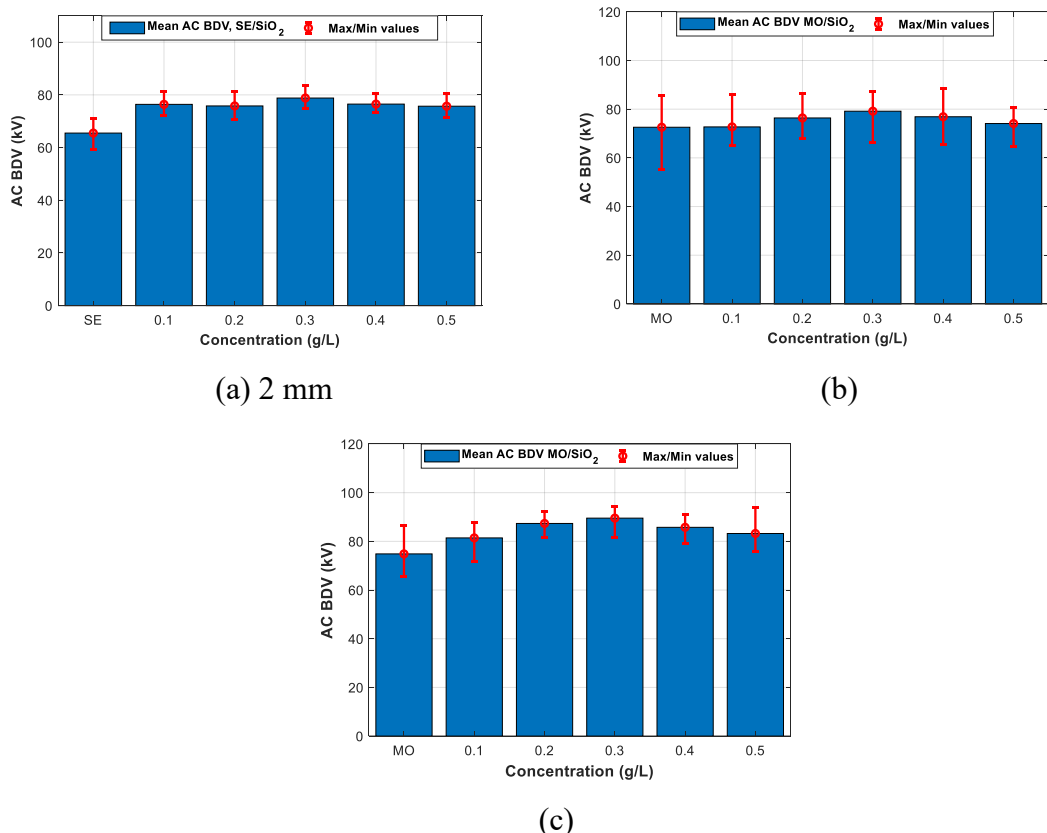


**Figure II.8** Tensions de claquage moyennes du nanofluide contenant du  $\text{SiO}_2$  à différentes concentrations pour (a) l'ester synthétique, (b) l'ester naturel et (c) l'huile minérale.

## **Discussion**

Bien que la plupart des études suggèrent que le comportement de piégeage des NP est responsable de l'amélioration du AC BDV des NF, ce mécanisme reste discutable. La clé pour comprendre ce mécanisme, l'effet des NP (conductrices, semi-conductrices ou isolantes) sur le claquage en AC du liquide de base, réside dans l'apparition d'une distribution de charges de surface à l'interface entre les NP et le liquide de base, causé par la différences des conductivités et/ou permittivités relatives entre NP et liquide de base, soumis à un champ électrique appliqué uniforme ( $E_0$ ). Selon Sima et al. [37] et Morgan et Green [100], la surface des NPs contient des charges induites et polarisées, charges induites dans le cas des NPs conductrices, et charges polarisées dans le cas des NPs isolantes (polarisation diélectrique) [37], [100]. Contrairement à l'idée qu'un matériau ne possède qu'une seule des deux propriétés (charges induites ou polarisées), certains matériaux en possèdent les deux (comme le  $\text{Fe}_3\text{O}_4$  conducteur avec une permittivité relative élevée, c'est-à-dire  $\epsilon = 80$ ). En outre, il existe une différence de densité de charge de part et d'autre de la particule, qui se traduit par un dipôle effectif ou induit à travers la particule (deux hémisphères de signes opposés) aligné sur le champ appliqué [100]. Ce concept est connu sous le nom de polarisabilité, comme le montre la figure II.9. Trois cas peuvent être distingués sur la base de ce qui précède :

- Le premier cas est celui où la polarisabilité de la NP est plus importante que celle du liquide de base. Cela signifie qu'il y a plus de charges à l'intérieur de l'interface (côté NP) qu'à l'extérieur (côté liquide), ce qui entraîne une différence de densité de charge de surface des deux côtés. Ainsi, un dipôle induit est aligné avec le champ appliqué à travers la particule [100]. Un exemple approprié de ce cas serait une NP conductrice (ou une NP "isolante ou conductrice" avec une constante diélectrique élevée) dans un liquide isolant avec une constante diélectrique faible.
- Le second cas est celui où la polarisabilité de la NP est moins importante que celle du liquide de base, c'est-à-dire qu'il y a moins de charges à l'intérieur de l'interface (côté NP) qu'à l'extérieur (côté liquide). Le dipôle qui en résulte pointe dans la direction opposée. Il peut s'agir d'une NP isolante en suspension dans un liquide ayant une constante diélectrique ou une conductivité élevée.
- Le troisième cas est celui où la polarisation du NP et du liquide de base est la même, sans dipôle net.

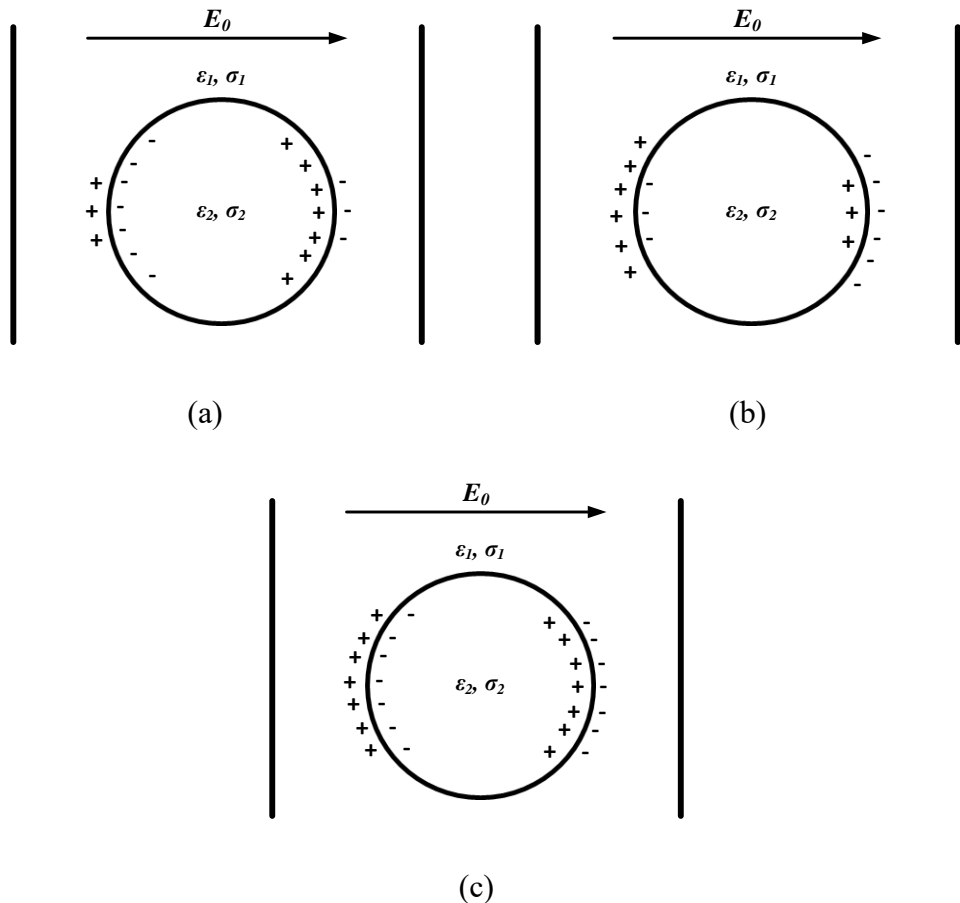


**Figure II.9** Diagramme illustrant la polarisation de particules diélectriques ayant (a) une capacité de polarisation plus élevée ou (b) plus faible, et (c) égale par rapport au liquide de base.

Évidemment, les deuxième et troisième cas ne correspondent pas à notre étude puisque, dans la plupart des cas, la conductivité et/ou la permittivité des NPs est supérieure à celle du liquide de base.

Dans le présent travail, des NP conductrices, semi-conductrices et isolantes sont étudiées, de sorte que le processus d'apparition de la charge varie de l'induction à la polarisation de la charge [37]. L'amélioration du AC BDV dans une configuration d'électrode sphère à sphère (champ électrique quasi-uniforme) lors de l'ajout de nanomatériaux conducteurs, semi-conducteurs et isolants à SE, NE et MO, soumis à une source de haute tension AC, est probablement due au piégeage des électrons causé par la formation de la densité de charge superficielle. Les électrons provenant de l'ionisation ou de l'injection se déplacent rapidement et sont piégés par le pôle chargé positivement jusqu'à saturation. À la saturation, les NP chargées négativement sont considérées comme

immobiles par rapport à la mobilité des électrons, ce qui ralentit la propagation du streamer en réduisant sa vitesse et en augmentant le BDV des NF par rapport aux liquides de base. Les NP conductrices (par exemple,  $\text{Fe}_3\text{O}_4$ ,  $\text{C}_{60}$  et Gr) induisent des charges et se chargent rapidement en raison de leur constante de temps de relaxation de charge rapide. Les NP diélectriques (par exemple,  $\text{Al}_2\text{O}_3$ ,  $\text{SiO}_2$ ,  $\text{ZrO}_2$ ) développent des charges de surface polarisées plus lentement. Les deux types de NP sont capables de capturer des électrons malgré leurs différences. La constante de temps de relaxation peut être calculée comme suit [37].

$$\tau = \left( \frac{2\epsilon_1 + \epsilon_2}{2\sigma_1 + \sigma_2} \right) \quad (\text{II.1})$$

Où  $\epsilon_{1,2}$ ,  $\sigma_{1,2}$  sont les permittivités et les conductivités du liquide de base et de la NP, respectivement. Les tableaux II.1 et II.2 montrent le temps de relaxation de différentes NP. Si le matériau est parfaitement conducteur, comme les NP de  $\text{Fe}_3\text{O}_4$ , le temps de relaxation est de l'ordre de  $10^{-14}$  à  $10^{-13}$  s, ce qui est très rapide comparé aux nanosecondes impliquées dans le développement des streamers. Dans le cas des NP isolantes, le temps de relaxation est très lent par rapport au temps de croissance du streamer. Ces résultats peuvent expliquer l'effet bénéfique des NP isolantes dans la suppression de la croissance des streamers. En fait, dans les NP isolantes ayant une permittivité élevée par rapport au liquide de base, le décalage de permittivité crée une charge de surface et, par conséquent, un mur de potentiel à l'interface NP/liquide de base est créé. La distribution de potentiel générée par la charge de surface induite et polarisée sur une NP conductrice et isolante s'exprime comme suit

$$\varphi_i = -E_0 r \cos(\theta) - \frac{1}{8} \times \left( \frac{\sigma_1 - \sigma_2}{2\sigma_1 + \sigma_2} \right) \times \frac{R^3 E_0}{r^2} \cos(\theta) \quad r \geq R \quad (\text{II.2})$$

$$\varphi_p = -\frac{1}{8} \times \left( \frac{\epsilon_1 - \epsilon_2}{2\epsilon_1 + \epsilon_2} \right) \times \frac{D^3 E_0}{r^2} \cos(\theta) \quad r \geq R \quad (\text{II.3})$$

Où  $D$  est le diamètre de la NP,  $r$  correspond à la distance de la surface de la NP, et  $E_0$  est le champ électrique. Ainsi, le processus de piégeage n'est pas non limité, et les charges de saturation, qui sont définies comme la quantité de charges que chaque NP peut

piéger, sont données par la formule 3.4 (pour les NP conductrices) et 3.5 (pour les NP isolantes), ci-dessous [37]

$$(\varphi_{sat})_{\text{Conducting}} = -12\pi\epsilon_1 E_0 R^2 \quad (\text{II.4})$$

$$(\varphi_{sat})_{\text{insulating}} = -12\pi\epsilon_1 E_0 R^2 \left( \frac{\epsilon_2}{2\epsilon_1 + \epsilon_2} \right) \quad (\text{II.5})$$

Si l'impact positif de l'ajout de NPs à une concentration optimale est expliqué, le déclin observé au-delà de la concentration optimale doit également être discuté. Pour expliquer l'impact négatif de l'ajout de certaines NP dans les liquides de base, les mécanismes varient selon que la concentration est inférieure ou supérieure à la

**Tableau II.1** Propriétés électriques des liquides de base et des NP conductrices, semi-conductrices et diélectriques.

	MO	SE	NE	Fe <sub>3</sub> O <sub>4</sub>	C <sub>60</sub>	Gr	ZnO	Al <sub>2</sub> O <sub>3</sub>	ZrO <sub>2</sub>	SiO <sub>2</sub>
$\epsilon$	2.2	3.8	3.2	80	2.2	6.6	9	9.8	25	4
$\sigma (S \cdot m^{-1})$				$10^{-12} - 10^{-10}$		$10^4$	$10^{-6}$	$10^4$	$10^{-6} - 10^{-3}$	$10^{-12}$

**Tableau II.2** Temps de relaxation des différents nanofluides.

NF	Temps de relaxation (s)		NF	Temps de relaxation (s)		NF	Temps de relaxation (s)	
<b>Nanoparticules conductrices</b>								
SE	7.75	$10^{-14}$	SE	8.67	$10^{-5}$	SE	1.25	$10^{-14}$
Fe <sub>3</sub> O <sub>4</sub>	NE	$7.64 \cdot 10^{-14}$	C <sub>60</sub>	NE	$7.60 \cdot 10^{-5}$	Gr	NE	$1.15 \cdot 10^{-14}$
MO		$7.47 \cdot 10^{-14}$	MO		$5.84 \cdot 10^{-6}$	MO		$0.97 \cdot 10^{-14}$
<b>Nanoparticules semi-conductrices</b>								
		SE		SE	$1.47 \cdot 10^{-7}$			
		ZnO	NE	NE	$1.36 \cdot 10^{-7}$			
			MO	MO	$1.18 \cdot 10^{-7}$			
<b>Nanoparticules isolantes</b>								
Al <sub>2</sub> O <sub>3</sub>	SE	51.33	ZrO <sub>2</sub>	SE	4.12	SiO <sub>2</sub>	SE	51.07
NE		47.79	NE		3.97	NE		45.79
MO		41.89	MO		3.71	MO		36.98

concentration optimale. Par exemple, lorsque la concentration en NP conductrices dépasse la concentration optimale, l'effet négatif sur l'AC BdV peut être attribué à la formation d'un chemin conducteur entre les électrodes dans le cas des NP conductrices. Cela se produit parce qu'une augmentation de la concentration réduit la distance entre les NP. Une autre raison possible est la réduction de la capacité de piégeage due à la formation d'agrégation (en raison des forces d'attraction de Van der Waals), qui réduit la surface effective nécessaire à la réussite des événements de piégeage. Les forces d'attraction de Van der Waals sont décrites ci-dessous.

$$vdW_F = \frac{H}{12\pi D_s^2} \quad (\text{II.6})$$

Où  $H$  est la constante de Hamaker et  $D_s$  la distance de séparation entre les NP. La  $vdW_F$  est inversement proportionnelle au carré de la distance entre les NP.  $D_s$  peut être exprimé comme suit.

$$D_s = \sqrt[3]{\frac{\left(\left(\frac{4}{3} \times \pi r^3\right) \times \rho\right)}{C}} \quad (\text{II.7})$$

Où  $r$ ,  $\rho$  (g/L), et  $C$  (g/L) sont le rayon et la densité des NP et la concentration des NP. L'analyse suppose une dispersion uniforme des NP, une distribution unique de la taille des NP (pas de distribution gaussienne) et l'absence d'agglomération initiale.

La figure II.10 montre l'évolution de la distance entre les NP de  $\text{Fe}_3\text{O}_4$ , de  $\text{ZnO}$  et d' $\text{Al}_2\text{O}_3$  (20-30 nm et 50 nm) en fonction de la concentration. On peut noter que lorsque la concentration augmente, la distance entre les NP diminue, ce qui accroît les forces d'attraction  $\text{vdW}_F$ , et par conséquent, les NPs ont tendance à s'agglomérer. En outre, dans le cas des NP de  $\text{Fe}_3\text{O}_4$ , la distance entre les deux NP diminue (moins de 50 nm) et se rapproche de leur diamètre (20 nm).

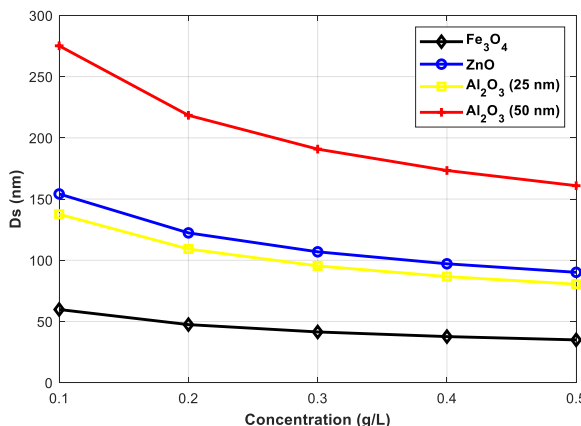


**Figure II.10** Distance inter-nanoparticules en fonction de la concentration de différents nanofluides.

En revanche, les NP d' $\text{Al}_2\text{O}_3$  (50 nm) présentent des risques réduits de réduction de la distance dans toutes les gammes de concentration. L' $\text{Al}_2\text{O}_3$  (20-30 nm) et le  $\text{ZnO}$  ont la même plage de distance inter-NP. Ainsi, les deux NP se comportent à peu près de la même manière lorsque la concentration augmente.

La réduction de la distance et la formation des agrégations peuvent justifier l'existence d'une concentration optimale, assurant un bon compromis entre le piégeage et l'espace entre les NP. Le processus de piégeage et de dépiégeage consiste à libérer les électrons capturés par la NP. Le piégeage et le dépiégeage des électrons réduisent leur mobilité, ce qui entraîne une recombinaison accrue de la densité de charge dans les NP et limite la densité des charges d'espace. Cela inhibe et retarde le développement des streamers, améliorant ainsi la tension du claquage.

## Conclusion

L'étude complète présentée dans cette section met en évidence l'impact significatif des additifs NPs sur les propriétés diélectriques de l'ester synthétique, de l'ester naturel et de l'huile minérale. Les résultats expérimentaux démontrent que l'incorporation de

nanoparticules telles que Fe<sub>3</sub>O<sub>4</sub>, C<sub>60</sub>, Gr, ZnO, Al<sub>2</sub>O<sub>3</sub>, ZrO<sub>2</sub>, et SiO<sub>2</sub> peut nettement améliorer la tension de claquage AC de ces liquides de base. Chaque type de nanoparticules présente des interactions uniques avec les liquides, les concentrations optimales étant identifiées pour une amélioration maximale du diélectrique. Ces résultats suggèrent des avancées prometteuses dans le développement de fluides diélectriques de haute performance pour les applications d'isolation électrique, ouvrant la voie à des recherches plus approfondies et à une mise en œuvre industrielle potentielle.

## **SECTION 3**

### **EFFET DES NANOPARTICULES SUR L'ACTIVITE DES DECHARGES PARTIELLES, LA TENDANCE A LA CHARGE ELECTROSTATIQUE ET LA DECHARGE SURFACIQUE**

L'étude expérimentale des NP dans les fluides isolants est cruciale pour comprendre leur impact sur les décharges partielles (DP), les tendances à la charge électrostatique (ECT) et les décharges surfaciques à l'interface solide/liquide. Lorsqu'elles sont dispersées dans des fluides diélectriques, les NP influencent les propriétés électriques de ces liquides et leur comportement dans des conditions de haute tension. Plus précisément, les nanoparticules peuvent affecter l'apparition et l'ampleur des décharges partielles, améliorant ou détériorant potentiellement les performances d'isolation en fonction de leur type et de leur concentration. L'ajout de nanoparticules telles que  $\text{Fe}_3\text{O}_4$ ,  $\text{Al}_2\text{O}_3$  ou  $\text{C}_{60}$  peut modifier la distribution du champ électrique et les propriétés diélectriques, affectant ainsi la tension d'amorçage, la fréquence et l'intensité de ces décharges. En améliorant la tension de claquage ou en réduisant la gravité des décharges, les nanoparticules peuvent améliorer la longévité et la fiabilité des équipements électriques. Cependant, l'effet des nanoparticules est complexe et varie en fonction du fluide de base et du matériau des nanoparticules, certaines combinaisons montrant une amélioration des performances et d'autres conduisant à une augmentation de l'activité des décharges.

L'ECT, un autre paramètre crucial, est affecté par la présence de NPs. L'accumulation de charges due au mouvement des fluides isolants peut entraîner une défaillance de l'équipement si elle n'est pas correctement gérée. Les NP peuvent influencer cette tendance en modifiant la mobilité et la dispersion des charges dans le liquide, réduisant ou augmentant ainsi l'accumulation de charges statiques.

Les NP influencent également les décharges surfaciques, qui se produisent le long de l'interface entre l'isolation solide et l'isolation liquide. Ces décharges peuvent dégrader les matériaux d'isolation au fil du temps, et les NP peuvent contribuer à supprimer ou à exacerber ce processus en modifiant les propriétés de surface et le comportement diélectrique des fluides.

Cette section explore ces effets, en présentant l'impact des différents types de NP sur les DP, l'ECT et le comportement de la décharge de surface dans divers fluides isolants. Il met en évidence les avantages et les limites potentiels de l'utilisation des NP dans les systèmes d'isolation électrique.

## Activité de décharge partielle

### NP conductrices

#### Esters synthétiques et naturels avec $Fe_3O_4$

La première étape de la méthodologie de l'essai de DP consiste à déterminer la tension d'amorçage (PDIV) pour chaque liquide, comme le montre la figure III.1. La tension est augmentée toutes les 10 secondes de 0.5 kV jusqu'à ce que la tension d'apparition soit atteinte pour un seuil de charge de 1 pC. Cette opération est répétée cinq fois. Ensuite, une tension d'amorçage moyenne est calculée. Dans un deuxième temps, chaque liquide est soumis à une tension de  $120\% * (PDIV)_{avg}$  pour s'assurer que le régime PD est atteint. Le profil de tension comprend cinq périodes identiques (figure III.2) ; chacune consiste en des phases croissantes/décroissantes avec une vitesse de 1 kV/s, un plateau de tension de 32 s ( $120\% * (PDIV)_{avg}$ ), et un temps de repos de 5 s. L'étude de DP est réalisée conformément à la norme IEC 60270. La charge moyenne ( $Q_{avg}$ ), la charge de maximale ( $Q_{peak}$ ) et le nombre de DP par seconde (NPDs/s) sont mesurés pendant le plateau pour chaque liquide, soit cinq fois au total, et la moyenne et l'écart type sont calculés. Les données recueillies représentent la moyenne des cinq mesures effectuées.

La PDIV du SE et du NE est comparée aux nanofluides correspondants avec  $Fe_3O_4$  pour les concentrations optimales, celles qui donnent l'AC BDV le plus élevé, et les

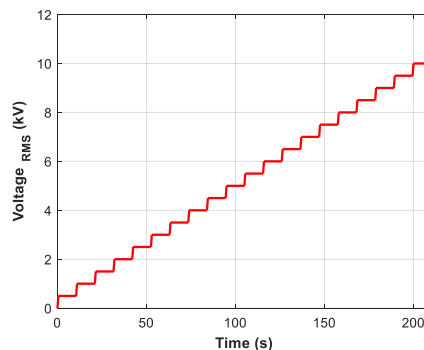


**Figure III.1** Protocole de montée en tension pour la recherche de la tension d'amorçage.

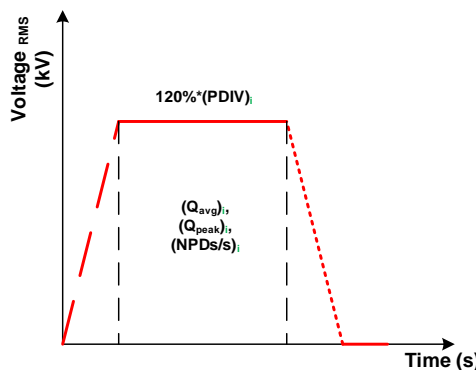


**Figure III.2** Profil de tension.

**Tableau III.1** Tension de démarrage, écart type et pourcentage d'amélioration des nanofluides synthétiques et à base d'esters naturels  $\text{Fe}_3\text{O}_4$

	Moyenne (kV)	St.Dev	Augmentation (%)
<b>SE</b>	9.04	0.38	-
<b>0.4 g/L <math>\text{Fe}_3\text{O}_4</math> NF</b>	9.22	0.64	1.99
<b>NE</b>	9.01	0.40	-
<b>0.4 g/L <math>\text{Fe}_3\text{O}_4</math> NF</b>	9.26	0.04	2.77

résultats sont donnés dans le tableau III.1. Le PDIV augmente de 9.04 kV à 9.22 kV lorsque 0.4 g/L de  $\text{Fe}_3\text{O}_4$  NPs sont ajoutés à SE. La même tendance peut être observée avec NE comme liquide de base ; l'ajout de 0.4 g/L de  $\text{Fe}_3\text{O}_4$  l'augmente de 9.04 kV à 9.26 kV.

Comme expliqué ci-dessus, pour s'assurer que le régime des DP est atteint, chaque liquide est soumis à une contrainte pendant le plateau, imposant  $120\% \times (\text{PDIV})_{avg}$ . Les résultats de cette analyse sont présentés dans le tableau III.2. Par rapport à la SE, moins de DP par seconde ont été observées pour les NF à base de  $\text{Fe}_3\text{O}_4$ . Les NP de  $\text{Fe}_3\text{O}_4$  ont un impact négatif sur les  $Q_{avg}$  et  $Q_{peak}$  de SE. Dans le cas de la NE comme liquide de base, l'ajout de NP de  $\text{Fe}_3\text{O}_4$  diminue le  $Q_{avg}$  et les NPDs/s tout en augmentant le  $Q_{peak}$ . L'ajout de NP de  $\text{Fe}_3\text{O}_4$  est plus favorable à la réduction de l'activité de DP avec la NE qu'avec la SE.

**Tableau III.2**  $Q_{peak}$ ,  $Q_{avg}$ , et NPDs/s, écart-type et pourcentage d'incrémentation des nanofluides synthétiques et à base d'esters naturels avec  $\text{Fe}_3\text{O}_4$

		$Q_{peak}$ (pC)	$Q_{avg}$ (pC)	NPDs/s (PDs/s)
<b>NF à base d'esters synthétiques</b>				
SE	<b>Moyenne</b>	190.8	13.77	60.14
	<b>St.Dev</b>	67.60	0.47	8.35
	<b>Incr. (%)</b>	-	-	-
<b>0.4 g/L <math>\text{Fe}_3\text{O}_4</math> NF</b>	<b>Moyenne</b>	427.32	17.25	45.55
	<b>St.Dev</b>	83.25	1.44	6.47
	<b>Incr. (%)</b>	123.96	25.27	-24.26
<b>NF à base d'esters naturels</b>				
NE	<b>Moyenne</b>	397.9	4.04	41.08
	<b>St.Dev</b>	101.3	0.46	3.53
	<b>Incr. (%)</b>	-	-	-
<b>0.4 g/L <math>\text{Fe}_3\text{O}_4</math> NF</b>	<b>Moyenne</b>	177.5	11.15	27.58
	<b>St.Dev</b>	56.50	0.613	3.845
	<b>Incr. (%)</b>	-55.39	175.4	-32.86

#### Esters synthétiques et naturels avec $C_{60}$

La figure III.3 montre le profil de la valeur efficace de la tension appliquée aux NF à base de SE avec  $C_{60}$  et Gr. Cette configuration a été mise en œuvre au début du travail de thèse et améliorée au fur et à mesure de l'avancement du projet (par rapport à la configuration finale présentée dans les figures III.1 et III.2). La tension monte et descend avec une vitesse de 1 kV/s, 12 kV étant la valeur maximale, maintenue pendant 30 secondes, et 5 secondes de repos sont respectées entre deux tests successifs. Ce profil de tension a été appliqué cinq fois pour chaque échantillon, et cinq tests de DP ont été réalisés pour chaque liquide.

Le tableau III.3 présente la moyenne et l'écart type des valeurs PDIV,  $Q_{avg}$ ,  $Q_{peak}$ , NPDs/s et PDEV obtenues à partir de mesures électriques pour les NF à base de SE et de SE avec 0.4 g/L de  $C_{60}$  pour un niveau seuil de PDs de 2 pC. La valeur PDIV des NF à base de SE avec  $C_{60}$  à 0.4 g/L est plus élevée que celle du SE, qui a été améliorée d'environ

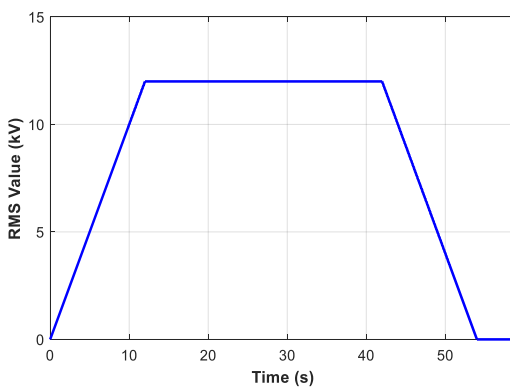


**Figure III.3** Profil de tension (valeur efficace) appliqué aux nanofluides à base de SE avec C<sub>60</sub> et Gr.

**Tableau III.3** Activité de DP des nanofluides à base d'ester synthétique et d'ester synthétique avec 0.4 g/L de C<sub>60</sub>

		PDIV (kV)	Q <sub>peak</sub> (pC)	Q <sub>avg</sub> (pC)	NPDs/s (PDs/s)	PDEV (kV)
SE	<b>Moyenne</b>	10.47	205	14.3	42	8.07
	<b>St.Dev</b>	0.58	68	1	2	0.73
	<b>Incr. (%)</b>	-	-	-	-	-
<b>0.4 g/L C<sub>60</sub> NF</b>	<b>Moyenne</b>	11.01	134	11.7	24	6.86
	<b>St.Dev</b>	0.362	9	1	1	1.48
	<b>Incr.(%)</b>	+5.1	-34.6	-18.1	-42	-14.98

5.1 % par rapport au liquide de base. En outre, les Q<sub>avg</sub>, Q<sub>peak</sub> et NPDs/s inférieurs pour la NF à base de SE avec C<sub>60</sub> démontrent que la NP C<sub>60</sub> a amélioré la performance du liquide SE avec une activité PD inférieure. Les résultats des PDEVs montrent que le SE pur donne la meilleure tension d'extinction par rapport aux NFs à base de C<sub>60</sub>. Elle a diminué d'environ 14.98 % avec les NF à base de SE avec C<sub>60</sub> par rapport au SE.

La PDIV des NF à base de NE et de NE avec 0.3 g/L et 0.4 g/L de C<sub>60</sub> est déterminée selon le protocole décrit dans les figures III.1 et III.2 ; les résultats sont présentés dans le tableau III.4. On peut observer que la PDIV diminue de 9.14 kV à 8.04 kV lorsque 0.3 g/L de NP de C<sub>60</sub> a été ajouté et diminue de 9.14 kV à 7.72 kV lorsque 0.4 g/L de NP de C<sub>60</sub> a été ajouté. Les diminutions sont de 12.11 % et 15.60 % dans le cas des NP C<sub>60</sub> à une concentration de 0.3 g/L et 0.4 g/L, respectivement. Le profil de tension décrit dans la figure III.2 est maintenant appliqué aux trois liquides, en imposant une tension de plateau

**Tableau III.4** Tension de démarrage, écart type et pourcentage d'amélioration des nanofluides à base d'ester naturel et de C<sub>60</sub>.

	Moyenne (kV)	St.Dev	Augmentation (%)
<b>NE</b>	9.14	0.65	-
<b>0,3 g/L C<sub>60</sub> NF</b>	8.04	0.5	-12.11
<b>0,4 g/L C<sub>60</sub> NF</b>	7.72	0.37	-15.60

**Tableau III.5** Q<sub>avg</sub>, Q<sub>peak</sub>, NPDs/s, écart type et pourcentage d'augmentation des nanofluides à base d'ester naturel et de C<sub>60</sub>

	Q <sub>peak</sub> (pC)	Q <sub>avg</sub> (pC)	NPDs/s (PDs/s)
<b>NF à base d'esters naturels</b>			
<b>NE</b>	<b>Moyenne</b>	812.86	43.25
	<b>St.Dev</b>	109.82	24.41
	<b>Incr. (%)</b>	-	-
<b>0,3 g/L C<sub>60</sub> NF</b>	<b>Moyenne</b>	105.31	9.10
	<b>St.Dev</b>	20.15	3.36
	<b>Incr. (%)</b>	-87.04	-78.95
<b>0,4 g/L C<sub>60</sub> NF</b>	<b>Moyenne</b>	127.28	15.19
	<b>St.Dev</b>	20.03	5.14
	<b>Incr. (%)</b>	-84.34	-64.87

égale à 120%\*PDIV. Les résultats sont présentés dans le tableau III.5. Les deux NF à base de NE avec C<sub>60</sub> ont observé plus de DP par seconde que le liquide de base.

Bien qu'un PDIV plus faible et des NPs/s plus élevés, un Q<sub>avg</sub> et un Q<sub>peak</sub> plus faibles pour les NF à base de NE avec C<sub>60</sub> par rapport au liquide de base, un Q<sub>peak</sub> plus faible indique que les NPs éliminent ou réduisent l'effet des DP avec une valeur de charge élevée. En outre, la réduction de Q<sub>avg</sub> est significative, ce qui signifie que même si le régime de DP est atteint à une valeur de tension légèrement inférieure à celle du liquide de base, cette réduction pourrait indiquer un régime de DP moins intense et, par conséquent, moins nocif pour le liquide.

### Ester synthétique avec Gr

La même configuration présentée à la figure III.3 a été utilisée à nouveau pour analyser les DP de SE et des NFs à base de SE avec Gr. Comme pour les NF avec C<sub>60</sub>, la tension monte et descend à une vitesse de 1 kV/s, 12 kV étant la valeur maximale, maintenue pendant 30 secondes, et 5 secondes de repos sont respectées entre deux tests successifs.

Le tableau III.6 présente la moyenne et l'écart type des valeurs PDIV, Q<sub>avg</sub>, Q<sub>peak</sub>, NPDs/s et PDEV pour les NF à base de SE et de SE avec 0.3 g/L de Gr à un niveau seuil de PDs de 2 pC. La valeur PDIV DE 0.3 g/L Gr NF est inférieure à celle du SE, qui a diminué d'environ 33 % par rapport au liquide de base. En outre, les Q<sub>avg</sub>, Q<sub>peak</sub> et NPDs/s plus élevés pour les NF à base de SE avec Gr démontrent que le Gr NP dégrade la performance du liquide SE avec une activité PD plus élevée. Les résultats de la PDEV montrent que la SE fournit la meilleure tension d'extinction par rapport aux NF à base de Gr. Elle a diminué d'environ 40 % avec les FN à base de SE avec Gr par rapport à la SE.

**Tableau III.6** Activité de DP des nanofluides à base d'ester synthétique et d'ester synthétique avec 0.3 g/L de Gr.

		PDIV (kV)	Q <sub>peak</sub> (pC)	Q <sub>avg</sub> (pC)	NPDs/s (PDs/s)	PDEV (kV)
<b>FN à base d'esters synthétiques</b>						
SE	<b>Moyenne</b>	10.47	205	14.3	42	8.07
	<b>St.Dev</b>	0.58	68	1	2	0.73
	<b>Incr. (%)</b>	-	-	-	-	-
0.3 g/L Gr NF	<b>Moyenne</b>	6.983	573	124.4	250	4.890
	<b>St.Dev</b>	0.582	67	5	3	0.387
	<b>Incr. (%)</b>	-33.34	+180	+770	+495	-39.40

### *NPs isolantes*

#### Ester synthétique et naturel avec Al<sub>2</sub>O<sub>3</sub> (20-30 nm)

Le même protocole présenté dans les figures III.1 et III.2 est utilisé pour la quantification de l'activité de DP pour SE et NE avec les NP d'Al<sub>2</sub>O<sub>3</sub> (20-30 nm). Les résultats révèlent que l'ajout de NP d'Al<sub>2</sub>O<sub>3</sub> (20-30 nm) influence divers aspects du comportement de la DP ; les résultats sont présentés dans le tableau III.7. L'ajout de 0.3

g/L NP d'Al<sub>2</sub>O<sub>3</sub> (20-30 nm) à SE entraîne une légère diminution du PDIV de 9.04 kV à 8.22 kV. De même, le PDIV diminue dans le de NE de 9.04 kV à 8.61 kV lorsque 0.2 g/L de Al<sub>2</sub>O<sub>3</sub> (20-30 nm) est ajouté, ce qui indique que les NP peuvent faciliter une initiation plus précoce de la DP. En ce qui concerne l'activité de DP, le Q<sub>avg</sub> diminue significativement de 52% dans SE, montrant une performance améliorée, alors que dans NE, le Q<sub>avg</sub> augmente de 53.69%, suggérant que les NP ont un effet variable en fonction du liquide de base. Le Q<sub>peak</sub> diminue de 33.45 % dans SE et de 70.83 % dans NE, ce qui révèle que les NP Al<sub>2</sub>O<sub>3</sub> (20-30 nm) réduisent efficacement les niveaux de charge de DP les plus élevés dans les deux liquides. En outre, la fréquence des événements de DP (NPDs/s) diminue de 17.09 % dans SE et de 49.70 % dans NE avec l'ajout de NP d'Al<sub>2</sub>O<sub>3</sub> (20-30 nm).

L'étude conclut que les NP d'Al<sub>2</sub>O<sub>3</sub> (20-30 nm) améliorent les caractéristiques de la DP en réduisant les niveaux de charge de maximale et les NPDs/s. Toutefois, leur impact sur la tension d'initiation et la charge moyenne varie entre SE et NE.

**Tableau III.7** Tension de démarrage, écart-type et pourcentage d'amélioration des nanofluides d'esters synthétiques et naturels Al O<sub>23</sub> (20-30 nm).

	Moyenne (kV)	St.Dev	Augmentation (%)
<b>SE</b>	9.04	0.38	-
<b>0,3 g/L Al O<sub>23</sub> NF</b>	8.22	0.02	-9.07
<b>NE</b>	9.01	0.40	-
<b>0,2 g/L Al O<sub>23</sub> NF</b>	8.61	0.49	-4.44

**Tableau III.8**  $Q_{peak}$ ,  $Q_{avg}$ , et NPDs/s, écart-type et pourcentage d'incrémentation des nanofluides d'esters synthétiques et naturels avec  $\text{Al}_2\text{O}_3$ .<sup>23</sup>

		$Q_{peak}$ (pC)	$Q_{avg}$ (pC)	NPDs/s (PDs/s)
<b>NF à base d'esters synthétiques</b>				
SE	<b>Moyenne</b>	190.8	13.77	60.14
	<b>St.Dev</b>	67.60	0.47	8.35
	<b>Incr. (%)</b>	-	-	-
<b>0.3 g/L <math>\text{Al}_2\text{O}_3</math> NF</b>	<b>Moyenne</b>	126.96	6.60	49.86
	<b>St.Dev</b>	98.6	1.50	8.29
	<b>Incr.(%)</b>	-33.45	-52	-17.09
<b>NF à base d'esters naturels</b>				
NE	<b>Moyenne</b>	397,9	4.04	41.08
	<b>St.Dev</b>	101.3	0.46	3.53
	<b>Incr.(%)</b>	-	-	-
<b>0.2 g/L <math>\text{Al}_2\text{O}_3</math> NF</b>	<b>Moyenne</b>	116.0	6.22	20.66
	<b>St.Dev</b>	35.20	0.50	4.89
	<b>Incr.(%)</b>	-70.83	+53.69	-49.70

### *Discussion de l'effet des NP sur l'activité des DP*

#### Effet du $\text{Fe}_3\text{O}_4$ et de l' $\text{Al}_2\text{O}_3$ sur les DP de SE et NE

Les résultats de cette étude donnent des indications importantes sur le rôle des NP dans l'amélioration des performances diélectriques des liquides isolants à base d'ester. L'introduction de NP de  $\text{Fe}_3\text{O}_4$  et d' $\text{Al}_2\text{O}_3$  a des effets variables sur l'activité de DP, en fonction du type de liquide de base utilisé.

Pour le SE, les NP de  $\text{Fe}_3\text{O}_4$  augmentent la sévérité des événements de DP, comme le montrent les valeurs plus élevées de  $Q_{avg}$  et  $Q_{peak}$ . Cela suggère que le  $\text{Fe}_3\text{O}_4$  peut retarder l'initiation de la DP mais peut également contribuer à une activité de décharge plus intense, compromettant potentiellement la performance de l'isolation. En revanche, les NP d' $\text{Al}_2\text{O}_3$  (20-30 nm) réduise de manière significative l'activité de DP dans la SE, réduisant le nombre de DP/s et la gravité des décharges. Cela met en évidence le potentiel de l' $\text{Al}_2\text{O}_3$  (20-30 nm) en tant que nanoparticules plus efficaces pour améliorer la résistivité des DP des esters synthétiques.

Pour NE, les NP de Fe<sub>3</sub>O<sub>4</sub> ont un impact mitigé, avec une réduction de Q<sub>avg</sub> mais une augmentation de Q<sub>peak</sub>, ce qui indique un compromis entre la fréquence et l'intensité des événements de DP. Les NP d'Al<sub>2</sub>O<sub>3</sub>, en revanche, ont un comportement plus complexe, augmentant Q<sub>avg</sub> mais réduisant Q<sub>peak</sub>. Cela suggère que si l'Al<sub>2</sub>O<sub>3</sub> peut réduire les niveaux de décharge maximum, il peut également conduire à des événements de DP plus fréquents dans les esters naturels.

En conclusion, l'étude souligne l'importance de sélectionner le type de nanoparticules approprié en fonction du liquide isolant spécifique et de la performance diélectrique souhaitée. Alors que les nanoparticules de Fe<sub>3</sub>O<sub>4</sub> peuvent offrir certains avantages en retardant l'initiation de la DP, les nanoparticules d'Al<sub>2</sub>O<sub>3</sub> semblent apporter une amélioration plus importante en réduisant la gravité et la fréquence de la DP, en particulier dans les liquides esters synthétiques. Il est recommandé de poursuivre les recherches afin d'optimiser les concentrations de nanoparticules et d'explorer leur stabilité à long terme dans différents environnements isolants.

#### Effet des NP C<sub>60</sub> et Gr sur les DP de SE et NE

Les effets des NP du C<sub>60</sub> et du Gr sur l'activité de DP révèlent des comportements contrastés. Le C<sub>60</sub> améliore généralement la résistance de DP, tandis que le graphène semble les dégrader. Pour les NP de C<sub>60</sub>, l'étude montre des résultats prometteurs, en particulier en SE. L'augmentation de la PDIV, associée à la réduction significative de Q<sub>avg</sub> et Q<sub>peak</sub>, suggère que C<sub>60</sub> peut effectivement supprimer l'activité PD et améliorer la rigidité diélectrique globale de SE. Cependant, dans le NE, alors que le C<sub>60</sub> réduit le Q<sub>peak</sub>, il augmente également la fréquence des DP, ce qui met en évidence une interaction complexe entre les NP et le liquide de base. Cela indique que si le C<sub>60</sub> a un potentiel en tant qu'additif pour améliorer les performances d'isolation, ses effets peuvent varier en fonction de l'ester utilisé.

D'autre part, les NP de Gr ont un effet néfaste sur les propriétés des DP des SE. La diminution significative du PDIV et l'augmentation significative du Q<sub>avg</sub> et du Q<sub>peak</sub> suggèrent que le graphène agrave l'activité de DP, entraînant des décharges plus fréquentes et plus graves. Cela indique que le graphène pourrait ne pas convenir en tant qu'additif de matériau isolant, en particulier pour les applications où la minimisation de l'activité de DP est essentielle.

En résumé, cette étude suggère que si les NP de C<sub>60</sub> peuvent améliorer les performances d'isolation des huiles d'ester, en particulier des esters synthétiques, les NP de Gr ne sont peut-être pas adaptées à ces applications.

### **Tendances à la charge électrostatique :**

Cette étude examine la tendance à la charge électrostatique (ECT) de diverses nanofluides à base des huiles de transformateur, en examinant plus particulièrement les esters synthétiques (SE), les esters naturels (NE) et les huiles minérales (MO) enrichis de différentes nanoparticules. La recherche s'est concentrée sur trois configurations expérimentales principales :

#### *Ester synthétique avec Fe<sub>3</sub>O<sub>4</sub>, CuO, et C<sub>60</sub> :*

- Étudié pour une concentration de 0.1 g/L
- Les trois nanoparticules réduisent l'ECT à une faible vitesse d'écoulement du liquide
- CuO et C<sub>60</sub> ont montré une réduction supérieure de l'ECT à des vitesses d'écoulement élevées.
- ECT a un comportement linéaire observé avec les nanoparticules Fe<sub>3</sub>O<sub>4</sub> et C<sub>60</sub>.

CuO et C<sub>60</sub> identifiés comme des alternatives potentielles aux inhibiteurs traditionnels de la BTA pour la réduction de l'ECT de SE.

#### *Ester naturel (Midel 1204) avec MgO :*

- Concentration optimale identifiée à 0.2 g/L qui maximise l'AC BDV et minimise l'activité de DP.
- Amélioration de 21.85 % de la tension de claquage en courant alternatif par rapport au SE.
- Réduction significative des caractéristiques de décharge partielle :
  - ❖ 72.55 % de diminution de la charge moyenne (Q<sub>avg</sub>)
  - ❖ Réduction de 66 % de la charge de pointe (Q<sub>peak</sub>)
  - ❖ Diminution de 15.51 % du nombre de décharges partielles par seconde

Les nanoparticules de MgO sont prometteuses en tant qu'inhibiteurs de l'ECT

**Ester naturel (FR3) avec C<sub>60</sub> :**

- Testé à des concentrations de 0.3 g/L et 0.4 g/L
- Les deux concentrations ont montré une réduction des niveaux d'ECT par rapport au FR3 pur.
- Les résultats s'alignent sur ceux d'études antérieures montrant l'efficacité de C<sub>60</sub> dans la réduction des ECT.

**Principales conclusions :**

- L'ajout de nanoparticules améliore généralement les performances d'ECT
- Les différentes nanoparticules ont montré une efficacité variable à différentes vitesses d'écoulement.
- L'optimisation de la concentration s'est avérée cruciale pour obtenir des performances maximales.
- Les résultats suggèrent des alternatives potentielles aux inhibiteurs traditionnels de l'ECT, moyennement d'utilisation des NPs.

L'étude démontre que des ajouts de nanoparticules soigneusement sélectionnés peuvent améliorer de manière significative les propriétés d'isolation électrique et réduire la tendance à la charge électrostatique dans les huiles de transformateur, certaines combinaisons spécifiques se révélant particulièrement prometteuses pour les applications industrielles.

## Décharge de surface

Les décharges de surface, également connues sous le nom de décharges glissantes, se produisent lorsqu'un champ électrique intense provoque des décharges à la surface des matériaux isolants. Si elles ne sont pas correctement évitées, ces décharges peuvent affaiblir la rigidité diélectrique des systèmes d'isolation et finalement conduire à une défaillance de l'équipement. Il a été démontré que les NP influencent le comportement des AC BDV, de l'activité PD et de l'ECT par différents mécanismes.

Cette section explorera comment différentes NP, telles que Fe<sub>3</sub>O<sub>4</sub>, Al<sub>2</sub>O<sub>3</sub>, et C<sub>60</sub>, affectent la décharge de surface des esters synthétiques et naturels, en particulier la longueur finale des décharges sous une tension impulsionnelle positive (1.2/50 µs). Un matériau solide en céramique de 6 mm est utilisé pour cette analyse. En comparant l'activité de décharge dans le liquide de base et différents NF, nous pouvons mieux comprendre le rôle des NPs dans la suppression ou la modification des décharges de

surface, ce qui est important pour améliorer la durabilité et la fiabilité des équipements à haute tension.

**Ester synthétique avec  $Fe_3O_4$ ,  $Al_2O_3$  (20-30 nm), et  $C_{60}$**

Modèle de la décharge de surface

Les figures III.4 (a)-(d) montrent des exemples de décharges rampantes se propageant à la surface d'un isolant solide immergé dans le SE et les NF correspondants (avec  $Fe_3O_4$ ,  $Al_2O_3$  (20-30 nm), et  $C_{60}$ ) sous une tension de polarité positive de 58 kV. Il est important de noter que les branches des décharges suivent des trajectoires circulaires (comportement radial) qui semblent tourner autour de l'électrode de pointe. Leur forme, leur longueur finale et la densité des branches dépendent de plusieurs paramètres, tels que la nature et l'épaisseur du matériau solide, l'amplitude de la tension appliquée et les NP ajoutées au liquide de base. D'autres ont également rapporté de telles observations[82],

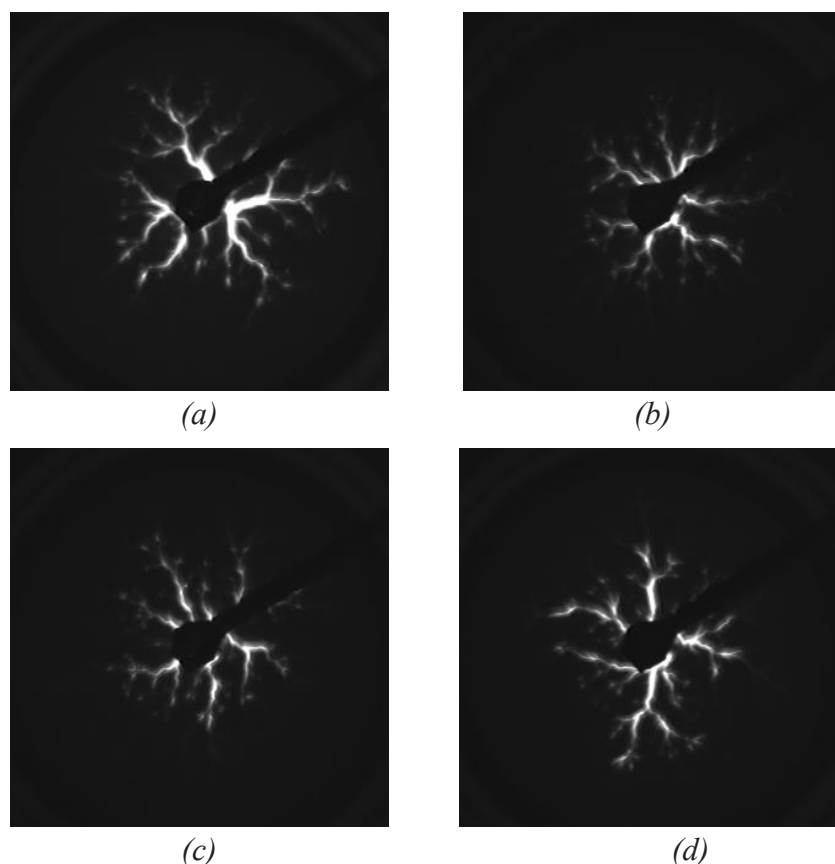


**Figure III.4** Image de décharge glissante à la surface d'un isolateur solide immergé dans (a) SE pur, (b) 0.4 g/L  $Fe_3O_4$  NF, (c) 0.3 g/L  $Al_2O_3$  (20-30 nm) NF, et (d) 0.3 g/L  $C_{60}$  NF.

[105]-[107]. Les décharges glissantes dans les NF à base de SE et de SE ont des formes similaires (en forme de buisson). Quel que soit le liquide testé, l'augmentation de la tension appliquée entraîne des décharges plus longues et des canaux de décharge plus brillants.

*Longueur d'arrêt des décharges glissantes*

La figure III.5 montre la longueur d'arrêt en fonction de la tension appliquée, allant de 48 à 58 kV pour SE et les NF correspondantes avec  $\text{Fe}_3\text{O}_4$ ,  $\text{Al}_2\text{O}_3$ , et  $\text{C}_{60}$ . Notez que la longueur d'arrêt pour une tension inférieure à 48 kV avec SE et supérieure à 58 kV avec  $\text{Fe}_3\text{O}_4$ ,  $\text{Al}_2\text{O}_3$ , et  $\text{C}_{60}$  NF a été mesurée. Cependant, à des fins de comparaison, seuls les points avec la même tension appliquée ont été représentés.

La longueur d'arrêt  $L_f$  augmente de façon quasi-linéaire avec la tension  $U$ , quel que soit le type de liquide/NF. Dans le cas du SE avec  $\text{Fe}_3\text{O}_4$  et à l'exception du 0.5 g/L à 54 kV, les concentrations de 0.3 g/L, 0.4 g/L et 0.5 g/L ont un impact positif sur la  $L_f$  quelle que soit l'amplitude de la tension. Dans la majorité des cas, les NFs 0.1 g/L et 0.2 g/L  $\text{Fe}_3\text{O}_4$  ont un impact négatif sur la  $L_f$ , quelle que soit l'amplitude de la tension. La NF avec 0.3 g/L  $\text{Fe}_3\text{O}_4$  montre les meilleures diminutions de  $L_f$  par rapport à SE. Dans le cas des NP d' $\text{Al}_2\text{O}_3$  (20-30) nm, des concentrations de 0.1-0.3 g/L affectent positivement le  $L_f$  de SE indépendamment de l'amplitude de la tension, tandis que des concentrations plus élevées augmentent le  $L_f$ . Ces résultats montrent la capacité de l'alumine à réduire les décharges de surface de SE à des concentrations plus faibles, contrairement au  $\text{Fe}_3\text{O}_4$ .

Dans le cas du C<sub>60</sub> NF, à l'exception de quelques points pour chaque concentration, le  $L_f$  est plus étendu avec le liquide de base que le NF correspondant pour une tension donnée. La diminution de la longueur d'arrêt se situe entre 1,49% (56 kV) et 13,23% (48 kV). Il est évident que l'incorporation de NPs de Fe<sub>3</sub>O<sub>4</sub>, Al<sub>2</sub>O<sub>3</sub>, et C<sub>60</sub> peut améliorer la résistance diélectrique des systèmes isolants solides et liquides.

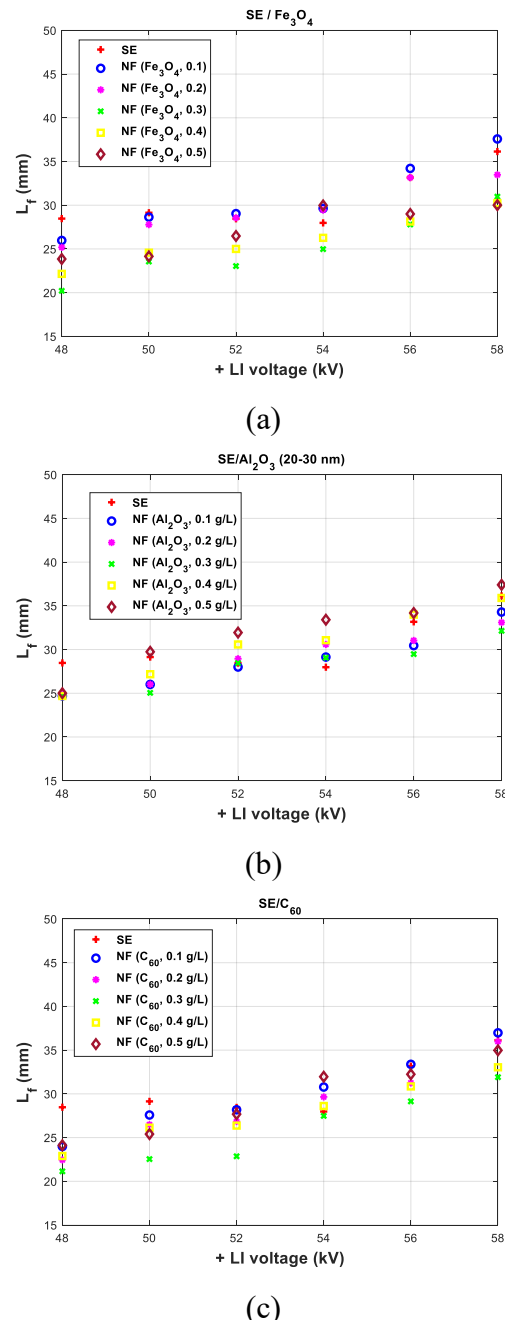


**Figure III.5** Longueur finale  $L_f$  de la décharge rampante en fonction de la tension appliquée pour (a) SE/Fe<sub>3</sub>O<sub>4</sub>, (b) SE/Al<sub>2</sub>O<sub>3</sub>, et (c) SE/C<sub>60</sub>.

***Ester naturel avec  $Fe_3O_4$ ,  $Al_2O_3$  (20-30 nm), et  $C_{60}$***

**Modèle de la décharge de surface**

Les figures III.6 (a)-(d) montrent des exemples de décharges rampantes se propageant à la surface de l'isolant solide immergé dans le FR3 et leurs NF correspondantes (avec  $Fe_3O_4$ ,  $Al_2O_3$ , et  $C_{60}$ ) sous une tension impulsionnelle de polarité positive de 58 kV. Comme pour les SE et les NF à base de SE, les branches des décharges semblent suivre des trajectoires circulaires (comportement radial) autour de l'électrode de pointe. Les décharges rampantes dans le liquide de base et les NF ont des motifs similaires (forme de buisson). En outre, deux différences significatives peuvent être soulignées : (1) les canaux principaux sont beaucoup plus épais dans le cas du NF  $C_{60}$ , avec plus de branches latérales que dans le liquide de base et les NF  $Fe_3O_4$  et  $Al_2O_3$ ; et (2) les branches sont encore plus denses, et la lumière émise est beaucoup plus faible que celle des autres liquides.

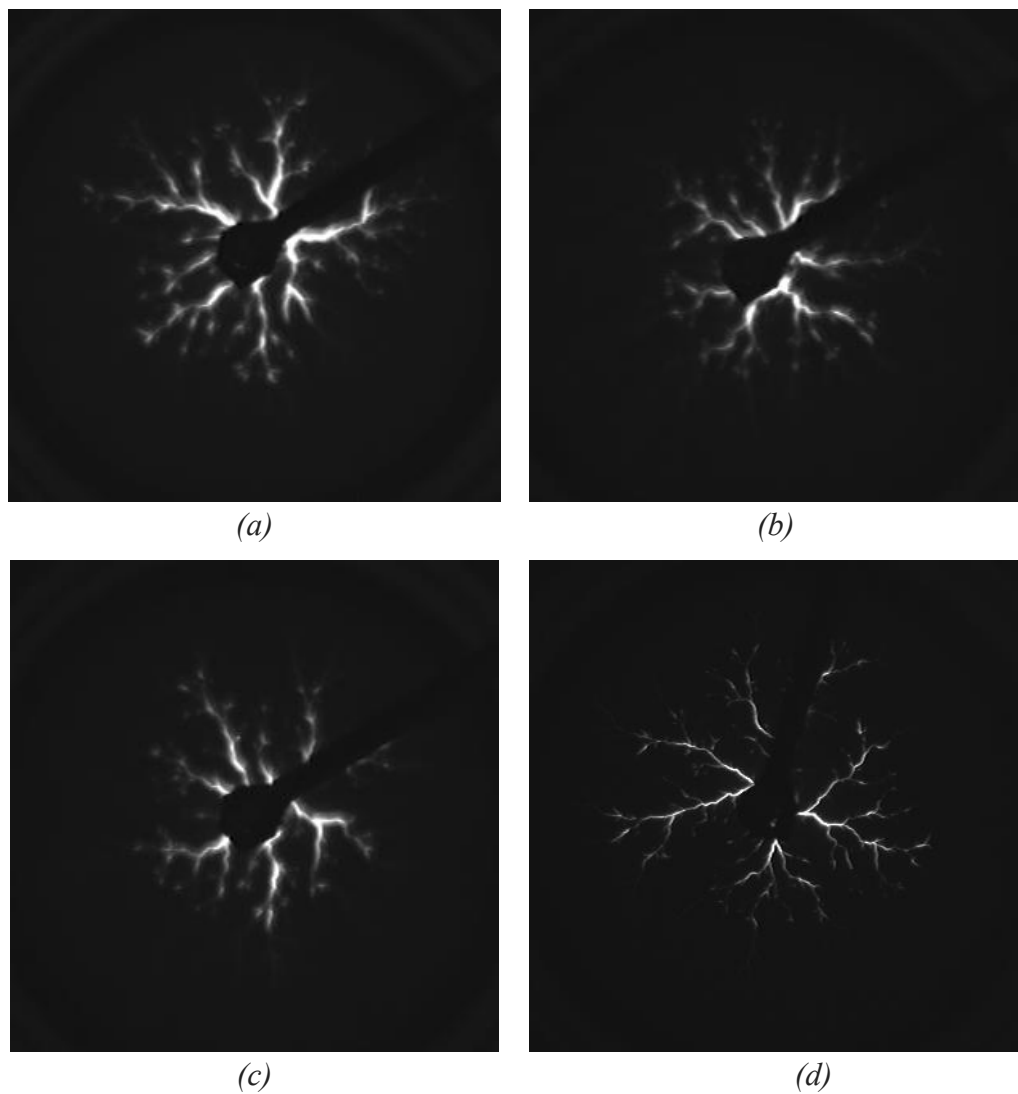
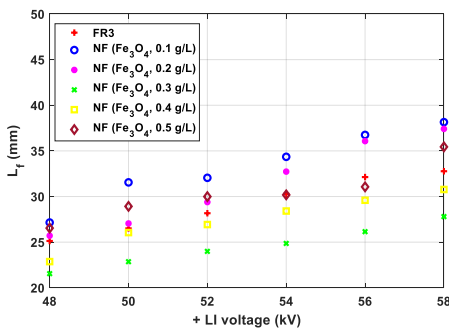


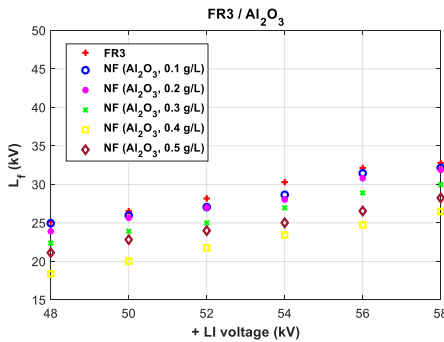
**Figure III.6** Image de décharge rampante à la surface d'un isolant solide immergé dans (a) FR3 pur, (b) 0.3 g/L  $\text{Fe}_3\text{O}_4$  NF, (c) 0.4 g/L  $\text{Al}_2\text{O}_3$  (20-30 nm) NF, et (d) 0.3 g/L  $\text{C}_{60}$  NF.

#### Longueur d'arrêt des décharges glissantes

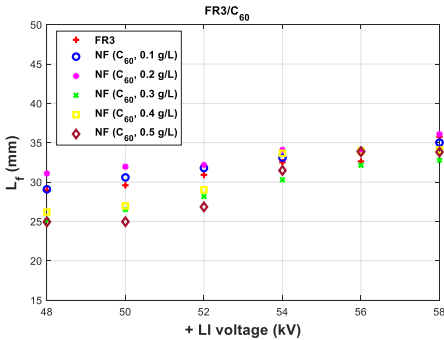
La figure III.7 illustre la relation entre  $L_f$  et la tension appliquée, allant de 48 à 58 kV pour FR3 et les NF correspondantes) contenant du  $\text{Fe}_3\text{O}_4$ , de l' $\text{Al}_2\text{O}_3$ , et du  $\text{C}_{60}$ . Conformément aux observations pour SE et leurs NF respectives,  $L_f$  a été mesurée pour des tensions inférieures à 48 kV avec FR3 et supérieures à 58 kV avec les NF  $\text{Fe}_3\text{O}_4$ ,  $\text{Al}_2\text{O}_3$ , et  $\text{C}_{60}$ . Cependant, seuls les points de données correspondant à la même tension appliquée ont été représentés. Le  $L_f$  augmente de manière quasi-linéaire avec la tension  $U$ , quel que soit le type de liquide/NF. Dans le cas du SE avec  $\text{Fe}_3\text{O}_4$ , seules deux concentrations (0.3 g/L et 0.4 g/L) ont un impact positif sur le  $L_f$ , quelle que soit



(a)



(b)



(c)

**Figure III.7** Longueur finale  $L_f$  de la décharge rampante en fonction de la tension appliquée pour (a) FR3/Fe<sub>3</sub>O<sub>4</sub>, (b) FR3/Al<sub>2</sub>O<sub>3</sub>, et (c) FR3/C<sub>60</sub>.

l'amplitude de la tension. Dans la plupart des cas, les NFs de 0.1 g/L, 0.2 g/L et 0.5 g/L de Fe<sub>3</sub>O<sub>4</sub> ont un impact négatif sur le  $L_f$ , quelle que soit l'amplitude de la tension. La NFs 0.3 g/L Fe<sub>3</sub>O<sub>4</sub> montre les meilleures diminutions de  $L_f$  par rapport à FR3. En revanche, les NP d'Al<sub>2</sub>O<sub>3</sub> (20-30) nm affectent positivement le  $L_f$  de FR3, indépendamment de l'amplitude et de la concentration des NP. Ces résultats montrent la capacité de l'alumine à réduire les décharges de surface.

Dans le cas de C<sub>60</sub> NF, à l'exception du premier point, la longueur d'arrêt est plus longue avec le liquide de base que le NF correspondant pour une tension donnée. La

diminution de la longueur d'arrêt se situe entre 1.49% (56 kV) et 13.23% (48 kV). Il ressort de ce qui précède que l'ajout de NPs de  $\text{Fe}_3\text{O}_4$ ,  $\text{Al}_2\text{O}_3$  et  $\text{C}_{60}$  pourrait être une solution pour améliorer la résistance diélectrique des systèmes isolants solide/liquide.

### ***Discussion***

#### *Impact de différentes nanoparticules sur la longueur de décharge finale*

L'analyse compare trois NP :  $\text{Fe}_3\text{O}_4$ ,  $\text{Al}_2\text{O}_3$  (20-30 nm), et  $\text{C}_{60}$ . L'objectif est de déterminer leur effet sur  $L_f$  des décharges de surface lorsqu'elles sont incorporées dans les liquides isolants SE et FR3. Pour les deux esters, la longueur de la décharge glissantes tend à augmenter de façon quasi-linéaire avec la tension appliquée. L'influence des NP peut soit renforcer soit supprimer cette augmentation en fonction de leur type et de leur concentration.

#### *Comparaison entre les nanofluides et les liquides de base*

##### a) Ester synthétique :

Les NP de  $\text{Fe}_3\text{O}_4$  ont des impacts variables sur  $L_f$  en fonction de la concentration. Les concentrations plus élevées (0.3 g/L et plus) allongent généralement la longueur de la décharge par rapport aux concentrations plus faibles (0.1 g/L), qui peuvent réduire  $L_f$ . Les NP d' $\text{Al}_2\text{O}_3$  réduisent systématiquement  $L_f$  à des concentrations plus faibles, ce qui les rend plus efficaces pour améliorer la résistance au décharge de surface à des charges plus faibles. Les NP de  $\text{C}_{60}$  présentent généralement un  $L_f$  plus long que le liquide de base dans la plupart des conditions, ce qui indique un impact moins favorable sur la suppression des décharges de surface.

##### b) Ester naturel :

Les tendances observées dans les tests SE se reflètent ici, avec quelques variations dans le degré de réduction de  $L_f$ . Par exemple, l' $\text{Al}_2\text{O}_3$  s'avère à nouveau efficace pour réduire la  $L_f$  à toutes les concentrations. L'impact des NP de  $\text{Fe}_3\text{O}_4$  n'est pas uniforme, seules des concentrations spécifiques entraînant des réductions notables de  $L_f$ , tandis que l'effet des NP de  $\text{C}_{60}$  reste moins favorable à la suppression des décharges de surface par rapport au liquide de base.

Les résultats de cette analyse indiquent que l' $\text{Al}_2\text{O}_3$  est la NP la plus fiable pour réduire la  $L_f$  des décharges glissantes, en particulier à des concentrations plus faibles.  $\text{Fe}_3\text{O}_4$  nécessite un choix précis de la concentration pour obtenir des performances

optimales, tandis que le rôle de C<sub>60</sub> dans la suppression des décharges reste moins cohérent.

## Conclusion

L'étude a fourni des informations précieuses sur la manière dont les NP influencent les propriétés électriques et les performances d'isolation des liquides isolants à base d'ester. Les résultats démontrent que différents types de NP, y compris Fe<sub>3</sub>O<sub>4</sub>, Al<sub>2</sub>O<sub>3</sub>, C<sub>60</sub>, et le graphène, ont des effets variables sur l'activité de décharge partielle (DP), les tendances à la charge électrostatique (ECT) et les décharges de surface, en fonction du type et de la concentration des NP et du liquide de base utilisé.

Les principales conclusions de ce chapitre sont les suivantes :

**Activité de décharge partielle** : L'introduction de NP peut soit supprimer soit exacerber l'activité de la décharge partielle en fonction du type de liquide de base et de la concentration de NP. Al O<sub>23</sub> réduit systématiquement la gravité et le nombre de décharges partielles par seconde, en particulier dans les SE, ce qui en fait un choix favorable pour l'amélioration des performances d'isolation. En revanche, l'impact du Fe O<sub>34</sub> varie, avec quelques améliorations pour retarder l'initiation de la DP et augmenter l'intensité de la décharge dans certaines conditions.

**Tendances à la charge électrostatique** : Les NP telles que CuO, MgO et C<sub>60</sub> ont montré un potentiel de réduction de l'ECT, en particulier à des vitesses d'écoulement de liquide plus élevées, ce qui suggère leur rôle d'additifs efficaces pour contrôler l'accumulation de charges statiques dans les systèmes isolants. Cependant, le type de NP, la concentration et la vitesse du liquide affectent le degré de réduction de l'ECT observé.

**Décharges de surface** : Les résultats du chapitre suggèrent que l'ajout de NP peut améliorer la rigidité diélectrique des systèmes isolants en réduisant la longueur finale ( $L_f$ ) des décharges de surface. Al O<sub>23</sub> apparaît comme la NP la plus efficace à cet égard, tandis que Fe O<sub>34</sub> et C<sub>60</sub> donnent des résultats mitigés en fonction de la tension et de la concentration appliquées.

## CONCLUSION GENERALE ET PERSPECTIVES

La recherche a fourni des preuves significatives du potentiel des nanofluides en tant que matériaux diélectriques avancés pour améliorer les performances d'isolation des huiles de transformateur. Les études expérimentales et les analyses statistiques révèlent que l'incorporation de NP telles que  $\text{Fe}_3\text{O}_4$ ,  $\text{Al}_2\text{O}_3$ ,  $\text{C}_{60}$ , et Gr influence de manière significative les propriétés électriques des esters synthétiques, des esters naturels et des huiles minérales. Les principales conclusions indiquent que l'ajout de ces nanoparticules peut améliorer la tension de claquage, réduire l'activité de décharge partielle, réduire les tendances à la charge electrostatique et les décharges de surface, bien que l'ampleur de l'amélioration dépende de divers facteurs, y compris le type de liquide de base, le matériau et la taille des nanoparticules, la concentration, etc.

Dans les esters synthétiques, les nanoparticules d' $\text{Al}_2\text{O}_3$  présentent systématiquement une réduction significative de la sévérité et de la fréquence des décharges partielles, ce qui en fait un choix approprié pour améliorer les performances diélectriques. Les nanoparticules de  $\text{Fe}_3\text{O}_4$ , tout en améliorant certaines propriétés diélectriques, présentent des effets mixtes en fonction de la concentration utilisée, certaines formulations montrant une augmentation de l'intensité des décharges partielles. Les matériaux à base de carbone, tels que le  $\text{C}_{60}$ , donnent des résultats prometteurs, notamment en réduisant la charge electrostatique, bien que leur efficacité puisse varier en fonction des différents liquides de base.

La recherche met en évidence la complexité de l'optimisation des formulations de nanofluides, car l'interaction entre les caractéristiques des NP et les propriétés diélectriques des fluides de base doit être gérée avec soin pour obtenir les performances souhaitées. En outre, les défis liés à la stabilité des NP, à la dispersion à long terme et aux risques potentiels pour la santé associés à la manipulation des nanomatériaux doivent être relevés pour faciliter l'utilisation sûre et efficace des NF dans les applications industrielles.

Les travaux futurs devraient se concentrer sur l'augmentation de la préparation de NF stables et performants, sur la réalisation d'études de vieillissement à long terme pour évaluer leur stabilité dans des conditions opérationnelles, et sur l'étude des interactions entre les NP et les produits de vieillissement dans les fluides diélectriques. En outre, l'exploration de nouvelles NP, telles que les nanomatériaux hybrides et les nanoparticules fonctionnalisées, pourrait ouvrir de nouvelles voies pour obtenir des améliorations encore

plus significatives de l'isolation électrique. Les résultats de cette recherche ouvrent la voie à l'application pratique des NP dans les transformateurs électriques et autres équipements à haute tension, contribuant ainsi à améliorer la fiabilité, la sécurité et l'efficacité dans le secteur de l'énergie.

## AUTORISATION DE SOUTENANCE

Vu les dispositions de l'arrêté du 25 mai 2016 modifié par l'arrêté du 26 août 2022,

Vu la demande du directeur de thèse

Monsieur A. BEROUAL

et les rapports de

M. S. AGNEL

Professeur - Institut d'Electronique du Sud (IES) - GEM, Université de Montpellier, CC079  
Place E. Bataillon - 34095 Montpellier cedex 05

et de

M. A. HADDAD

Professeur - Cardiff University - United Kingdom

**Monsieur KHELIFA Hocine**

est autorisé à soutenir une thèse pour l'obtention du grade de **DOCTEUR**

**Ecole doctorale ELECTRONIQUE, ELECTROTECHNIQUE, AUTOMATIQUE**

Fait à Ecully, le 5 décembre 2024

Pour le directeur de l'École Centrale de Lyon  
Le directeur de la recherche



Christophe CORRE

## ABSTRACT

This thesis explores developing, preparing, and characterizing nanofluids (NFs) to enhance the dielectric performance of insulation liquids commonly used in power transformers, including synthetic esters, natural esters, and mineral oils by incorporating different types of nanoparticles (NPs). These later being conducting ( $\text{Fe}_3\text{O}_4$ ,  $\text{C}_{60}$ , Gr), semi-conducting ( $\text{ZnO}$  and  $\text{CuO}$ ), and insulating ( $\text{Al}_2\text{O}_3$ ,  $\text{ZrO}_2$ ,  $\text{SiO}_2$ , and  $\text{MgO}$ ). The study aims to improve dielectric properties, including the AC breakdown voltage, partial discharge (PD) resistance, electrostatic charging tendency, and surface discharge characteristics. A comprehensive analysis covering the historical evolution, preparation techniques (one-step and two-step methods), and stabilization mechanisms essential for achieving stable nanofluids with optimal dielectric properties is presented. The preparation protocols of NFs, as well as the various experimental set-ups and methods used to characterize them dielectrically, are then described. The impact of NP characteristics, such as the type, size, concentration, and surface treatment, on the dielectric performance of base liquids is systematically assessed. The experimental data are then analyzed using statistical tools such as the Anderson-Darling goodness-of-fit test and Weibull probability analysis, and the voltages corresponding to 1%, 10%, and 50% risk levels were determined. The involved mechanisms in the improvement/deterioration of AC breakdown voltage are discussed. The experimental results indicate that nanofluids (NFs) significantly enhance the dielectric properties by reducing partial discharge activity, the electrostatic charging tendency, and the stopping length of surface discharges. This improvement is achieved by influencing charge mobility within the liquids. Both conducting and insulating nanoparticles (NPs), particularly  $\text{Fe}_3\text{O}_4$  and  $\text{Al}_2\text{O}_3$ , demonstrate substantial benefits, which can help mitigate breakdown events and extend equipment longevity. Additionally, the interaction of nanoparticles at solid-liquid interfaces affects surface discharge behaviors, further supporting the role of nanofluids in enhancing insulation durability.

**Keywords:** Nanofluids, Transformers oils, Metal Oxides Nanoparticles, Carbonic Nanoparticles, dielectric Properties.

## RESUME

### “PROPRIÉTÉS DIÉLECTRIQUES DES NANOFUIDES : RIGIDITÉ DIÉLECTRIQUE, TENDANCE À LA CHARGE ÉLECTROSTATIQUE, DÉCHARGES PARTIELLES ET DÉCHARGES SURFACIQUES”

Cette thèse explore le développement, la préparation et la caractérisation des nanofuides (NF) pour améliorer la performance diélectrique des liquides d'isolation couramment utilisés dans les transformateurs de puissance, y compris les esters synthétiques, les esters naturels et les huiles minérales en incorporant différents types de nanoparticules (NPs). Ces dernières sont conductrices ( $\text{Fe}_3\text{O}_4$ ,  $\text{C}_{60}$ , and Gr), semi-conductrices ( $\text{ZnO}$  et  $\text{CuO}$ ) et isolantes ( $\text{Al}_2\text{O}_3$ ,  $\text{ZrO}_2$ ,  $\text{SiO}_2$  et  $\text{MgO}$ ). L'étude vise à améliorer les propriétés diélectriques, notamment la tension de claquage en courant alternatif, la résistance aux décharges partielles, la tendance à la charge électrostatique et les caractéristiques de décharge de surface. Une analyse complète couvrant l'évolution historique, les techniques de préparation (méthodes en une ou deux étapes) et les mécanismes de stabilisation essentiels pour obtenir des nanofuides stables avec des propriétés diélectriques optimales est présentée. Les protocoles de préparation des NP, ainsi que les différents montages expérimentaux et les méthodes utilisées pour les caractériser sur le plan diélectrique, sont ensuite décrits. L'impact des caractéristiques des NP, telles que le type, la taille, la concentration et le traitement de surface, sur les performances diélectriques des liquides de base est systématiquement évalué. Les données expérimentales sont ensuite analysées à l'aide d'outils statistiques tels que le test d'adéquation d'Anderson-Darling et l'analyse de probabilité de Weibull, et les tensions correspondant à des niveaux de risque de 1 %, 10 % et 50 % ont été déterminées. Les mécanismes impliqués dans l'amélioration/la détérioration de la tension de claquage en courant alternatif sont discutés. Les résultats expérimentaux indiquent que les nanofuides (NF) améliorent de manière significative les propriétés diélectriques en réduisant l'activité de décharge partielle, la tendance à la charge électrostatique et la longueur d'arrêt des décharges de surface. Cette amélioration est obtenue en influençant la mobilité des charges dans les liquides. Les nanoparticules (NPs) conductrices et isolantes, en particulier  $\text{Fe}_3\text{O}_4$  et  $\text{Al}_2\text{O}_3$ , présentent des avantages substantiels qui peuvent contribuer à atténuer les événements de rupture et à prolonger la longévité des équipements. En outre, l'interaction des nanoparticules aux interfaces solide-liquide affecte les comportements

de décharge de surface, ce qui renforce le rôle des nanofluides dans l'amélioration de la durabilité de l'isolation.

**Mots-clés :** Nanofluides, huiles pour transformateurs, nanoparticules d'oxydes métalliques, nanoparticules carboniques, propriétés diélectriques.